Américo José Gonzalez Duarte

Mestre em Bioquímica Estrutural e Funcional

Characterization of Nitric Oxide Reductase (NOR) from *Pseudomonas nautica*, a Study on Biologic Nitric Oxide Reduction

Dissertação para obtenção do Grau de Doutor em Bioquímica

Orientador: Isabel Moura, Professora Catedrática, Faculdade de Ciências e Tecnologia da Universidade Nova de Lisboa

Presidente: Prof. Doutor António Manuel Dias de Sá Nunes dos Santos

Arguentes: Prof. Doutora Margarida Maria Portela Correia dos Santos Romão
Prof. Doutor José João Galhardas de Moura

Vogais: Prof. Doutora Maria de Lurdes Afonso Barreira Alves de Mira
Prof. Doutora Maria Conceição Santos Silva Rangel Gonçalves
Prof. Doutor Manuel Aureliano Pereira Martins Alves
Prof. Doutora Maria Margarida Catalão Almiro e Castro
Doutora Cristina Maria Grade Couto da Silva Cordas

FACULDADE DE CIÊNCIAS E TECNOLOGIA
UNIVERSIDADE NOVA DE LISBOA

Outubro 2011

Américo José Gonzalez Duarte

Characterization of Nitric oxide reductase (NOR) from *Pseudomonas nautica*, a study on biologic nitric oxide reduction.

Dissertação apresentada para a obtenção do grau de doutor em Bioquímica, especialidade em Bioquímica-Fisica, pela Faculdade de Ciências e Tecnologia da Universidade Nova de Lisboa.

Dissertation submitted to obtain the phD degree in Biochemistry, specialty in Physical-Biochemistry, by the Faculdade de Ciências e Tecnologia from the Universidade Nova de Lisboa.

Lisboa 2011

"Saber interpor-se constantemente entre si próprio e as coisas
é o mais alto grau de sabedoria e prudência"

in Livro do Desassossego

Acknowledgments

Em primeiro lugar gostaria de agradecer à minha orientadora, a Professora Doutora Isabel Moura, não só por me ter acolhido na sua equipa, bem como por sempre se ter mostrado presente durante todo o tempo que permaneci no seu laboratório. Acabei por ser mal acostumado por ela, por duas razões: primeiro nunca se negou a ver e/ou discutir um resultado por mim obtido e segundo por nos brindar regularmente, a mim e a todos os demais com as suas iguarias gastronómicas. Ao Professor José J.G. Moura, pela sua disponibilidade e também por me ter permitido inserir no seu grupo de investigação, o Bioin.

Não posso deixar de agradecer à Professora Dr.ª Alice Pereira e ao Professor Dr. Pedro Tavares que sempre se mostraram disponíveis para me ouvir, aconselhar e ajudar, mesmo nas conversas rápidas que tínhamos. Todos os conselhos que me deram foram determinantes para a minha progressão nos estudos apresentados nesta tese, portanto o meu mais sincero obrigado, a ambos.

À Cristina Cordas, não existem palavras para descrever a minha gratidão, não só pela sua amizade e companheirismo, tanto no trabalho como fora deste. Gostava também de agradecer ao Carlos Martins, por toda a informação que me disponibilizou sobre o sistema estudado, e em especial por todas aquelas amostras que lhe fui "roubando", com a sua autorização, da sua gaveta, muito obrigado, pois sempre me poupaste umas horas de trabalho.

Não menos importantes, terei de agradecer a enorme amizade do Filipe Folgosa, do Rui Almeida, e da Susana Ramos, pois tiveram um contributo importante nesta jornada. À restante equipa dos grupos Bioin e Bioprot, com elementos que nela se inserem e/ou inseriram, à Sofia à Cristina Timóteo, ao Cristiano Mota, à Ana Teresa, à Marta, à Raquel, à Luísa ao Pablo à Gabi, ao Luís Nobre, e aos restantes "Césares" que por ali foram passando.

Não poderei deixar de agradecer à minha família: à mana Isabel e ao meu cunhado Beto por todo o apoio incondicional e sobretudo por me terem dado o Bernardo para tomar conta, sempre me aliviou a cabeça e me pintou uns sorrisos na cara. Quando defendi a passada tese de mestrado estavam vós atendendo a chegada do pequeno Bernardo, será que na defesa desta tese de doutoramento estareis vós à espera de um

irmão/ã do Bernardo? Ao meu Pai que embora presentemente ausente, nunca travou o meu caminho e claro, não menos importante à Carmen, que igualmente me encorajou.

É imperativo prestar um sentido agradecimento ao meu "gang" de amigos. Nem este conjunto de agradecimentos estaria completo sem tal menção. Ao Zé que mesmo fora de Lisboa me encorajou, apoiou, escutou e com ele descobri que há um refrão de uma música eterna que está completamente errado quando é transposto para o quotidiano. Às meninas dos meus olhos: à Jack pela sua eterna amizade, à Vera pela sua alegria contagiante, que piora cada vez que nos juntamos, vai sempre tudo a baixo. À Pat (riqueza) pelo seu carinho, à minha Sue (pureza) pela sua pseudo terapia. Ao Hugo, que retirou a palavra menos do meu dicionário, ao Tiago que sempre me acalmou a ansiedade, ao Miguel pela sua presença e sim, existe alguém mais irrequieto que eu, e claro ao Bruno pelo seu constante modo de festa. À Gi a e ao Plim, que sempre me encorajaram e mostraram quem é o capitão, ao João Leandro pela sua infinita bondade e amizade. E um especial agradecimento à Ana Bicho, simplesmente por ser inesperada, incansavelmente verdadeira e um exemplo de força a seguir. Não menos importante, um agradecimento à Joana Gordo, que me aturou todos os dias à hora de almoço e nunca deixou que eu me fosse a baixo. Um especial agradecimento terá de ser feito a alguns dos amigos anteriores que perderam de uns minutos a algumas horas do seu tempo a elaborar os separadores desta tese.

Quero agradecer ao CQFB / Departamento de Química da FCT/UNL pelas condições de trabalho proporcionadas.

O meu agradecimento à Fundação para a Ciência e Tecnologia pelo financiamento, a bolsa de doutoramento atribuída (SFRH/BD/39009/2007), sem a qual a execução deste trabalho não seria possível.

Sei que se começasse a enunciar os restantes que se cruzaram comigo durante esta jornada, iria esquecer uma boa dezena de nomes importantes, não querendo parecer banal, agradeço a todos aqueles que me ajudaram e acima de tudo, que sempre acreditaram que eu seria capaz de chegar ao final. A todos vós, o meu mais sincero obrigado.

Publication List

1. Sofia R. Pauleta, **Américo G. Duarte**, Marta S. Carepo, Alice S. Pereira, Pedro Tavares, Isabel Moura, José J. G. Moura, "NMR assignment of the apo-form of a *Desulfovibrio* gigas protein containing a novel Mo-Cu cluster", Biomolecular NMR Assignment Journal (2007). Jul 1;(1):81-3.

2. Shabir. Najmudin, Cecília. Bonifácio, **Américo G. Duarte**, Sofia R. Pauleta, Isabel Moura, José J. Moura, Maria J. Romão. "Crystallization and crystallographic analysis of the apo form of the orange protein (ORP) from Desulfovibrio gigas", Acta Crystallogr Sect F Struct Biol Cryst Commun. (2009) Jul 1;65(Pt 7):730-2.

3. Andrea Santos, **Américo G. Duarte**, Alexander Fedorov, José M.G. Martinho, Isabel Moura. "Rubredoxin mutant A51C unfolding dynamics: a Förster Resonance Energy Transfer study", Biophysical Chemistry (2010), May; 148(1-3):131-7.

4. Cristina G. Timoteo, Alice S. Pereira, Carlos S. Martins, Sunil G. Naik, **Américo G. Duarte**, José J. G. Moura, Pedro Tavares, Boi, H. Huynh, Isabel Moura. "Low Spin heme b_3 in the Cathalytic Center of Nitric Oxide Reductase from *Pseudomonas nautica*", Biochemistry (2011), March 31, 50, 4251-4262.

Resumo

A desnitrificação ou redução dissimilativa do nitrato é uma via metabólica que se insere no ciclo do nitrogénio. Esta via metabólica envolve quatro reacções de redução: o nitrato é reduzido a nitrito, o nitrito a óxido nítrico (NO), este a óxido nitroso (N_2O) e o último passo a dinitrogénio. Cada um destes passos envolve metaloenzimas específicas que catalizam as anteriores reacções, nomeadamente as reductases do nitrato, as reductases do nitrito, as reductases do óxido nítrico (NOR) e as reductases do óxido nitroso, respectivamente.

A NOR é uma metaloenzima que realiza a redução do NO. Esta reacção envolve dois electrões e dois protões, tendo como produto o N_2O e H_2O. Esta proteína insere-se na super-família das oxidases terminais, pois são proteínas integrais de membrana com 12 hélices α transmembranares, numa disposição altamente conservada. As cNORs são compostas por duas subunidades. A subunidade NorC, com uma massa molecular de 17 kDa, que contém um hemo *c* de spin-baixo, ligado covalentemente à cadeia polipeptídica, com uma coordenação His/Met. A segunda subunidade, a NorB, também designada por subunidade catalítica, apresenta uma massa molecular de 56 kDa. Contém um centro hémico de spin-baixo (hemo *b*), um centro hémico de spin-alto (hemo b_3) e um ferro não-hémico (Fe_B). Estes dois últimos centros encontra-se acoplados antiferromagneticamente e ligados em ponte por um oxigénio/grupo hidroxilo, formando assim o centro catalítico da enzima. Recentemente, utilizando espectroscopia de Mössbauer, foi comprovado inequivocamente que o hemo catalítico é na verdade hexa-coordenado, quando o átomo de Fe se encontra no estado férrico ou ferroso. Estes resultados estão em concordância com a estrutura tridimensional da NOR isolada da bactéria *Pseudomonas (Ps.) aeruginosa*, que mostra a presença do ligando axial (His) e do ligando em ponte na forma como isolada.

O mecanismo e redução do NO é um assunto controverso, existindo contudo duas hipóteses consideradas: o mecanismo *cis* que descreve a redução de duas moléculas de substrato, com a coordenação das mesmas a um único átomo de Fe do centro catalítico, e o mecanismo *trans*, onde ambos os átomos de Fe do coordenam uma molécula de substrato. Esta classe de enzimas não cataliza apenas a redução de NO a N_2O, cataliza igualmente a redução de O_2 a H_2O, numa reacção que envolve quatro electrões e quatro protões. O mecanismo de redução do O_2 é também um assunto pouco esclarecido, sendo provável o envolvimento do hemo catalítico b_3, à semelhança das oxidases terminais.

O principal objectivo deste trabalho foi a purificação e caracterização da NOR de *Ps. nautica*, através da aplicação de diferentes técnicas bioquímicas, electroquímicas e espectroscopias, tais como a espectroscopia de ultra-violeta–visível e Ressonância Paramagnética Electrónica (RPE).

Neste trabalho é apresentada a optimização do protocolo de purificação da forma nativa da NOR de *Ps. nautica*. As fracções purificadas evidenciam um elevado grau de pureza, a correcta estequiometria dos co-factores metálicos.

Os resultados espectroscópicos obtidos evidenciam novas características estruturais, nomeadamente:

i) Os dados de UV-visível sugerem que o hemo b_3 apresenta uma conformação de spin-baixo.

ii) Os dados de RPE comprovam a existência de uma nova espécie de spin-inteiro, espécie esta que provém do acoplamento antiferromagnético do hemo b_3 com o Fe não-hémico, ambos no estado férrico (b_3-Fe^{III}-Fe_B^{III}).

Foram ainda realizados ensaios de transferência electrónica, utilizando a enzima em estudo, imobilizada na superfície de um eléctrodo de grafite. Os dados obtidos mostram pela primeira vez, quatro processos de oxidação/redução (redox), correspondentes a cada um dos centros metálicos da NOR de *Ps. nautica*. A figura que se segue resume os valores obtidos para cada um dos centros de Fe da proteína em estudo.

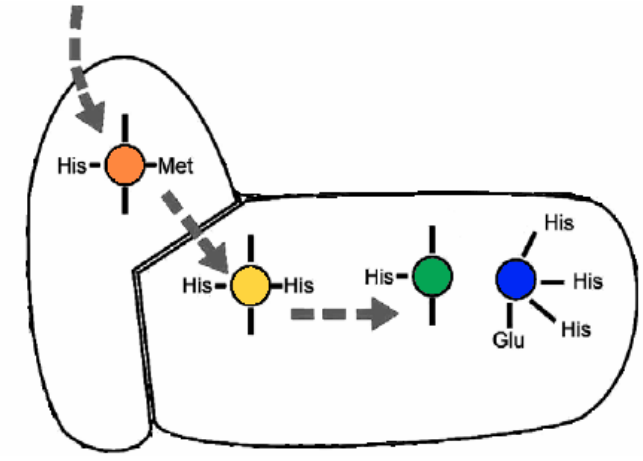

	Hemo *c*	Hemo *b*	Hemo b_3	Fe_B
cNOR/*Ps. nautica*	**+ 208**	**+ 43**	**-162**	**-369**

Figura – Valores de potencial redox obtidos para os centros metálicos da NOR de *Pseudomonas nautica*. A figura mostra uma representação esquemática da enzima e os valores referem-se aos potenciais obtidos para cada um dos co-factores da enzima (*vs.* ENH).

Os resultados obtidos através dos ensaios de resposta electroquímica directa utilizando a NOR de *Ps. nautica* são:

i) O Fe não-hémico apresenta o potencial redox mais reduzido (-369 mV *vs.* ENH).
ii) O potencial redox mais elevado pertence ao hemo do tipo *c* (+ 208 mV *vs.* ENH).
iii) Os resultados do potencial redox para cada um dos centros metálicos, obtidos com a dependência do pH, sugerem a existência de resíduos polares conservados, em redor dos grupos prostéticos da enzima, que podem estabilizar as cadeiras propiónicas destes.

Paralelamente, a subunidade NorC recombinante foi imobilizada na superfície de um eléctrodo de grafite, sendo estudada a sua resposta electroquímica directa. Com os resultados obtidos foi comprovado inequivocamente o potencial redox do hemo *c*. A comparação deste valor com o resultado obtido para a proteína nativa, propõe a existência de alterações estruturais, em redor do centro hémico, provavelmente devido à inexistência da subunidade NorB.

Durante a realização deste trabalho e através de técnicas electroquímicas, foi investigada a resposta catalítica da enzima na presença de NO e O_2. Foi determinado o número de electrões necessários aos processes de redução de cada um dos substratos, sendo ainda comprovado que o produto da redução do O_2 é a H_2O, sem que ocorra a formação de H_2O_2.

Ensaios cinéticos no estado estacionário, realizados com esta enzima, permitiram a dedução de modelos cinéticos e a determinação de constantes cinéticas para a redução de NO e O_2. Estes ensaios foram obtidos utilizando o cit. c_{552} (isolado de *Ps. nautica*) previamente reduzido, ou a enzima imobilizada num eléctrodo rotativo de grafite, sendo os electrões necessários à reacção fornecidos pelo mesmo.

Este é o primeiro caso onde são reportados ensaios cinéticos na presença de O_2 simultaneamente com o seu dador electrónico (cit. c_{552}). Os ensaios cinéticos mostram:

i) Uma elevada afinidade para o NO em detrimento do O_2.

ii) Duas moléculas de NO a coordenarem-se consecutivamente à enzima, de forma a catalizar o substrato.

iii) A redução de O_2 apresenta um perfil inibitório, pela presença do substrato.

Ensaios cinéticos na presença de NO, com dependência do pH, evidenciam a presença de grupos ionizáveis acídicos, provavelmente Glu ou Asp, que podem pertencer ao conjunto de resíduos conservados de entrada de protões, para o centro catalítico. Um dos valores obtidos nunca tinha sido antes determinado (pK_{a1} = 3.27) e provavelmente refere-se a um dos resíduos da via anteriormente mencionada, com uma maior exposição ao solvente.

Abstract

Denitrification is a metabolic pathway from the nitrogen cycle where nitrate is reduced to dinitrogen. This pathway involves four reduction steps: the nitrate reduction to nitrite, followed by the reduction to nitric oxide (NO), from this to nitrous oxide (N_2O), and finally to dinitrogen. The enzymes involved in the mentioned steps are the nitrate reductases, the nitrite reductases, the nitric oxide reductases (NOR) and the nitrous oxide reductases, respectively.

The NORs perform the NO reduction to N_2O, using two substrate molecules, two protons and two electrons with the consequent product formation and water. These enzymes belong to the heme copper oxidase superfamily, since they are integral membrane proteins, with 12 transmembrane α-helixes and a set of conserved residues. They are composed by two subunits. The NorC subunit with a molecular weight of 17 kDa, comprises a low-spin heme *c* covalently bound to the polypeptide chain, with a His/Met coordination. The second subunit, NorB, also named the catalytic subunit, with a molecular weight of 56 kDa, harbouring two *b*-type hemes, one low-spin bis-His coordinated (heme *b*), a high-spin heme *b* (heme b_3), His coordinated and a non-heme Fe_B. These last two iron centers are antiferromagnetic coupled and bridged by a μ-oxo/hydroxo group, and together they compose the catalytic diiron center. Recently Mössbauer spectroscopy proved that the catalytic heme b_3 is in fact low-spin in both ferric and ferrous states, indicating a six-coordination environment for this iron center in both redox states. The *Pseudomonas (Ps.) aeruginosa* NOR crystal structure shows the presence of the His ligand simultaneously with the μ-oxo bridge in the as-isolated form.

The substrate reduction mechanism is an issue of intense discussion, with the *cis* and *trans*-mechanisms taken in consideration. The *cis*-mechanism descries that NO reduction occurs in the catalytic center and only one of the iron atoms is coordinating the substrate during catalysis. The *trans*-mechanism describes NO reduction with the binding of one substrate molecule to each one of the iron atoms of the catalytic center. Different isolated NORs have the ability of reducing O_2 to H_2O in a four electrons/four protons reaction. The mechanism for O_2 reduction is unknown, but it is presumed that substrate binds to the catalytic heme b_3, analogous to the terminal oxidases.

The main objective of this work was to isolate and characterize the *Ps. nautica* NOR, using different biochemical, and spectroscopic techniques.

Here, it is presented the optimized protocol for the purification of the native *Ps. nautica* NOR. The achieved enzyme fractions were consistent, since they present high purity and the correct metal stoichiometry.

The spectroscopic characterization made revealed new structural features:

i) The UV-visible absorption spectra suggest a low-spin conformation for the catalytic heme b_3.

ii) The EPR spectroscopy results show the existence of a new integer-spin species rising from the heme b_3-Fe^{III}-Fe_B^{III} antiferromagnetic coupling.

Direct electron transference between the immobilized *Ps. nautica* NOR and an electrode was accomplished. This is the first time four redox processes were distinguished using this approach and indexed to the four Fe centers. The following figure show a summary of the midpoint redox potentials determined for the *Ps. nautica* NOR.

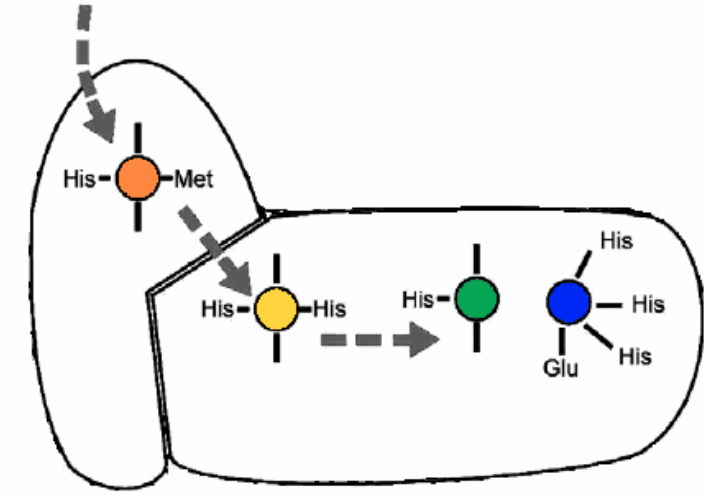

	Heme *c*	Heme *b*	Heme b_3	Fe_B
cNOR/*Ps. nautica*	**+ 208**	**+ 43**	**-162**	**-369**

Figure – Midpoint redox potentials for the NOR metal centers. Top, schematic representation of the NOR structure emphasising the four co-factors, with the correspondent ligands. Bottom, summary table of the midpoint redox potentials (*vs.* NHE), obtained in this work.

The results present in this work show:

i) The non-heme Fe_B present the lowest redox potential (-369 mV *vs.* NHE).

ii) The heme *c* presents the higher midpoint redox potential (-+ 208 mV *vs.* NHE).

iii) The results obtained for the midpoint redox potentials in pH dependence, for all the Fe centers, suggest the presence of a hydrogen bound network surrounding the heme propionate side chains.

In parallel, the recombinant NorC subunit (rNorC) was immobilized in an electrode surface and used in direct electrochemical experiments. This is the first time that direct electron transfer is studied with this subunit, separately from the catalytic subunit NorB. The results show unequivocally that the heme *c* is the metal center with the higher positive redox potential. The comparison of the value for the rNorc with the obtained for the native enzyme suggests structural changes around the low-spin heme *c*, due to the subunit separation.

In this work is reported the direct electrochemical measurements for the immobilized *Ps. nautica* NOR, under catalytic conditions, showing the electrocatalytic response for NO and O_2. This is the first time the quantification of electrons involved in these reactions is performed, using an electrochemical method. The results here presented, show beyond doubt that O_2 is reduce to H_2O, without H_2O_2 formation.

Steady-state kinetic assays were made in order to deduce kinetic mechanisms, and determine relevant kinetic parameters for the NO and O_2 reduction. The experiments were done using the reduced *Ps. nautica* cyt.c_{552} or the immobilized *Ps. nautica* NOR to a graphite RDE, where the enzyme receives the electrons directly from the electrode. This is the first report on oxidoreductase activity measurements assayed with the enzyme's physiological electron donor. Both electron donor systems show beyond doubt:

i) A high affinity for NO rather than for O_2.

ii) Two NO molecules bind to the enzyme in a consecutive mechanism.

iii) The O_2 reduction presents a substrate inhibitory pattern.

The pH dependence experiments show the presence of a new protonable residue probably an acidic residue (Glu or Asp), belonging to the conserved proton pathway with a high exposure to the solvent, that has never been reported in pH dependence experiments (pK_{a1} = 3.27).

Symbols

Γ	Surface coverage
ε	Molar extintion coeficiente
ν	Scan rate
ω	Angular speed

Abbreviations

AMPSO	N-(1,1-Dimethyl-2-hydroxyethyl)-3-amino-2-hydroxypropanesulfonic acid
ASC	Sodium ascorbate
ATP	Adenosine 5'-triphosphate
BCA	Bicinchoninic acid
BH4	6R-tretrahydroviopterin
BSA	Bovine serum albumin
C*c*O	Cytochrome c oxidase
CHT	Ceramic hydroxyapatite
CV	Cyclic voltammetry
cyt.	Cytochrome
Da	Dalton
DDM	n-dodecyl-β-D-maltoside
DEAE	Diethylaminoethyl
E. coli	*Escherichia coli*
EDTA	Ethylenediamine tetraacetic acid
FAD	Flavin adenine dinucleotide
HARC	hexa-aminеruthenium(II)-chloride
HCuO	Heme copper oxidase
Hepes	4-(2-Hydroxyethyl)piperazine-1-ethanesulfonic acid
HH	Horse heart
IPTG	Isopropyl β-D-1-thiogalactopyranoside
KPB	Potassium phosphate buffer
k_s	Heterogeneous rate constant
MES	2-(N-Morpholino)ethanesulfonic acid

N_2O	Nitrous oxide
N_2OR	Nitrous oxide reductase
NADPH	β-Nicotinamide adenine dinucleotide phosphate
Nar	Nitrate reductase
NHE	Normal hydrogen electrode
Nir	Nitrite reductase
nm	nanometer
NO	Nitric oxide
NOR	Nitric oxide reductase
ORF	Open reading frame
Pa.	*Paracoccus*
PDB	Protein data bank
PE	(S)-(-)-Phenylethanol
PFV	Protein film voltammetry
PMS	Phenazinemetasulfate
Ps.	*Pseudomonas*
RDE	Rotative disk electrode
rNorC	Recombinant NorC subunit
SAM	Self assembled monolayer
SCE	Saturated calomel electrode
TMBZ	3,3',5,5'-Tetramethylbenzidine
TMPD	*N*,*N*,*N*',*N*'-Tetramethyl-*p*-phenylenediamine
TPTZ	2,4,6-Tris(2-pyridyl)-s-triazine
Tris-HCl	Tris(hydroxymethyl)aminomethane
UV	Ultra-violet
VHH03	NOR specific fragment antibody
wt	Wild-type
X-gal	5-Bromo-4-chloro-3-indolyl β-D-galactopyranoside

Index

Chapter 5 Main Conclusions

Supporting information

Figure Index

Table Index

CHAPTER 1

INTRODUCTION

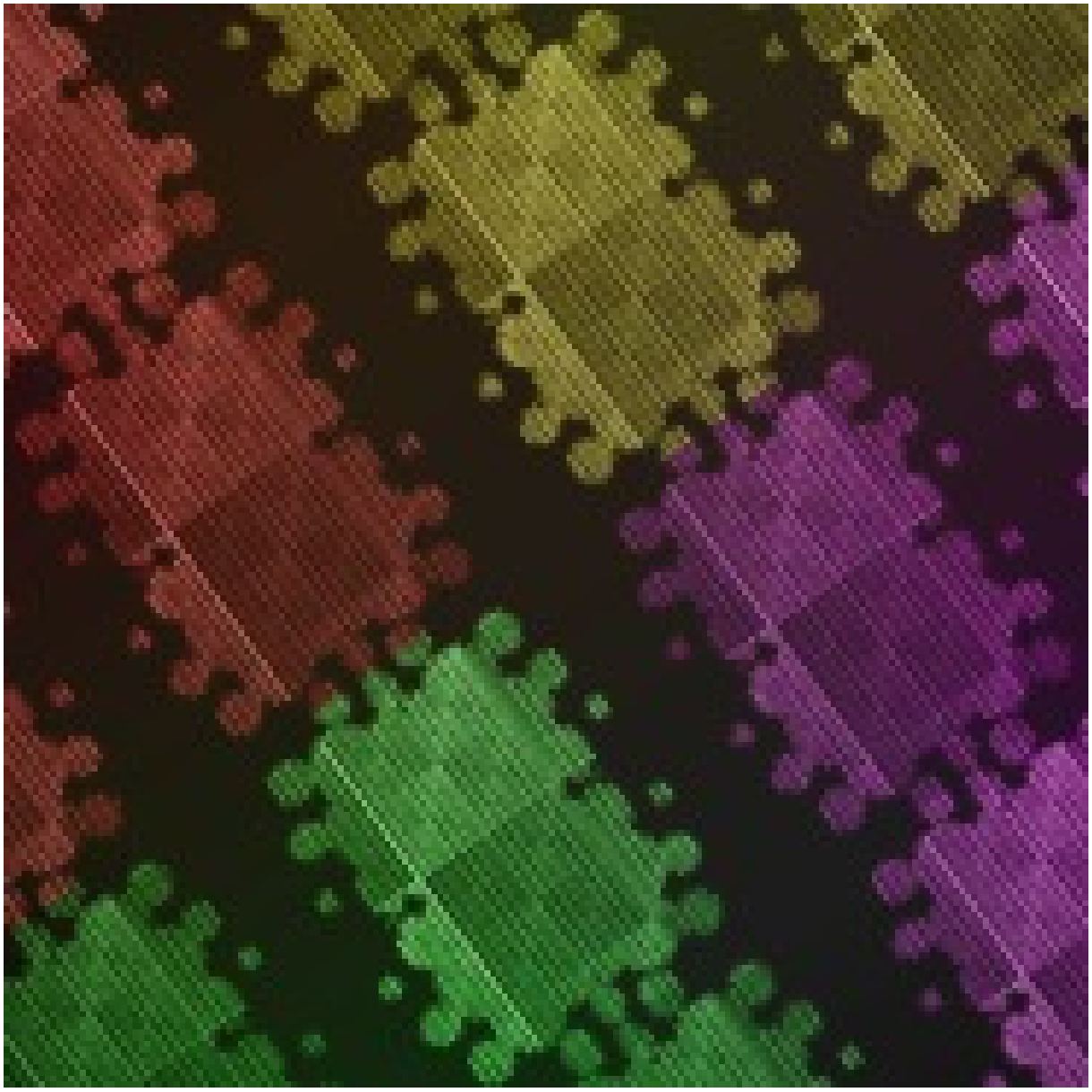

Chapter 1 Introduction

1. Introduction

1.1. Nitric Oxide: Chemistry and Role in Biology

Nitric oxide (NO) is a diatomic molecule among the simplest molecules. Its structure and reaction chemistry has been the subject of study by chemists for many years [1]. NO was long thought of as a poisonous, pungent-smelling gas, an unpleasant and dangerous product of the oxidation of ammonia and of the incomplete combustion of gasoline in motor vehicle exhausts.

From the chemical point of view, the NO molecule is a stable free radical with the molecular orbital diagram showing an unpaired electron residing in a π^* molecular orbital. This electronic configuration explains the high reactivity of the NO. Its oxidation leads to the nitrosoniumion (NO^+) and its reduction to the nitroxide ion (NO^-). Its reactivity reaches beyond the simple ionization and NO is extremely reactive with other simple molecules such as oxygen (O_2) or halogens, and metals, like iron, and it is why it is used to reveal structural and mechanistic insights in metalloproteins [2].

Several N-oxides were identified by bacteria fermentation of plant material in the second half of the 19th century, and these microorganisms were designated as denitrifiers [3]. In the 60's decade, NO was suggested to play a role as an intermediate of this pathway, and at the same time, it was identified as a crucial biological intermediate of the denitrification processes by the marine bacterium *Pseudomonas perfectomarinus* [4]. Years after, in the 80's, NO was discovered to be one of the most important physiological regulators [2]. Nitric oxide synthase (NOS) was found to synthesize this signalling and protective molecule that could be extremely helpful in different processes in mammals. NO was identified as an endothelium relaxing factor, as a key cytotoxic agent of the immune system, or even as a signalling molecule in the nervous system [4]. In bacteria, NO also play an important role. Not only is an intermediate of the nitrogen (N) cycle, as it is a signalling molecule, for example in bacterial biofilm dispear [5].

Nevertheless, above certain concentration levels, NO and its reactive species may prove to be toxic to cells, and this phenomenon is designated by nitrosative stress. Some microorganisms have the ability to produce NO. Others may also have specific metabolic pathways which allow them to resist to this kind of stress. They are able to reduce NO to

nitrous oxide (N_2O) or to ammonia (NH_4^+), by the denitrification pathway or by other detoxification mechanisms. [3].

1.2. The Nitrogen Cycle

1.2.1. Overview of the Nitrogen Cycle

Nitrogen (N) is the fifth most abundant element in the solar system, and it is also well represented in essential biomolecules, being an important constituent of nucleic acids and proteins, the two most important polymers in life. The N-cycle is the process by which nitrogen is converted between in its different molecular forms (figure 1.1). The chemistry of this element is almost entirely dependent on reduction-oxidation (redox) reactions [6]. The chemical forms are transformed via specific enzymes, able to oxidize and reduce the N-compounds. In the cycle, nitrate (NO_3^-) and ammonia (NH_4^+) present the higher (+5) and lower (-3) redox states for the N atom, respectively, and the other molecules of the cycle present different intermediate redox states (figure 1.1).

Earth's earliest N-cycle was tightly controlled by a robust natural negative feedback mechanism between atmospheric reactions, slow geological and microbial processes. In the previous century, human intervention drastically disrupted the N-cycle by developing industrial processes to reduce dinitrogen (N_2) to NH_4^+, by implementing new agricultural practices in order to boost crop yields, and by burning fossile fuels [6]. In particular there has been an abusive use of nitrogen fertilizers which does not translate to a higher yield in agricultural products, since only a part of the inorganic material is used to produce biomass. Fertilizers are mainly composed of NH_4^+, and aerobic nitrification can not be avoided, causing an accumulation of NO_3^- and nitrite (NO_2^-) at the Earth's crust [6]. These particular reactions are controlled by three enzymes: the ammonium monooxygenase (Amo), the hydroxyalanine oxidoreductase (Hao) and the nitrite oxidoreductase (Nxr) (figure 1.1).

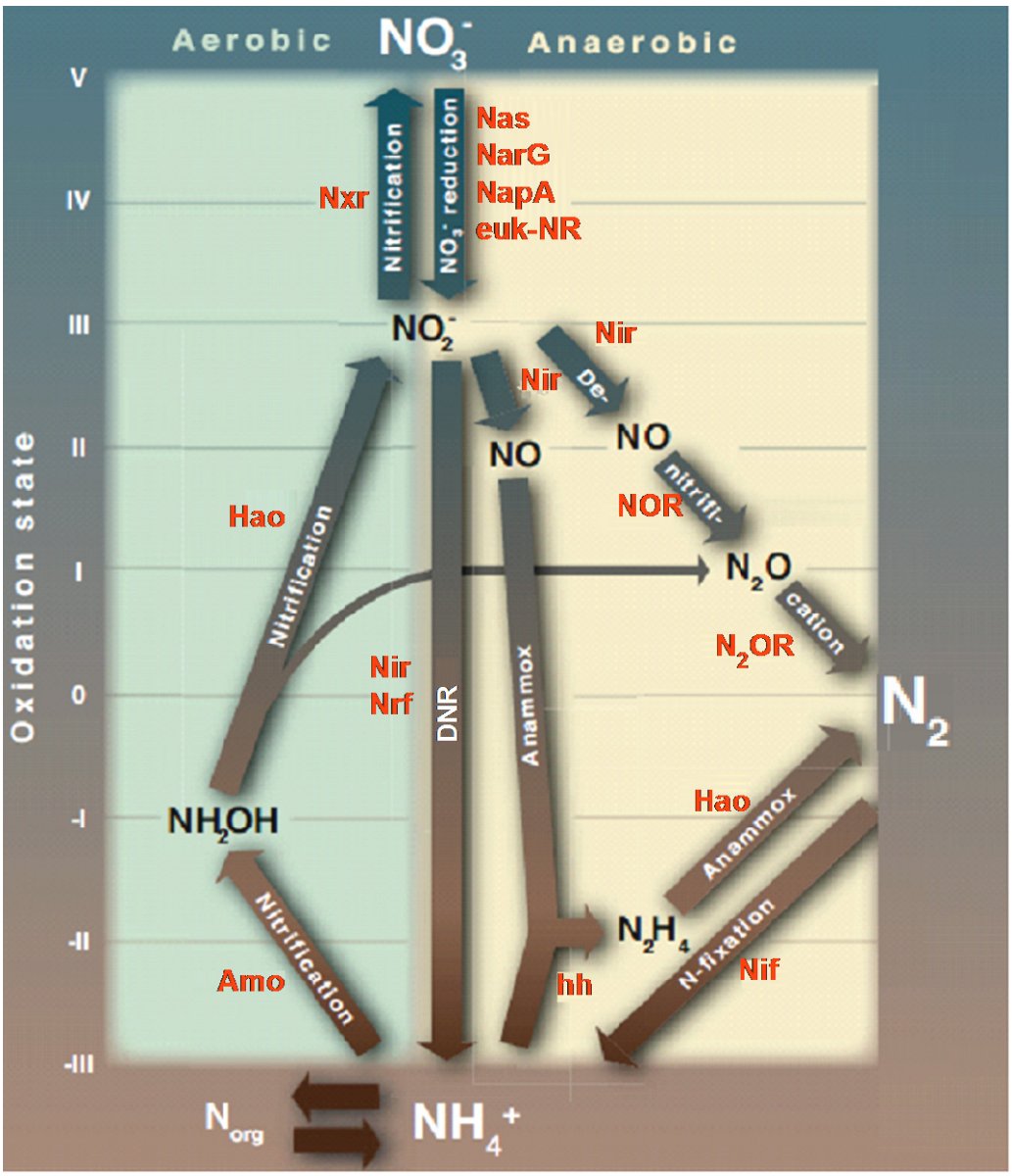

Figure 1.1 – The N-cycle schematic representation. Arrows describe the principle pathways and the enzymes involved in each reaction are in red. Nitrate reductase: Nas - cytoplamatic, prokaryote assimilatory pathway; euk-NR- cytoplamatic, eukaryote – assimilatory pathway; NarG- membrane bound, dissimilatory pathway; NapA – periplasmic, dissimilatory pathway; Nitrite reductase, Nir - various kinds, Nrf - associated with periplasmic NR's (Nap); nitric oxide reductase, NOR; nitrous oxide reductase N_2OR; nitrogenase, Nif; ammonium monooxygenase, Amo; hydroxylamine oxidoreductase, Hao; nitrite oxidoreductase, Nxr; hydrazine hydrolase, hh. Adapted from [6].

As a compensatory mechanism for the human production of oxidized molecules, anaerobic microorganisms are able to reduce of the amount of NO_3^- and NO_2^- by three pathways: denitrification, dissimilatory nitrite reduction and anaerobic ammonium oxidation.

Denitrification is the pathway where NO_3^- is reduced to N_2. It is composed by four reduction steps, controlled by metalloenzymes: NO_3^- is reduced to NO_2^- via the nitrate

reductases (NRs); NO_2^- is reduced to NO by the nitrite reductases; NO is reduced to N_2O by nitric oxide reductase (NOR); and in a last step N_2O is reduced to N_2, by the nitrous oxide reductase (N_2OR). The denitrification pathway will be discussed in the following section.

Anaerobic ammonium oxidation, currently called anammox, describes the reduction of the N-oxides as NO_3^- and NO_2^- to NO, by nitrate reductases (NRs) and nitrite reductases (Nir), respectively, and further reduction to hydrazine (N_2H_4). Alternatively, it is also possible to oxidize NH_4^+ to N_2H_4, under the hydrazine hydrolase (hh) control. Subsequent N_2H_4 oxidation is possible, catalyzed by hydroxylamine oxidoreductase (Hao).

Direct NO_2^- reduction to NH_4^+ can be accomplished by microorganisms that harbour the nitrite reductases (Nir or Nfr) coupled to the nitrite reductase system. This pathway is designated as dissimilatory nitrite reduction (DNR), or dissimilatory reduction of nitrite in anoxic conditions. As an example there is the penta-heme cytochromes *c* nitrate reductase (ccNir or Nrf), able to reduce NO_2^-or NO directly to NH_4^+.

The N_2 reduction to NH_4^+ is performed by nitrogenase (Nif), a multimeric enzyme that catalyzes this exergonic reaction, since this reduction consumes 16 molecules of ATP per reduced N_2 molecule [6]. These enzymes are characteristic of the symbiotic connection between bacteria and plant roots.

1.2.2. The Denitrification Pathway

Denitrification, or dissimilative nitrate reduction, is an anaerobic process used by some bacteria for energy generation. The study of this metabolic pathway is relevant, since NO_3^- and NO_2^- became one of the worst water pollutants, a major concern being the removal of NO_3^- from the water before it can be supplied to costumers [7].

Reduction of NO_3^- to nitrogen gas (N_2) is done in four different steps:

$$NO_3^- + 2\,e^- + 2\,H^+ \longrightarrow NO_2^- + H_2O \qquad \text{(eq. 1.1)}$$

$$NO_2^- + e^- + 2\,H^+ \longrightarrow NO + H_2O \qquad \text{(eq. 1.2)}$$

$$2\,NO + 2\,e^- + 2\,H^+ \longrightarrow N_2O + H_2O \qquad \text{(eq. 1.3)}$$

$$N_2O + 2\,e^- + 2\,H^+ \longrightarrow N_2 + H_2O \qquad \text{(eq. 1.4)}$$

NO_3^- is reduced to NO_2^- in a two electron reaction, followed by one electron reduction to NO, and by a two electron-two proton reduction to N_2O, and a final two electron reduction to N_2. Equations 1.1 to 1.4 show the electrons involved in each reaction process. These processes are catalyzed by different metalloenzymes as pointed in figure 1.2.

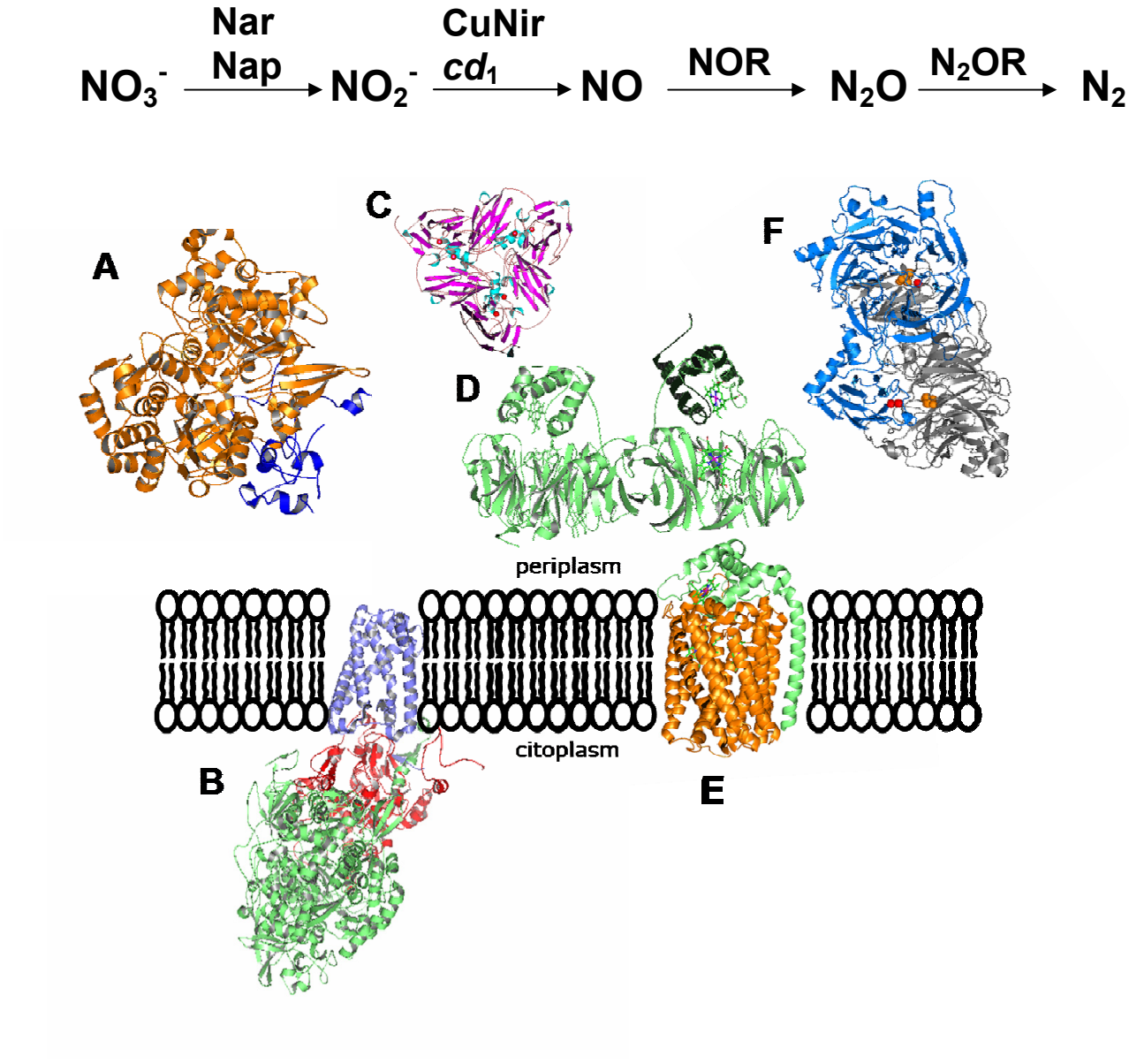

Figure 1.2 – The denitrification pathway. Different resolved structures for the metalloenzymes involved in this metabolic route: A- *Cupriavidus necator* Nar (PDB:3ML1) [8], B- *Escherichia coli* Nar (PDB:1Q16) [9], C- *Achromobacter cycloclastes* CuNir (PDB:2BW4) [10, 11], D- *Paracoccus pantotrophus* cyt. cd_1 (PDB:1H9X)[12], E- *Pseudomonas aeruginosa* NOR (PDB: 3O0R) [13] and F- *Pseudomonas nautica* 617 N_2OR (PDB: 1QNI) [14]. The PDB files were edited with *Pymol* software.

The **Nitrate reductases** (NRs) catalyze the reduction of NO_3^- to $NO_2^-$and they are ubiquitous, from bacteria to eukaryotes. Organisms reduce NO_3^- for three main reasons: i) incorporation of N into molecules (assimilatory ammonification), ii) to generate energy for cellular functions (respiration, denitrification) and iii) to eliminate energy excess generated by cell metabolism (dissimilatory ammonification) [15]. The NRs are mainly molybdenum (Mo)-containing enzymes. Additional to the catalytic Mo center, the enzymes carry redox co-factors such as iron-sulfur clusters or hemes that mediate the electron transfer. Classification of these proteins have been made according to different criteria, such as cell localization, protein structure, catalytic center molecular properties, metabolic routes and others. According to their localization, they are divided in four groups: the eukaryotic NO_3^- reductases (euk-nar), the assimilatory NO_3^- reductases (Nas), the respiratory NO_3^- reductases (Nar) (figure 1.2 B) and the periplasmic (Nap) (figure 1.2 A) [16]. All NRs present an active center which is similar to the center of dimethyl sulfoxide (DMSO) reductase family, with exception for the eukaryotic enzymes which are part of the sulfite oxidase family [7]. Eukaryiotic NRs and Nas are cytoplasmatic enzymes involved in the NO_3^- assimilation, whereas Nars are periplasmic and are involved exclusively in the denitrification pathway.

Focusing in the prokaryotic NRs, these enzymes are involved in generating a proton motive force across the membranes. They are constituted by three subunits: NarGHI ($\alpha\beta\gamma$, respectively), narG subunit harbouring the Mo active center, and the remaining subunits maintaining the electron transfer centers. They can be isolated from different bacteria such as *Escherichia coli* [17], *Ps. nautica* [15] and *Cupriavidus necator* [18]. The isolated form can be a trimeric or a dimeric form, since the anchored γ-subunit (NarI) can be isolated or not, depending on the purification procedure [7]. NarI is the small subunit, presenting a molecular weight of 19-26 kDa and comprising two heme *b* groups (b_D and b_P). Moreover, *Pseudomonas nautica* 617[1] revealed the presence of an unexpected *c*-type heme in this subunit [15]. The β subunit, has a molecular weight of 55-64 kDa, carries four iron-sulfur clusters: three [4Fe-4S] designated FS1 FS2 and FS3, and one [3Fe-4S] named FS4. The larger subunit NarG (118-150 kDa), harbours the Mo catalytic center, coordinated to a molybdopterin guanine dinucleotide (MGD) as observed typically in the

[1] Is also known as *Marinobacter hydrocarbonoclasticus* 617 [19] . In this report the designation *Pseudomonas nautica* 617 will be adopted

DMSO mononuclear Mo enzymes. The other Mo ligands are from the protein peptide chain, normally sulfur ligands from Cys or selenocysteine (Se-Cys) residues. There is an additional electron transfer center in this subunit, a [4Fe-4S] cluster named FS0. All the redox cofactors are located along an electron transfer pathway ($b_D \rightarrow b_P \rightarrow FS4 \rightarrow FS3 \rightarrow FS2 \rightarrow FS1 \rightarrow FS0 \rightarrow Mo$) from which the nitrate receives the electrons provided by the quinol pool (figure 1.3) [7, 15].

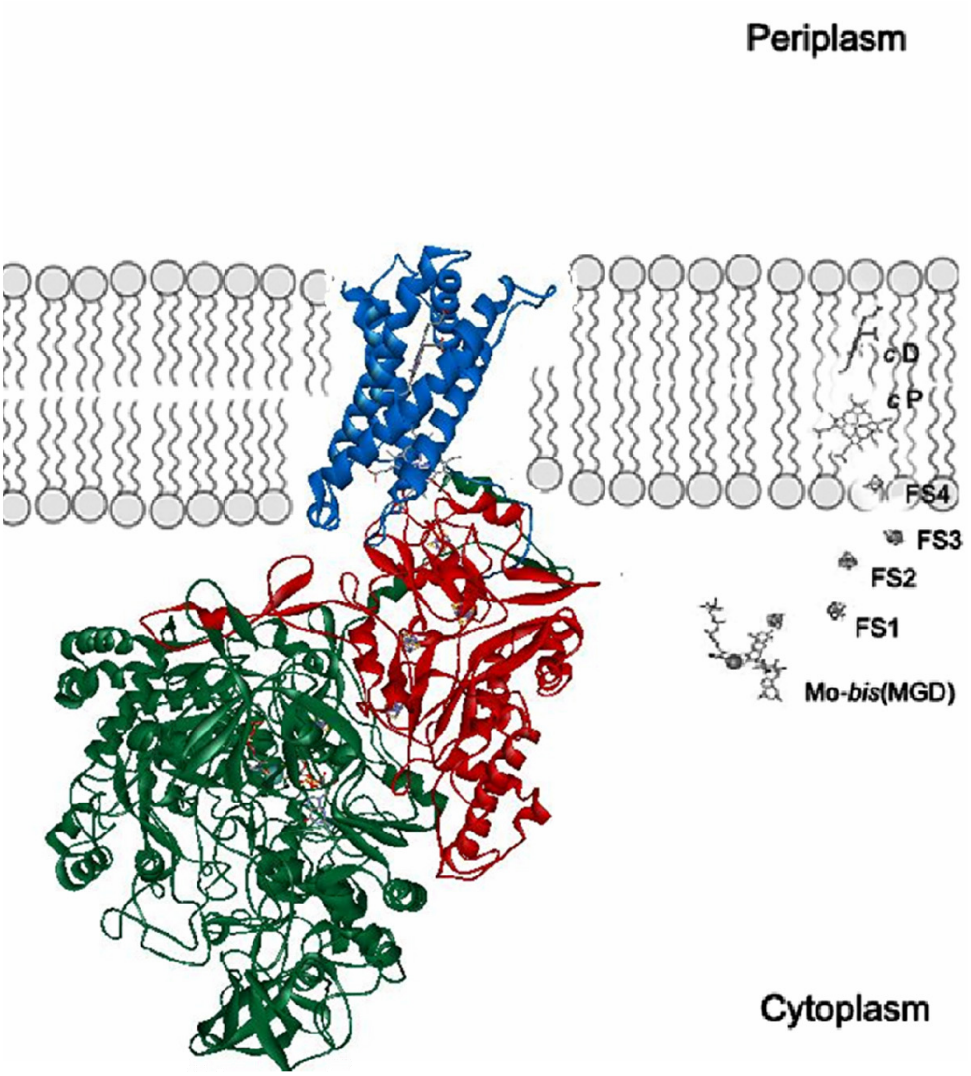

Figure 1.3 – *Escherichia coli* NarGHI complex (PDB:1Q16) [9]. Overall three-dimensional structure is presented. For better visualisation, the diagram of the enzyme electron transfer co-factors was shifted to the right. The PDB file was edited with *Pymol* software.

The reaction mechanism suggested for nitrate reductases is still a matter of controversy. Originally a unique reaction mechanism was suggested for all nitrate reductases regardless of their subclassification. This reaction mechanism, which was mainly based on the crystal structure of the periplasmic nitrate reductase from *Desulfovibrio*

desulfuricans [20], implies the replacement of the sixth coordinating ligand to molybdenum (originally proposed to be a hydroxyl/water molecule) by nitrate, the transfer of two electrons from Mo(IV) to nitrate, and the release of nitrite. The presence of an Asp residue coordinated to molybdenum in a bidentate fashion in NarGHI from *E. coli* [9] suggests that this mechanism can be feasible only if the bidentate coordination is opened and an oxygenic species enters in the sixth coordinating position of the molybdenum atom, as was determined in the crystal structure of NarGH [21]. This hypothesis is also supported by the EPR results for both as-isolated and nitrate-reacted *Pseudomonas nautica* 617 Nar that point to a molybdenum ion coordinated to a hydroxyl/water ligand, which could act as the labile group in a mechanism involving a direct nitrate–molybdenum interaction [15]. Most recently, theoretical and computational tools were used to revise the catalytic mechanism of NRs. The basis was the crystallographic data from the NapA isolated from *Desulfovibrio desulfuricans* (PDB: 2v3v). Results show that both Mo species have an active role on the mechanism but in different phases. The Mo^{VI} is required for the NO_3^- reduction to NO_2^- and the Mo^{V} is involved in the second part of the mechanism where one water molecule is formed and enzyme turnover occurs [22].

The **Nitrite reductases** can be divided in two major groups, according the nature of their metal co-factor: there are the copper–containing nitrite reductases (Cu-Nir, figure 1.2 C) and the heme or Fe containing nitrite reductases (Fe-Nir, figure 1.2 D), also known as cytochrome cd_1. While the Fe-Nirs are more abundant in nature, Cu-Nirs are found in a greater variety of ecological systems and therefore demonstrate more physiological diversity. To date, no biological system has been shown to contain both Fe- and Cu-Nirs. Nirs catalyze the one electron reduction of NO_2^- to NO [23].

Cu-Nir enzymes have been isolated from several organisms, such as *Achromobacter cycloclaste* [10, 11], *Ps. aureofaciens* and *Alcaligenes xylosodixans* [7]. The enzyme presents a trimeric structure with six copper atoms, divided in two types: the T1Cu, buried inside the protein core and the T2Cu, the catalytic center, located in the interface of each two subunits. The enzymes can be divided in two groups, according to the spectroscopic properties of their T1Cu centers. The green reductases present an axially flattened tetrahedron with an axial EPR signal and characteristic visible band at 590 nm. The blue reductases present an axially distorted tetrahedron with a rhombic EPR signal and a

visible absorption spectra with different characteristic features (at 460 and 600 nm) [7, 24].

The electrons are donated by the physiological donor, presumably the cyt. c_{551} or pseudozurin, to the T1Cu center and then transferred to the catalytic T2Cu center through a chemical path involving conserved residues. The model for the catalytic mechanism of Cu-Nir supposes that NO_2^- binds to the oxidized form of the T2Cu center, displacing a solvent molecule. After reduction of the T2Cu center with an electron from the T1Cu center, a intermediate compound, O=N-O-H is formed, and consequently the product (NO) is released [7]. Figure 1.4, left side shows the proposed mechanism for the NO_2^- reduction by the Cu-Nir.

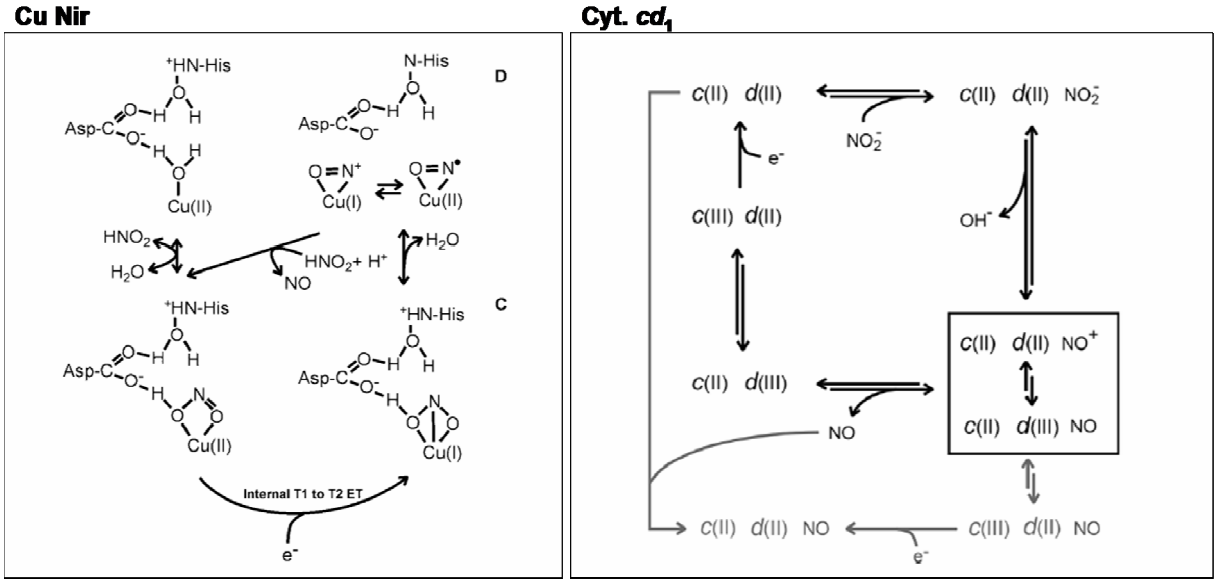

Figure 1.4 – Nitrite reduction mechanism proposed for the Cu-Nir (left side) and for the cytochrome cd_1 (right side), adapted from [7].

Cytochrome cd_1 is a periplasmic soluble homodimer, with a molecular weight of 60 kDa and two hemes, one heme *c* and one heme d_1 per monomer. It was isolated from *Pseudomonas* strains like *aeruginosa* [25] and *stutzeri*, and *Pa. denitrificans* [7]. The heme *c* is located in the N-terminal region; it is six-coordinated with two His ligands and is involved in the electron transfer between the physiological donor and the catalytic heme *d*. The heme *d* is the site for NO_2^- reduction, and presents specific spectroscopic features, namely distinct visible absorption spectra. EPR spectroscopy proves that heme *d* is also six-coordinated in the oxidized state, with a His/Tyr coordination, but reduction

produces the lost of the Tyr axial ligand. The putative catalytic mechanism for NO_2^-reduction points for the binding of a NO_2^- molecule to the ferrous heme *d*, in a high-spin conformation. Dehydration leads to the formation of a nitrosyl intermediate, and release of NO and concomitant intramolecular electron transfer from heme *c* to heme d, completing the mechanism cycle (figure 1.4) [7].

The **Nitric oxide reductases** (NOR) catalyze the third step in the denitrification pathway. Protein sequence alignment with members from this classe can be checked in the supporting information S1. They are divided in three different classes, according to their physiological electron donor: the cytochromes (cNOR), quinol (qNOR) and the copper quinol (qCuNOR) [7] (figure 1.5). These enzymes are integral membrane proteins, and they belong to the heme copper oxidase (HCuO) superfamily, sharing a high structural homology of the catalytic subunit. In this class of enzymes, there is variation in the type of electron transfer co-factors and in the number of subunits, but very well conserved is the unusual binuclear diiron center, composed by a *b*-type heme (heme b_3) bridged to a non-heme Fe_B [26].

The **cNORs** present two subunits and receive electrons from soluble cytochromes or cupredoxin. The **qNORs** lack one electron transfer co-factor and are composed by a unique subunit, they receive electrons directly from the periplasmic quinol pool. The **qCuNORs** are composed by two subunits, one comprising a binuclear Cu_A center similar to the present in some HCuO members, and the other is the catalytic subunit. These last can accept electrons directly from menaquinol or from soluble cytochromes via the Cu_A center.

Mechanisms for NO reduction are issue in of intensive discussion. However, all the proposed models consider substrate reduction in the binuclear Fe center with electron transfer from the other metal co-factors to the binuclear cluster [7, 27]. Since the protein here studied is a cNOR, a detailed description of the cNORs follows in section 1.2.2.1.

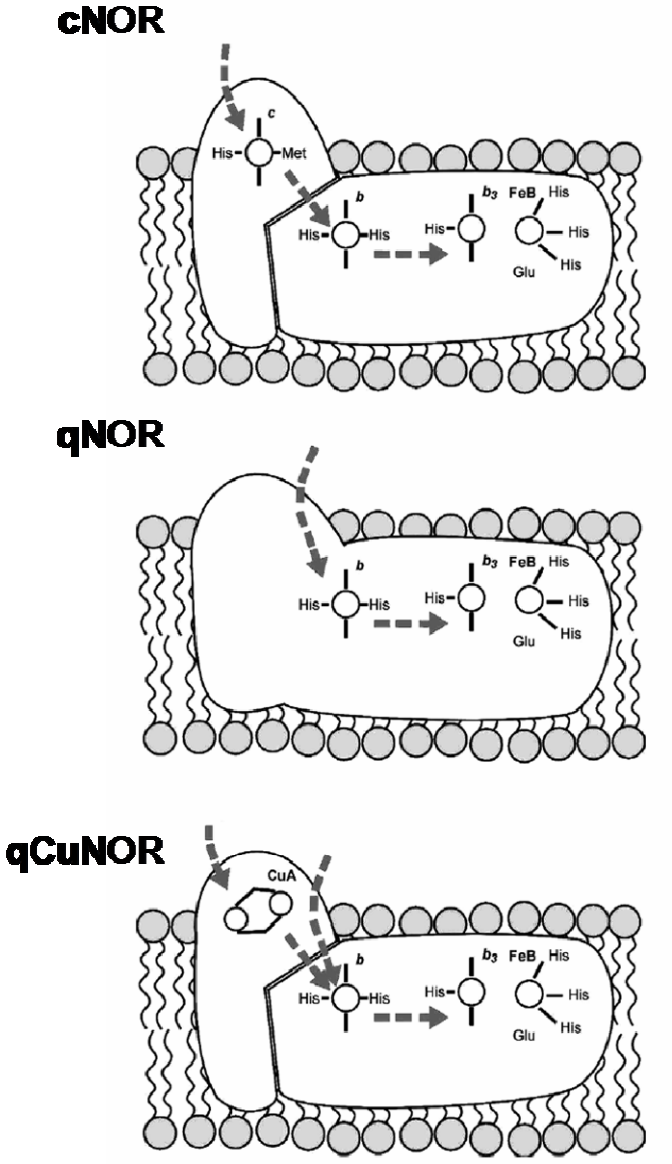

Figure 1.5 – Schematic representation of the known NOR classes. Grey broken arrows represent the proposed electron transfer pathways from a periplasmic electron donor towards the active site, adapted from [7].

The **Nitrous oxide reductase** (N_2OR) is the last enzyme of the denitrification pathway, catalyzing the N_2O reduction to N_2. It has been intensively characterized and isolated from different denitrifying organisms such as *Ps. nautica* [14], *stutzeri* [28, 29], *Pa. denitrificans* [30], *Achromobacter cycloclastes* [31] and *Wolinella succinogenes* [32, 33]. The isolated periplasmic enzymes are purified in a homodimeric form with approximately 65 kDa per monomer. Each subunit contains two Cu centers: a multi-copper catalytic center (Cu_Z) and a binuclear Cu site (Cu_A) similar to the ones observed in some members of the HCuO, involved in electron transfer [7, 34]. There are two exceptions: i) the N_2OR

isolated from *Wolinella,* which presents an additional extension of approximately 200 aminoacids with *c*-type heme motif in its C-terminal [7, 34], and ii) the enzyme from *Flexibacter canadensis*, which interacts with the cytoplasmatic membrane [7]. The homodimeric form presents a large dimerization interface, in such a way that the Cu_A center from one subunit is very close to the catalytic Cu_Z center from the other subunit (figure 1.6). In the Cu_A center, the two Cu atoms are bridged by two Cys ligands, the Cu_I metal presents an addition His and Met residue coordination, and Cu_{II} presents a His and a carbonyl group from a Trp residue. The catalytic Cu_Z center, is a μ4-sulfide bridged tetranuclear copper center, coordinated by His residues [7, 14].

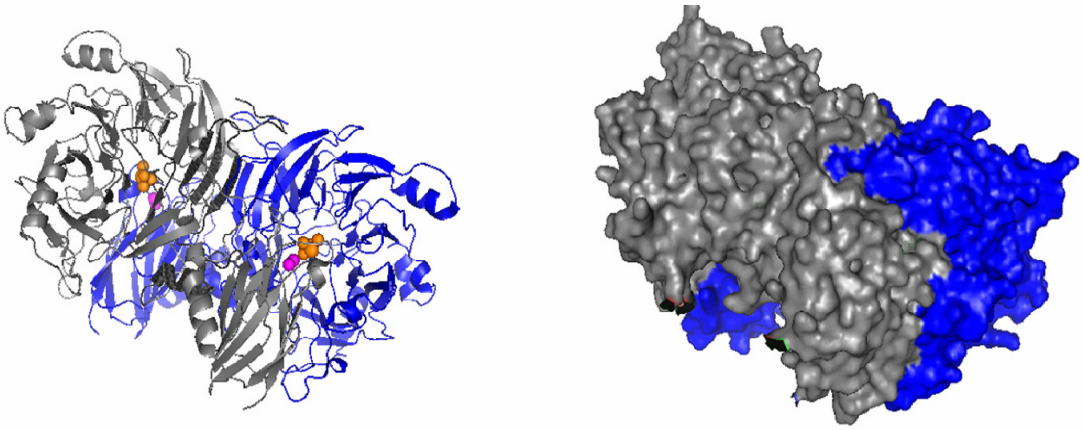

Figure 1.6 – The *Pseudomonas nautica* N_2OR (PDB: 1QNI) [14] structure. Monomers are coloured in blue and grey. Pink and orange spheres are evidence the Cu_A and Cu_Z centers, respectively. The PDB files were edited with *Pymol* software.

Several mechanisms for the N_2O reduction have been proposed [7, 34-36]. The density functional theory (DFT) calculations suggested the binding of a N_2O molecule between Cu_I and Cu_{IV} atoms from the Cu_Z center. The cycle seems to involve two sequential proton-electron transfer steps after N_2 release, followed by the restoration of the enzyme active form by release of one H_2O molecule. Recent reports describe a catalytic mechanism with emphasis in the interconversion between the active and inactive form of the enzyme, where relevant catalytic intermediate species were detected and characterized by spectroscopic methods [34, 35].

1.2.2.1. The Nitric Oxide Reductase

The NOR belongs to the Heme copper oxidase superfamily (HCuO), because this type of enzymes presents a high structural homology, in means of their catalytic subunit, as well as in the ligands that coordinate the redos centers. The major difference between them is the catalytic center. In oxidases it is composed by a mixed cluster of Fe and Cu while in NOR is composed by a binuclear Fe center. Some authors believe that NOR was present in several ancestral organisms. During evolution, the disappearance of a reductive environment and appearance of an oxidative atmosphere, produced the insolubility of Fe, and induce species to replace Fe by Cu [3, 37].

1.2.2.1.1. Heme Copper Oxidases Superfamily

Terminal oxidases of membrane-bound electron transfer chains catalyze the reduction of dioxygen (O_2) to water, coupling the redox energy to proton translocation through the cytoplasmatic or mitochondrial/chloroplast membrane. Most of the terminal oxidases belong to the HCuO. This large family can present different electron donors, subunit composition, and heme type. Common to all the members is the presence of a catalytic subunit harbouring a six-coordinated low-spin heme and an unusual binuclear catalytic center, giving rise to its name, composed by a high-spin heme and a copper ion Cu_B.

The HCuO catalytic subunit or subunit I is composed, at least, by 12 transmembrane α-helices, carrying the binuclear active center and the immediate low-spin electron transfer heme. These three metal centers present six well conserved His residues ligands: two coordinate the low-spin heme, one coordinates the catalytic high-spin heme and the remaining three ligands support the catalytic Cu_B. Prokaryotic oxidases may contain quite diverse heme, such as heme *a*, *b* or *o*, commonly used to designate the enzymes. However, the type of heme does not correlate with the organisms' phylogeny, the type of electron donor, nor with sequence similarities, and therefore it is inappropriate to classify the oxidase family based on the heme types [38]. A very simple way of illustrating all the HCuO was described by Garcia-Horsman [39], which separates the superfamily in the cytochromes c oxidases (*CcO*) , the ones that accept electrons from soluble cytochromes

and the quinol oxidases, where the physiological electron donor is the quinol molecule (figure 1.7).

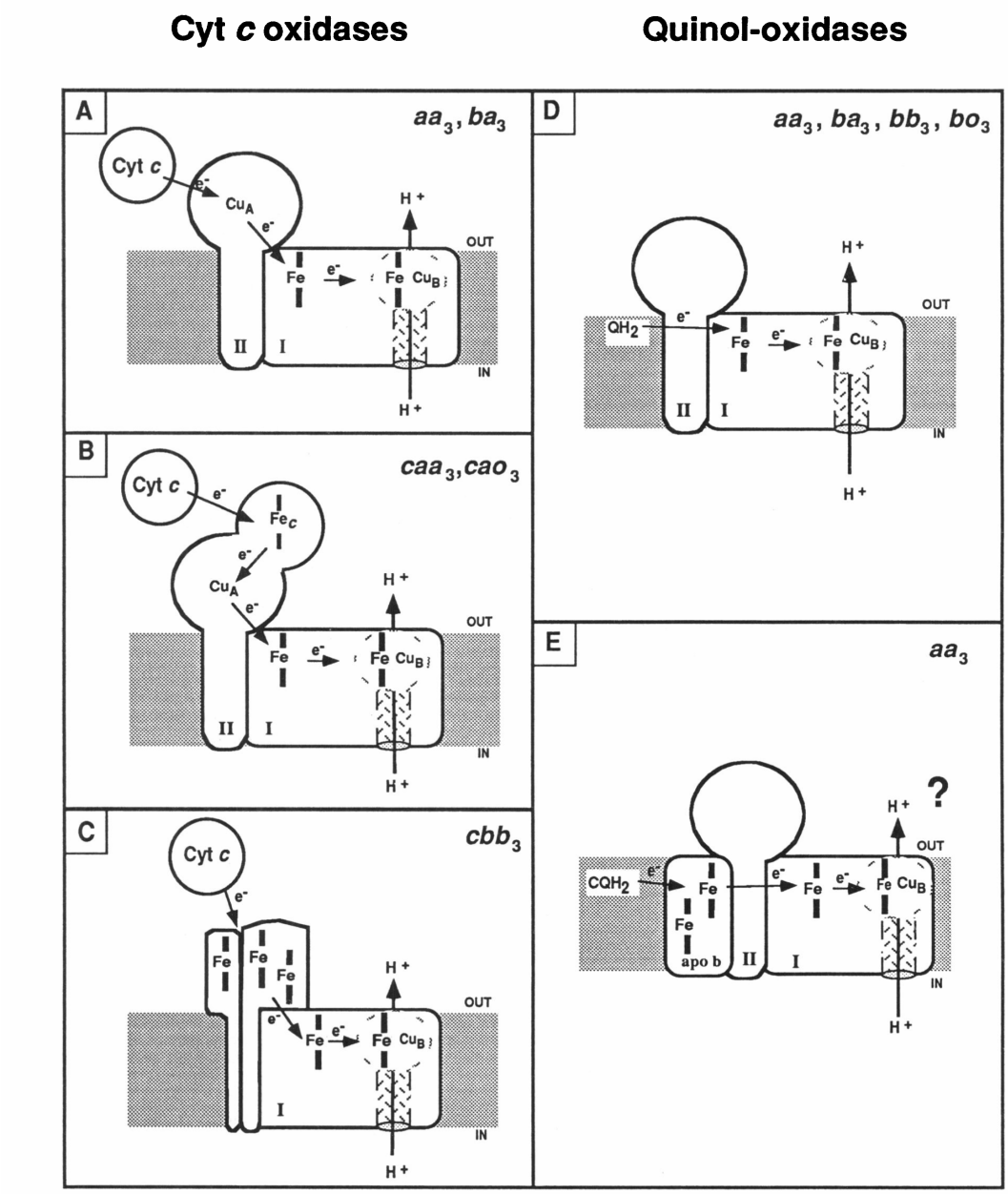

Figure 1.7 – Schematic illustration showing the similarities and differences between five subclasses of the heme-copper oxidase superfamily. Panels A-C, cytochromes c oxidases (C*c*O); panels D and E, quinol oxidases [39].

The His ligands coordinating the co-factors in the HCuO catalytic subunit are extremely well conserved as it can be seen in figure 1.8. Sequence alignment show protein five sequences of HCuO members, including a NOR. The transmembrane α-helixes are dispersed in three type arches in a round disposition around the metal co-factors, where

these are inside the proposed pores created by the helixes special arrangement [23, 38]. A schematic representation of the helices disposition is illustrated in the inset of figure 1.8.

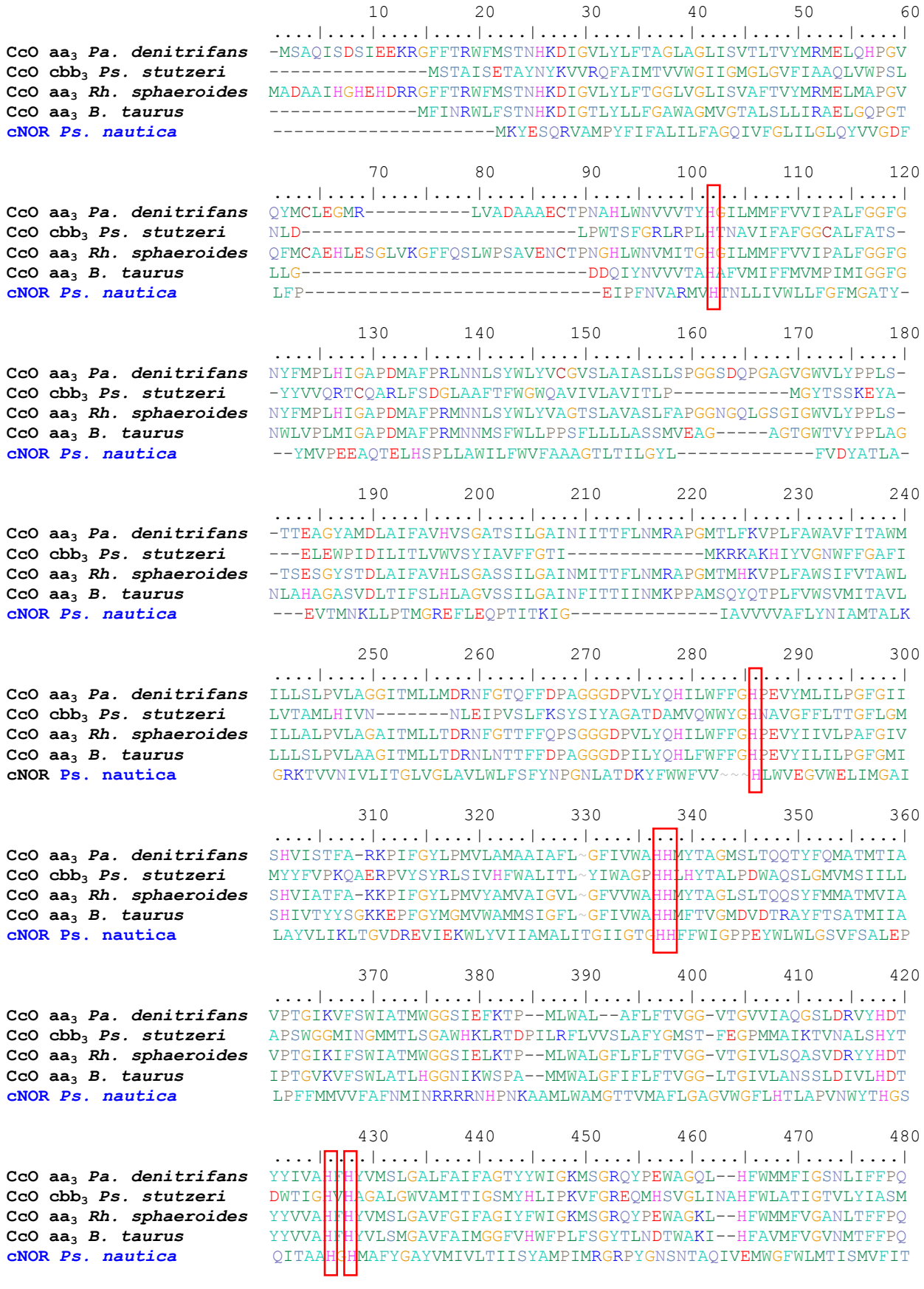

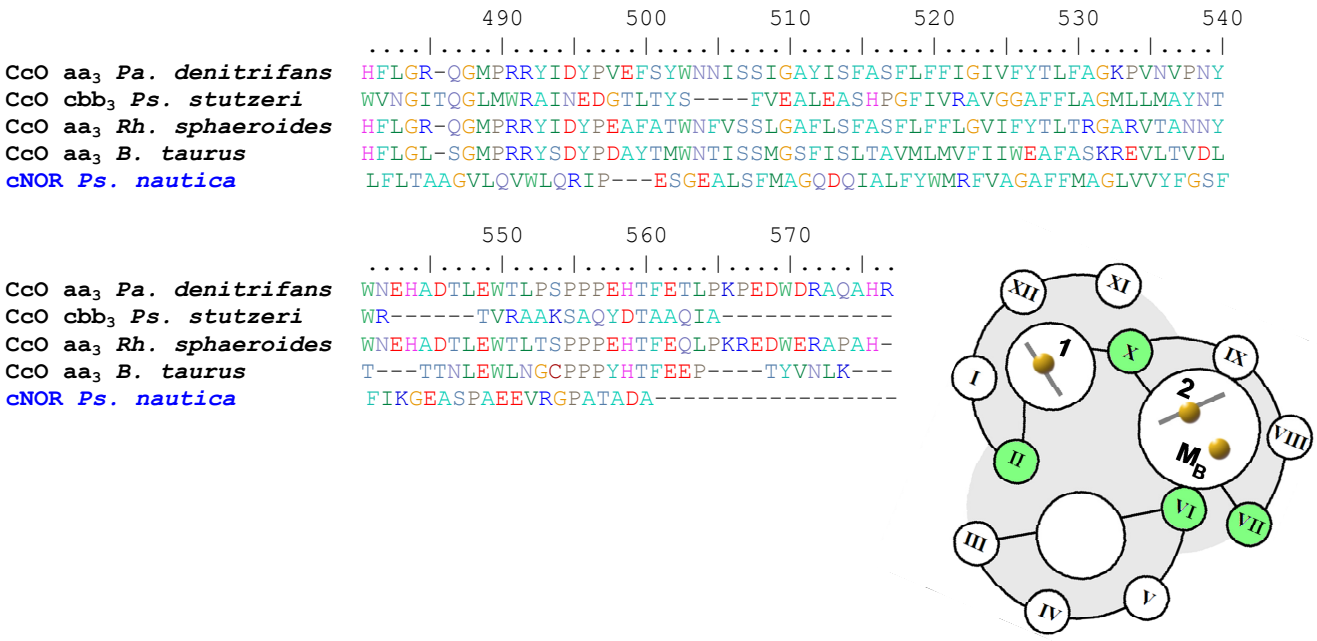

Figure 1.8 – Sequence alignment for the catalytic subunit of five members from the HCuO superfamily. *CcO* aa_3-type from *Paracoccus denitrificans*, cbb_3 type from *Pseudomonas stutzeri*, aa_3-type from *Rhodobacter sphaeroides*, aa_3-type from *Bos taurus* and cNOR from *Pseudomonas nautica 617*. Bottom inset: schematic top view of the HCuO superfamily catalytic subunit; roman numerals indicate the helixes number and green circules indicate the helixes with the His ligands (adapted from [23]). 1 stands for the low-spin heme electron transfer center, 2 is the catalytic high-spin heme center and M_B is either a Cu or a non-heme Fe.

1.2.2.1.2. The Nitric Oxide Reductase Subclasses

The nitric oxide reductase (NOR) subclass is characterized by a diiron center. This is the major difference between NORs and other HCuO members that have a mixed binuclear center (Fe/Cu). The ligands that coordinate the metal centers are, nevertheless, conserved. The non-heme Fe_B prefers an six-coordination environment instead of the tetrahedic like Cu typical for the HCuO. For many years, assumptions were made for a possible ligand. Molecular modelling and sequence alignment predicted a Glu residue near the catalytic center to stabilize the Fe_B [3, 40]. The first crystal structure for a NOR was obtained only recently, confirming the existence of an extra Glu ligand to the non-heme Fe_B center [13]. Figure 1.9 (red rectangles) shows the sequence alignments with the Glu residue conserved in several NORs, extremely important for substrate reduction [40, 41].

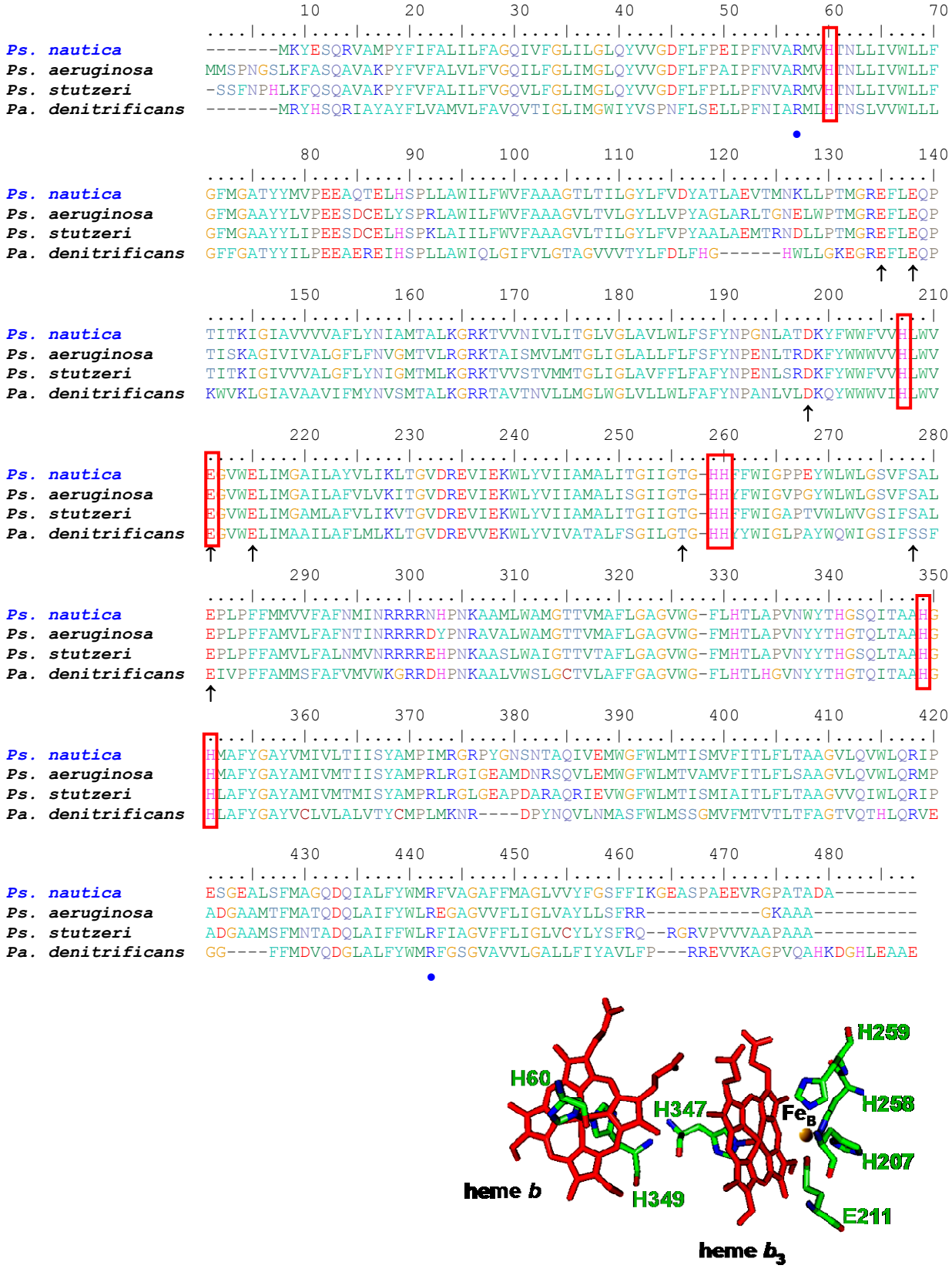

Figure 1.9 – Sequence alignment for the catalytic subunit (NorB) of cNOR from *Pseudomonas nautica* 617, *Pseudomonas aeruginosa*, *Pseudomonas stutzeri* and *Paracoccus denitrificans*. Rectangles enclose the iron co-factors' ligands, blue dots are the conserved Arg residues and the black arrows indicate the conserved aminoacids for protons entrance towards the active site. Inset, schematic representation of the electron transfer heme and the catalytic binuclear Fe center, adapted from *Pseudomonas aeruginosa* NorB sbunit resolved structure (PDB: 3O0R) [13].

cNOR (Cytochrome NOR)

Enzymes from the cNOR type have been extensively studied and characterized from different denitrifying bacteria such as *Paracoccus denitrificans* [42, 43], *Halomonas halodenitrificans* [44, 45], *Pseudomonas stutzeri* [46, 47], *aeruginosa* [48] and *nautica* [49]. These enzymes receive electrons from soluble cytochromes such as cyt. c_{551}, c_{552} [3, 13, 50, 51], or from other soluble electron transfer proteins, such as pseudoazurin, which was identified as a possible electron donor in the cNOR isolated from *Pa. denitrificans* [51].

They are purified as heterodimers and the two subunits are non-covalently bound and known as NorB and NorC.

The large subunit, NorB, presents a molecular weight of 56 kDa, contains a bis-His low-spin heme *b* as the immediate electron transfer co-factor. The catalytic center, encompassed in this subunit, is composed by a high-spin heme *b* (heme b_3), His-coordinated and with a μ-oxo/hydroxo bridge coupled to a non-heme iron (Fe_B). Recent crystallographic data from the *Ps. aeruginosa* cNOR structure confirmed the presence of a His in the heme b_3 axial position, in the as-purified state [13]. It was believed that the coordinating His residue could have a dynamic character, binding and unbinding the heme Fe in the different redox states and steps of the catalysis. The *Ps. nautica* cNOR spectroscopic characterization proved unequivocally that heme b_3 is hexacoordinated in both ferric and ferrous states [49].

Sequence alignment for the NorB subunits from different isolated cNORs revealed, not only their high homology, but also the conserved His residues that coordinate the Fe co-factors in the HCuO superfamily (figure 1.9). As mentioned before, an additional Glu residue coordination the non-heme Fe_B is responsible for the trigonal bipyramid molecular geometry [13].

The small subunit, NorC, is anchored to the cytoplasmatic membrane, has a molecular weight of 17 kDa and harbours a *c*-type heme. Its primary sequence is equally conserved amoung the members of this type of NORs as it shown in the alignment present in figure 1.10.

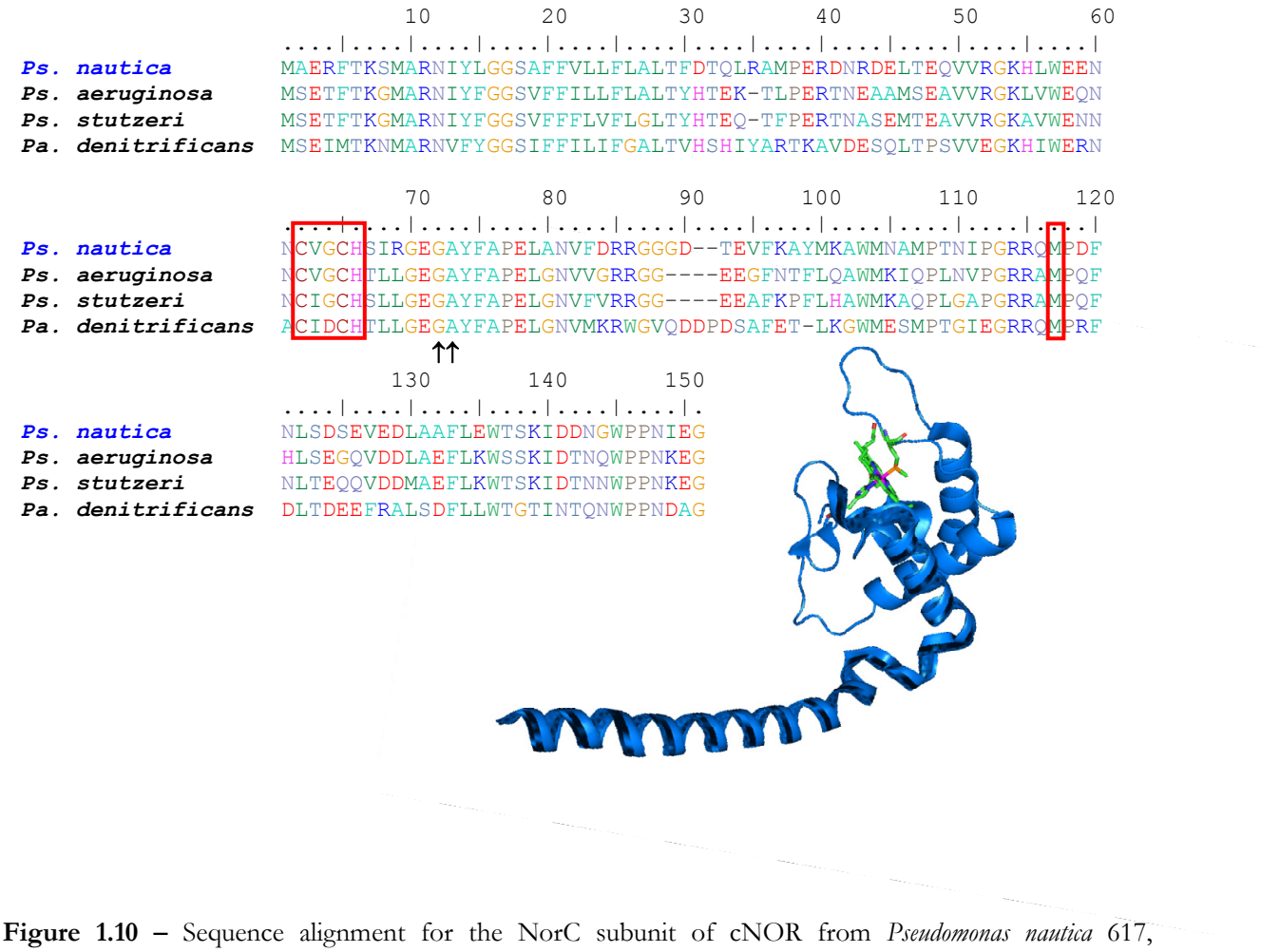

Figure 1.10 – Sequence alignment for the NorC subunit of cNOR from *Pseudomonas nautica* 617, *Pseudomonas aeruginosa*, *Pseudomonas stutzeri* and *Paracoccus denitrificans*. Rectangles enclose the heme *c* binding motif (CXXCH) and the axial Met ligand. Black arrows indicate the two conserved residues involved in the possible electron transfer between heme *c* and heme *b*. Inset shows NorC subunit structure, evidencing the heme *c* motif with its axial ligands His 65 and Met 112 (*Ps. aeruginiosa* numbering, PDB: 3O0R) [13].

The protein sequence demonstrates a unique heme *c* binding motif, with the usual CXXCH sequence revealing the His ligand (His 65, *aeruginosa* numbering) as well as the two conserved Cys residues responsible for the prosthetic group covalent binding to the polypeptide chain (see figure 1.10). The sixth ligand of the heme iron is a methionine residue (Met 112, *Ps. aeruginosa* numbering) and the center exhibits a high anisotropic EPR signal [49, 52].

As mentioned previously, cNORs receive their electrons typically from cytochromes. Intermolecular electron transfer occurs, with electrons flowing from the electron donor to the low-spin heme *c*, and from this, to the low-spin heme *b*, until they reach the catalytic binuclear center. To conduct the electrons, two highly conserved residues are present in

the NorC subunit (Gly 71 and Ala 72, *Ps. aeurginosa* numbering), in the interface between NorC and NorB (marked in figure 1.10). It is postulated that electrons flow from the heme *c*, to the Ala residue, and from their, they can go to the low-spin heme *b*, and pass to heme b_3 via a conserved Phe residue (Phe 352, *Ps. aeurginosa* numbering), or to the putative Ca atom bridging the two propionate side chains from the *b*-type hemes in the NorB subunit, and from there to the catalytic center. These electron routes were proposed with the achievement of the first NOR crystal structure and further experiments should be conducted to evaluate the importance of this residues and element (Ca) [13].

The first cNOR crystal structure points to the presence of one Ca^{2+} ion [13]. This element is postulated to be bridging the heme aliphatic chains of the prosthetic groups in the NorB subunit. Curiously, in *CcO* there are Arg residues that seem to be important in stabilizing the anionic form of the heme propionate side chains. Site directed mutants in which these residues have been modified, not only revealed a destabilization in the propionate anionic form, such as resulted in the loss of proton pumping [53]. [53]Recently the *Ps. stutzeri* cbb_3 *CcO* shown the presence of these two conserved Arg residues, stabilizing their heme *b* side chains with one additional putative Ca atom [54]. The presence of these aminoacids in some cNORs primary sequences is highly conserved (figure 1.9) and molecular modelling predicted the exact same role for this Arg residues in NOR's [40].

The *c*-type NORs have been intensively isolated and characterized, using different biochemical and spectroscopic techniques [42-44, 55, 56]. Since these enzymes are hemic proteins, their UV-visible absorption spectra exhibit a Sortet band at 410 nm, and the α, β bands are centred at 550 nm. Since the protein carries different heme types, the 552 nm band was assigned to the heme *c* and the small shoulder developed at 558 nm was assigned to the low-spin electron transfer heme *b*. Some isolated NORs present a UV-visible band around 595 nm [55, 57]. This band was addressed to the ligand-to-ligand metal charge transfer band associated with the high-spin ferric beme b_3 without the proximal His ligand [58].

The EPR spectra of different cNORs is reported in the literature [51, 55, 57, 59]. The as-isolated form presents two sets of low-spin signals: one indexed to the low-spin heme *b*, due to its bis-His coordination [59], and an other, where only the g_{max} has been detected, was assigned to the heme *c* [52]. The catalytic center was assumed to be EPR

silent due to the antiferromagnetical coupling of the two catalytic irons. The signals rising at g = 6 region and g = 4.3, where attributed to a small fraction of uncoupled heme b_3 and to the non-heme Fe_B, respectively [55, 57]. Most recently, Mössbauer spectroscopy revealed new insights in the *Ps. nautica* NOR enzyme, suggesting a six-coordination for the catalytic heme b_3 in both ferric and ferrous stares of the enzyme, claiming a new assignment for the g = 6 signals present in the EPR cNOR signature [56].

The midpoint redox potentials for the *Pa. denitrificans* NOR co-factors were reported by Grönberg and co-workers, using visible absorption titration (at pH 7.6) [60]. The results show a large positive potential for the heme *c*, heme *b* and the non-heme Fe_B, 310, 345 and 320 mV (*vs.* NHE) respectively, with a much lower redox potential for the heme b_3, 60 mV. The large redox potentials, around 300-350 mV were explained as a benefit for the rapid electron transfer from the physiological electron donor towards the active site [60]. The rather low potential for the heme b_3, some 200 mV below the other potentials was attributed to a thermodynamic barrier to the complete reduction of the dinuclear center. *Ps. nautica* NOR visible oxidation/reduction titration point a heme *c* and heme *b* redox potential in the same magnitude as it was reported in the literature [56, 60]. To achieve the redox potential of the binuclear catalytic center, direct electrochemistry was applied in the *Ps. nautica* NOR and a lower redox potential value was indexed to the heme b_3 [61].

The *Ps. nautica* NOR EPR characterization and direct electrochemical were major topics in this thesis and the results obtained are exposed in chapters 2 and 3.

qNOR (quinol NOR)

A second class of NOR indicated in the previous figure 1.5, is represented by the quinol NORs (qNORs). While presenting a similar primary structure to cNOR, qNORs are single subunit enzymes with a molecular weight of 84.5 kDa, accepting electrons directly from quinols [7]. The primary sequence alignment with other NOR's (supporting information S.1) presents a N-terminal extension of approximately 280 aminoacids residues, quite similar to the NorC subunit and a C-terminal similar to the NorB subunit [7]. The observed structure lead to the proposal that qNOR was formed by a gene fusion of NorC and NorB. In such case, during evolution, qNOR would have lost the heme *c*

center and gained a quinol-binding site [7]. These enzymes where isolated from *Ralstonia eutropha* [62], *Pyrobaculum aerophilum* [63] and were identified in the genome of several pathogenic strains [64, 65].

In comparison with other NORs, these enzymes lack one electron transfer co-factor, either heme *c* or Cu_A; they only comprise the binuclear iron center and the low-spin heme *b*. In this case, electrons are directly transferred from quinol to the low-spin center (figure 1.5 grey broken arrows), and from this to the catalytic center.

qCuNOR (quinol-copper NOR)

The third type of NORs is the quinol copper NOR (qCuNOR, figure 1.5), was isolated and characterized from *Bacillus azotoformans* [66, 67] and it is composed by two subunits. The large one maintains its similarity with the NorB subunit from cNORs and the HCuO subunit I, ubiquitous to all NORs. The small subunit lacks the *c*-type heme and contains instead a binuclear Cu_A center identical to the reported for several HCuO [39, 67].

The qCuNORs can use menaquinol as an electron donor, as well as the soluble cyt c_{551}. Kinetic assays with menaquinol demonstrate a 4-fold higher maximum activity as compared to those with cytochrome c_{551}. Because of these, it was proposed that electron donation via menaquinol is used for NO detoxification [7].

1.3. Nitric Oxide Reduction by Nitric Oxide Reductases

The catalytic mechanism for NO reduction is a hot topic under intense discussion. Since the catalytic center is composed by two iron atoms, the heme b_3 and the non-heme Fe_B, connected by a μ-oxo/hydroxo bridge, different possibilities can be assumed for the substrate binding at the active center. They can be divided in two major groups: the *trans*-mechanism describing the NO binding to each one of the Fe atoms of the diiron center [48, 55, 68] and the *cis*-mechanism, where both NO molecules bind to the same Fe atom. For this last mechanism, two possibilities were predicted: a *cis*-Fe_B mechanism with both substrate molecules binding the non-heme Fe_B [69], and a *cis*-b_3 mechanism when they bind to the heme b_3 iron [37, 70].

The trans-mechanism

The *trans*-mechanism (figure 1.11) describes one substrate molecule binding to each one of the catalytic irons. This model was first suggested by Girsch and co-workers [55], and it is supported by Raman [68] and EPR spectroscopies [26, 45, 48]. Substrate reduction is described by a first NO molecule binding the heme b_3, leading to the protonation of the μ-oxo bridge, and a second NO molecule binding to the non-heme Fe_B [23, 27]. The formation of a hyponitrite intermediate is assumed. However, no catalytic intermediate of this reaction as ever been detected, which renders the N-N coupling speculative [71].

All the proposed mechanisms assume a high-spin heme b_3 in the resting state of the enzyme (fully oxidized state). A recent study on *Ps. nautica* NOR proves that heme b_3 is low-spin in both its ferric and ferrous states [56]. Other studies also proved that a six-coordinated heme nitrosyl compound weakens the Fe-NO and the N-O bond, relatively to a five-coordinated species, which could somehow help to activate the NO molecule [71].

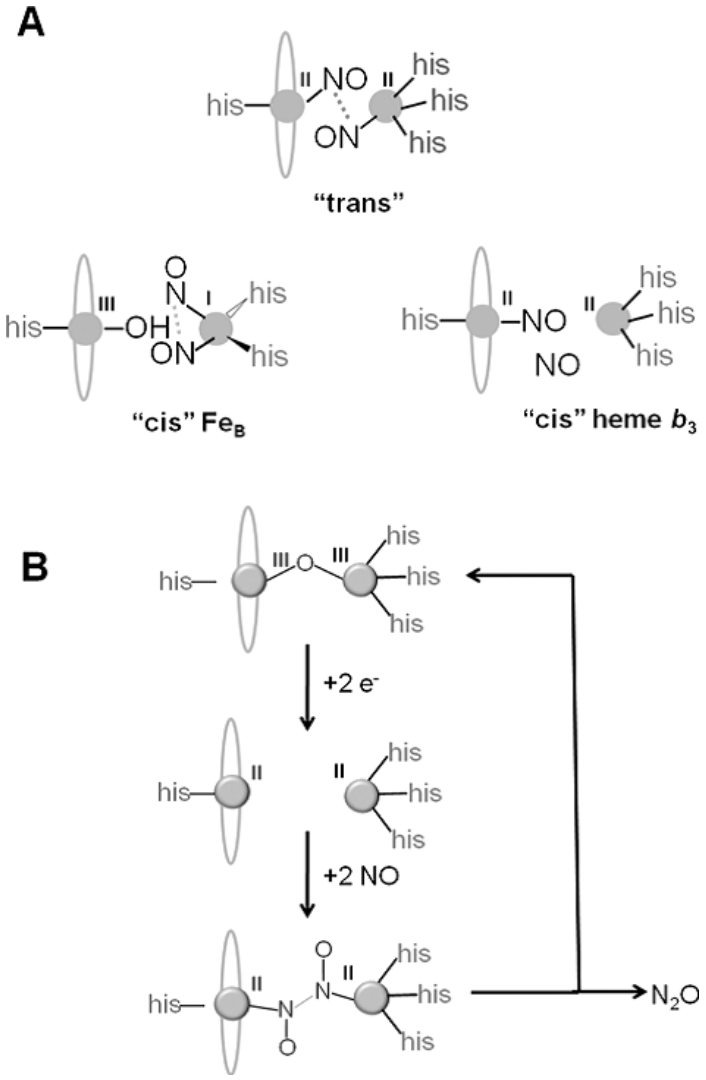

Figure 1.11 – Possible modes for NO binding to the binuclear centre of NOR: *Cis* and *Trans*. A-Three different modes of accommodating two molecules of NO at the active site of NOR; B-Schematic representation of the *trans*-mechanism model (adapted from [27]).

The cis-mechanism

The *cis*-mechanism is assumed when only one of the Fe atoms of the catalytic center binds the substrate, being the other iron atom responsible for giving the reducing equivalents.

The *cis*-heme b_3 mechanism has only been predicted by theoretical models. Blomberg and co-workers shown a complete analysis for possible intermediate species in the NO reduction mechanism, considering the possibility of a second NO molecule interacting with a first one bound to the heme b_3 (figure 1.11) [70].

The *cis*-Fe_B mechanism was proposed, based in the presence of one non-heme Fe_B per NOR molecule, because non-heme organometallic compounds suggest a reactive coupling with two NO molecules and the chemical conversion of NO to N_2O [69]. Theoretical models assuming an octahedral coordination for the Fe_B with the three His and the Glu ligands were studied [70]. Nevertheless, up to date, there is no available information on any intermediates that can support this mechanism.

Oxygen as an Alternative Substrate to Nitric Oxide

Oxygen (O_2) is an alternative substrate to the NORs. This is a common mechanism to *Ps. nautica* and *Pa denitrificans* NOR enzymes, and possibly to other isolated NO-reductases. Comparative studies of O_2 steady-state reduction kinetics, between wild-type and mutants of *Pa. denitrificans* NOR have provided insight on both mechanistic and structural features of the enzyme [40, 41, 72, 73]. This alternative natural substrate has been greatly used in experimental protocols, since it mimics the NO molecule in catalysis and it is much easier to handle. Nevertheless, there is no information on the catalytic mechanism for O_2 reduction, namely on the substrate binding to the catalytic diiron center and in the detection of relevant kinetic intermediates. Flow-flash experiments indicated that O_2 binds to the heme b_3 center, analogous to the HCuO mechanism [74-76].

The steady-state kinetic features for O_2 reduction by *Ps. nautica* NOR was a major focus of this thesis, and the results are presented in chapters 3 and 4.

Proton Gateways are Necessary for Reduction

Attention is mainly focused on NO and O_2, but protons are an essential co-substrate for the reduction mechanism. Two protons are required for the NO reduction and subsequent N_2O formation, while O_2 reduction to water involves four protons. There is evidence that electrons come from physiological donors and enter to the catalytic site, via the electron transfer co-factor.

At first, NORs were postulated to pump protons across the membrane, as described for the terminal oxidases. These enzymes generate an electrical gradient by using electrons and protons derived from opposite sides of the cytoplasmatic membrane. Protons are transferred from the cytoplasmatic surface of the protein into the active site through the D and K- pathways [40].

Latter on, NO and O_2 reduction were proved to be non-electrogenic, i.e., not coupled to charge translocation across the membrane [40, 77]. Experiments using cNOR closed in vesicles indicated that substrate protons are taken from the periplasmic side of the membrane [40]. The protons seem to enter via a conserved set of protonable residues (figure 1.12) and putative water molecules. Site directed mutagenesis experiments shown that some of these residues, such as Glu 122 and Glu 125 (*Pa. denitrificans* numbering), are essential for substrate reduction, implicating these residues in proton channelling [41].

The protonable residues are also conserved in cNORs and qNORs as it can be seen in the support information S.1 and reported by Reimann *et al.* [40].

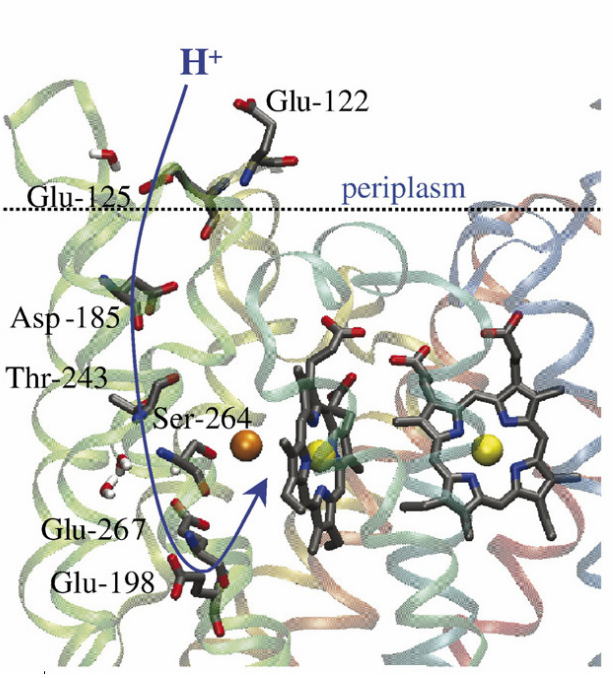

Figure 1.12 – Pathway for protons on the NOR catalytic subunit. *Paracoccus denitrificans* NorB subunit molecular model evidencing the protonable residues for protons translocation towards the active site. Yellow and orange spheres represent the heme *b* and non-heme Fe_B, respectively, adapted from [40].

1.4. NO Related Enzymes: NO Synthases and Reductases

NO synthases

Nitric oxide synthases (NOSs) are highly regulated multidomain metalloenzymes that catalyze the oxidation of l-Arginine (Arg) to NO and L-citrulline (Cit), via a stable intermediate the, N^{ω}-hydroxy-l-arginine (NOHA). These enzymes comprise a NOS oxygenase domain and a C-terminal flavoprotein reductase domain. The first domain contains the catalytic center, a *c*-type heme that binds the substrate (Arg) and the redox active co-factor 6R-tretrahydroviopterin (BH4). The second domain has binding sites for flavine and similar co-factors (FAD, FMN, and NADPH) that act as source of reducing equivalents. [4].

The NOS where primarily identified in mammalian cells, and present different regulations. The biochemical attempts to detect NO activity in various culture isolates lead to the discovery of bacterial NOS and NOS-like proteins. Bacterial NOSs produce NO *in vivo*, which function includes toxin biosynthesis, protection against oxidative damage and as a signal to regulate growth responses. Genome sequencing of prokaryotes revealed bacterial open reading frames (ORFs) coding for proteins with high sequence homology for the mammalian NOS oxygenase domain and with conserved catalytic motifs, suggesting that bacterial NOS would be involved in the NO synthesis. They are mostly found in gram positive bacteria, such as *Deinococcus radioduras*, and *Bacilli* species. Crystal structures revealed a strong resemblance with the mammalian NOS oxygenase domain with absence of the N-terminal domain [4].

Cytochrome c Nir

The penta-heme nitrite reductase, also known as cytochromes *c* nitrite reductase (ccNir or Nrf), is a periplasmic multi-hemic protein, that has been isolated and its X-ray structure resolved from *E. coli* [78], *Wolinella succinogenes* [79] and *Desulfovibrio desulfuricans* [80]. Due to their role in the denitrification pathway, these proteins were early included in the N-cycle (figure 1.1), where they catalyse the reduction of NO_2^- to NO. Additionally, they are able to reduce NO_2^- or NO to NH_4^+.

The enzymes belonging to this class are oligomers with two subunits, one of which is anchored to the membrane. The complex harbours five *c*-type hemes. The catalytic heme (heme I) is easy to identify since it is the only heme with a Lys residue in its axial ligand, showing a new heme-binding motif CXXCK. The remaining four hemes exhibit a bis-His coordination and they are responsible for the electron transfer towards the active site [3, 24, 78-80].

Electrochemical response of the *E. coli* ccNir demonstrated a higher affinity for NO than for NO_2^- leading to the believe that this enzyme plays a significant role in NO detoxification [3, 81].

Flavodiiron Proteins

The flavodiiron proteins, originally called A-type flavoproteins, are enzymes which catalyze the two electron-two protons NO reduction to N_2O. They are present in Archea, bacteria and some protozoan pathogens (mostly anaerobes), and they play an important role in the NO and O_2 detoxification [82].

These enzymes have a two domain structure: an N-terminal β-lactamase fold and a C-terminal short-chain flavodoxin-like fold, and they receive electrons from the NADH:rubredoxin oxidoreductase [3, 82, 83].

Flavorubredoxin seam to be the combination of the A-type flavoprotein and rubredoxin, and they have been are equally studied and isolated, as well as the as the flavodiiron proteins [84, 85].

Primarily, it was thought that these proteins were O_2-scavenging enzymes. Today, they where assigned to be deeply involved in the nitrosative and/or oxidative stress [82].

Fungal P450$_{nor}$

Fungal nitric oxide reductase cytochrome (P450$_{nor}$) is a unique heme-thiolate protein involved in fungal denitrification by reducing NO to N_2O [86].

P450$_{nor}$ was originally isolated from the filamentous fungus *Fusarium oxysporum* [87], indicating for the first time that denitrification is not restricted to prokaryotes. As part of the whole denitrification procedure, fungal denitrification contains reduction steps of nitrogen sources, from nitrate to nitrous oxide. P450$_{nor}$ [87]. The enzyme seems to receive electrons directly from NADH to reduce NO, without any help from a flavoprotein.

The finding of P450$_{nor}$ in a broad range of eukaryotes raised the attention of the scientific community working in NO_3^-/ NO_2^- reduction pathways. Being analogous to ccNir and the flavodiiron, it is likely that P450$_{nor}$ plays a role in NO detoxification in certain organisms [86, 87].

Heme Copper Oxidases

As mentioned before (section 1.2.2.1.1.) the HCuO are a superfamily of enzymes that comprise several terminal oxidases and the NORs.

Subject of discussion is the oxidoreductase activity of NOR (section 1.3). There are several HCuOs, such as the *ba*$_3$ and *caa*$_3$ oxidases from *Thermus thermophilus* and cytochrome *cbb*$_3$ oxidase from *Pseudomonas stutzeri*, which displayed NO reactivity. Contrarily, other oxidases, such as C*c*O from bovine heart, show no NO reductase activity [88-91]. For the purified enzymes that are able to reduce NO there is no reference to their catalytic mechanism. Nevertheless, spectroscopic results suggest NO binding to the Cu_B atom in order to produce N_2O [92].

Rational design of structural models for the cytochrome oxidase catalytic center was proformed, starting from the coding sequence of sperm whale myoglobin and using site direct mutagenesis [93]. The recombinant mutated protein obtained was fully characterized but only presented its functionality for NO reduction [94].

1.4.1. Model Compounds

To understand the NOR catalytic mechanism, inorganic compounds where synthesized in order to mimic the unusual binuclear iron center. This strategy has been applied to several other metalloenzymes. Unfortunately, it is difficult to exactly reproduce the chemical environment around the desired metal centers.

For many years, synthetic compounds where synthesized to mimic the heme/non-heme diiron compounds, but they missed the proximal His heme ligand, and the carboxyl group original from the conserved Glu in the native enzyme [95-97]. Some of artificial compounds exhibit reactivity with diatomic molecules like NO, O_2 and CO. Collman *et al.* synthesized a novel NOR active site (figure 1.13), accounting for the proximal His heme ligand and the postulated non-heme Fe_B carboxyl ligand [98, 99]. This was the first report for a functional NOR model that was able to reduce NO to N_2O stoichiometrically, apparently by a *trans* mechanism [100].

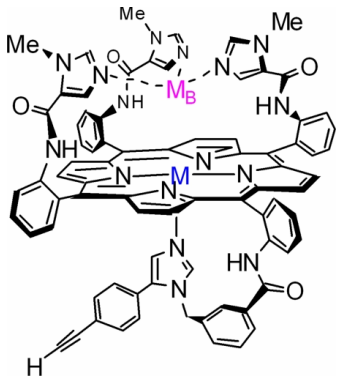

Figure 1.13 – Representation of the functional model compound able to reduce NO to N_2O, adapted from [100]. M and MB stand for the metal porphyrin (Fe) and for the non-heme metal (Fe_B).

The same compound was tested for the O_2 reduction, using electrochemical techniques. The diiron model compound was linked to a self assembled monolayer (SAM) and preformed an efficient four electron reduction of O_2 to water [101], showing the versatility of the unusual NO catalytic center.

1.4.2. Rational Design in Alternative Proteins

In silico design of proteins and enzymes has emerged as a powerful tool to design application-tailored proteins and catalysts for a wide range of applications.

Several enzymes exploit the unique features of metal co-factors to achieve catalytic activity otherwise unattainable through the use of only natural amino acid residues [102]. As an alternative, insertion or construction of a catalytically competent moiety inside a polypeptide scaffold is reported in literature [102-104]. Unluckily, these constructions rarely rival the natural enzymes in terms of catalytic efficiency, but they often yield invaluable structural and mechanistic information [105].

Using the myoglobin, Sigman *et al.* changed different aminoacids in the heme pocket of the protein, in order to obtain a chemical environment for Cu binding, aiming a soluble artificial enzyme harbouring the *CcO* catalytic center [93] Curiously, similar to other HCuO, this artificial enzyme presents NO reductase activity [94]. Similar work was done by Yeung *et al.*, but in this case, the binuclear Fe center of the NOR was accomplished (figure 1.14) [106]. The introduction of a Glu ligand in the myoglobin heme pocket enhanced the Fe binding with a favourable geometry, and therefore, the unusual diiron center from NORs was available in a much smaller and soluble protein. Biochemical and spectroscopic characterization of this artificial enzyme revealed that heme and non-heme Fe are magnetically coupled and capable of reducing NO to N_2O [106].

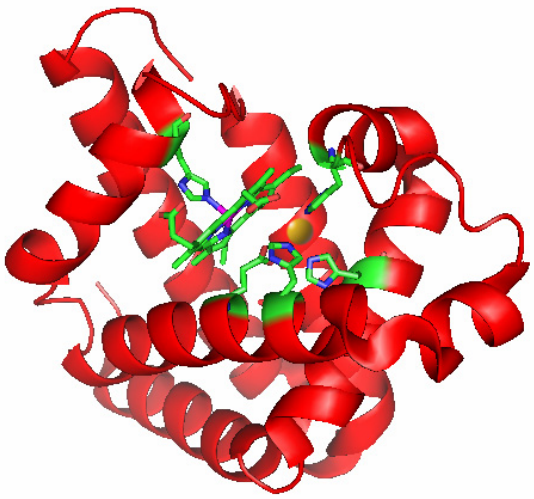

Figure 1.14 – The sperm whale myoglobin rotational design three-dimensional structure (PDB: 3K9Z). In red is evidenced the polypeptide chain, in green the ligands coordinating the diiron center and in yellow the non-heme Fe_B. The PDB file was edited with *Pymol* software.

1.5. The State of the Art and Aims

The NOR enzyme is an integral membrane protein purified from different denitrifying organisms. It is isolated as a heterodimer and it has been intensively characterized using biochemical and spectroscopic methods. In the end of 2010, new insights in this class of proteins were achieved.

The first NOR X-ray crystal structure was determined (figure 1.15), the as isolated form, shows the catalytic heme b_3 coordinated to its proximal His ligand (His 347, *Ps. aeruginosa* numbering), and to the μ-oxo bridge that connects to the non-heme Fe_B, suggesting a six-coordinated catalytic heme, contrarily to the reported in the literature [13].

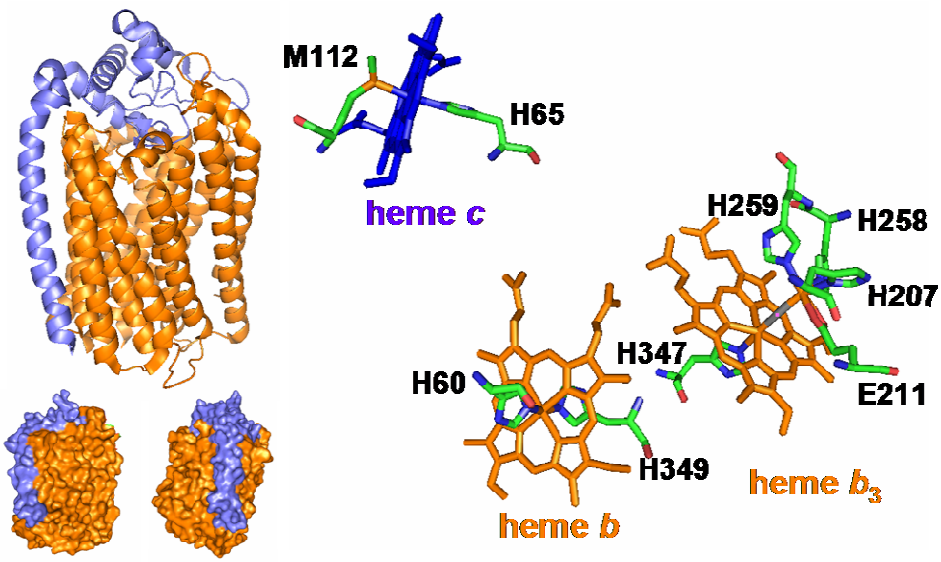

Figure 1.15 – The *Pseudomonas aeruginosa* NOR 2.7 Å crystal structure. On the left side is illustrated the two subunit interaction (NorC subunit in blue and NorB subunit in orange), with the helixes arrangement or with correspondent subunit surface. On the right side, is abstracted the polypeptide chain and is showed the co-factors disposition with the correspondent ligands. The PDB (3O0R) file was edited with *Pymol* .software.

Mössbauer spectroscopic results were recently achieved for the first time in this class of enzymes. The ^{57}Fe labelled *Ps. nautica* NOR was purified and characterized in our research group. The data show unequivocally that the catalytic heme b_3, contrarily to the previously supposed, is in fact low-spin for both ferric and ferrous states. This called for a

reconsideration on the EPR signals previously described in the literature [56]. The EPR signals rising at low field (g = 6) were assigned to the uncoupled ferric heme b_3. Since this is in fact a low-spin Fe center, the attribution of this signal to the catalytic heme center will be discussed further in this thesis (chapter 2). Careful analysis of the Mössbauer data, suggest a lower redox potential for both Fe atoms from the catalytic diiron center, since they are only reduced in the presence of a strong reducing agent, such as sodium dithionite (- 0.66 V, *vs.* NHE, at pH 7.0 [107]).

Spectroelectrochemistry revealed the redox centers at the active site of *Pa. denitrificans* NOR are isopotential, (+ 80 mV), and after the electron transfer low-spin heme *b* reduction, the μ-oxo bridge opens, in a favourable process for substrate binding [108].

These results were determined by a reappraisal of the values determined before by Gronberg *et al.* [60]. The midpoint redox potential of the metal co-factors in the NOR enzyme it is an issue of controversy. This subject will be elucidated in the chapter 3 of this thesis, with a detailed description of the *Ps. nautica* NOR midpoint redox potentials for the iron co-factors, assigned by direct electrochemical measurements.

There are still many questions to answer in the biological NO reduction field. The mechanism for substrate reduction is still a subject under intense discussion. Currently two mechanisms are being considered, namely the *cis* and *trans*-mechanism. To both hypotheses there is no information on possible kinetic intermediates that can support one of the proposed mechanisms. The reduction mechanism for NO reduction and for secondary substrates such as O_2 where investigated under steady-state conditions, an issue with low relevance in the literature, and the results are shown in chapter 4.

The aim of this thesis was:

i) to purify and characterize the *Ps. nautica* NOR;

ii) to characterize biochemically and spectroscopically the purified enzyme;

iii) to study the kinetics of this enzyme towards NO and O_2.

The achieved results were:

i) the biochemical and spectroscopic characterization of the enzyme;

ii) direct electrochemical response for the four Fe centers, using the immobilized enzyme;

iii) quantification of the number of electron involved in NO and O_2 reduction;

iv) steady-state kinetic features for the NO and O_2 reduction, using different electron donors.

1.6. References

[1] Richter-Addo, G.B., P. Legzdins and J. Burstyn, *Introduction: Nitric oxide chemistry.* Chem Rev, 2002. **102**(4): p. 857-859.

[2] McCleverty, J.A., *Chemistry of nitric oxide relevant to biology.* Chem Rev, 2004. **104**(2): p. 403-418.

[3] Zumft, W.G., *Nitric oxide reductases of prokaryotes with emphasis on the respiratory, heme-copper oxidase type.* J Inorg Biochem, 2005. **99**(1): p. 194-215.

[4] Crane, B.R., J. Sudhamsu and B.A. Patel, *Bacterial Nitric Oxide Synthases.* Annual Review of Biochemistry, Vol 79, 2010. **79**: p. 445-470.

[5] Barraud, N., D.J. Hassett, S.H. Hwang, S.A. Rice, S. Kjelleberg and J.S. Webb, *Involvement of nitric oxide in biofilm dispersal of Pseudomonas aeruginosa.* J Bacteriol, 2006. **188**(21): p. 7344-7353.

[6] Canfield, D.E., A.N. Glazer and P.G. Falkowski, *The Evolution and Future of Earth's Nitrogen Cycle.* Science, 2010. **330**(6001): p. 192-196.

[7] Tavares, P., A.S. Pereira, J.J. Moura and I. Moura, *Metalloenzymes of the denitrification pathway.* J Inorg Biochem, 2006. **100**(12): p. 2087-100.

[8] Coelho, C., P.J. Gonzalez, J.G. Moura, I. Moura, J. Trincao and M. Joao Romao, *The Crystal Structure of Cupriavidus necator Nitrate Reductase in Oxidized and Partially Reduced States.* J Mol Biol. **408**(5): p. 932-48.

[9] Bertero, M.G., R.A. Rothery, M. Palak, C. Hou, D. Lim, F. Blasco, J.H. Weiner and N.C. Strynadka, *Insights into the respiratory electron transfer pathway from the structure of nitrate reductase A.* Nat Struct Biol, 2003. **10**(9): p. 681-7.

[10] Adman, E.T., J.W. Godden and S. Turley, *The structure of copper-nitrite reductase from Achromobacter cycloclastes at five pH values, with NO2- bound and with type II copper depleted.* J Biol Chem, 1995. **270**(46): p. 27458-74.

[11] Antonyuk, S.V., R.W. Strange, G. Sawers, R.R. Eady and S.S. Hasnain, *Atomic resolution structures of resting-state, substrate- and product-complexed Cu-nitrite reductase provide insight into catalytic mechanism.* Proc Natl Acad Sci U S A, 2005. **102**(34): p. 12041-6.

[12] Sjogren, T. and J. Hajdu, *The Structure of an alternative form of Paracoccus pantotrophus cytochrome cd(1) nitrite reductase.* J Biol Chem, 2001. **276**(31): p. 29450-5.

[13] Hino, T., Y. Matsumoto, S. Nagano, H. Sugimoto, Y. Fukumori, T. Murata, S. Iwata and Y. Shiro, *Structural basis of biological N2O generation by bacterial nitric oxide reductase.* Science, 2010. **330**(6011): p. 1666-70.

[14] Prudencio, M., A.S. Pereira, P. Tavares, S. Besson, I. Cabrito, K. Brown, B. Samyn, B. Devreese, J. Van Beeumen, F. Rusnak, G. Fauque, J.J. Moura, M. Tegoni, C. Cambillau and I. Moura, *Purification, characterization, and preliminary crystallographic study of copper-containing nitrous oxide reductase from Pseudomonas nautica 617*. Biochemistry, 2000. **39**(14): p. 3899-907.

[15] Correia, C., S. Besson, C.D. Brondino, P.J. Gonzalez, G. Fauque, J. Lampreia, I. Moura and J.J. Moura, *Biochemical and spectroscopic characterization of the membrane-bound nitrate reductase from Marinobacter hydrocarbonoclasticus 617*. J Biol Inorg Chem, 2008. **13**(8): p. 1321-33.

[16] Gonzalez, P.J., M.G. Rivas, C.D. Brondino, S.A. Bursakov, I. Moura and J.J. Moura, *EPR and redox properties of periplasmic nitrate reductase from Desulfovibrio desulfuricans ATCC 27774*. J Biol Inorg Chem, 2006. **11**(5): p. 609-16.

[17] Jepson, B.J., S. Mohan, T.A. Clarke, A.J. Gates, J.A. Cole, C.S. Butler, J.N. Butt, A.M. Hemmings and D.J. Richardson, *Spectropotentiometric and structural analysis of the periplasmic nitrate reductase from Escherichia coli*. J Biol Chem, 2007. **282**(9): p. 6425-37.

[18] Coelho, C., P.J. Gonzalez, J. Trincao, A.L. Carvalho, S. Najmudin, T. Hettman, S. Dieckman, J.J. Moura, I. Moura and M.J. Romao, *Heterodimeric nitrate reductase (NapAB) from Cupriavidus necator H16: purification, crystallization and preliminary X-ray analysis*. Acta Crystallogr Sect F Struct Biol Cryst Commun, 2007. **63**(Pt 6): p. 516-9.

[19] Marquez, M.C. and A. Ventosa, *Marinobacter hydrocarbonoclasticus Gauthier et al. 1992 and Marinobacter aquaeolei Nguyen et al. 1999 are heterotypic synonyms*. Int J Syst Evol Microbiol, 2005. **55**(Pt 3): p. 1349-51.

[20] Dias, J.M., M.E. Than, A. Humm, R. Huber, G.P. Bourenkov, H.D. Bartunik, S. Bursakov, J. Calvete, J. Caldeira, C. Carneiro, J.J. Moura, I. Moura and M.J. Romao, *Crystal structure of the first dissimilatory nitrate reductase at 1.9 A solved by MAD methods*. Structure, 1999. **7**(1): p. 65-79.

[21] Jormakka, M., D. Richardson, B. Byrne and S. Iwata, *Architecture of NarGH reveals a structural classification of Mo-bisMGD enzymes*. Structure, 2004. **12**(1): p. 95-104.

[22] Cerqueira, N.M., P.J. Gonzalez, C.D. Brondino, M.J. Romao, C.C. Romao, I. Moura and J.J. Moura, *The effect of the sixth sulfur ligand in the catalytic mechanism of periplasmic nitrate reductase*. J Comput Chem, 2009. **30**(15): p. 2466-84.

[23] Wasser, I.M., S. de Vries, P. Moenne-Loccoz, I. Schroder and K.D. Karlin, *Nitric oxide in biological denitrification: Fe/Cu metalloenzyme and metal complex NO(x) redox chemistry*. Chem Rev, 2002. **102**(4): p. 1201-34.

[24] Moura, I., S.R. Pauleta and J.J. Moura, *Enzymatic activity mastered by altering metal coordination spheres*. J Biol Inorg Chem, 2008. **13**(8): p. 1185-95.

[25] Nurizzo, D., M.C. Silvestrini, M. Mathieu, F. Cutruzzola, D. Bourgeois, V. Fulop, J. Hajdu, M. Brunori, M. Tegoni and C. Cambillau, *N-terminal arm exchange is observed in the*

2.15 A crystal structure of oxidized nitrite reductase from Pseudomonas aeruginosa. Structure, 1997. **5**(9): p. 1157-71.

[26] Hendriks, J., A. Warne, U. Gohlke, T. Haltia, C. Ludovici, M. Lubben and M. Saraste, *The active site of the bacterial nitric oxide reductase is a dinuclear iron center.* Biochemistry, 1998. **37**(38): p. 13102-9.

[27] Watmough, N.J., S.J. Field, R.J. Hughes and D.J. Richardson, *The bacterial respiratory nitric oxide reductase.* Biochem Soc Trans, 2009. **37**(Pt 2): p. 392-9.

[28] Coyle, C.L., W.G. Zumft, P.M. Kroneck, H. Korner and W. Jakob, *Nitrous oxide reductase from denitrifying Pseudomonas perfectomarina. Purification and properties of a novel multicopper enzyme.* Eur J Biochem, 1985. **153**(3): p. 459-67.

[29] Riester, J., W.G. Zumft and P.M. Kroneck, *Nitrous oxide reductase from Pseudomonas stutzeri. Redox properties and spectroscopic characterization of different forms of the multicopper enzyme.* Eur J Biochem, 1989. **178**(3): p. 751-62.

[30] Brown, K., K. Djinovic-Carugo, T. Haltia, I. Cabrito, M. Saraste, J.J. Moura, I. Moura, M. Tegoni and C. Cambillau, *Revisiting the catalytic CuZ cluster of nitrous oxide (N2O) reductase. Evidence of a bridging inorganic sulfur.* J Biol Chem, 2000. **275**(52): p. 41133-6.

[31] Paraskevopoulos, K., S.V. Antonyuk, R.G. Sawers, R.R. Eady and S.S. Hasnain, *Insight into catalysis of nitrous oxide reductase from high-resolution structures of resting and inhibitor-bound enzyme from Achromobacter cycloclastes.* J Mol Biol, 2006. **362**(1): p. 55-65.

[32] Simon, J., O. Einsle, P.M. Kroneck and W.G. Zumft, *The unprecedented nos gene cluster of Wolinella succinogenes encodes a novel respiratory electron transfer pathway to cytochrome c nitrous oxide reductase.* FEBS Lett, 2004. **569**(1-3): p. 7-12.

[33] Teraguchi, S. and T.C. Hollocher, *Purification and some characteristics of a cytochrome c-containing nitrous oxide reductase from Wolinella succinogenes.* J Biol Chem, 1989. **264**(4): p. 1972-9.

[34] Dell'Acqua, S., S.R. Pauleta, I. Moura and J.J. Moura, *The tetranuclear copper active site of nitrous oxide reductase: the CuZ center.* J Biol Inorg Chem, 2011. **16**(2): p. 183-94.

[35] Dell'Acqua, S., S.R. Pauleta, P.M. Paes de Sousa, E. Monzani, L. Casella, J.J. Moura and I. Moura, *A new CuZ active form in the catalytic reduction of N(2)O by nitrous oxide reductase from Pseudomonas nautica.* J Biol Inorg Chem, 2010. **15**(6): p. 967-76.

[36] Bar-Nahum, I., A.K. Gupta, S.M. Huber, M.Z. Ertem, C.J. Cramer and W.B. Tolman, *Reduction of nitrous oxide to dinitrogen by a mixed valent tricopper-disulfido cluster.* J Am Chem Soc, 2009. **131**(8): p. 2812-4.

[37] Moenne-Loccoz, P., *Spectroscopic characterization of heme iron-nitrosyl species and their role in NO reductase mechanisms in diiron proteins.* Nat Prod Rep, 2007. **24**(3): p. 610-20.

[38] Pereira, M.M., M. Santana and M. Teixeira, *A novel scenario for the evolution of haem-copper oxygen reductases.* Biochim Biophys Acta, 2001. **1505**(2-3): p. 185-208.

[39] Garcia-Horsman, J.A., B. Barquera, J. Rumbley, J. Ma and R.B. Gennis, *The superfamily of heme-copper respiratory oxidases.* J Bacteriol, 1994. **176**(18): p. 5587-600.

[40] Reimann, J., U. Flock, H. Lepp, A. Honigmann and P. Adelroth, *A pathway for protons in nitric oxide reductase from Paracoccus denitrificans.* Biochim Biophys Acta, 2007. **1767**(5): p. 362-73.

[41] Butland, G., S. Spiro, N.J. Watmough and D.J. Richardson, *Two conserved glutamates in the bacterial nitric oxide reductase are essential for activity but not assembly of the enzyme.* J Bacteriol, 2001. **183**(1): p. 189-99.

[42] Carr, G.J. and S.J. Ferguson, *The nitric oxide reductase of Paracoccus denitrificans.* Biochem J, 1990. **269**(2): p. 423-9.

[43] Hoglen, J. and T.C. Hollocher, *Purification and some characteristics of nitric oxide reductase-containing vesicles from Paracoccus denitrificans.* J Biol Chem, 1989. **264**(13): p. 7556-63.

[44] Sakurai, T., S. Nakashima, K. Kataoka, D. Seo and N. Sakurai, *Diverse NO reduction by Halomonas halodenitrificans nitric oxide reductase.* Biochem Biophys Res Commun, 2005. **333**(2): p. 483-7.

[45] Sakurai, T., N. Sakurai, H. Matsumoto, S. Hirota and O. Yamauchi, *Roles of four iron centers in Paracoccus halodenitrificans nitric oxide reductase.* Biochem Biophys Res Commun, 1998. **251**(1): p. 248-51.

[46] Heiss, B., K. Frunzke and W.G. Zumft, *Formation of the N-N bond from nitric oxide by a membrane-bound cytochrome bc complex of nitrate-respiring (denitrifying) Pseudomonas stutzeri.* J Bacteriol, 1989. **171**(6): p. 3288-97.

[47] Kastrau, D.H., B. Heiss, P.M. Kroneck and W.G. Zumft, *Nitric oxide reductase from Pseudomonas stutzeri, a novel cytochrome bc complex. Phospholipid requirement, electron paramagnetic resonance and redox properties.* Eur J Biochem, 1994. **222**(2): p. 293-303.

[48] Kumita, H., K. Matsuura, T. Hino, S. Takahashi, H. Hori, Y. Fukumori, I. Morishima and Y. Shiro, *NO reduction by nitric-oxide reductase from denitrifying bacterium Pseudomonas aeruginosa: characterization of reaction intermediates that appear in the single turnover cycle.* J Biol Chem, 2004. **279**(53): p. 55247-54.

[49] Timoteo, C.G., *Estudos Estruturais e Mecanisticos em enzimas Multihémicas Isoladas de Bactérias Desnitrificantes.* 2004, pHD Thesis Universidade Nova de Lisboa: Lisboa.

[50] Conrath, K., A.S. Pereira, C.E. Martins, C.G. Timoteo, P. Tavares, S. Spinelli, J. Kinne, C. Flaudrops, C. Cambillau, S. Muyldermans, I. Moura, J.J. Moura, M. Tegoni and A. Desmyter, *Camelid nanobodies raised against an integral membrane enzyme, nitric oxide reductase.* Protein Sci, 2009. **18**(3): p. 619-28.

[51] Field, S.J., F.H. Thorndycroft, A.D. Matorin, D.J. Richardson and N.J. Watmough, *The respiratory nitric oxide reductase (NorBC) from Paracoccus denitrificans.* Methods Enzymol, 2008. **437**: p. 79-101.

[52] Oubrie, A., S. Gemeinhardt, S. Field, S. Marritt, A.J. Thomson, M. Saraste and D.J. Richardson, *Properties of a soluble domain of subunit C of a bacterial nitric oxide reductase.* Biochemistry, 2002. **41**(35): p. 10858-65.

[53] Branden, G., M. Branden, B. Schmidt, D.A. Mills, S. Ferguson-Miller and P. Brzezinski, *The protonation state of a heme propionate controls electron transfer in cytochrome c oxidase.* Biochemistry, 2005. **44**(31): p. 10466-74.

[54] Buschmann, S., E. Warkentin, H. Xie, J.D. Langer, U. Ermler and H. Michel, *The structure of cbb3 cytochrome oxidase provides insights into proton pumping.* Science. **329**(5989): p. 327-30.

[55] Girsch, P. and S. de Vries, *Purification and initial kinetic and spectroscopic characterization of NO reductase from Paracoccus denitrificans.* Biochim Biophys Acta, 1997. **1318**(1-2): p. 202-16.

[56] Timoteo, C.G., A.S. Pereira, C.E. Martins, S.G. Naik, A.G. Duarte, J.J. Moura, P. Tavares, B.H. Huynh and I. Moura, *Low-Spin Heme b3 in the Catalytic Center of Nitric Oxide Reductase from Pseudomonas nautica.* Biochemistry, 2011. **50**(20): p. 4251-4262.

[57] Sakurai, N. and T. Sakurai, *Isolation and characterization of nitric oxide reductase from Paracoccus halodenitrificans.* Biochemistry, 1997. **36**(45): p. 13809-15.

[58] Field, S.J., L. Prior, M.D. Roldan, M.R. Cheesman, A.J. Thomson, S. Spiro, J.N. Butt, N.J. Watmough and D.J. Richardson, *Spectral properties of bacterial nitric-oxide reductase: resolution of pH-dependent forms of the active site heme b3.* J Biol Chem, 2002. **277**(23): p. 20146-50.

[59] Cheesman, M.R., W.G. Zumft and A.J. Thomson, *The MCD and EPR of the heme centers of nitric oxide reductase from Pseudomonas stutzeri: Evidence that the enzyme is structurally related to the heme-copper oxidases.* Biochemistry, 1998. **37**(11): p. 3994-4000.

[60] Gronberg, K.L., M.D. Roldan, L. Prior, G. Butland, M.R. Cheesman, D.J. Richardson, S. Spiro, A.J. Thomson and N.J. Watmough, *A low-redox potential heme in the dinuclear center of bacterial nitric oxide reductase: implications for the evolution of energy-conserving heme-copper oxidases.* Biochemistry, 1999. **38**(42): p. 13780-6.

[61] Cordas, C.M., A.S. Pereira, C.E. Martins, C.G. Timoteo, I. Moura, J.J. Moura and P. Tavares, *Nitric oxide reductase: direct electrochemistry and electrocatalytic activity.* Chembiochem, 2006. **7**(12): p. 1878-81.

[62] Cramm, R., A. Pohlmann and B. Friedrich, *Purification and characterization of the single-component nitric oxide reductase from Ralstonia eutropha H16.* FEBS Lett, 1999. **460**(1): p. 6-10.

[63] de Vries, S., M.J. Strampraad, S. Lu, P. Moenne-Loccoz and I. Schroder, *Purification and characterization of the MQH2:NO oxidoreductase from the hyperthermophilic archaeon Pyrobaculum aerophilum.* J Biol Chem, 2003. **278**(38): p. 35861-8.

[64] Hendriks, J., A. Oubrie, J. Castresana, A. Urbani, S. Gemeinhardt and M. Saraste, *Nitric oxide reductases in bacteria.* Biochim Biophys Acta, 2000. **1459**(2-3): p. 266-73.

[65] Householder, T.C., E.M. Fozo, J.A. Cardinale and V.L. Clark, *Gonococcal nitric oxide reductase is encoded by a single gene, norB, which is required for anaerobic growth and is induced by nitric oxide.* Infect Immun, 2000. **68**(9): p. 5241-6.

[66] Suharti, H.A. Heering and S. de Vries, *NO reductase from Bacillus azotoformans is a bifunctional enzyme accepting electrons from menaquinol and a specific endogenous membrane-bound cytochrome c551.* Biochemistry, 2004. **43**(42): p. 13487-95.

[67] Suharti, M.J. Strampraad, I. Schroder and S. de Vries, *A novel copper A containing menaquinol NO reductase from Bacillus azotoformans.* Biochemistry, 2001. **40**(8): p. 2632-9.

[68] Moenne-Loccoz, P.d.V., S., *Structural Characterization of the Catalytic High-Spin Heme b of Nitric Oxide Reductase: A Resonance Raman Study.* J Am Chem Soc, 1998. **120**: p. 5147-5152.

[69] Ye, R.W., B.A. Averill and J.M. Tiedje, *Denitrification: production and consumption of nitric oxide.* Appl Environ Microbiol, 1994. **60**(4): p. 1053-8.

[70] Blomberg, L.M., M.R. Blomberg and P.E. Siegbahn, *Reduction of nitric oxide in bacterial nitric oxide reductase--a theoretical model study.* Biochim Biophys Acta, 2006. **1757**(4): p. 240-52.

[71] Goodrich, L.E., F. Paulat, V.K. Praneeth and N. Lehnert, *Electronic structure of heme-nitrosyls and its significance for nitric oxide reactivity, sensing, transport, and toxicity in biological systems.* Inorg Chem. **49**(14): p. 6293-316.

[72] Flock, U., J. Reimann and P. Adelroth, *Proton transfer in bacterial nitric oxide reductase.* Biochem Soc Trans, 2006. **34**(Pt 1): p. 188-90.

[73] Flock, U., N.J. Watmough and P. Adelroth, *Electron/proton coupling in bacterial nitric oxide reductase during reduction of oxygen.* Biochemistry, 2005. **44**(31): p. 10711-9.

[74] Brzezinski, P. and R.B. Gennis, *Cytochrome c oxidase: exciting progress and remaining mysteries.* J Bioenerg Biomembr, 2008. **40**(5): p. 521-31.

[75] Flock, U., P. Lachmann, J. Reimann, N.J. Watmough and P. Adelroth, *Exploring the terminal region of the proton pathway in the bacterial nitric oxide reductase.* J Inorg Biochem, 2009. **103**(5): p. 845-50.

[76] Lachmann, P., Y. Huang, J. Reimann, U. Flock and P. Adelroth, *Substrate control of internal electron transfer in bacterial nitric-oxide reductase.* J Biol Chem, 2010. **285**(33): p. 25531-7.

[77] Hendriks, J.H., A. Jasaitis, M. Saraste and M.I. Verkhovsky, *Proton and electron pathways in the bacterial nitric oxide reductase.* Biochemistry, 2002. **41**(7): p. 2331-40.

[78] Bamford, V.A., H.C. Angove, H.E. Seward, A.J. Thomson, J.A. Cole, J.N. Butt, A.M. Hemmings and D.J. Richardson, *Structure and spectroscopy of the periplasmic cytochrome c nitrite reductase from Escherichia coli.* Biochemistry, 2002. **41**(9): p. 2921-31.

[79] Einsle, O., P. Stach, A. Messerschmidt, J. Simon, A. Kroger, R. Huber and P.M. Kroneck, *Cytochrome c nitrite reductase from Wolinella succinogenes. Structure at 1.6 A resolution, inhibitor binding, and heme-packing motifs.* J Biol Chem, 2000. **275**(50): p. 39608-16.

[80] Cunha, C.A., S. Macieira, J.M. Dias, G. Almeida, L.L. Goncalves, C. Costa, J. Lampreia, R. Huber, J.J. Moura, I. Moura and M.J. Romao, *Cytochrome c nitrite reductase from Desulfovibrio desulfuricans ATCC 27774. The relevance of the two calcium sites in the structure of the catalytic subunit (NrfA).* J Biol Chem, 2003. **278**(19): p. 17455-65.

[81] van Wonderen, J.H., B. Burlat, D.J. Richardson, M.R. Cheesman and J.N. Butt, *The nitric oxide reductase activity of cytochrome c nitrite reductase from Escherichia coli.* J Biol Chem, 2008. **283**(15): p. 9587-94.

[82] Vicente, J.B., F.M. Scandurra, E. Forte, M. Brunori, P. Sarti, M. Teixeira and A. Giuffre, *Kinetic characterization of the Escherichia coli nitric oxide reductase flavorubredoxin.* Methods Enzymol, 2008. **437**: p. 47-62.

[83] Vicente, J.B., M.C. Justino, V.L. Goncalves, L.M. Saraiva and M. Teixeira, *Biochemical, spectroscopic, and thermodynamic properties of flavodiiron proteins.* Methods Enzymol, 2008. **437**: p. 21-45.

[84] Saraiva, L.M., J.B. Vicente and M. Teixeira, *The role of the flavodiiron proteins in microbial nitric oxide detoxification.* Adv Microb Physiol, 2004. **49**: p. 77-129.

[85] Toogood, H.S., D. Leys and N.S. Scrutton, *Dynamics driving function: new insights from electron transferring flavoproteins and partner complexes.* Febs J, 2007. **274**(21): p. 5481-504.

[86] Zhang, L. and H. Shoun, *Purification and functional analysis of fungal nitric oxide reductase cytochrome P450nor.* Methods Enzymol, 2008. **437**: p. 117-33.

[87] Daiber, A., H. Shoun and V. Ullrich, *Nitric oxide reductase (P450nor) from Fusarium oxysporum.* J Inorg Biochem, 2005. **99**(1): p. 185-93.

[88] Giuffre, A., G. Stubauer, P. Sarti, M. Brunori, W.G. Zumft, G. Buse and T. Soulimane, *The heme-copper oxidases of Thermus thermophilus catalyze the reduction of nitric oxide: evolutionary implications.* Proc Natl Acad Sci U S A, 1999. **96**(26): p. 14718-23.

[89] Pinakoulaki, E., T. Ohta, T. Soulimane, T. Kitagawa and C. Varotsis, *Detection of the His-heme Fe2+-NO species in the reduction of NO to N2O by ba3-oxidase from thermus thermophilus.* J Am Chem Soc, 2005. **127**(43): p. 15161-7.

[90] Pinakoulaki, E., S. Stavrakis, A. Urbani and C. Varotsis, *Resonance Raman detection of a ferrous five-coordinate nitrosylheme b(3) complex in cytochrome cbb(3) oxidase from Pseudomonas stutzeri.* J Am Chem Soc, 2002. **124**(32): p. 9378-9.

[91] Forte, E., A. Urbani, M. Saraste, P. Sarti, M. Brunori and A. Giuffre, *The cytochrome cbb3 from Pseudomonas stutzeri displays nitric oxide reductase activity.* Eur J Biochem, 2001. **268**(24): p. 6486-91.

[92] Butler, C.S., H.E. Seward, C. Greenwood and A.J. Thomson, *Fast cytochrome bo from Escherichia coli binds two molecules of nitric oxide at CuB.* Biochemistry, 1997. **36**(51): p. 16259-66.

[93] Sigman, J., B.C. Kwok and Y. Lu, *From Myoglobin to Heme-Copper Oxidase: Design and Engineering of a CuB Center into Sperm Whale Myoglobin.* J Am Chem Soc, 2000. **122**: p. 8192-8196.

[94] Zhao, X., N. Yeung, B.S. Russell, D.K. Garner and Y. Lu, *Catalytic reduction of NO to N2O by a designed heme copper center in myoglobin: implications for the role of metal ions.* J Am Chem Soc, 2006. **128**(21): p. 6766-7.

[95] Wasser, I.M., H.W. Huang, P. Moenne-Loccoz and K.D. Karlin, *Heme/non-heme diiron(II) complexes and O2, CO, and NO adducts as reduced and substrate-bound models for the active site of bacterial nitric oxide reductase.* J Am Chem Soc, 2005. **127**(10): p. 3310-20.

[96] Ju, T., D., A.S. Woods, R.J. Cotter, P. Moenne-Loccoz and K.D. Karlin, *Dioxygen and nitric oxide reactivity of a reduced heme/non-heme diiron(II) complex 8(5L)FeII...FeII-Cl-]+. Using a tethered tetraarylporphyrin for de development of an active site reactivity model for bacterial nitric oxide reductase.* . Inorganica Chimica Acta, 2000. **297**: p. 362-372.

[97] Wasser, I.M., C.F. Martens, C.N. Verani, E. Rentschler, H.W. Huang, P. Moenne-Loccoz, L.N. Zakharov, A.L. Rheingold and K.D. Karlin, *Synthesis and spectroscopy of micro-oxo (O(2)(-))-bridged heme/non-heme diiron complexes: models for the active site of nitric oxide reductase.* Inorg Chem, 2004. **43**(2): p. 651-62.

[98] Collman, J.P., Y.L. Yan, J. Lei and P.H. Dinolfo, *Active-site models of bacterial nitric oxide reductase featuring tris-histidyl and glutamic acid mimics: influence of a carboxylate ligand on Fe(B) binding and the heme Fe/Fe(B) redox potential.* Inorg Chem, 2006. **45**(19): p. 7581-3.

[99] Collman, J.P., Y. Yang and R.A. Decreau, *Synthesis of nitric oxide reductase active site models bearing key components at both distal and proximal sites.* Org Lett, 2007. **9**(15): p. 2855-8.

[100] Collman, J.P., Y. Yang, A. Dey, R.A. Decreau, S. Ghosh, T. Ohta and E.I. Solomon, *A functional nitric oxide reductase model.* Proc Natl Acad Sci U S A, 2008. **105**(41): p. 15660-5.

[101] Collman, J.P., A. Dey, Y. Yang, S. Ghosh and R.A. Decreau, *O2 reduction by a functional heme/nonheme bis-iron NOR model complex.* Proc Natl Acad Sci U S A, 2009. **106**(26): p. 10528-33.

[102] Mazzucco, N., S. Zanconato, D. De Lucrezia, E. Argese, I. Poli and G. Minervini, *Design and dynamic simulation of minimal metallo-proteins.* J Mol Model.

[103] Oliveri, V. and G. Vecchio, *A novel artificial superoxide dismutase: non-covalent conjugation of albumin with a Mn(III) salophen type complex.* Eur J Med Chem. **46**(3): p. 961-5.

[104] Nakajima, H., K. Ramanathan, N. Kawaba and Y. Watanabe, *Rational engineering of Thermus thermophilus cytochrome c552 to a thermally tolerant artificial peroxidase.* Dalton Trans. **39**(12): p. 3105-14.

[105] Kohler, V. and T.R. Ward, *Design of a functional nitric oxide reductase within a myoglobin scaffold.* Chembiochem. **11**(8): p. 1049-51.

[106] Yeung, N., Y.W. Lin, Y.G. Gao, X. Zhao, B.S. Russell, L. Lei, K.D. Miner, H. Robinson and Y. Lu, *Rational design of a structural and functional nitric oxide reductase.* Nature, 2009. **462**(7276): p. 1079-82.

[107] Mayhew, S.G., *The redox potential of dithionite and SO-2 from equilibrium reactions with flavodoxins, methyl viologen and hydrogen plus hydrogenase.* Eur J Biochem, 1978. **85**(2): p. 535-47.

[108] Field, S.J., M.D. Roldan, S.J. Marritt, J.N. Butt, D.J. Richardson and N.J. Watmough, *Electron transfer to the active site of the bacterial nitric oxide reductase is controlled by ligand binding to heme b(3).* Biochim Biophys Acta, 2011. **1807**(4): p. 451-7.

CHAPTER 2

Pseudomonas nautica NOR: PURIFICATION AND CHARACTERIZATION

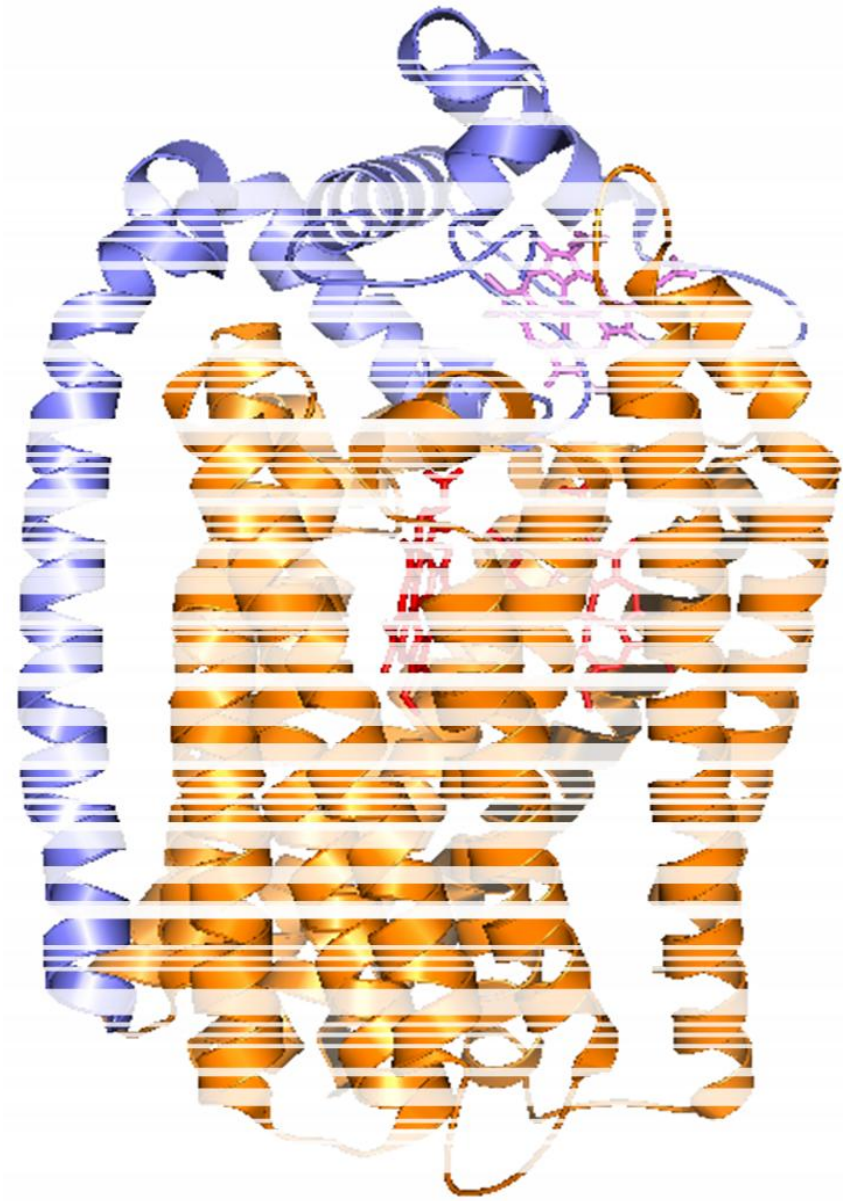

Chapter 2 *Pseudomonas nautica* NOR: Purification and Characterization

2. *Pseudomonas nautica* NOR: Purification and Characterization

2.1. Purification Strategy

The target enzyme is an integral membrane protein. The primary step of this part of the work is to isolate the membrane fraction, of *Pseudomonas nautica* 617[1] for further total protein extraction. To achieve this goal, it is imperative to use a surfactant, such as n-dodecyl-β-D-maltoside (DDM) used here, able to mimic the cytoplasmatic membrane in order to avoid protein precipitation. The surfactant used will be present in the remaining purification steps.

2.1.1. Preparation of *Pseudomonas nautica* Membranes

After cell disruption, the homogenate is centrifuged at 8000 ×g, for 20-30 minutes, to separate cell debris and undisrupted cells. The supernatant is then centrifuged at 138 000 ×g, for 90 minutes to separate the soluble and membrane fractions. The pellets containing the membranes were pooled and ressuspended in 50 mM Tris–HCl pH 8, 100 mM KCl to a final concentration of 10 mg/ml of total protein. Membranes were sonicated in a 500 ml portion, in an ice bath, with a 200 watts sonicator, at 24 kHz ultrasonic frequency, equipped with a S7 tip (7 mm diameter). The sonicator amplitude was set to 60% and the pulse to 0.5 seconds. The sonication period was 10 minutes and this procedure was repeated twice. Afterwards the homogenate was centrifuged at 138 000 ×g, for 90 minutes. The insoluble fraction containing the membranes was homogenized in 50 mM Tris-HCl pH 8, diluted to 10 mg/ml of total protein, and the last centrifugation step was repeated in order to wash to membranes and to remove the KCl. A scheme resuming these procedures is presented in figure 2.1.

[1] The bacterial cultures were grown as described in reference [1].

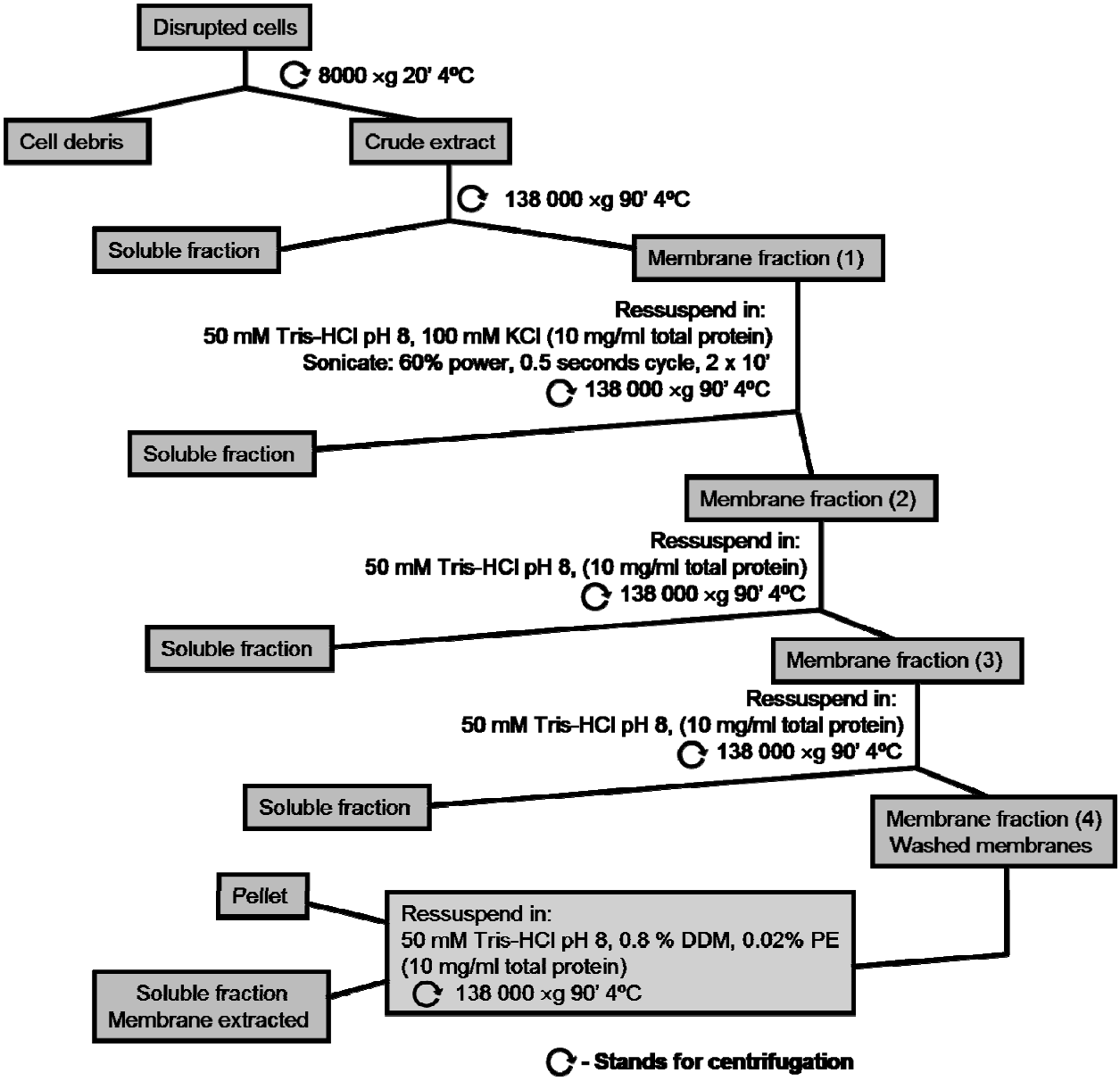

Figure 2.1 – *Pseudomonas nautica* membrane fraction isolation. The scheme shows the steps used in order to separate membrane fraction, containing the NOR. All steps were optimized for each particular preparation.

The sonication procedure and the treatment with KCl-based buffer were done in order to remove contaminating proteins that are weakly bound to the cell membrane.

2.1.2. Purification of the NOR from the Membrane Extract

Washed membrane fractions were dosed in total protein amount content to proceed to the membrane protein extraction step. This extraction is obtained by incubation with 0.8 % (w/v) n-dodecyl-β-D-maltoside (DDM), and 0.02 % (v/v) of S-(-)-phenylethanol (PE), at a final protein concentration of 10 mg/ml. Steering was maintained throughout the process, during 30 minutes at 4ºC.

The extracted fraction was separated by centrifugation (138 000×g, 90 minutes). The supernatant was applied to a DEAE bio-gel (*Bio-Rad*) column (Ø 50 × 350 mm), equilibrated with 50 mM Tris-HCl pH 8.0, 0.02 % (w/v) DDM, 0.01% (v/v) PE. After washing the column, a linear gradient of 2 litres was applied from 0 to 500 mM of NaCl in order to remove the adsorbed proteins. Fractions were collected in test tubes and NO reductase activity was assayed using a NO-sensor, as described in the supporting information S.8.4. The tubes that exhibited NO reductase activity were pooled and concentrated in an ultrafiltration apparatus. The ionic strength was lowered to 50 mM Tris-HCl pH 8, 0.02 % (w/v) DDM, 0.01 % (v/v) PE, using the same device. The NOR rich fraction was loaded in a CHT type II (*Bio-Rad*) column (Ø 16 × 350 mm). Protein elution was done, with a linear gradient, using 1.5 M KPB pH 7.0, 0.02 % DDM, 0.01 % PE, as the second buffer. The presence of NOR in each fraction was analysed by tricine sodium dodecyl sulfate electrophoresis (SDS-PAGE), the fractions containing the enzyme were joined and the ionic strength adjusted to 100 mM KPB pH 7.0 0.02 % (w/v) DDM, 0.01 % (v/v) PE by ultrafiltration. The NOR rich fraction, was loaded in a prepacked (20 ml) CHT type I (*Bio-Rad*) column equilibrated with 100 mM KPB pH 7.0, 0.02 % (w/v) DDM, 0.01 % (v/v)PE. A linear gradient was applied from 100 mM up to 1.5 M KPB pH 7, 0.02 % (w/v) DDM, 0.01 % (v/v) PE. The length of the gradient was optimized for each column, in order to achieve a better resolution. NOR fractions were eluted at an ionic strength close to 400-500 mM (≅ 40%).

The final fraction was concentrated and buffer exchanged to 100 mM KPB pH 7.0, 0.02 % (w/v) DDM, 0.01 % (v/v) PE. Purity was evaluated by UV-Visible absorption spectra and tricine SDS-PAGE. Protein staining was preformed using the blue coomassie

staining protocol, and heme staining was accomplished in parallel (supporting information S.8). All the protein quantification was made using the BCA method (*Sigma*). A scheme resuming these procedures is presented in figure 2.2.

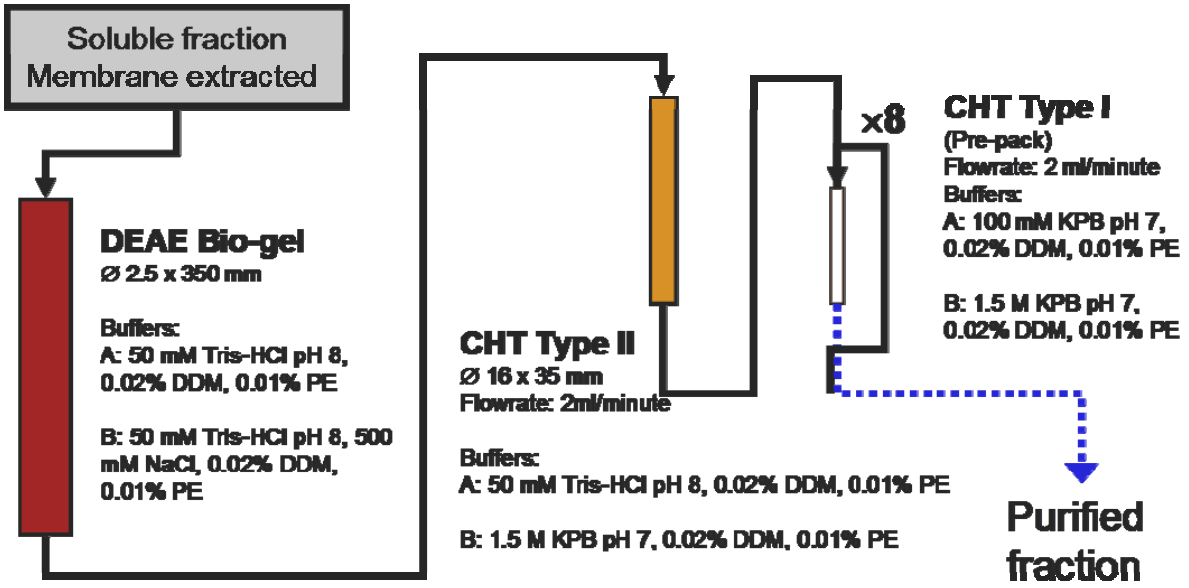

Figure 2.2 – The *Pseudomonas nautica* NOR purification scheme. The diagram resumes the chromatographic steps used for the protein purification, starting from the solubilized membrane fraction.

2.1.3. Purification Table

A purification table can be performed in order to obtain the purification yield and evaluate which was the best chromatographic step. Membranes were washed as described, but only half of the total washed membranes were used to continue in the downstream process, that is why the purification table (table 2.1) is separated in two parts (grey and white rows).

Table 2.1 - Purification table for the *Pseudomonas nautica* NOR. The table is separated in two parts, first part (grey) with the centrifugation and sonication steps for washing the membranes and the second part (white) starting from the detergent solubilized fraction.

	Volume (ml)	C (mg/ml)	Activity[a]	Total activity[b]	Specific activity[c]	Yield (%)	Purification fold
Membrane fraction 2	4550	10	0.02	-	-		
Membrane fraction 3	3400	10	0.07	-	-		
Soluble fraction	1756	10	0.05	87.8	2.84	100	1
DEAE Bio-gel	896	6.7	0.03	26.88	5.01	31	1.8
CHT (Type II/I)	18	3.3	0.16	2.88	2700	3.28	952

Units:

[a] μM NO. sec^{-1}

[b] μM NO. sec^{-1}.ml protein

[c] μM NO. sec^{-1}.mg $protein^{-1}$

The chromatographic steps were grouped according to the used solid support. The DEAE biogel support and the CHT type II were used only once (for primary crude extracts), wile the CHT-type I (prepacked) was re-used in order to obtain the last fraction which came out of the column consistently with a higher purity, explaining the extreme high value for the purification fold when using this chromatographic support (see purification table). Moreover, this last procedure was repeated up to 8×. This makes the protein purification extremely time consuming, but it was previously known by our research group that this ceramic resin was the best chromatographic support for the protein purification, amongst others. Unfortunately, only approximately 3 % of the total solubilized proteins are obtained, and as it is showed, the specific activity increases with the purification steps, as expected.

2.2. Biochemical and Spectroscopic Characterization

Type-*c* NORs have been identified in the genome of several organisms [2, 3], however they have only been isolated and characterized from a few denitrifying bacteria, such as *Pa. denitrificans* [4, 5], *Halomonas halodenitrificans* [6, 7], and the *Pseudomonas* species, *stutzeri* [8, 9], *aeruginosa* [10, 11] and *nautica* [12]. qNOR's and qCuNOR's here equally studied and isolated from *Rastonia eutropha* [13, 14], and *Bacillus azotoformans* [15].

In the following sections, the detailed biochemical and spectroscopic characterization of the isolated *Ps. nautica* 617 NOR is presented.

2.2.1. Tricine Sodium Dodecyl Sulfate Electrophoresis

Electrophoresis under denaturating conditions was performed constantly during purification steps, in order to evaluate the purity of the obtained fractions. Tricine SDS-PAGE gels [16] were done, and stained for total protein and peroxidatic heme detection. Experimental details and methodologies are described in supporting information S.8.1.

As it is shown in figure 2.3, the isolated protein presents two subunits, non-covalently bound, with 17 and 56 kDa, corresponding to the NorC and NorB subunits, respectively. The above mentioned value for the NorB subunit molecular weight was determined according to the primary sequence.

In gel electrophoresis was observed a band with higher eletrophoretic mobility (between 35 and 40 kDa) due to the high hydrophobic character of this subunit (figure 2.3). This result was already reported in different cNORs [7, 9, 17]. Heme staining presents a single band at 17 kDa, pointing the presence of a covalently bound *c*-type heme to the small subunit (NorC).

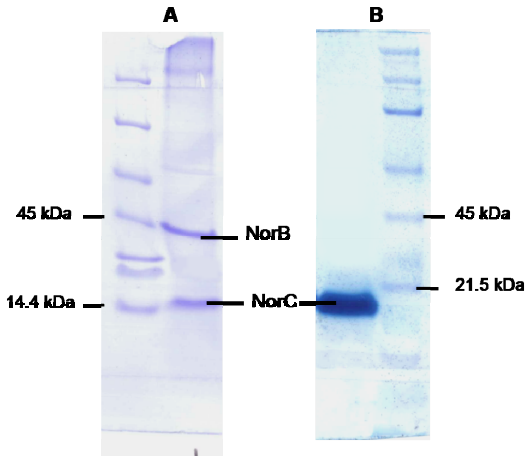

Figure 2.3 – Tricine SDS-PAGE gel (10 %) of the *Pseudomonas nautica* NOR purified fraction. Panel A: coomassie blue staining, showing the total protein content. Panel B: heme staining using the TMBZ method, which evidences the peroxidatic type hemes. Experimental details in supporting information S.8.

2.2.2. Metal Quantification

In order to determine the metal content in the purified sample, different quantifications were performed. Heme iron was determined according to the pyridine-hemocromogen method as described by Berry and Trumpower [18]. Total Fe and Ca were determined by plasma emission. Non–heme iron was determined by difference between total iron and heme iron. This calculation was adopted in replacement of the TPTZ method [19] since the quantifications in our research group revealed that the values obtained were similar (table 2.2) [12].

Table 2.2 - Metal quantification results obtained for the isolated NOR.

	Fe / cNOR				Ca / cNOR
	Heme		Total	Non-heme	
	c-type	*b*-type			
cNOR	0.9 ± 0.1	1.7 ± 0.2	4 ± 0.8	1.2 ± 0.1	0.7 ± 0.2

The values point to the presence of a 1:2:1 stoichiometry for the heme *c*, *b* and non-heme Fe_B respectively. This result is in agreement with previous values reported for other isolated cNORs e.g.[2, 20]. Ca determination reveals a substoichiometry value, although

one Ca atom per protein molecule was recently reported [10]. Comments to a possible Ca presence in the protein structure will be made further in this thesis (section 3.4).

2.2.3. UV-Visible Absorption

The UV-visible absorption spectrum of the as-isolated NOR is presented in figure 2.4 (blue line). The spectrum is typical of heme containing proteins and very similar to those of other purified cNORs [12, 21]. It shows a 280 nm peak, characteristic of all proteins, a Soret band at 411 nm, and a broad band at higher wavelengths, centered at 550 nm, with two small peaks at 558 and 528 nm, characteristic for the α and β regions, respectively. The appearance of the small absorption peaks in the as-isolated form of the enzyme indicate the presence of a small amount of reduced low spin heme, in agreement with the Mössbauer data reported in literature [12]. The absorbance ratio of the Soret band to the protein band (Abs 411/280) was determined to be 1.2. A molar extinction coefficient was previously determined for the as-isolated form and used to estimate protein concentration in all assays (ε_{411nm} = 295 $mM^{-1}cm^{-1}$) [12]. Other isolated NOR exhibit an absorption band at 595 nm [17, 22], however such band is absent in the as-isolated form of the *Ps. nautica* NOR [12]. This band was suggested to be due to a ligand-to-metal charge transfer associated with a high-spin ferric heme b_3 without the proximal His ligand [23]. The absence of an absorption band at 595 nm in the as-purified sample, suggests a different spin state and/or a different coordination environment for heme b_3, most probably six-coordinated, in agreement with the more recent reports [10, 12].

Ascorbate reduction of the sample red-shifts the Soret peak to 418 nm and sharpens the optical bands in the α β absorption region, revealing defined peaks at 523 nm and 552 nm, with a shoulder at 558 nm (figure 2.4, orange line), consistent with the reduction of low-spin heme groups. The absorption band at 552 nm was assigned to heme *c* and 558 nm indexed to the heme *b* [4, 24, 25]. Optical data, as well as EPR data (see bellow), indicate that heme *b* and heme *c* are reduced by ascorbate.

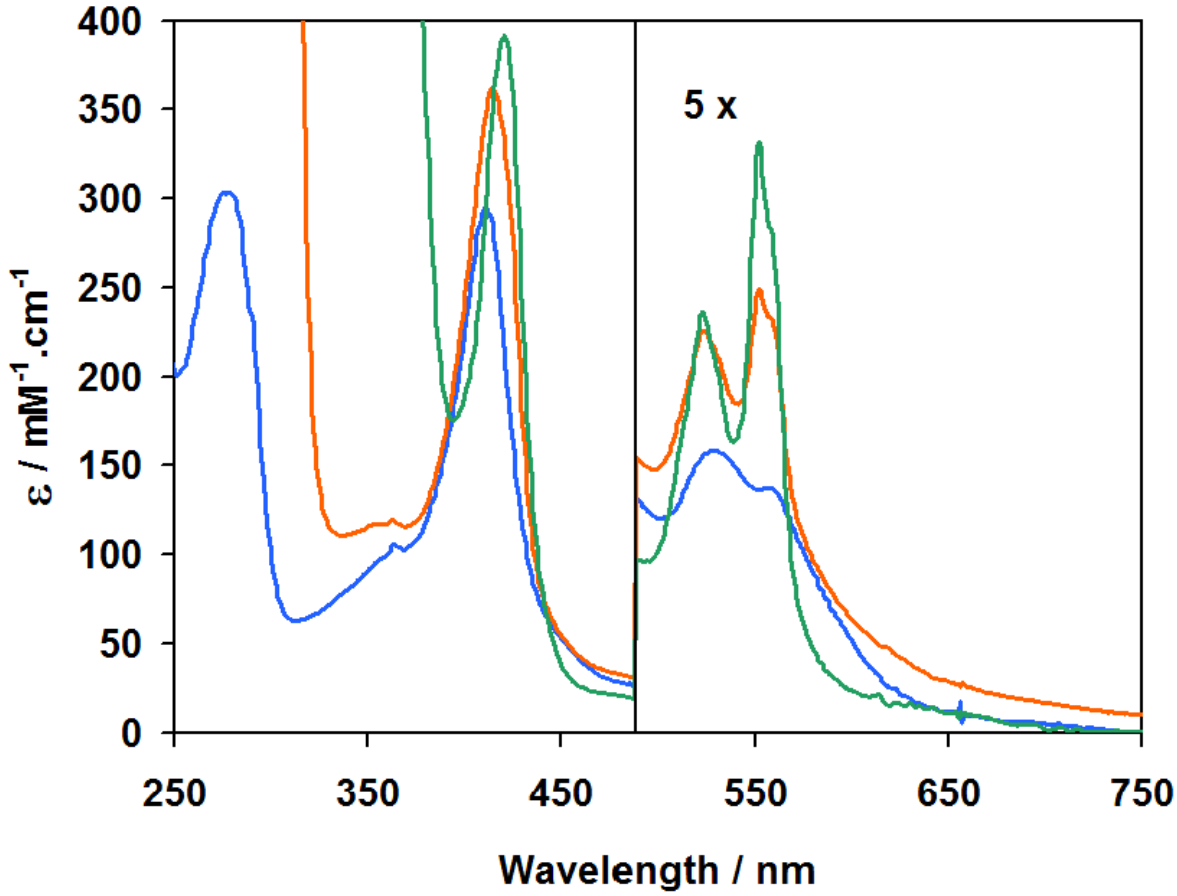

Figure 2.4 – The UV-visible absorption spectra of the purified *Pseudomonas nautica* NOR in different redox states: as-isolated form (blue line), sodium ascorbate reduced (orange line) and sodium dithionite reduced (green line). Complete reduction was accomplished by consecutive addiction of excess reducing agent. Spectra were done in 100 mM KPB pH 7.0, 0.02 % (w/v) DDM, 0.01 % (v/v) PE.

Sodium dithionite reduction of the sample shifts the Soret maximum to 421 nm and the α β bands become more intense indicating heme groups reduction (figure 2.4 green line).

Difference spectrum between the dithionite and ascorbate reduced forms of the enzyme (figure 2.5) suggests low-spin heme reduction, upon dithionite addiction. As showed, low-spin electron transfer hemes were reduced with ascorbate, This result is corroborated by Mössbauer results, since predicted a ferric low-spin configuration for the heme b_3 on the ascorbate reduced sample [12].

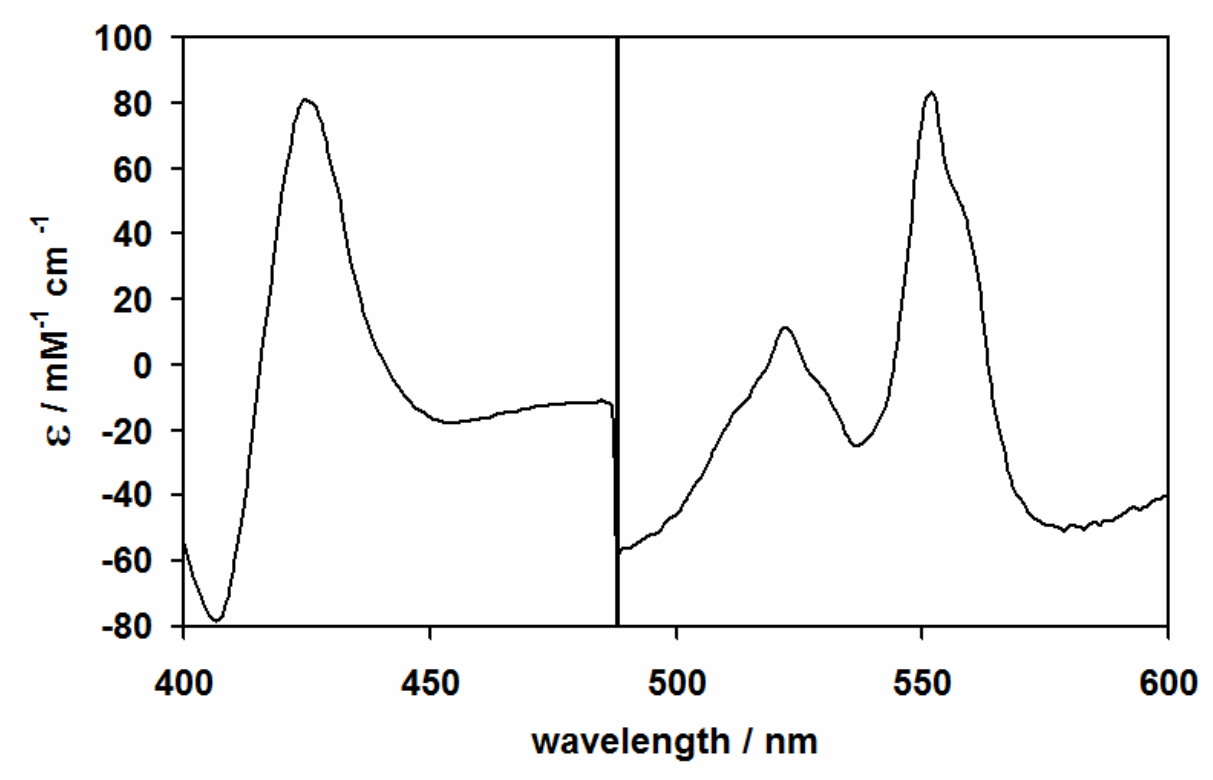

Figure 2.5 – UV-visible difference spectrum between the sodium dithionite and sodium ascorbate reduced forms of the *Pseudomonas nautica* NOR. Spectra were acquired in 100 mM KPB pH 7, 0.02 % DDM, 0.01 % PE.

2.2.4. Electron Paramagnetic Ressonance (EPR)

Similarly to the UV-visible absorption spectra, EPR spectra were acquired in the same three redox states: as-purified, sodium ascorbate and sodium dithionite reduced.

The as-purified *Ps. nautica* NOR exhibits an EPR spectrum quite similar to those reported for other isolated cNORs [17, 25, 26]. Two sets of low-spin heme signals were detected. One with g values of 2.99, 2.25 and 1.43, which have been attributed to the bis-His low-spin heme *b* [26], and the extreme anisotropic set of signals, from which only the g_{max} value of 3.59 can be observed, which have been attributed to the heme *c* of the NorC subunit (figure 2.6-A) [27].

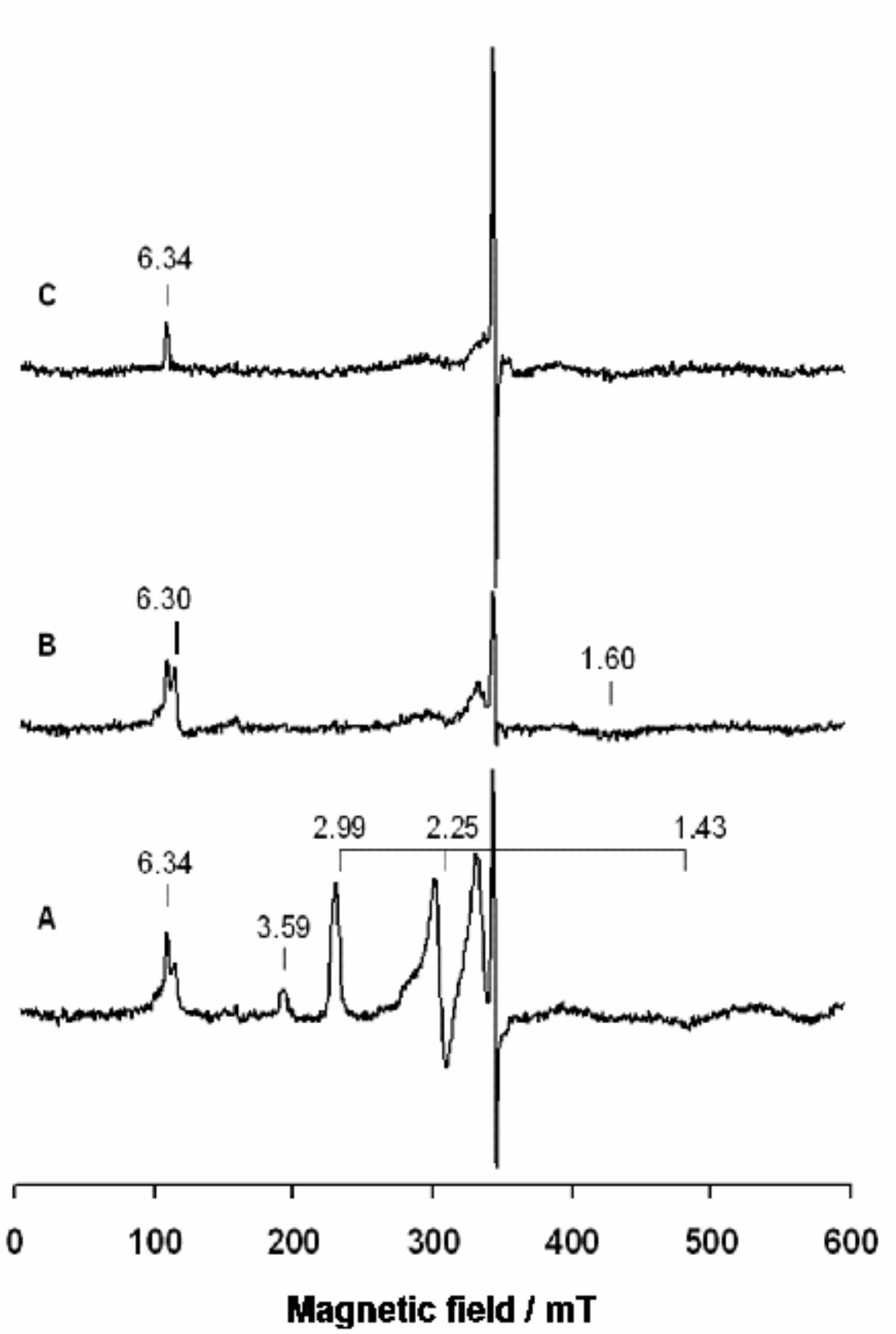

Figure 2.6 – EPR spectra at 9.653 GHz of the as-isolated (A), ascorbate-reduced (B) and dithionite reduced (C) *Ps. nautica* cNOR (265 μM in 100 mM KPB, pH 7.0, 0.02% (w/v) DDM, 0.01% (v/v) PE). Experimental conditions of spectra: temperature = 12 K, microwave power = 0.2 mW, modulation frequency = 100 kHz, modulation amplitude = 0.5 mT, receiver gain = 1×10^5, conversion time = 163.84 ms and time constant = 81.92 ms.

Spin quantitation of these two low-spin ferric heme signals was done using the Aasa and Vanngard method [28] and modified according to De Vries *et al.* [29]. The spectrum simulation is shown in supporting information S.2. Approximately 0.9 and 0.7 spin/molecule was determined for the heme *b* and heme *c* signals, respectively, indicating their presence in the analysed sample.

The NOR catalytic center has been described as a high-spin heme b_3 (S = 5/2), antiferromagnetically coupled to the high-spin ferric non–heme Fe_B (S = 5/2) [25, 27]. Therefore, the coupling of these two ferric centers would produce a diamagnetic specie (S = 0) ground state. No EPR signal was expected to arise from the oxidized catalytic binuclear center. In the analysed samples, the signals present at the g = 6 region were assigned to a fraction of uncoupled heme b_3 and the g = 4.3 signal accounted to the uncoupled high-spin non-heme Fe_B [25, 27].

Recent findings, revealed that heme b_3 is a low-spin, in both ferric and ferrous states [12]. Thus, magnetic coupling of the low-spin heme b_3 (S = 1/2) and the high-spin non-heme Fe_B (S = 5/2) would produce a integer-spin ground state with S = 2 or S = 3 that may not be EPR silent [30].

When the sample is reduced with sodium ascorbate, the electron transfer low-spin heme *b* and heme *c* signatures (g = 3.59, 2.99, 2.25 and 1.43) clearly disappear, while the signals around g = 6.30, 2.05, 2.01 and 1.60 are retained (figure 2.6 B). The disappearance of the ferric low-spin signals is consistent with the visible absorption spectroscopy results previously discussed (section 2.2.3), the published Mössbauer data [12] and the electrochemistry results discussed in further sections (section 3.3.). The remaining signals at the g = 6 region and a broad signal at 1.60 can be still observed. The signal at low field will be discussed further in the text (see below). The g = 2.05 and 1.60 signals are equally present in other purified cNOR's, such as the isolated from *Pa. denitrificans* and *Ps. aeruginosa* [11, 21], and not yet assigned.

Dithionite addiction to the sample, reduces the intensity in the g = 6.34 signal, but not completely (figure 2.6, C).

A comparative analysis of the three redox state samples can be made. The signal rising at the g = 6.34 position was previous attributed to the supposed high-spin heme b_3. It should be noted that this signal is present in all the acquired spectrum (figure2.6). Additionally, one needs to keep in mind that: i) the *Ps. nautica* NOR heme b_3 is a low spin, ii) this center reduction is only accomplished at low redox potential, and that by other

means only a strong reducing agent will be able to fully reduce it, and iii) dithionite is not able to fully reduce both iron centers from the NORs active site, with Mössbauer determining 60 % reduction upon dithionite addition [12]. Therefore, this set of signals seems to arise from the catalytic diiron center and it corresponds to a heme-b_3-Fe^{III} species, combined with a ferric or ferrous Fe_B. The possibility of a mixed valence state for heme b_3-Fe^{III}-non-heme Fe_B^{II} should be excluded, since this species signal would increase under more reductive conditions, and the low field g = 6.34 signal decreases its intensity. Both Mössbauer and EPR spectroscopy show equal population ratios, measured either by the ferric /non-heme Fe_B percentage or by the intensity ratio of the g = 6.34 signal respectively, as it can be seen by the values presented in table 2.3. So, it is most likely that this signal is due to an integer-spin state rising from the low-spin heme b_3 - Fe^{III}-non-heme Fe_B^{III} [12].

Table 2.3 – Ratios determined with the Mössbuer and EPR results. The values where achieved by using the attributed percentage, or the intensity of the g = 6.34 signal, for Mössbauer and EPR, respectively [12].
.

	Mössbauer % total % (relative %)		**Ratio**	
	Heme b_3 –Fe^{III}	**Fe_B^{III}**	**Mössbauer**	**EPR**
As isolated	25 (100)	17 (68)	1	1
Ascorbate reduced	25 (100)	14 (56)	0.82	0.82
Dithionite reduced	10 (40)	10 (40)	0.59	0.59

The temperature dependence of the assumed g = 6 integer spin signal was characterized, as illustrated in figure 2.7, showing the decrease of its intensity with the rising temperatures. This result is in accordance with a ground state species for the assumed heme b_3-Fe^{III}-Fe_B^{III}.

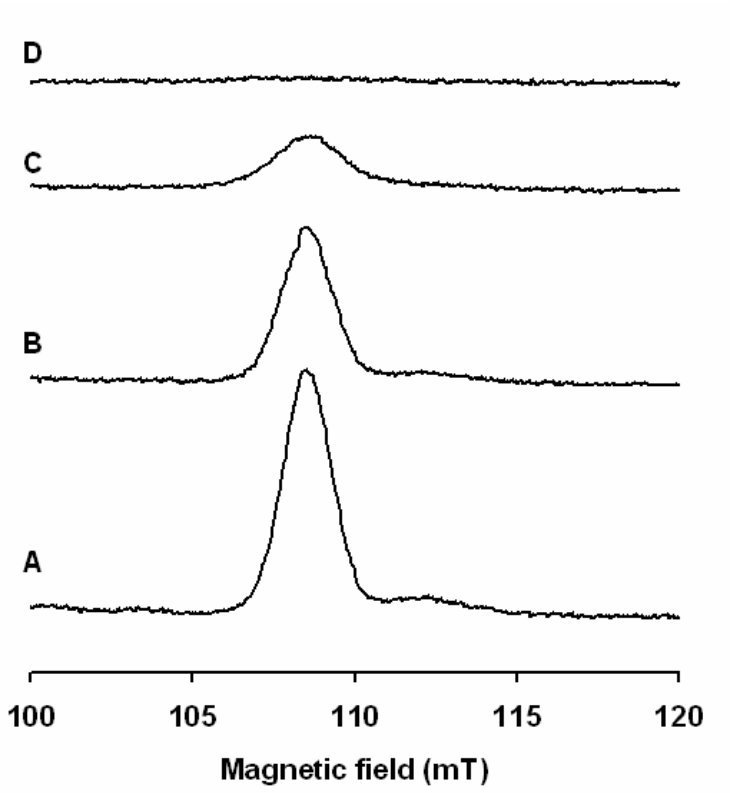

Figure 2.7 – Temperature dependence EPR spectra at 9.653 GHz of the dithionite reduced *Pseudomonas nautica* NOR (265 μM in 100 mM KPB, pH 7, 0.02% DDM, 0.01% PE). Experimental conditions of spectra: microwave power = 6.3 mW, modulation frequency = 100 kHz, modulation amplitude = 0.4 mT, receiver gain = 2×105, conversion time = 81.92 ms and time constant = 40.96 ms. Spectrum A was collected at 5.5 K, B at 7.0 K, C at 12 K, and spectrum D at 22.5 K.

The possibility of g = 6.34 to be due a ground state integer-spin can be further investigated under parallel mode. Preliminary spectra of the *Ps. nautica* NOR were recorded in parallel mode for the as-isolated and dithionate reduced sample. The change in the field orientation should bring evidence a more intense signal (up to 3×), but no relevant signal was detected in the low field region. Integer-spin systems exhibit powder sub-spectra with a high valued effected g_z, (spectral feature at low field) and two other low-valued effective g_{xy} values (usually at fields beyond detection). So the presence of a signal increase at low-field under parallel mode EPR should be followed by weaker and broader g_{xy} signals at slightly higher field in perpendicular mode [31]. Literature reports only a few binuclear iron center integer-spin systems, most of them composed by high-spin non-heme irons [32, 33]. Notably some exceptions exist, namely with the g = 12 resonance in *CcO*, attributed to a weak antiferromagnetic coupled ferric heme (S = 5/2) and a cupric ion (S =1/2), in which the parallel to perpendicular signal intensity ratio is much more smaller than the expected [30].

2.2.5. Three-Dimensional Structure Prediction

Nowadays it is possible to predict the three-dimensional structure of a certain protein based on its primary sequence. The SWISS-MODEL platform is a magnificent tool for this propose, since it is a fully automated protein structure homology-modelling server [34]. In this workspace is possible to submit a primary protein sequence, and in return, the program offers a three-dimensional model, based in homologue resolved structures.

Similar bioinformatic tools were used by others to predict the three-dimensional structure of the NorB subunit [2, 3]. Recently, *Ps. aeuruginosa* NOR crystal structure was solved and since the enzyme studied in this work shows a high homology with this one (62 % and 75 % for the NorC and NorB subunits, respectively), the predicted model obtained was based in this known structure [10].

Concerning the structure, the purpose of this section is to highlight once more the similarity between the *Ps. nautica* NOR and the other members of the HCuO superfamily, and in particular with the members of the cNOR subclass. The models achieved for the NorB and NorC subunits are presented in figure 2.8.

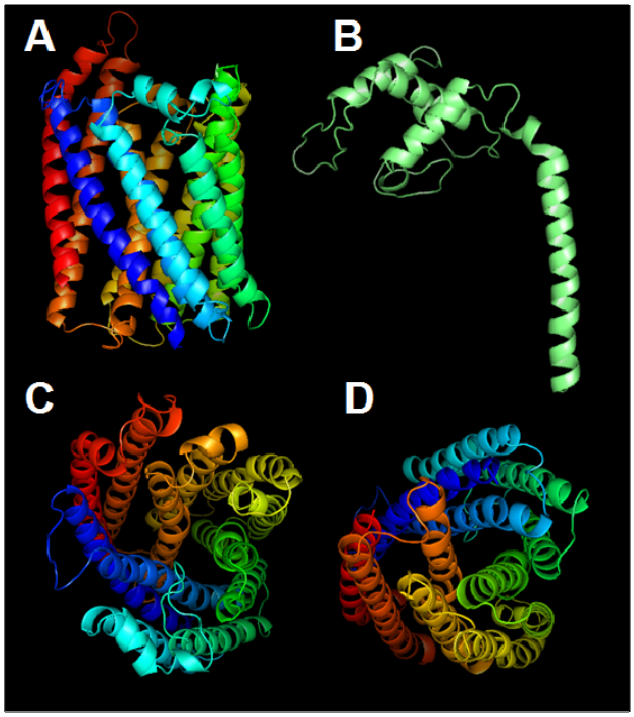

Figure 2.8 – Three-dimensional structure, predicted for the *Pseudomonas nautica* cNOR subunits. A, C and D show NorB subunit side, top and bottom view respectively. C shows NorC subunit. Models were achieved using SWISS-MODEL platform, and the obtained files treated with *Pymol* software.

The NorB molecular model generated is very similar to the ones previous predicted for this subunit in *Pa. denitrificans* and *Ps. stutzeri* [2, 3], showing an extremely hydrophobic subunit containing 12 transmembrane α-helixes, in accordance with the homologues from the *CcO* superfamily. The helixes surround the two heme *b* centers as well as the non-heme Fe_B [10] (as can be seen in figure 2.8 panel C and D). The NorC subunit seems to contain an N-terminal transmembrane α-helix, non-covalently bound to the NorB subunit, as revealed by the biochemical characterization, (figure 2.3) .

Steady-state kinetics assays using *Ps. nautica* NOR and its physiological electron donor (cyt. c_{552}), in the presence and abcence of specific fragment antibodies, point to the existence of a unique docking area for the cyt. c_{552} [35]. Several algorithms can be used in the future to predict docking implantations between a cNOR solved structure (or molecular models) with potential electron donors.

2.3. Concluding Remarks

The results described in this chapter show that the *Ps. nautica* NOR can be purified from the bacterial membrane fraction using DDM-based buffers. The purification yield is low, approximately only 3 % of the total protein extracted from the membrane. The purification protocol was optimized, in order to achieve reproducible samples, containing equal amount of co-factors, and purity, but still this task is extremely time consuming. The maximal purity coefficient obtained in this work was 1.2 (Abs 411/Abs 280) and the correct proportionality of the iron co-factors was accomplished.

The UV-visible results, demonstrate that the purified NOR exhibits the characteristic spectroscopic features of the reported cNORs [12, 21]. However, the lacking of a 595 nm charge transfer band in the enzyme spectra, and the appearance of a low-spin heme signal upon dithionite reduction to the previous ascorbate reduced sample, leads to believe that the catalytic heme iron is in a low-spin conformation [12]. This issue was solved using the Mössbauer spectroscopy results obtained by our research group [12], combined with the EPR results presented in this thesis. Together, they confirm irrefutably that the *Ps. nautica* NOR heme b_3 is six-coordinated, for both ferric and ferrous states.

The EPR data show for the first time preliminary results on a possible integer-spin species, rising from the antiferromagnetic coupled diiron catalytic center. A complete study of this binuclear iron center could be accomplished with low temperature EPR in both perpendicular and parallel mode, with temperature dependence, in order to pursuit the integer-spin signature as well as the possible presence of mixed valence species. These experiments can also give clues to the signals at g = 2.05 and 1.6, not yet assigned.

2.4. References

[1] Brown, K., M. Tegoni, M. Prudencio, A.S. Pereira, S. Besson, J.J. Moura, I. Moura and C. Cambillau, *A novel type of catalytic copper cluster in nitrous oxide reductase.* Nat Struct Biol, 2000. **7**(3): p. 191-5.

[2] Zumft, W.G., *Nitric oxide reductases of prokaryotes with emphasis on the respiratory, heme-copper oxidase type.* J Inorg Biochem, 2005. **99**(1): p. 194-215.

[3] Reimann, J., U. Flock, H. Lepp, A. Honigmann and P. Adelroth, *A pathway for protons in nitric oxide reductase from Paracoccus denitrificans.* Biochim Biophys Acta, 2007. **1767**(5): p. 362-73.

[4] Carr, G.J. and S.J. Ferguson, *The nitric oxide reductase of Paracoccus denitrificans.* Biochem J, 1990. **269**(2): p. 423-9.

[5] Hoglen, J. and T.C. Hollocher, *Purification and some characteristics of nitric oxide reductase-containing vesicles from Paracoccus denitrificans.* J Biol Chem, 1989. **264**(13): p. 7556-63.

[6] Sakurai, T., S. Nakashima, K. Kataoka, D. Seo and N. Sakurai, *Diverse NO reduction by Halomonas halodenitrificans nitric oxide reductase.* Biochem Biophys Res Commun, 2005. **333**(2): p. 483-7.

[7] Sakurai, T., N. Sakurai, H. Matsumoto, S. Hirota and O. Yamauchi, *Roles of four iron centers in Paracoccus halodenitrificans nitric oxide reductase.* Biochem Biophys Res Commun, 1998. **251**(1): p. 248-51.

[8] Heiss, B., K. Frunzke and W.G. Zumft, *Formation of the N-N bond from nitric oxide by a membrane-bound cytochrome bc complex of nitrate-respiring (denitrifying) Pseudomonas stutzeri.* J Bacteriol, 1989. **171**(6): p. 3288-97.

[9] Kastrau, D.H., B. Heiss, P.M. Kroneck and W.G. Zumft, *Nitric oxide reductase from Pseudomonas stutzeri, a novel cytochrome bc complex. Phospholipid requirement, electron paramagnetic resonance and redox properties.* Eur J Biochem, 1994. **222**(2): p. 293-303.

[10] Hino, T., Y. Matsumoto, S. Nagano, H. Sugimoto, Y. Fukumori, T. Murata, S. Iwata and Y. Shiro, *Structural basis of biological N2O generation by bacterial nitric oxide reductase.* Science, 2010. **330**(6011): p. 1666-70.

[11] Kumita, H., K. Matsuura, T. Hino, S. Takahashi, H. Hori, Y. Fukumori, I. Morishima and Y. Shiro, *NO reduction by nitric-oxide reductase from denitrifying bacterium Pseudomonas aeruginosa: characterization of reaction intermediates that appear in the single turnover cycle.* J Biol Chem, 2004. **279**(53): p. 55247-54.

[12] Timoteo, C.G., A.S. Pereira, C.E. Martins, S.G. Naik, A.G. Duarte, J.J. Moura, P. Tavares, B.H. Huynh and I. Moura, *Low-Spin Heme b3 in the Catalytic Center of Nitric Oxide Reductase from Pseudomonas nautica.* Biochemistry, 2011. **50**(20): p. 4251-4262.

[13] Cramm, R., A. Pohlmann and B. Friedrich, *Purification and characterization of the single-component nitric oxide reductase from Ralstonia eutropha H16.* FEBS Lett, 1999. **460**(1): p. 6-10.

[14] de Vries, S., M.J. Strampraad, S. Lu, P. Moenne-Loccoz and I. Schroder, *Purification and characterization of the MQH2:NO oxidoreductase from the hyperthermophilic archaeon Pyrobaculum aerophilum.* J Biol Chem, 2003. **278**(38): p. 35861-8.

[15] Suharti, M.J. Strampraad, I. Schroder and S. de Vries, *A novel copper A containing menaquinol NO reductase from Bacillus azotoformans.* Biochemistry, 2001. **40**(8): p. 2632-9.

[16] Schagger, H. and G. Vonjagow, *Tricine Sodium Dodecyl-Sulfate Polyacrylamide-Gel Electrophoresis for the Separation of Proteins in the Range from 1-Kda to 100-Kda.* Analytical Biochemistry, 1987. **166**(2): p. 368-379.

[17] Girsch, P. and S. de Vries, *Purification and initial kinetic and spectroscopic characterization of NO reductase from Paracoccus denitrificans.* Biochim Biophys Acta, 1997. **1318**(1-2): p. 202-16.

[18] Berry, E.A. and B.L. Trumpower, *Simultaneous Determination of Hemes-a, Hemes-B, and Hemes-C from Pyridine Hemochrome Spectra.* Analytical Biochemistry, 1987. **161**(1): p. 1-15.

[19] Fischer, D.S. and D.C. Price, *Simple Serum Iron Method Using New Sensitive Chromogen Tripyridyl-S-Triazine.* Clinical Chemistry, 1964. **10**(1): p. 21-&.

[20] Watmough, N.J., S.J. Field, R.J. Hughes and D.J. Richardson, *The bacterial respiratory nitric oxide reductase.* Biochem Soc Trans, 2009. **37**(Pt 2): p. 392-9.

[21] Field, S.J., F.H. Thorndycroft, A.D. Matorin, D.J. Richardson and N.J. Watmough, *The respiratory nitric oxide reductase (NorBC) from Paracoccus denitrificans.* Methods Enzymol, 2008. **437**: p. 79-101.

[22] Hendriks, J., A. Warne, U. Gohlke, T. Haltia, C. Ludovici, M. Lubben and M. Saraste, *The active site of the bacterial nitric oxide reductase is a dinuclear iron center.* Biochemistry, 1998. **37**(38): p. 13102-9.

[23] Field, S.J., L. Prior, M.D. Roldan, M.R. Cheesman, A.J. Thomson, S. Spiro, J.N. Butt, N.J. Watmough and D.J. Richardson, *Spectral properties of bacterial nitric-oxide reductase: resolution of pH-dependent forms of the active site heme b3.* J Biol Chem, 2002. **277**(23): p. 20146-50.

[24] Fujiwara, T. and Y. Fukumori, *Cytochrome cb-type nitric oxide reductase with cytochrome c oxidase activity from Paracoccus denitrificans ATCC 35512.* J Bacteriol, 1996. **178**(7): p. 1866-71.

[25] Sakurai, N. and T. Sakurai, *Isolation and characterization of nitric oxide reductase from Paracoccus halodenitrificans.* Biochemistry, 1997. **36**(45): p. 13809-15.

[26] Cheesman, M.R., W.G. Zumft and A.J. Thomson, *The MCD and EPR of the heme centers of nitric oxide reductase from Pseudomonas stutzeri: Evidence that the enzyme is structurally related to the heme-copper oxidases.* Biochemistry, 1998. **37**(11): p. 3994-4000.

[27] Oubrie, A., S. Gemeinhardt, S. Field, S. Marritt, A.J. Thomson, M. Saraste and D.J. Richardson, *Properties of a soluble domain of subunit C of a bacterial nitric oxide reductase.* Biochemistry, 2002. **41**(35): p. 10858-65.

[28] Aasa, R. and T. Vanngard, *Epr Signal Intensity and Powder Shapes - Re-Examination.* Journal of Magnetic Resonance, 1975. **19**(3): p. 308-315.

[29] De Vries, S. and S.P.J. Albracht, *Intensity of Highly Anisotropic Low-Spin Heme Epr Signals.* Biochim Biophys Acta, 1979. **546**(2): p. 334-340.

[30] Hendrich, M.P. and P.G. Debrunner, *Integer-Spin Electron-Paramagnetic Resonance of Iron Proteins.* Biophysical Journal, 1989. **56**(3): p. 489-506.

[31] Hagen, W.R., *EPR spectroscopy as a probe of metal centres in biological systems.* Dalton Transactions, 2006(37): p. 4415-4434.

[32] Pikus, J.D., J.M. Studts, C. Achim, K.E. Kauffmann, E. Munck, R.J. Steffan, K. McClay and B.G. Fox, *Recombinant toluene-4-monooxygenase: Catalytic and Mossbauer studies of the purified diiron and Rieske components of a four-protein complex.* Biochemistry, 1996. **35**(28): p. 9106-9119.

[33] Cadieux, E., V. Vrajmasu, C. Achim, J. Powlowski and E. Munck, *Biochemical, Mossbauer, and EPR studies of the Diiron cluster of phenol hydroxylase from Pseudomonas sp strain CF 600.* Biochemistry, 2002. **41**(34): p. 10680-10691.

[34] Arnold, K., L. Bordoli, J. Kopp and T. Schwede, *The SWISS-MODEL workspace: a web-based environment for protein structure homology modelling.* Bioinformatics, 2006. **22**(2): p. 195-201.

[35] Conrath, K., A.S. Pereira, C.E. Martins, C.G. Timoteo, P. Tavares, S. Spinelli, J. Kinne, C. Flaudrops, C. Cambillau, S. Muyldermans, I. Moura, J.J. Moura, M. Tegoni and A. Desmyter, *Camelid nanobodies raised against an integral membrane enzyme, nitric oxide reductase.* Protein Sci, 2009. **18**(3): p. 619-28.

CHAPTER 3

Pseudomonas nautica NOR: ELECTROCHEMICAL CHARACTERIZATION

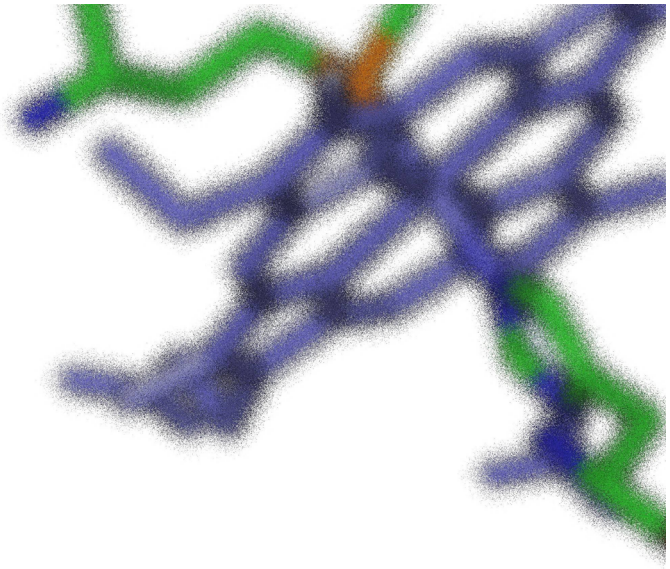

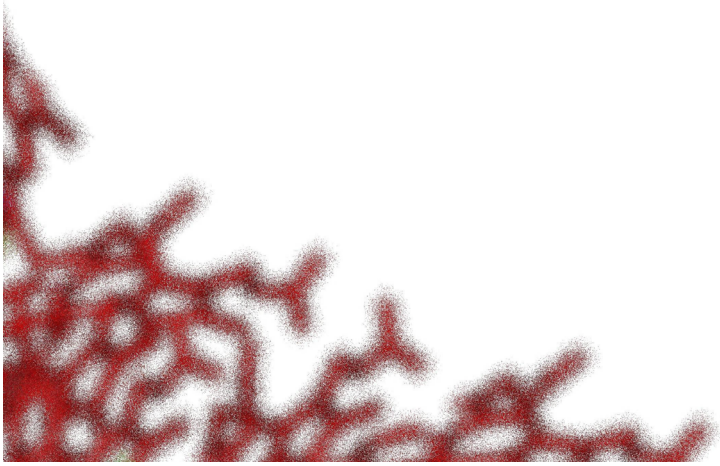

Chapter 3 *Pseudomonas nautica* NOR: Electrochemical Characterization

3. *Pseudomonas nautica* NOR: Electrochemical Characterization

3.1. Applied Methods and Objectives

Over the last years, electrochemistry has proven to be both, a useful means to understand the biochemistry of metalloproteins and enzymes, and a powerful method for the exploration of these proteins in biosensors and bioelectronics. The principles underlining electrochemical methods are well established and knowledge of the structure/function of metalloproteins is increasingly available [1].

When using proteins in direct electrochemical experiments, the main goal is to replace the protein's electron donor for an electrode, and therefore study the electroactive or electrocatalytic response, in case of an enzyme. Many strategies have been used to enhance the electronic transfer from and through the proteins and electrodes. Different methods can go from a simple classic bulk solution, in the presence or absence of chemical mediators, to more complex methods such as the immobilization of the biological material at the electrode surface. For this propose there are several approaches that can depend on the electrode material, surface, and the biological sample's nature. Examples of typical techniques used to immobilize proteins can be mentioned, such as: protein bound to gold electrodes via a specific residue, typically a Cys; protein anchored via a His-tag or a biotin-avidin group; the protein immobilization in a lipid layer membrane; protein adsorbed on a Self Assembled Monolayer (SAM) of alkanothiol groups; or the entrapment of the biological material in a layer-by-layer system. Several changes to these techniques are reported constantly in order to achieve a better electrochemical response [1-4].

Protein immobilization has demonstrated to be an effective methodology for studying high electron transfer rates, conferring advantages since it is simple, easy to prepare, economic, and in some cases, simplification of the theoretical analysis can be done, since without diffusion, Laviron's approximation can be applied [4-11].

Cyclic voltammetry (CV) is an electrochemical technique, in which the potential is ramped linearly versus time. When the potential reaches a set maximal value, the potential ramp is inverted. This inversion potential can be multiple and set according to the studied system. The current is plotted against the applied voltage to give the voltammogram trace [12]. Cyclic voltammetry is a useful method to apply in electrochemical studies and has

been used to study metalloproteins and their active sites for the passed decades [11]. This technique became a routine tool for determining formal potential of redox centers and it is also a powerful method to study the catalytic activity of a specific enzyme [13, 14]

The NOR was purified from *Ps. nautica* membranes extracts, biochemical and spectroscopically characterized, as described in the chapter 2. The major aim of this part of the studies is the investigation of the direct electrochemical response of this protein, in the presence and absence of substrate, in order to:

i) discriminate between the four redox processes associated to the different metal co-factors;
ii) study the electrocatalytic response of the enzyme towards NO and O_2;
iii) quantify the number of electrons involved in the two catalytic processes.

3.2. The NOR Redox Potentials Overview

The *Pa. denitrificans* NOR formal redox potentials were reported by Grönberg and co-workers, and their results show a large positive potential for the heme *c*, heme *b* and the non-heme Fe_B (310, 345 and 320 mV *vs* NHE, pH 7.6, respectively), and a much lower redox potential for the heme b_3 (60 mV *vs* NHE, pH 7.6). The large difference of the redox potentials, between the heme b_3 and the other centers was explained as a benefit for the rapid electron transfer from the physiological electron donor towards the active site and as a thermodynamic barrier to the complete reduction of the binuclear Fe center [15]. A reprisal of this values was performed recently confirming the previous reported, suggesting that the heme b_3 and the non-heme Fe_B are isopotetntial [16].

Ps. nautica NOR visible oxidation/reduction titration points toward a heme *c* and heme *b* redox potential in the same magnitude, separated from the heme b_3 by approximately 200 mV, confirming the values previously reported: + 232 mV (*vs* NHE, pH 7.0) for the heme *c* and *b* and -16 mV (*vs* NHE, pH 7.0) for the catalytic heme b_3 [15, 17]. Direct electrochemistry was used to study the *Ps. nautica* NOR, the results show the presence of a redox process, highly scan rate dependent. This process presented a midpoint redox potential of -126 mV (*vs* NHE, pH 7.6) and was indexed to the catalytic diiron center, probably to the, until then, assumed high-spin heme b_3 [6].

3.3. The *Ps. nautica* NOR: Direct Electron Transfer

The *Ps. nautica* NOR electrochemical response was accomplished in this work, by adsorbing the enzyme to a pyrolytic graphite electrode. CV was used in order to investigate this enzyme redox processes on a graphite modified electrode.

The enzyme was immobilized to the electrode surface using the cast away technique (experimental details). The electrode was immersed in a mixed buffer solution, chosen in agreement with previous experiments conducted in our research group [6]. The buffer ionic strength (20 mM) revealed to be appropriated to conduct all the experiments, since it is a mixed buffer, designed to a wide pH range. Also the system presented good

conductivity not showing ohmic drop issues and the buffer concentration is high enough to eliminate mass transfer due to migration.

During these studies, different preparations were made. The achieved results were consistent, revealing the reproducibility of the studied system. It should be mentioned that the *Ps. nautica* NOR film at the electrode was stable, since it was possible to work in some cases, during 10 hours, performing more than 150 cyclic voltammograms and in the end, the electrochemical response obtained was comparable. The stability of the enzyme film can be due to the presence of detergent in the protein buffer, added to avoid protein loss of structure, as reported before [6].

In the obtained results it is possible to distinguish four redox processes (figure 3.1). Two of them were observed at positive potential values, between 0 and 300 mV (*vs.* NHE), and they were attributed to the electron transfer heme centers, the hemes *c* and *b* (processes III and IV, section 3.3.1.). The remaining processes (I and II), are present at low potential values, between 0 and -400 mV (*vs.* NHE), and they are most likely rising from the catalytic center heme b_3 and Fe_B (section 3.3.3.).

Different scan rates were used to study the *Ps. nautica* NOR modified electrode (from 5 to 5000 mVs^{-1}), since different processes can only be observed at high scan rate (process I and II) and others processes (III and IV) are better observed at low scan rates (not higher than 500 mVs^{-1}).

The potential range used was chosen according to the experiments. Although this potential window was not increased further in the negative potential range, since at extreme negative potentials, H_2 is formed due to solvent reduction. The potential was not gone further than 600 mV (*vs.* NHE), due to the possible formation of oxide species in the graphite surface.

Figure 3.1 shows a set of cyclic voltammograms obtained with the immobilized *Ps. nautica* NOR. The presented insets show a detailed view of the anodic and cathodic waves (figure 3.1, panel B and C, respectively). The overlap of these voltammetric curves is intended to show the different dependence of each signal with the scan rate. To determine the peak redox potential for each one of the processes, every acquired voltammogram was analysed independently and with the correspondent control experiment, performed in the same electrolyte solution, at the same scan rate, without the immobilized enzyme, or in some cases, in the presence of equal amount (in volume) of

the enzyme's buffer (since this buffer contains a surfactant, used to avoid the protein's precipitation).

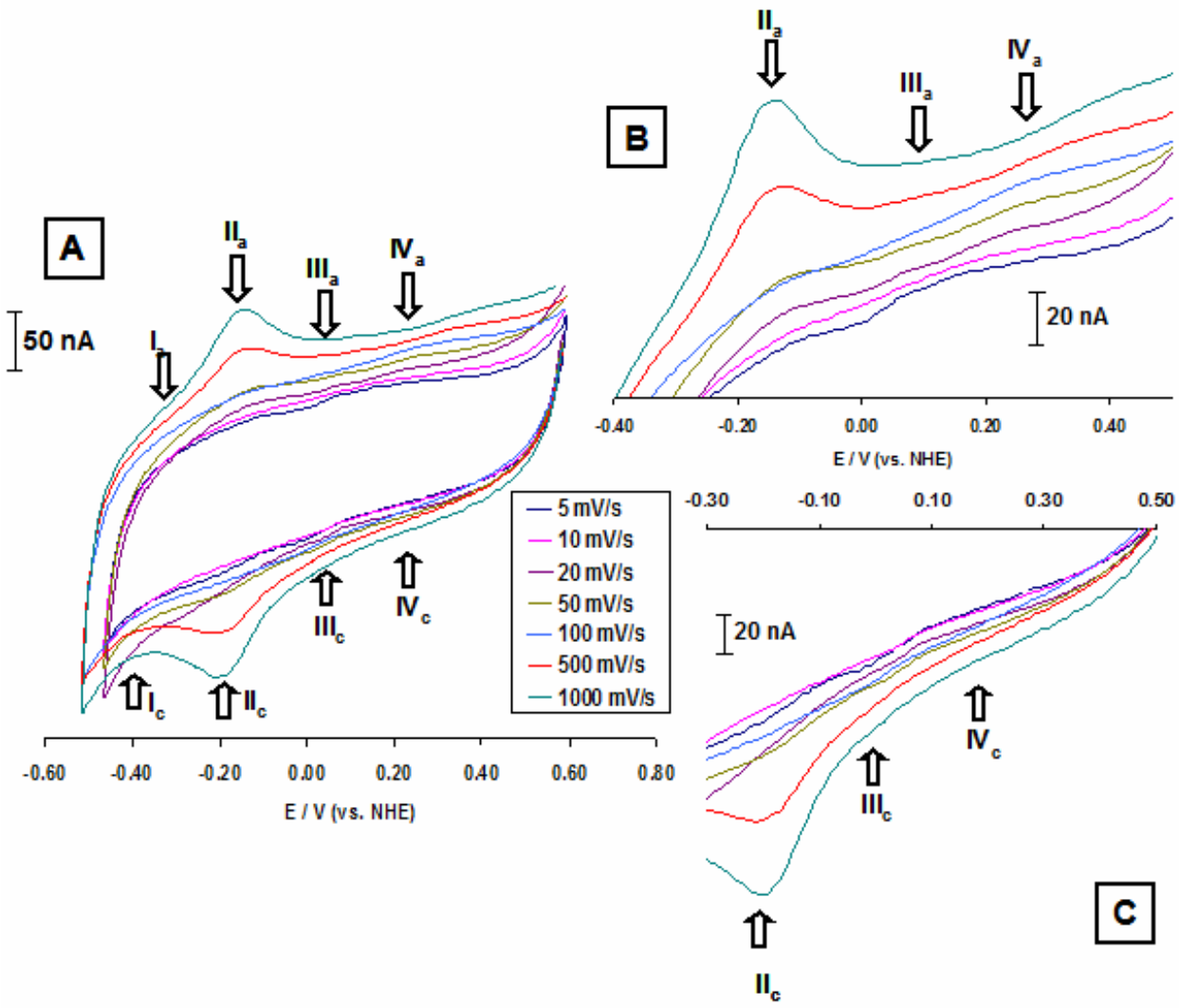

Figure 3.1 – Plot of the *Pseudomonas nautica* NOR cyclic voltammograms at different scan rates. Arrows point the region where the processes I to IV are developed in the anodic and cathodic waves (panel A). Panel B and C show an detailed view of the anodic and cathodic waves, respectively. The current intensities for the voltammograms performed with scan rates larger than 5 mVs^{-1} were corrected with convenient correction factors, in order to make comparison easier. The voltammograms were obtained as described in experimental details and the electrolyte solution was a 20 mM mixture buffer equilibrated at pH 7.63.

When overlapping the voltammograms performed at different scan rates, process I is not distinguished. Moreover, several voltammograms will be shown in detail to elucidate the four redox processes.

As studied before [6], process II shows a high scan rate dependence, increasing the current intensity with the scan rate increase. The same was observed for process I and an opposite effect in processes III and IV that became more evident when using scan rates not higher than 500 mVs^{-1}. From this observation, qualitative information can be extracted. Since process I and II are more evident when using high scan rates, it is most likely that they present higher heterogeneous rate constants (k_s) when compared with processes III and IV.

Figure 3.2 shown one of the voltammograms obtained with the immobilized *Ps. nautica* NOR, performed at 500 mVs^{-1}, with the correspondent control experiment, achieved with the same electrode, without the immobilized protein (panel A). This voltammogram were chosen from a typical set of experimental results obtained (for more examples check supporting information S.9.1), with the aim to elucidate the result analysis performed for the different scan rates studied (and pH values, section 3.4). A cautious analysis of the ΔEp (values presented in support information S.9.2) lead to believe that the process is reversible.

Observing these two voltammograms, the first process to be identified was the process II, due to the previously mentioned high scan rate dependence [6]. A closer observation of the negative potential region suggests the presence of a redox couple (process I), being this confirmed when a subtraction is performed between the referred voltammograms (panel B). Analogously, a careful observation of the positive potential region of the figure 3.2 (panel A), proposes the presence of the mentioned redox couples III and IV, and the subtraction (panel B) clearly shows them.

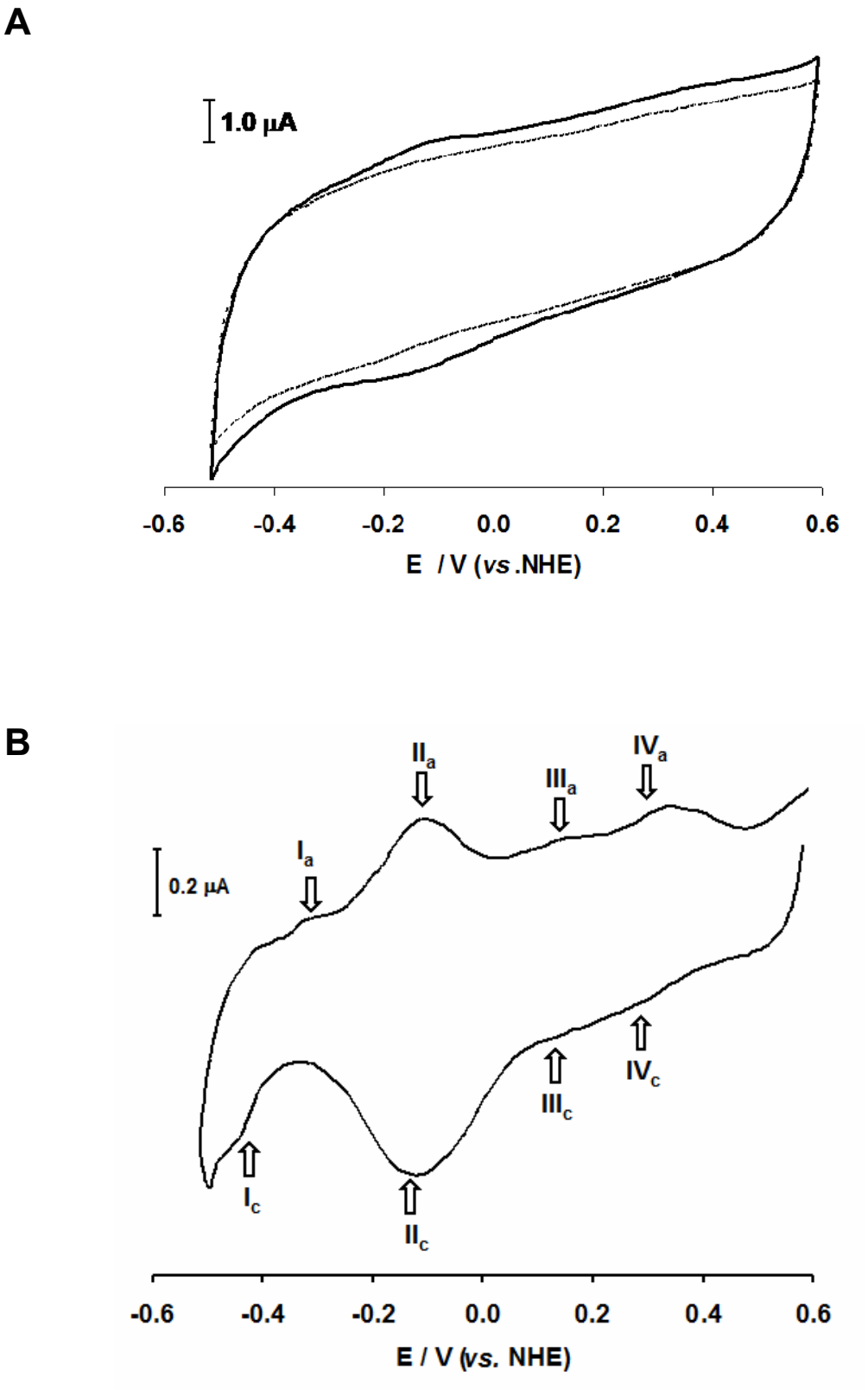

Figure 3.2 – Cyclic voltammogram of the immobilized *Pseudomonas nautica* NOR. Panel A shows the cyclic voltammogram at 500 $mV.s^{-1}$ (black line) and the correspondent control experiment (without protein, dashed line). Panel B shows the previous voltammograms subtraction (black line minus dashed line). The arrows point towards the anodic and cathodic peaks for the identified redox processes. Experiments were conducted in 20 mM mixture buffer (experimental details) pH 7.15.

To the redox processes I to IV it was attributed a one electron transfer process, suggested by the peak width at half height (experimental results presented in supporting information S.9.2). According to the equation 3.1, and assuming a reversible process, it is possible to estimate the number of electrons involved in each one of the identified redox couples.

$$\Delta E_{P,1/2} = 3.53\frac{RT}{nF} \qquad \text{(eq. 3.1)}$$

In this equation the terms R, T and F stand for the ideal gas constant (8.31 J $mol^{-1}K^{-1}$), temperature (K), and the Faraday constant (96485 C mol^{-1}), respectively, and n the number of electrons involved in the redox process. The achieved values for $Ep_{w.1/2}$ are resumed in supporting information S.9.2, as well as the number of electrons estimated for each redox process. In the present work the temperature was 20 ºC.

Surface coverage (Γ) for each trial can be estimated using the process II, applying the following equation:

$$\Gamma = \frac{Q}{nFA} \qquad \text{(eq. 3.2)}$$

where Q is the charge involved in the reaction process, n the number of electrons transferred, F the Faraday constant and A the electrode area [6, 12]. In this case Γ can be used to normalize kinetic experiment results (chapter 4) since it determines the number of active enzyme molecules at the electrode surface, and can also be used to identify the presence of a protein multilayer layer at the electrode surface. Considering n = 1 and the electrode geometric area (0.126 cm^2), the average value attained was $1.72 \pm 0.77 \times 10^{-11}$ $mol.cm^{-2}$ was and the maximum value attained was $2.37 \pm 0.27 \times 10^{-11}$ $mol.cm^{-2}$, from all the executed preparations. However it will be impossible to evaluate the presence of a multilayer, since only the X-ray structure of the *Ps. aeruginosa* NOR is available, as well as molecular models for other homologue proteins [18-20], like the one presented for the *Ps. nautica* NOR in the previous chapter. Using the information from the molecular models can lead to a wrong estimative for the presence of a multilayer at the electrode surface.

It is possible to assume the physical adsorption of the protein to the electrode surface, because:

i) The voltammograms made without protein (control experiments) are clearly different from the obtained with the immobilized protein (figure 3.2, panel A).

ii) All the redox processes present a small and constant separation between their potential peaks (ΔEp) with the scan rate variation.

iii) The current intensity increases with the scan rate, and the ratio between the intensity of the cathodic and anodic peaks is close to one.

These characteristics are common for a surface confined process [6, 7, 21]. Usually, for a reversible process the ΔEp should be zero, however for quasi-reversible processes the ΔEp is different from zero. The midpoint redox potentials for each process were determined by the average of the cathodic and anodic peak potentials ($(Ep_c + Ep_a) / 2$). [12].

The results obtained for the four redox processes will be further shown within this chapter.

3.3.1. The Electron Transfer Heme *b* and Heme *c*

The processes III and IV, observed at higher redox potentials, were attributed to the electron transfer hemes, the low-spin heme *b* and heme *c*. These processes are more well defined when using scan rates not higher than 500 mVs^{-1}.

The identification of the redox processes within the window of potential used can be very difficult, because there is the possibility of oxide species formation at the graphite electrode surface, leading to misinterpretation of the voltammograms. The analysis of the results required the use of control experiments, file subtractions for the multiple scan rate voltammetric waves obtained. A difference between voltammograms is presented in figure 3.3 (panel D) and the processes highlighted by arrows.

The spectroscopic studies done here (chapter 2) demonstrated that electron transfer hemes *b* and *c* are totally reduced in the presence of sodium ascorbate, suggesting a midpoint redox potential higher than 0 mV (*vs.* NHE) [16, 17, 22]. The processes exhibited 43 and 208 mV (*vs.* NHE) at pH 7.63 for III and IV, respectively. Process IV is indexed to the low-spin heme *c* unequivocally. It corresponds to the higher redox potential, since it is believed that NorC subunit interacts directly with the NOR's physiological electron donor, the cyt. c_{552} and therefore it may be the co-factor responsible for the electrons entrance [23], and consequent transference to the next electron transfer co-factor (heme *b*). Additionally, electrochemical experiments performed with the recombinant NorC subunit (rNorC, described in section 3.3.2), show a redox potential in the same range

The remaining process III is attributed to the heme *b*. It presents a lower midpoint redox potential, when compared with the heme *c*, favourable for the electron transfer between the two centers, a common feature in intramolecular redox processes already proposed for the NORs and other proteins such as the bacterial cytochrome *c* peroxidase [15, 24, 25].

.

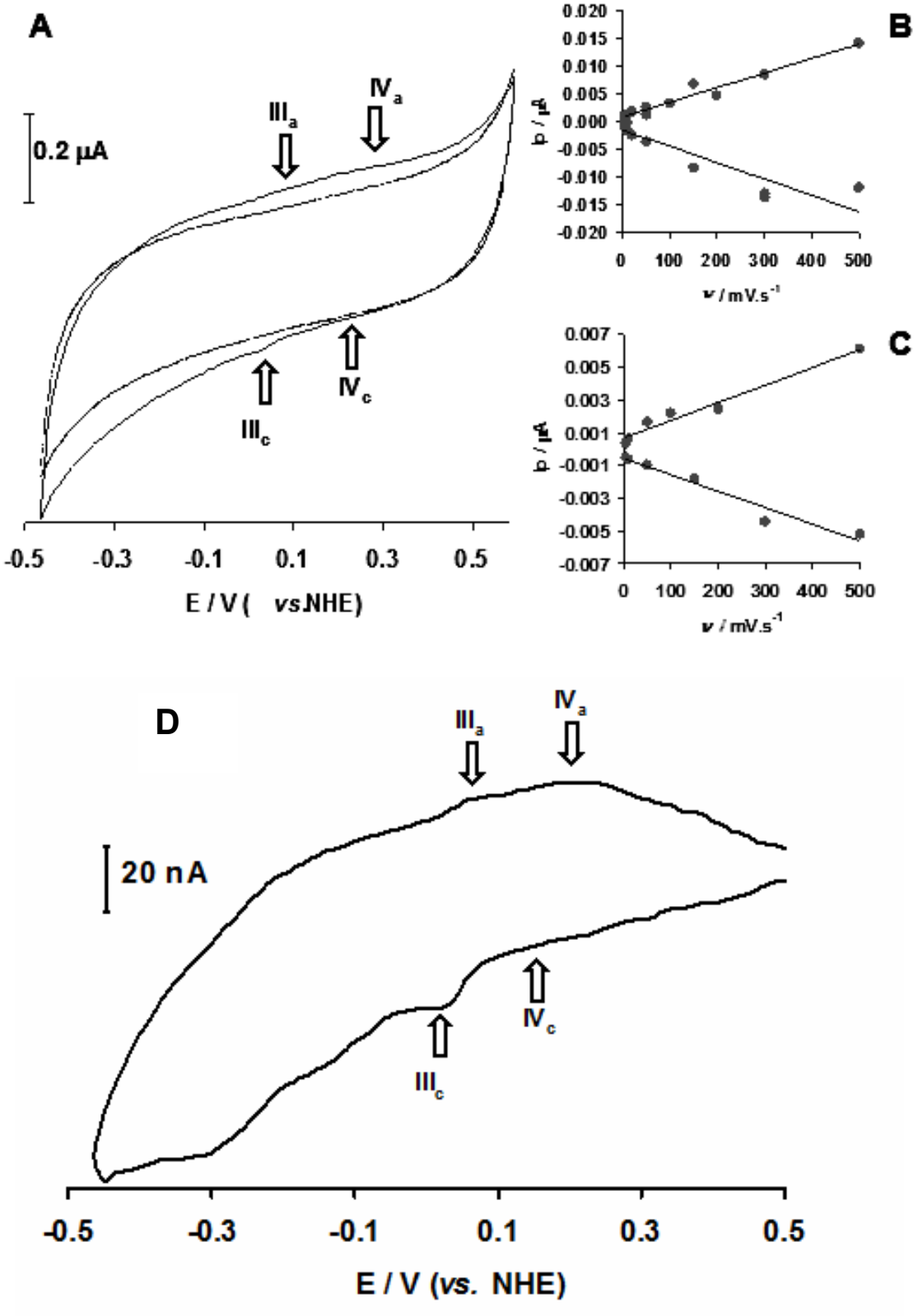

Figure 3.3 – Low–spin electron transfer heme redox processes. Panel A shows the low scan rate cyclic voltammogram (20 mV.s^{-1}) of the immobilized *Pseudomonas nautica* NOR on a graphite electrode (black line) and control experiment (without protein, dashed line), panel D shows the previous voltammograms subtraction (black line minus dashed line), the arrows point the anodic and cathodic peaks for identified redox processes. Panel B and C present the plot of the peak current *vs.* scan rate for processes III and IV respectively. For an adsorbed process with no mass transfer limitations, the current intensity (I) is given by the expression: $I = n^2F^2\nu A\Gamma/4RT$. Experiments were conducted in 20 mM mixture buffer (experimental details) pH 7.63.

The low-spin heme *b* and heme *c* redox potentials are lower than the previously described by visible titration [15, 17]. This fact can be due to protein immobilization, besides there are studies that show that the immobilization on a surface can lower the midpoint redox potential value of the proteins metallic centers [26, 27].

Using the Laviron's formulation (supporting information S.4) [8] it is possible to determine the k_s for both redox centers. The values obtained for the heme *c* and heme *b* are similar, 47 and 46 s^{-1} respectively. This is in agreement with other electron transfer rates determined for heme proteins [28].

Figure 3.3, panel B and C show the current peak intensity on scan rate dependence for both cathodic and anodic peaks. As it is shown, they increase proportionally and their ratio is close to one. Together with the previous mention facts (small peak potential separation and different line shapes for the assayed voltammograms and control experiments), it is assumed the *Ps. nautica* NOR immobilization.

3.3.2. The Recombinant NorC Subunit

To confirm the high redox potential attributed to the heme *c* co-factor, the direct electrochemical response of the purified recombinant NorC subunit (rNorC) was investigated.

The open reading frame (ORF) containing the NorC coding sequence was cloned as it is described in supporting information S.3. Heterologous overexpression, purification, biochemical and spectroscopic characterization were done in our research group [29]. In summary, the sample was purified from *E. coli* extracts using specific fragment antibodies [23]. The use of biochemical and spectroscopic techniques, revealed that the purified sample contained a heme:protein ratio of 1.3, achieved by the pyridine-hemocromogen method. UV-visible and EPR data pointed heme *c* characteristic features in the isolated sample [29, 30] .

The antibody-rNorC complex was immobilized in the pyrolytic graphite electrode, and cyclic voltammetry was used to investigate its direct electron transference. Analogously to the previous described for the native *Ps. nautica* NOR assays, control experiments were done in parallel without the adsorbed rNorC, but in the presence, (or without) of the protein's buffer. The buffer used was a 100 mM KPB pH 7, 0.02 % (w/v) DDM, 0.01 % (v/v) PE, equal to the one present in the native NOR, because the rNorC sample was buffer exchange to this same buffer (experimental details).

Scan rate dependence was performed using the rNorC modified electrode, and the assays were done, as described previously for the experiments performed with the native NOR enzyme.

One of the many performed cyclic voltammograms obtained with the antibody-rNorC complex immobilized on the electrode surface is presented in figure 3.4 (additional voltammograms and subtraction are present in supporting information S.9.3), as well as a linear baseline correction and a voltammogram subtraction. As it can be seen, the voltammogram trace for the control experiment is different from the assayed, indicating the physical adsorption of the protein.

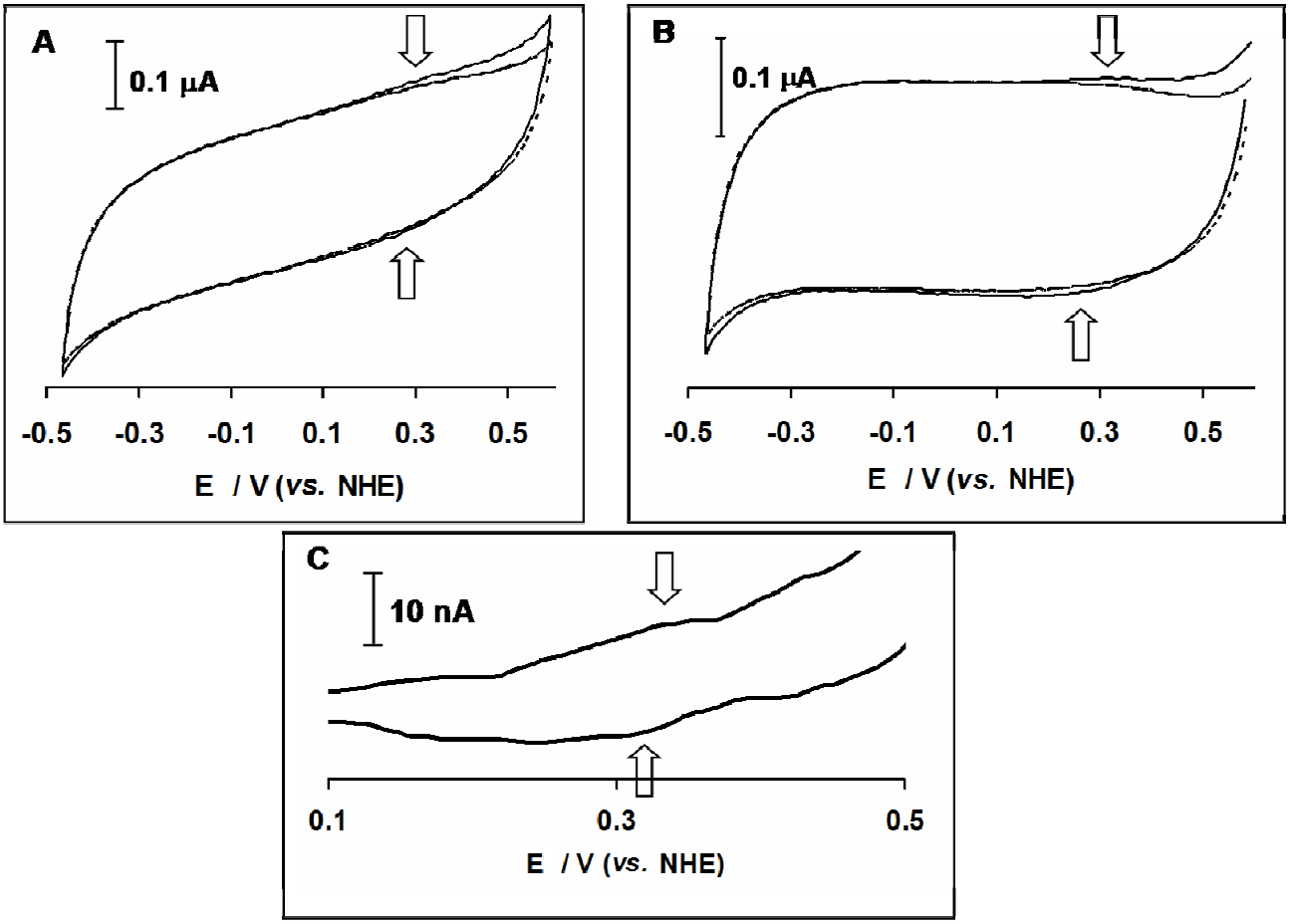

Figure 3.4 – Cyclic voltammogram of the immobilized recombinant *Pseudomonas nautica* rNorC subunit. Panel A and B show the cyclic voltammogram (10 $mV.s^{-1}$) and a linear corrected voltammogram (black lines) respectively, with the correspondent control experiment (without protein, dashed line). Panel C shows the difference voltammograms present in the panel A (black line minus dashed line). Experiments were conducted in 20 mM mixture buffer (experimental details) pH 7.63.

The identification of the cathodic and anodic peaks was extremely difficult, not only they have a low current intensity, due to the low concentration of the sample, but also they can be misunderstood by the oxide species formation at the electrodes surface, at high potential.

The analysis of the achieved voltammograms performed at different scan rates was done independently, in order to determine the midpoint redox potential, of the observed redox process (figure 3.4), which gave a value of 298 ± 19 mV.

The recombinant subunit presents a slightly higher redox potential when compared to the previously assigned process IV (208 mV, *vs.* NHE). It should be noted that the rNorC

protein used forms a complex with the specific antibody, from which there is no information on the epitopes coordinates, nor on the surface interface in contact with the electrode. The unique information available is the high dissociation constant between this two proteins, and that the physiological electron donor is unable to interact with the native enzyme when the antibody is bound (VHH 03) [23]. The presence of the specific antibody fragment and the absence of the NorB subunit could lead to a higher midpoint redox potential, for the heme *c* in the rNorC.

An increase in the heme redox potential can be due to other reasons. Literature suggests higher midpoint redox potential for heme proteins that are totally fold and that confine the heme cavity to a smaller solvent exposure [31]. It is unwise to say that the rNorC presents a smaller heme *c* exposure to the solvent, when dissociated from the NorB subunit and connected to the antibody. However, one should mention, the difference detected between the heme *c* midpoint redox potential determined in the wild-type NOR and in the rNorC subunit, which is probably due to structural changes in the three-dimensional structure, near the heme center.

The k_s was not determined for the antibody–rNorC complex, since the peaks were poorly defined which could lead to a wrong estimated value, and also because the value would not be comparable to the one obtained using the heterodimeric NOR.

3.3.3. The Diiron Catalytic Center

The remaining redox potentials (process I and II, figure 3.5) are attributable to the catalytic binuclear center. So far, the midpoint redox potential for the catalytic heme co-factor has been suggested to be lower than the non-heme Fe_B (proposed to be close to the value determined for the other co-factors, heme *b* and *c*) [15]. Spectroscopic titrations point to a midpoint redox potential for the heme b_3 of + 60 mV (*vs.* NHE) in the *Pa. denitrificans* NOR [15] and -38 mV (*vs.* NHE) in the *Ps. nautica* NOR [17]. More recently it was proposed that when the bridge between the two irons is cleaved and substrate connects to the low-spin heme b_3, this value reaches the same magnitude of the electron transfer heme *b* [16]. However it should be noted that most of the reported experiments were done with spectroscopic techniques using the ligand-to-metal charge transfer band at 595 nm, associated with the high-spin ferric heme b_3 without the proximal His ligand [15, 16, 32]. The studies performed in the *Ps. nautica* NOR by our group prove unequivocally that heme b_3 is a low-spin and that the active site reduction is only possible in the presence of a strong reducing agent [17]. The direct electrochemical response of this enzyme was studied by cyclic voltammetry in the same research group, where it was characterized a well-defined redox couple with a midpoint redox potential of -126 mV (*vs.* NHE) and highly scan rate dependent [6].

The experiments done here show a low redox potential value for the catalytic binuclear center (figure 3.5, A). The process II was indexed to the low-spin heme b_3 center since a similar value of -162 ± 19 mV (*vs.* NHE) was determined [6]. The present results point to a non-heme Fe_B midpoint redox potential (process I) more negative than the determined for the heme b_3.

The lower midpoint redox potential achieved was -369 ± 14 mV (*vs.* NHE) and was indexed to the non-heme Fe_B (process I, figure 3.5). Until the publication of this thesis, only UV-visible titrations were able to determine this co-factor redox potential, and the value was similar to the electron transfer heme centers [15]. This work is the first evidence of a redox process occurring within the negative potential range, beyond the catalytic heme b_3 midpoint redox potential. A lower redox potential for the catalytic diiron center is also suggested by biochemical and spectroscopic studies in the *Ps. nautica* NOR. This enzyme active form is the four electron reduced form, and Mössbauer spectroscopy

confirms that the catalytic center is not reduced in the presence of ascorbate, like the electron transfer hemes. Its reduction is only obtained with the use of a strong reducing agent (such as sodium dithionite, -0.66 mV at pH 7.0 [33]), suggesting a lower redox potential for the heme b_3 and the Fe_B, since this reducing agent is only able to reduce 60% of the catalytic binuclear site [17].

Here, the *Ps. nautica* NOR shows a difference of approximately 300 mV between the low-spin heme *c* and the heme b_3 co-factors midpoint redox potentials. This is in agreement with other works which reported cNORs redox potential intervals of 200-300 mV [15, 17]. Another common feature of the cNORs is the high heme *c* potential, coupled to the acceptance of electrons to the enzyme from the physiological electron donor, and its intramolecular transfer to the centers with lower redox potential.

Interestingly, the value of the catalytic heme b_3 redox potential varies between -162 mV (found here with electrochemical analysis, and -126 mV ref. [6]) and -38 or + 60 mV done by visible titrations [15, 17]. This could be due to the different techniques applied, since the enzyme immobilization on a surface can lower the midpoint redox potential value of the proteins metallic centers [26, 27], and/or to the experimental conditions, such as pH and ionic strength which varied between the different works.

In addition, spectroelectrochemistry applied to a rational designed myoglobin, that contained a NOR catalytic center, show that the heme b_3 redox potential is of the same magnitude of the reported, but highly dependent on the metal that is in the other position of the catalytic center (the Fe_B site) [34, 35].

The low midpoint redox potential of the heme b_3, was suggested to be a thermodynamic barrier to the complete catalytic center reduction [15]. The results here presented seem to indicate that the non-heme Fe_B is the responsible for this barrier, since is the redox center with the lowest potential.

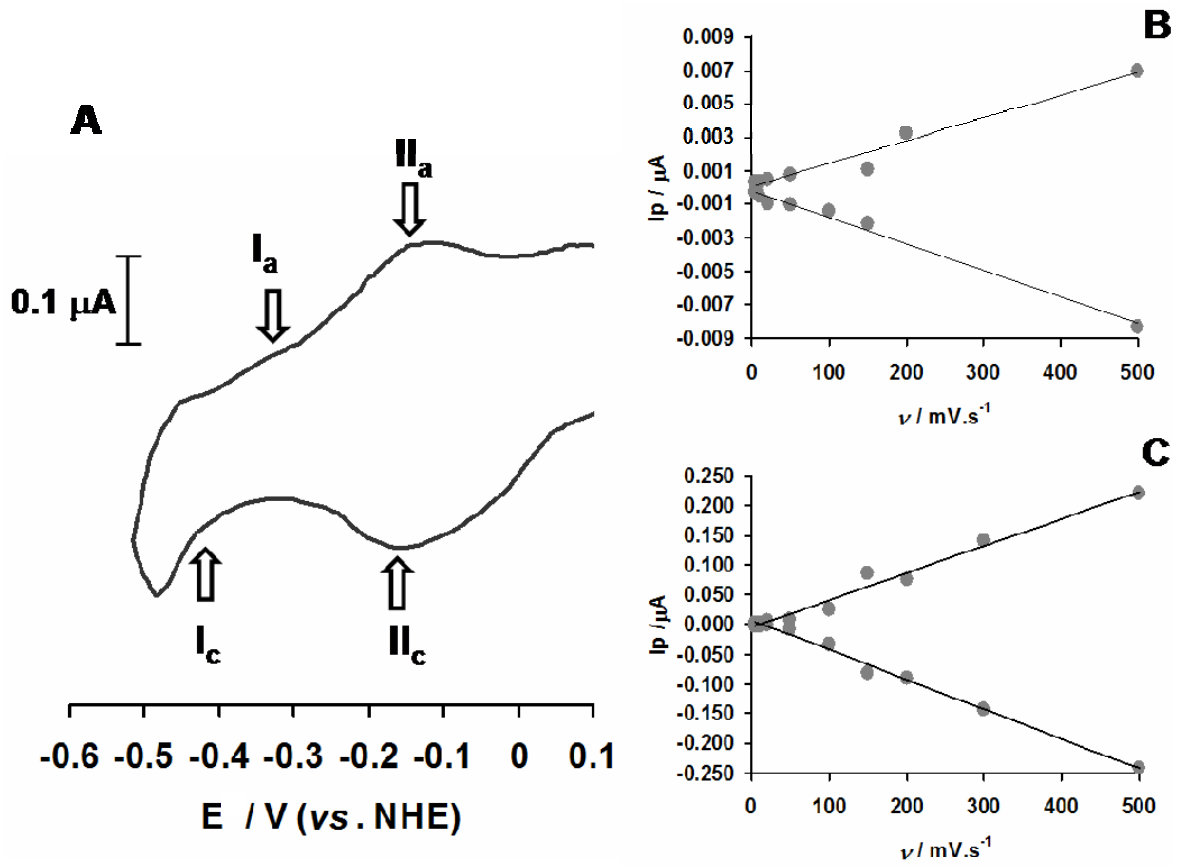

Figure 3.5 – The *Pseudomonas nautica* NOR binuclear active site redox processes. Panel A shows the cyclic voltammogram (200 $mV.s^{-1}$) of the immobilized *Pseudomonas nautica* NOR on a graphite electrode (black line) and the correspondent control experiment (without protein, dash line). The arrows point to the anodic and cathodic peaks for the mentioned redox processes. Panel B and C present the plot of peak current *vs.* scan rate for processes I and II respectively. For an adsorbed process with no mass transfer limitations, the current intensity (I) is given by the expression: $I = n^2F^2\nu A\Gamma/4RT$. Experiments were done in 20 mM mixture buffer (experimental details) pH 7.63.

For both redox processes (I and II), the anodic and cathodic intensity current *vs.* scan rate plot show a straight relationship with their ratio is close to one (figure 3.5, panels B and C). A low difference between the cathodic and anodic peaks is observed (ΔEp). This value is kept constant with the scan rate variation. For the reference process II the ΔEp observed is never higher than 89 mV (see supporting information S.9.2). This strongly suggests the physical adsorption of the enzyme to the electrode surface.

A k_s was calculated, and the achieved values for the non-heme Fe_B (73 s^{-1}) and for the low–spin heme b_3 (129 s^{-1}) are larger than the obtained for the previous co-factors. This had been predicted, since these two redox couples are highly scan rate dependent.

3.3.4. Remarks in the *Ps. nautica* NOR Direct Electron Transfer

For the first time, the midpoint redox potential of the four iron centers present in the *Ps. nautica* NOR enzyme were determined, using direct electrochemical experiments (table 3.1). The results show a surface confined process with the physical adsorption of the protein to the electrode surface.

The k_s values determined according Laviron's formulation (for the case of $\Delta Ep < 200$ mV and assumig $\alpha = 0.5$), agree with the observation made before in the text (section 3.3, figure 3.1), when it was analysed the variation of the current intensity of each redox process with the scan rate (table 3.1). Comparison of the values suggests a favourable electron pathway from the catalytic center towards the electrode rather than for the electron transfer hemes (heme *b* and *c*). Since graphite is charged negatively, the protein molecules probably will be oriented with a region positively charged.

Table 3.1 – The *Pseudomonas nautica* NOR midpoint redox potentials. The table shows the midpoint redox potentials and k_s of the NOR iron centers, and the antibody-rNorC complex.

Iron center	E/ mV (*vs.* NHE)	k_s / s^{-1}
	at pH 7.6, 5 Vs^{-1} used for k_s determination)	
Heme *c*	208 ± 12	47
Heme *b*	43 ± 12	46
Heme b_3	-162 ± 19	129
Fe_B	-369 ± 14	73
rNorC	298 ± 19	-

By using bioinformatics tools and the *Ps. aeruginosa* crystal structure (PDB 30OR) or the models presented in the previous chapter for the *Ps. nautica* NOR subunits, it would be possible to elaborate charge surface models that can help to elucidate the orientation of the molecule towards the electrode. However the *Ps. aeruginosa* NOR has aproximantly 70 % of homology with the studied enzyme and the structure was obtained with fragment antibodies, which are present in the structure. The models for the *Ps. nautica* NOR were determined separately (NorB and NorC) and the information of the co-factors position could only be made by the conserved coordinating ligands. Gathering all this information

and not forgetting that the enzyme is solubilized by detergent (DDM), charge surface diagrams were made using the mentioned structure and models, but no specific region could be unequivocally pointed as region of adsorption to the electrode.

The electron transfer centers, heme *c* and heme *b*, exhibited the higher midpoint redox potential values. The attained, results, well as the slightly lower value for the heme *b*, are in agreement with the electron transfer namely from heme *c* to heme *b*. The achieved values are also in agreement with the published results determined, using UV visible methods [17].

The catalytic binuclear center presents a heme b_3 redox potential similar to the predicted value, reported by others, using direct electrochemical and spectroscopic methods. [6, 15, 17]. Contrarily to the generally accepted, the non-heme Fe_B has a more negative midpoint redox potential than the catalytic heme b_3. This result is in agreement with the Mössbauer data obtained by our research group, that determined a negative redox potential for the diiron center, instead of a non-heme Fe_B redox potential close to the value determined for the electron transfer hemes [17]. This result seems to show that for this particular enzyme, which was studied, the non-heme Fe_B presents the lower redox potential from all the iron co-factors of the enzyme.

Mossbauer data indicates the presence of a small fraction of reduced non-heme FeB, in the as purified sample. This seams wired, since the iron center presents such negative midpoint redoox potential. However this can be due to a small fraction of uncoupling in the binuclear center [35, 36] or by the presence/absence of ligands stabilizing the first coordination sphere of the non-heme Fe_B [19, 37].

The possible presence of Ca^{2+} ion in the vicinity of the low-spin heme *b* centers can not be proved by the obtained results. As discussed previously, the *Ps. nautica* NOR presents a substoichiometric value for this element and the electrochemical experiments done could not give insights to its presence, since Ca has a strong reducing power, and it is no possible to input its reduction.

3.4. Midpoint Redox Potential Titration of the *Ps. nautica* NOR

The pH can change the strength of interaction between the protein metallic centres and the surrounding residues, enhancing electrochemical perturbations, due to protonation and deprotonation. With the resolved *Ps. aeruginosa* NOR crystallographic structure, the proposed models for the *Ps. stutzeri*, *Pa denitrificans* NOR [19, 20, 38], and the model presented in chapter 2 (section 2.2.5), it is possible to predict small conformational changes in the enzyme structure, specially in the neighbourhood of each metal center.

In order to study the midpoint redox potential on a pH scale (2.5 < pH < 9.7), the *Ps. nautica* NOR modified pyrolytic graphite electrode was used in different pH buffered solutions (supporting information S.9.4). For each pH trial, the scan rate was varied (between 5 and 1000 mVs^{-1}) in order to pursuit the four midpoint redox potentials, indexed to the four iron centers. Once more, the obtained results show a high reproducibility, since the immobilized enzyme maintained similar electrochemical response after intense electrochemical measurements and after extreme pH conditions.

The results obtained show the midpoint redox potentials, for the *Ps. nautica* NOR, on a pH scale (figure 3.6). The experimental data were simulated using the Nernst equation (eq. 3.3) [39] accordingly, and the best fit describing the data is presented in figure 3.6.

$$E^{o} = E^{o\prime} - 0.059 \cdot \log\left(\frac{\left[H^{+}\right]^{x} + \left[H^{+}\right]^{x-1} K_{ox_1} + \left[H^{+}\right]^{x-2} K_{ox_1} K_{ox_2} ..... K_{ox_1} K_{ox_2} ... K_{ox_n}}{\left[H^{+}\right]^{y} + \left[H^{+}\right]^{y-1} K_{red_1} + \left[H^{+}\right]^{y-2} K_{red_1} K_{red_2} ..... K_{red_1} K_{red_2} ... K_{red_m}} \right) \quad \text{(eq. 3.3)}$$

To each of the redox co-factors under study, the pK_{ox} and pK_{red} values were determined (table 3.2). Previously, two pK values were accounted for the catalytic heme b_3 redox process [6]. Equivalent values were achieved in this work, with an additional pK due to the existence of more experimental data.

The acidic pKs determined for the heme groups (4.11/5.12, 3.88/5.16, and 3.55/3.94, check table 3.2) can be attributed to the propionic acid side chain ionization. These side chains normally show a pK_{ox} value near 6.2. Nevertheless, the variation in the heme propionate pK_a value has not been adequately explained on a structural level but is

strongly affected by electrostatic interactions. When these side chains are exposed to the solvent, they tend to decrease the p*K*, but if they are buried inside the protein the opposite effect is observed, depending on the proximity to the protein surface, to other charges or groups. Addicionaly, the pK_a of a propionic acid side chain can be lowered when a favourable hydrogen bounding network is present [19, 39-42].

In the NorB subunit, there are two Arg residues (Arg 50 and 433 in *Ps. nautica* numbering figure 1.9 chapter 1), conserved in several NORs, that are pointed to stabilize the aliphatic side chains of the low-spin *b*-type hemes [20, 38]. In this same subunit, His 332 and Asn 328 are also conserved and, like in the *Ps. stutzeri* NOR model they could accomplish the H-bond for the propionate side chain of heme b_3 [20]. The NOR structure from *Ps. aeruginosa* shows a strong H-bond network for the heme propionates of heme *b* and b_3, but no relevance for the conserved Arg is made [19]. In its place it is shown the presence of a Ca atom, stabilizing the proprionic side chains. Ca atoms and/or conserved polar aminoacid residues near the heme propionate side chains are common in members of the C*c*O family and some of them are essential for activity [17, 43, 44] (and references therein).

The *Ps. aeruginosa* NorC subunit crystal structure points to the presence of a conserved Arg residue in the heme *c* cavity, lying close to the propionic side chains. Curiously, this residue is conserved among NorC sequences and is contiguous to the Met axial ligand of the metal co-factor (see figure 1.10, Chapter 1). Based on what it already known from the literature and the similarities between the *Ps. nautica* NOR and the other *c*-type NORs, it is most likely that all the heme co-factors present in the *Ps. nautica* enzyme are stabilized by a H-bound network surrounding the propionic side chains and therefore, their p*K*s are more acidic than the predicted value of 6.2. However, several experiments should be conducted in order to determine the importance of these polar residues in both NOR subunits.

The remaining p*K*s can be attributed to different aminoacids from the co-factors neighbourhood. Namely His that have a p*K* range of 5.9 – 7.0 because there is at least one coordinating each metal center, or a Glu residue, since this polar aminoacid was proved to have a p*K* range from 8.5 to 8.8 when buried inside protein cores [6, 45].

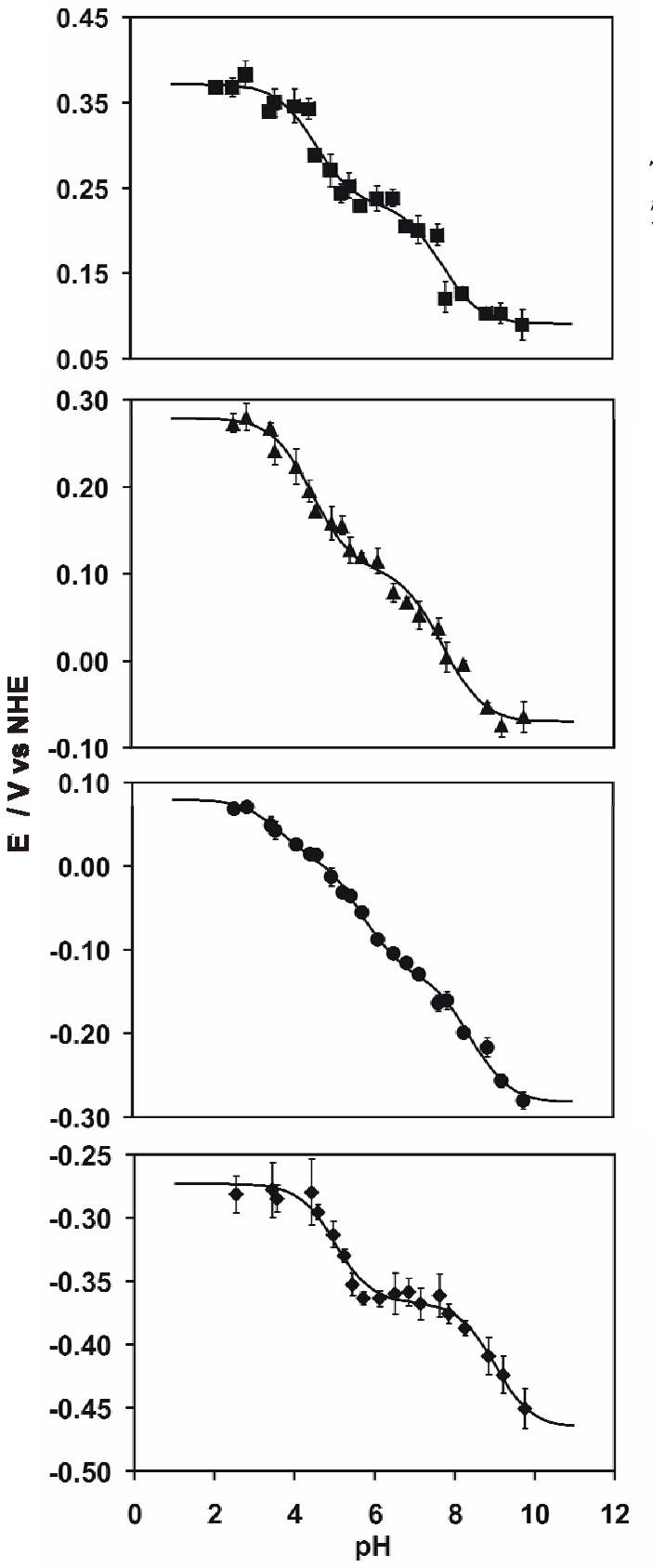

Table 3.2 - pK_{ox} and pK_{red} of the *Pseudomonas nautica* NOR iron centers.

	pK_{ox}	pK_{red}
Heme *c*	4.11 ± 0.1	5.12 ± 0.05
	7.23 ± 0.07	8.24 ± 0.07
Heme *b*	3.88 ± 0.04	5.16 ± 0.05
	7.12 ± 0.05	8.39 ± 0.05
Heme b_3	3.45 ± 0.10	3.94 ± 0.13
	5.27 ± 0.08	6.30 ± 0.08
	7.94 ± 0.11	9.07 ± 0.12
Fe_B	4.70 ± 0.02	5.37 ± 0.02
	8.64 ± 0.03	9.36 ± 0.06

Figure 3.6 – pH dependence of the midpoint redox potential for the *Pseudomonas nautica* redox co-factors. ■ Heme *c*, ▲ heme *b*, ● heme b_3 and ♦ non-heme Fe_B. Experimental data were fitted using the Nernst equation.
Experiments were done in 20 mM mixture buffer (experimental details, section 3.7) at different pH values.

3.5. Catalytic Activity Towards Nitric Oxide and Oxygen

In this section, the *Ps. nautica* NOR activity towards NO and O_2 was investigated to observe the different electrochemical features.

Different NORs present catalytic activity towards NO and O_2, with distinct constant rates [46-51]. Further discussion on the kinetic features for the NO and O_2 reduction, and the assumed mechanism for its reduction, is present in the next chapter, where dynamic voltammetry was applied to characterize the immobilized *Ps. nautica* NOR.

In this section it is only presented the electrochemical proof for the NO and O_2 reduction by the enzyme in study, as well as the quantification of the number of electrons involved in both reduction processes. For these last electrochemical experiments is imperative to use a rotative disk electrode (RDE). This is one of the few convective electrode systems for which the hydrodynamic equations and the convective-diffusion equation have been solved rigorously for the steady-state. The electrode construction is quite simple, consisting in a disk of the electrode material imbedded in a rod of an insulating material, connected to a motor able to input a rotation at a certain frequency (f) ($\omega = 2\pi f$). The advantage of a hydrodynamic method is that a steady-state is attained rather fast, and measurements can be made with high precision. The simplest treatments of convective systems are based on a diffusion layer approach. In this model, it is assumed that the convective flow maintains the concentration of all species uniform, therefore the concentration of a certain specie at the electrode surface is equal to the bulk solution [12].

The electrocatalytic response of the *Ps. nautica* NOR was studied elsewhere [6, 52] using a stationary pyrolytic graphite electrode. In this work both electrodes where used, the stationary and the rotative graphite electrodes, in order to confirm the obtained results.

The use of a RDE required the optimization of the experimental conditions, performing dependence in parameters such as the scan rate, angular speed, protein amount and substrate concentration. The results shown in the following sections (ν = 50 mVs^{-1}, ω = 5000 RPM and $[O_2]$ = 56 μM or [NO] = 20 μM) are used to elucidate the catalytic feature of the immobilized NOR towards both substrates, and they were chosen

from the set of experiments conducted to optimize the assays done for determine the number of electrons involved in both substrates reduction (section 3.5.1).

Oxygen Reduction

The *Ps. nautica* NOR oxidoreductase activity was assayed using the protein immobilized on a graphite electrode. The enzyme was adsorbed to the graphite RDE, and to a stationary pyrolytic graphite electrode, and the surface coverage was characterized by fast scan rate CV. The O_2 reduction by both modified electrodes is shown in figure 3.7, with the correspondent control experiments.

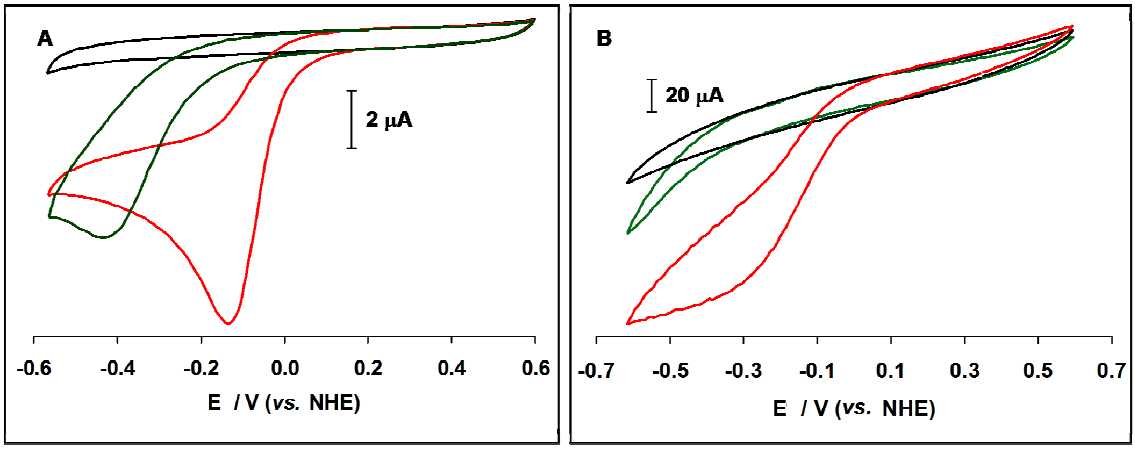

Figure 3.7 – Oxygen reduction using the *Pseudomonas nautica* NOR modified electrodes. Panels A and B show the obtained results using stationary graphite electrode or a rotative disk graphite electrode, respectively. Black and red line describe the electrochemical response of the NOR modified graphite electrodes, in the absence and presence of O_2, respectively. The green line describes the control experiment (without protein) in the presence of O_2. Electrolyte solution was a 20 mM mixture buffer (experimental details, section 3.7) pH 7.6, $\nu = 50$ mV.s^{-1}, ($\omega = 5000$ RPM, RDE), [O_2] = 56 μM.

When O_2 is added to the bulk solution, the shape of the voltammograms is modified. A reduction peak starts to develop near – 74 mV (*vs.* NHE) when the enzyme is adsorbed to the stationary electrode (figure 3.7, panel A, red trace), and when this is absent, the reduction peak is shifted to a lower potential (figure 3.7, panel A, green trace). The potential change with the presence of the protein demonstrates the catalytic reduction of O_2 by the *Ps. nautica* NOR. This process was already reported and proved to be dependent upon O_2 concentration [6, 52]. The switch for a dynamic regime (figure 3.7, panel B)

alters slightly the voltammogram shape. Instead of a cathodic peak, a limit current is detected beginning at a similar potential value (-66 mV, *vs.* NHE). The shift to higher redox potential values of this catalytic current upon NOR presence demonstrates O_2 reduction by the enzyme (figure 3.7, panel B, red and green trace). The developing of a limit current instead of a peak is due a dynamic system, since with this type of electrode, the concentration of the reduced specie in solution is maintained constant at the electrode surface.

Nitric Oxide Reduction

Similar to the previously described, the same modified electrodes were used to investigate the NO reduction. Figure 3.8 shows the corresponding results, as well as the control experiments.

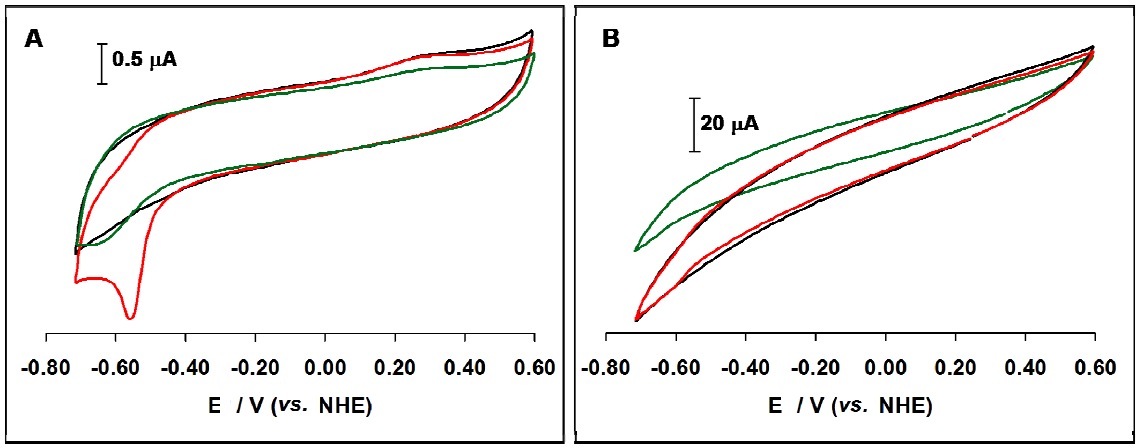

Figure 3.8 –Nitric oxide reduction using the *Pseudomonas nautica* NOR modified electrodes. Panels A and B show the obtained results using stationary graphite electrode or a rotative disk graphite electrode, respectively. Black and red line describe the electrochemical response of the NOR modified graphite electrodes, in the absence and presence of NO, respectively. The green line describes the control experiment (without protein) in the presence of NO. Electrolyte solution was a 20 mM mixture buffer (experimental details, section 3.7) pH 7.6, ν = 50 mV.s^{-1}, (ω = 5000 RPM, RDE), [NO] = 20 µM.

The results obtained are similar to the ones achieved for the O_2 reduction (the behaviour of the cathodic waves). When NO is introduced into the system with the NOR modified stationary electrode, a catalytic peak is present, starting to develop at -518 ± 20 mV (figure 3.8 panel A, red line). Equally, in the dynamic system and when using the equivalent rotative electrode, a limit current starts to be observed at -469 ± 23 mV (figure 3.8, panel B, red line). The inexistence of enzyme adsorbed to the electrodes brings a

catalytic peak or a limit current development at more negative redox potentials for the stationary and rotative systems, respectively (figure 3.8, green line, panel A and B). The potential shift in the presence of *Ps. nautica* NOR, supports its participation in the NO reduction [6, 52] (more voltammograms can be seen in supporting information S.9.5).

The limit current developed for the NO reduction is not so pronounced as the curve obtained for the NOR oxidoreductase activity (figure 3.7). Since limit current is proportional to the angular speed and to the concentration of the electroactive species (Levich equation, eq. 3.4), this observation may be due to: i) a lower substrate concentration (20 μM for NO and 56 μM for O_2); ii) a higher NO diffusion in the protein hydrophobic core and/or adsorbed film, due to the proposed channels for NO diffusion in the protein structure [19]; and iii) the enzyme's high turnover for the natural substrate.

Literature reported a non functional inorganic Fe compound that mimics the Fe_B from the NOR catalytic center. This model compound shows a midpoint redox potential of about 200-250 mV (*vs.* NHE), when used in organic solvents. The nitrosyl form of this complex, exhibits a much lower redox potential (approximately -330 mV, *vs.* NHE). A low redox potential for the model complex could suggest the involvement of the *Ps. nautica* NOR non-heme Fe_B in the NO reduction mechanism. Nevertheless, the authors admit that further studies are required to the complete characterization of the model compound specially in the redox potential adjustment for achieving a functional model [53].

3.5.1. Electron Quantification for Both Substrates Under Catalytic Conditions

The ultimate goal of the experiments described in this chapter is to determine the number of electrons involved in the O_2 and NO reduction. In order to maintain a convective flow of the substrate towards the electrode is imperative to use a RDE. As previously mentioned, with this kind of electrode is possible to assume that the concentration of the dissolved species on the electrode surface is equal to the concentration in the bulk solution. Therefore is possible to use the Levich equation (eq. 3.4):

$$I_{\lim it} = 0.62nFAD^{\frac{2}{3}}\nu^{\frac{-1}{6}}C\omega^{\frac{1}{2}} \qquad \text{(eq. 3.4)}$$

where n is the number of electrons involved in the process, F the Faraday constant (96485 C.mol^{-1}), A the electrode area (cm^2), D the diffusion constant of the electroactive specie (D_{NO}= 2.07 × 10^{-5} cm^2.s^{-1}, D_{O2}= 2.01 × 10^{-5} cm^2.s^{-1}), ν the water kinematic viscosity (8.90 × 10^{-7} m^2.s^{-1}), C the electroactive molar concentration (mol.cm^{-3}) and ω the rotation frequency (s $^{-1/2}$) [54-56].

The equation shows a limit current proportional to the electroactive species concentration and the angular speed square root. To determine the number of electrons involved in each substrate reduction, it is necessary to maintain the substrate concentration at a constant value, while changing switch angular speed in order to obtain a straight relation between $\omega^{1/2}$ and I_{limit}. The other parameters of the equation are constants.

The use of Levich equation, or a derivation of this equation (Koutechy-Levich equation), has been used before to determine the amount of electrons exchanged in an enzymatic catalytic process [57, 58].

It is possible to use this equation, since the enzyme is adsorbed to the electrode surface and the catalytic center is buried in the polypeptide chain. Literature also shows redox and chemical catalysis in monolayer and multilayer coated electrodes, as well as the use of CV for the kinetic analysis of the catalytic systems [59]. Therefore, the catalytic

current observed when it is used the *Ps. nautica* NOR modified electrode, outcomes from the enzyme reduction and re-oxidation, in the presence of the substrate and can be used to estimate the number of electrons involved in each of the reduction reactions.

Experimentally the catalytic reduction of NO seems to be extremely fast, which makes it difficult to maintain a constant substrate concentration in the system. Thereby CV assays were changed for normal linear sweep voltammetry and only one cycle was used in order to maintain the substrate concentration constant for the different angular speed values.

Results obtained for both substrates are presented in figure 3.9, corresponding to 3.99 ± 0.50 and 1.67 ± 0.13 electrons for the O_2 and NO reduction respectively.

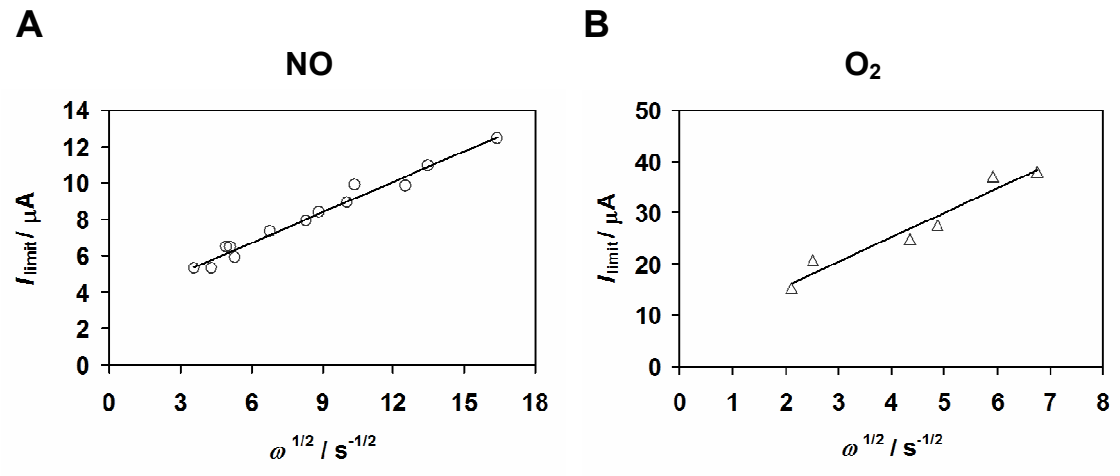

Figure 3.9 – Determination of the number of electrons involved in the NO and O_2 reduction, by the *Pseudomonas nautica* NOR. Limit current *vs.* $\omega^{1/2}$ representation for (A) NO and (B) O_2 reduction. Slopes: 5.60 ± 0.27 × 10^{-7} and 4.24 ± 0.47 × 10^{-6} for NO and O_2 reduction respectively. Experiments were done in a 20 mM mixture buffer (experimental details, section 3.7) pH 7.63, ν = 50 mV.s^{-1}, [NO] = 16.67 µM and [O_2] = 53.82 µM.

The estimated values are in complete agreement with the literature that describe NO reduction as a two electron, two proton process and O_2 reduction as a four electron process. However, it was investigated the possibility of O_2 reduction to H_2O_2 [60]. Flock and co-workers demonstrated that O_2 was reduced in a four electron process, using steady-state kinetic assays [60].

To exclude the possibility of the reduction of O_2 to H_2O_2 catalyzed by the *Ps. nautica* NOR, assays with combined enzymes (*Ps. nautica* NOR and a commercial peroxidase)

were made to search for possible H_2O_2 formation. The assays were conducted in aerobic environment and using TMPD as the chemical electron donor for both enzymes (supporting information S.5). The reaction was followed by absorbance changes at 520 nm a specific wavelength for the chemical electron donor oxidation and the results are resumed in figure 3.10.

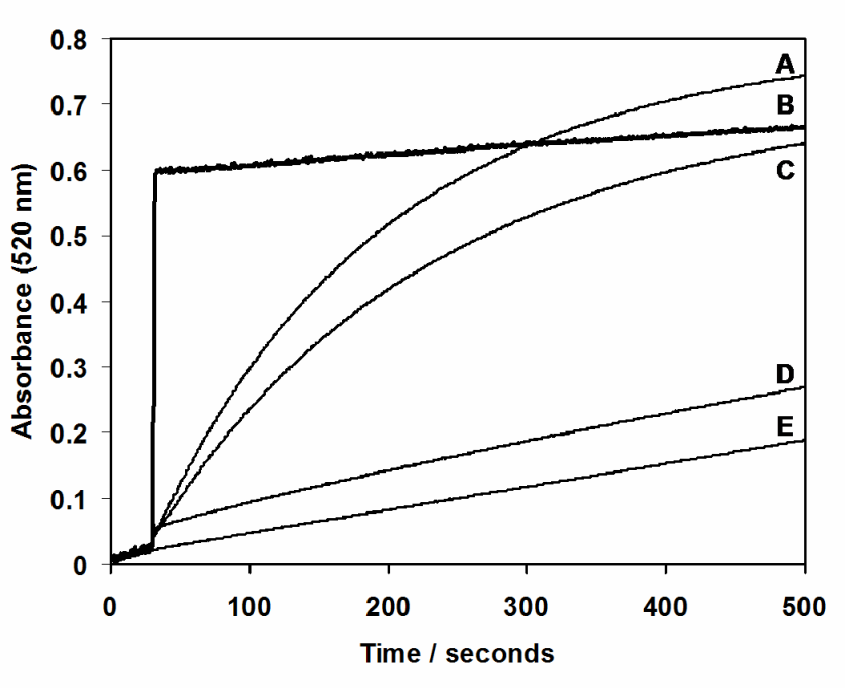

Figure 3.10 – Oxidoreductase activity assays for the *Pseudomonas nautica* NOR combined with commercial peroxidase. The figure shows differences at the absorbance measured at 520 nm for the reactions in the presence of (A) – NOR (0.5 μM) , (B) – Peroxidase (0.5 μM) + H_2O_2 (2.5 μM), (C) – Peroxidase (0.5 μM) + NOR (0.5 μM), (D) – Peroxidase (0.5 μM), (E) – TMPD (1 mM) oxidation. Experimental details: 100 mM KPB pH 6, 0.02 %; 1 mM TMPD. Reactions were done in a quartz cuvette in aerobic conditions.

As a control to the experiment peroxidase activity was assayed separately (figure 3.10, curve B). Since both enzymes can use TMPD as the electron donor (supporting information S.7). A mixture of these two enzymes was used in aerobic conditions (curve C), and was similar to the obtained with the *Ps. nautica* NOR as single catalyst (curve A), showing that *Ps. nautica* NOR reduces O_2 directly to H_2O, without the formation of H_2O_2 The TMPD self oxidation curve (trace E), and its oxidation in the presence of peroxidase (curve D) in the absence of H_2O_2 were used as control experiments.

3.6. Concluding Remarks

The direct electrochemical experiments done with the immobilized *Ps. nautica* NOR revealed, for the first time, the four redox potentials for all the iron co-factors of this enzyme.

The NO reduction mechanism has been intensively studied over the years, and rising controversy [61]. This work shows a highly negative redox potential for the non-heme Fe_B metal site. Since the *Ps. nautica* active form seems to be the full reduced state, this means that Fe_B must be reduced so that catalysis can start, suggesting the formation of a Fe_B-(di)nytrosyl as an intermediate of the NO reduction [17, 25]. However more experiments must be conducted in order to elucidate the catalytic mechanism.

pH dependence experiments on the midpoint redox potential suggest a possible hydrogen network surrounding the heme propionates, established by the response of conserved residues, near the heme co-factors. These results may claim for the design of specific experiments in order to elucidate the role of several residues in the electron transfer and catalytic activity.

The enzyme under study is able to reduce NO to N_2O and O_2 to H_2O, in processes that involve two and four electrons, respectively. This is the first time that the electrons involved in a NOR catalysis were analytically quantified for different substrate reactions. O_2 reduction is accomplished by the *Ps. nautica* NOR and the reduction potential starts developing at -60 mV (*vs.* NHE). The NO reduction is shifted for much lower redox potentials (-330 mV *vs.* NHE), in agreement with recent experiments done using nitrosyl-Fe model compounds, suggesting the involvement of the non-heme Fe_B in the NO reduction mechanism [53].

3.7. Experimental details

Protein purification: *Ps. nautica* NOR purification was made as described in the chapter 2, as well as its biochemical and spectroscopic characterization. Recombinant NorC was cloned as described in the supporting information S.3. Purification and characterization of this recombinant protein is reported elsewhere [29]. Purified rNorC was concentrated in an ultrafiltration apparatus and buffer exchanged to 100 mM KPB pH 7, 0.02 % (w/v), 0.01 % (PE).

Protein immobilization protein immobilization on graphite electrodes was accomplished by adsorption, using the solvent casting technique. Drops of 7 to 14 μL of a 45 or 265 μM pure protein sample equilibrated in 100 mM KPB pH 7, 0.02 % (v/v) DDM, 0.01 % (v/v) PE was used as the stock solution. The supporting electrolyte was a 20 mM mixture of sodium citrate, MES, HEPES, AMPSO buffered at different pH values.

Electrochemical methods and instrumentation: The experiments were conducted in a μAUTOLAB type II potentiostat, using a three electrode configuration in a one-compartment electrochemical cell. The working electrode was a graphite rotative disk electrode (RDE) or a stationary pyrolytic graphite electrode. A platinum wire and a saturated calomel electrode (SCE) were used as counter and reference electrodes, respectively. Both graphite electrodes were previously treated trough immersion in a diluted nitric acid solution, rinsed in water, polished with 5.0, 1.0 and 0.3 μm alumina, briefly sonnicated and rinsed with deionized water. Cyclic voltammetry (CV) assays were preformed at different scan rates. O_2 and NO dependence experiments were preformed by adding different volumes of water solutions containing the dissolved gas. Separated water gastight flasks were saturated with the gases and each concentration was estimated considering its solubility in water according to the literature [62, 63]. O_2 saturation was made by direct bubbling. NO saturation was achieved by bubbling a 5 % NO / 95 % He mixture in 5M KOH solution, passing from this to a non buffered water solution pH 3, before deionized water saturation. This procedure was applied in order to remove possible NOx formation. Additions were made using a Hamilton gastight syringe.

The experiments were conducted at room temperature, in controlled atmosphere, using an anaerobic chamber. All the acquired data were analysed with GPES software. Unless mentioned, the presented voltammograms are always the second cycle experiment.

3.8. References

[1] Gilardi, G., A. Fantuzzi and S.J. Sadeghi, *Engineering and design in the bioelectrochemistry of metalloproteins.* Curr Opin Struct Biol, 2001. **11**(4): p. 491-9.

[2] Liu, X., L. Shang, Z. Sun and G. Li, *Direct electrochemistry of hemoglobin in dimethyldioctadecyl ammonium bromide film and its electrocatalysis to nitric oxide.* J Biochem Biophys Methods, 2005. **62**(2): p. 143-51.

[3] Leger, C. and P. Bertrand, *Direct electrochemistry of redox enzymes as a tool for mechanistic studies.* Chem Rev, 2008. **108**(7): p. 2379-438.

[4] Heering, H.A., F.G. Wiertz, C. Dekker and S. de Vries, *Direct immobilization of native yeast iso-1 cytochrome C on bare gold: fast electron relay to redox enzymes and zeptomole protein-film voltammetry.* J Am Chem Soc, 2004. **126**(35): p. 11103-12.

[5] Dell'Acqua, S., S.R. Pauleta, P.M. Paes de Sousa, E. Monzani, L. Casella, J.J. Moura and I. Moura, *A new CuZ active form in the catalytic reduction of N(2)O by nitrous oxide reductase from Pseudomonas nautica.* J Biol Inorg Chem, 2010. **15**(6): p. 967-76.

[6] Cordas, C.M., A.S. Pereira, C.E. Martins, C.G. Timoteo, I. Moura, J.J. Moura and P. Tavares, *Nitric oxide reductase: direct electrochemistry and electrocatalytic activity.* Chembiochem, 2006. **7**(12): p. 1878-81.

[7] Correia dos Santos, M.M., P.M. Sousa, M.L. Goncalves, M.J. Romao, I. Moura and J.J. Moura, *Direct electrochemistry of the Desulfovibrio gigas aldehyde oxidoreductase.* Eur J Biochem, 2004. **271**(7): p. 1329-38.

[8] Laviron, E., *General expression of the linear potential sweep voltammogram in the case of diffusionless electochemical system* Journal Electroanal. Chem., 1979. **101**: p. 19-28.

[9] Laviron, E., *The use of Linear sweep voltammetry and of a.c. voltammetry for the study of the surface electrochemical reaction of strongly adsorbed systems and of redox modified electrodes.* Journal Electroanal. Chem., 1979. **100**: p. 263-270.

[10] de Sousa, P.M., S.R. Pauleta, M.L. Goncalves, G.W. Pettigrew, I. Moura, M.M. Dos Santos and J.J. Moura, *Mediated catalysis of Paracoccus pantotrophus cytochrome c peroxidase by P. pantotrophus pseudoazurin: kinetics of intermolecular electron transfer.* J Biol Inorg Chem, 2007. **12**(5): p. 691-8.

[11] Armstrong, F.A., J.N. Butt and A. Sucheta, *Voltammetric studies of redox-active centers in metalloproteins adsorbed on electrodes.* Methods Enzymol, 1993. **227**: p. 479-500.

[12] Bard, A.J. and L.R. Faulkener, *Electrochemical Methods* ed. s. edition. 2001, USA: John Wiley & Sons. INC.

[13] Armstrong, F.A., *Recent developments in dynamic electrochemical studies of adsorbed enzymes and their active sites.* Curr Opin Chem Biol, 2005. **9**(2): p. 110-7.

[14] Armstrong, F.A. and G.S. Wilson, *Recent developments in faradic bioelectrochemistry.* Electrochimica Acta, 2000. **45**: p. 2623-2645.

[15] Gronberg, K.L., M.D. Roldan, L. Prior, G. Butland, M.R. Cheesman, D.J. Richardson, S. Spiro, A.J. Thomson and N.J. Watmough, *A low-redox potential heme in the dinuclear center of bacterial nitric oxide reductase: implications for the evolution of energy-conserving heme-copper oxidases.* Biochemistry, 1999. **38**(42): p. 13780-6.

[16] Field, S.J., M.D. Roldan, S.J. Marritt, J.N. Butt, D.J. Richardson and N.J. Watmough, *Electron transfer to the active site of the bacterial nitric oxide reductase is controlled by ligand binding to heme b(3).* Biochim Biophys Acta, 2011. **1807**(4): p. 451-7.

[17] Timoteo, C.G., A.S. Pereira, C.E. Martins, S.G. Naik, A.G. Duarte, J.J. Moura, P. Tavares, B.H. Huynh and I. Moura, *Low-Spin Heme b3 in the Catalytic Center of Nitric Oxide Reductase from Pseudomonas nautica.* Biochemistry, 2011. **50**(20): p. 4251-4262.

[18] Flock, U., J. Reimann and P. Adelroth, *Proton transfer in bacterial nitric oxide reductase.* Biochem Soc Trans, 2006. **34**(Pt 1): p. 188-90.

[19] Hino, T., Y. Matsumoto, S. Nagano, H. Sugimoto, Y. Fukumori, T. Murata, S. Iwata and Y. Shiro, *Structural basis of biological N2O generation by bacterial nitric oxide reductase.* Science, 2010. **330**(6011): p. 1666-70.

[20] Zumft, W.G., *Nitric oxide reductases of prokaryotes with emphasis on the respiratory, heme-copper oxidase type.* J Inorg Biochem, 2005. **99**(1): p. 194-215.

[21] Zheng, N., X. Zhou, W. Yang, X. Li and Z. Yuan, *Direct electrochemistry and electrocatalysis of hemoglobin immobilized in a magnetic nanoparticles-chitosan film.* Talanta, 2009. **79**(3): p. 780-6.

[22] Field, S.J., F.H. Thorndycroft, A.D. Matorin, D.J. Richardson and N.J. Watmough, *The respiratory nitric oxide reductase (NorBC) from Paracoccus denitrificans.* Methods Enzymol, 2008. **437**: p. 79-101.

[23] Conrath, K., A.S. Pereira, C.E. Martins, C.G. Timoteo, P. Tavares, S. Spinelli, J. Kinne, C. Flaudrops, C. Cambillau, S. Muyldermans, I. Moura, J.J. Moura, M. Tegoni and A. Desmyter, *Camelid nanobodies raised against an integral membrane enzyme, nitric oxide reductase.* Protein Sci, 2009. **18**(3): p. 619-28.

[24] De Smet, L., G.W. Pettigrew and J.J. Van Beeumen, *Cloning, overproduction and characterization of cytochrome c peroxidase from the purple phototrophic bacterium Rhodobacter capsulatus.* Eur J Biochem, 2001. **268**(24): p. 6559-68.

[25] Lachmann, P., Y. Huang, J. Reimann, U. Flock and P. Adelroth, *Substrate control of internal electron transfer in bacterial nitric-oxide reductase.* J Biol Chem, 2010. **285**(33): p. 25531-7.

[26] Hirst, J., *Elucidating the mechanisms of coupled electron transfer and catalytic reactions by protein film voltammetry*. Biochim Biophys Acta, 2006. **1757**(4): p. 225-39.

[27] Zhang, W. and G. Li, *Third-generation biosensors based on the direct electron transfer of proteins*. Anal Sci, 2004. **20**(4): p. 603-9.

[28] Ye, T., R. Kaur, X. Wen, K.L. Bren and S.J. Elliott, *Redox properties of wild-type and heme-binding loop mutants of bacterial cytochromes C measured by direct electrochemistry*. Inorg Chem, 2005. **44**(24): p. 8999-9006.

[29] Mesquita, K.A., *Produção e caracterização da subunidade c recombinante da redutase do óxido nítrico*, in *Chemistry Department* 2008, Universidade Nova de Lisboa: Lisbon p. 44.

[30] Oubrie, A., S. Gemeinhardt, S. Field, S. Marritt, A.J. Thomson, M. Saraste and D.J. Richardson, *Properties of a soluble domain of subunit C of a bacterial nitric oxide reductase*. Biochemistry, 2002. **41**(35): p. 10858-65.

[31] Wirtz, M., V. Oganesyan, X. Zhang, J. Studer and M. Rivera, *Modulation of redox potential in electron transfer proteins: effects of complex formation on the active site microenvironment of cytochrome b5*. Faraday Discuss, 2000(116): p. 221-34; discussion 257-68.

[32] Field, S.J., L. Prior, M.D. Roldan, M.R. Cheesman, A.J. Thomson, S. Spiro, J.N. Butt, N.J. Watmough and D.J. Richardson, *Spectral properties of bacterial nitric-oxide reductase: resolution of pH-dependent forms of the active site heme b3*. J Biol Chem, 2002. **277**(23): p. 20146-50.

[33] Mayhew, S.G., *The redox potential of dithionite and SO-2 from equilibrium reactions with flavodoxins, methyl viologen and hydrogen plus hydrogenase*. Eur J Biochem, 1978. **85**(2): p. 535-47.

[34] Yeung, N., Y.W. Lin, Y.G. Gao, X. Zhao, B.S. Russell, L. Lei, K.D. Miner, H. Robinson and Y. Lu, *Rational design of a structural and functional nitric oxide reductase*. Nature, 2009. **462**(7276): p. 1079-82.

[35] Lin, Y.W., N. Yeung, Y.G. Gao, K.D. Miner, S. Tian, H. Robinson and Y. Lu, *Roles of glutamates and metal ions in a rationally designed nitric oxide reductase based on myoglobin*. Proc Natl Acad Sci U S A, 2010. **107**(19): p. 8581-6.

[36] Zhao, X., N. Yeung, B.S. Russell, D.K. Garner and Y. Lu, *Catalytic reduction of NO to N2O by a designed heme copper center in myoglobin: implications for the role of metal ions*. J Am Chem Soc, 2006. **128**(21): p. 6766-7.

[37] Hino, T., S. Nagano, H. Sugimoto, T. Tosha and Y. Shiro, *Molecular structure and function of bacterial nitric oxide reductase*. Biochim Biophys Acta, 2011.

[38] Reimann, J., U. Flock, H. Lepp, A. Honigmann and P. Adelroth, *A pathway for protons in nitric oxide reductase from Paracoccus denitrificans*. Biochim Biophys Acta, 2007. **1767**(5): p. 362-73.

[39] Moore, G.R.P., G. W. , *Cytochromes c evolutionary, Structural and Physicochemical Aspects*. 1990: Springer-Verlang.

[40] Mikami, S., H. Tai and Y. Yamamoto, *Effect of the redox-dependent ionization state of the heme propionic acid side chain on the entropic contribution to the redox potential of Pseudomonas aeruginosa cytochrome c551*. Biochemistry, 2009. **48**(33): p. 8062-9.

[41] Takayama, S.J., S. Mikami, N. Terui, H. Mita, J. Hasegawa, Y. Sambongi and Y. Yamamoto, *Control of the redox potential of Pseudomonas aeruginosa cytochrome c551 through the Fe-Met coordination bond strength and pKa of a buried heme propionic acid side chain.* Biochemistry, 2005. **44**(14): p. 5488-94.

[42] Hauser, K., J. Mao and M.R. Gunner, *pH dependence of heme electrochemistry in cytochromes investigated by multiconformation continuum electrostatic calculations.* Biopolymers, 2004. **74**(1-2): p. 51-4.

[43] Buschmann, S., E. Warkentin, H. Xie, J.D. Langer, U. Ermler and H. Michel, *The structure of cbb3 cytochrome oxidase provides insights into proton pumping.* Science. **329**(5989): p. 327-30.

[44] Lee, H.J., L. Ojemyr, A. Vakkasoglu, P. Brzezinski and R.B. Gennis, *Properties of Arg481 mutants of the aa3-type cytochrome c oxidase from Rhodobacter sphaeroides suggest that neither R481 nor the nearby D-propionate of heme a3 is likely to be the proton loading site of the proton pump.* Biochemistry, 2009. **48**(30): p. 7123-31.

[45] Fitch, C.A., D.A. Karp, K.K. Lee, W.E. Stites, E.E. Lattman and E.B. Garcia-Moreno, *Experimental pK(a) values of buried residues: analysis with continuum methods and role of water penetration.* Biophys J, 2002. **82**(6): p. 3289-304.

[46] Flock, U., P. Lachmann, J. Reimann, N.J. Watmough and P. Adelroth, *Exploring the terminal region of the proton pathway in the bacterial nitric oxide reductase.* J Inorg Biochem, 2009. **103**(5): p. 845-50.

[47] Forte, E., A. Urbani, M. Saraste, P. Sarti, M. Brunori and A. Giuffre, *The cytochrome cbb3 from Pseudomonas stutzeri displays nitric oxide reductase activity.* Eur J Biochem, 2001. **268**(24): p. 6486-91.

[48] Giuffre, A., G. Stubauer, P. Sarti, M. Brunori, W.G. Zumft, G. Buse and T. Soulimane, *The heme-copper oxidases of Thermus thermophilus catalyze the reduction of nitric oxide: evolutionary implications.* Proc Natl Acad Sci U S A, 1999. **96**(26): p. 14718-23.

[49] Huang, Y., J. Reimann, H. Lepp, N. Drici and P. Adelroth, *Vectorial proton transfer coupled to reduction of O2 and NO by a heme-copper oxidase.* Proc Natl Acad Sci U S A, 2008. **105**(51): p. 20257-62.

[50] Matsushita, K., E. Shinagawa, O. Adachi and M. Ameyama, *o-Type cytochrome oxidase in the membrane of aerobically grown Pseudomonas aeruginosa.* FEBS Lett, 1982. **139**(2): p. 255-8.

[51] Hayashi, T., M.T. Lin, K. Ganesan, Y. Chen, J.A. Fee, R.B. Gennis and P. Moenne-Loccoz, *Accommodation of two diatomic molecules in cytochrome bo: insights into NO reductase activity in terminal oxidases.* Biochemistry, 2009. **48**(5): p. 883-90.

[52] Cordas, C.M., *Electrochemical Studies of Electron Transfer Proteins and Electroactive Biofilms*. 2007, Universidade Nova de Lisboa: Lisboa. p. 183.

[53] Berto, T.C., M.B. Hoffman, Y. Murata, K.B. Landenberger, E.E. Alp, J. Zhao and N. Lehnert, *Structural and Electronic Characterization of Non-Heme Fe(II)-Nitrosyls as Biomimetic Models of the FeB Center of Bacterial Nitric Oxide Reductase (NorBC).* J Am Chem Soc, 2011.

[54] Lide, D.R., *CRC Handbook of chemistry and physics a ready reference book of chemical and physical data*. 88th ed. 2007-2008, London, New york CRC press, Taylor & Francis group.

[55] Wise, D.L. and G. Houghton, *Diffusion coefficients on neon, krypton, xernon, carbon monoxide and nitric oxide in water at 10-60 ºC.* Chem Engng Sci, 1968. **23**(1): p. 1211-1216.

[56] Zacharia, I.G. and W.M. Deen, *Diffusivity and solubility of nitric oxide in water and saline.* Ann Biomed Eng, 2005. **33**(2): p. 214-22.

[57] Vincent, K.A., A. Parkin and F.A. Armstrong, *Investigating and exploiting the electrocatalytic properties of hydrogenases.* Chem Rev, 2007. **107**(10): p. 4366-413.

[58] Udit, A.K., N. Hindoyan, M.G. Hill, F.H. Arnold and H.B. Gray, *Protein-surfactant film voltammetry of wild-type and mutant cytochrome P450 BM3.* Inorg Chem, 2005. **44**(12): p. 4109-11.

[59] Savéant, J.M., *Elements of Molecular and Biomolecular Electrochemistry, An Electrochemical Approach to Electron Transfer Chemistry*. 2006, USA: Wiley-Interscience.

[60] Flock, U., N.J. Watmough and P. Adelroth, *Electron/proton coupling in bacterial nitric oxide reductase during reduction of oxygen.* Biochemistry, 2005. **44**(31): p. 10711-9.

[61] Watmough, N.J., S.J. Field, R.J. Hughes and D.J. Richardson, *The bacterial respiratory nitric oxide reductase.* Biochem Soc Trans, 2009. **37**(Pt 2): p. 392-9.

[62] Girsch, P. and S. de Vries, *Purification and initial kinetic and spectroscopic characterization of NO reductase from Paracoccus denitrificans.* Biochim Biophys Acta, 1997. **1318**(1-2): p. 202-16.

[63] Instruments, W.P., *Isolate dissolved oxygen meter and oxygen electrode.* 2001, United Kingdom World Precision Instruments

CHAPTER 4

NOR KINETICS:
NO AND O_2 REDUCTION

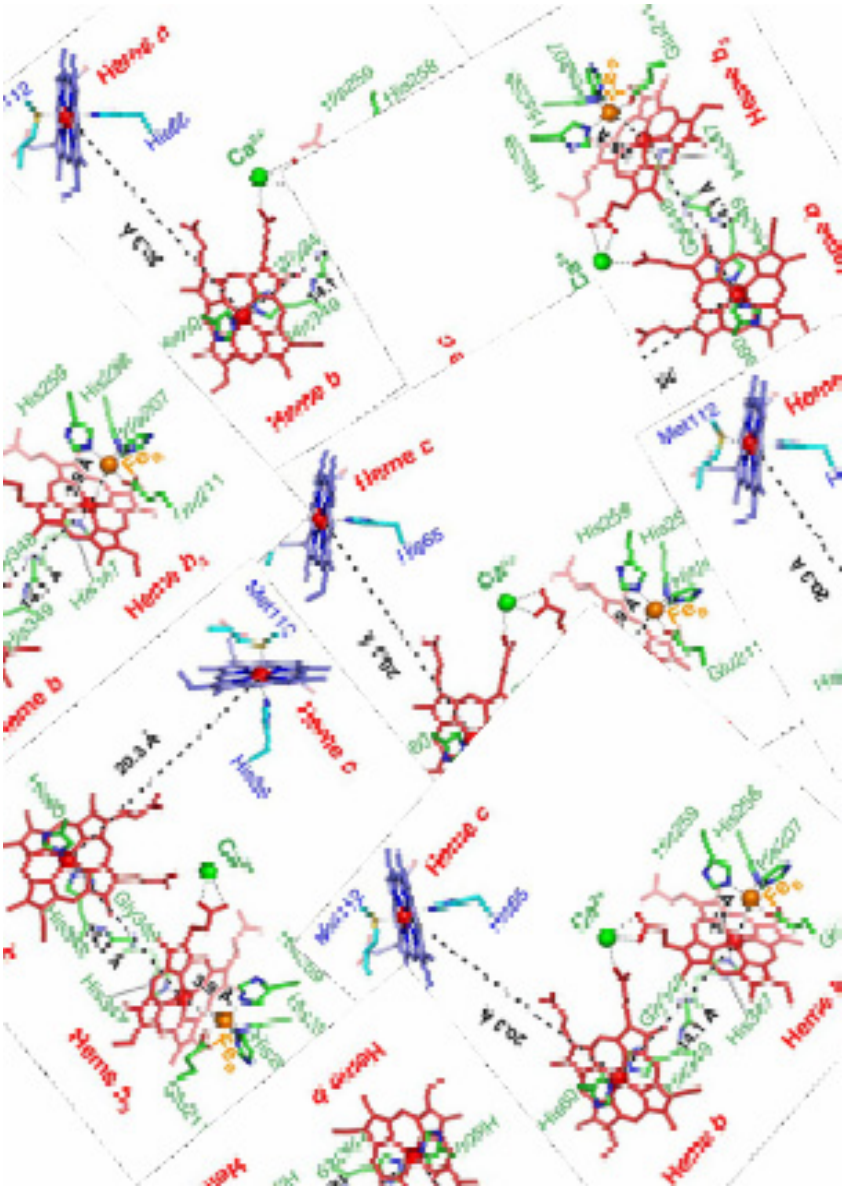

Chapter 4 Nitric Oxide Reductase Kinetics: Nitric Oxide and Oxygen Reduction

4. Nitric Oxide Reductase Kinetics: Nitric Oxide and Oxygen Activity

4.1. The Nitric Oxide Reductase Activity

NO reduction has been studied for different NORs [1-6] and other members of the HCuO superfamily such as the *cbb*$_3$, *ba*$_3$ and *bo*$_3$ type C*c*O in different buffers, electron donors and pH solutions [7-9].

Here, NO reduction by *Ps. nautica* NOR was studied. The reaction uses two electrons, as quantified using electrochemical techniques, (chapter 3, section 3.5.1) and two protons, with the formation of N_2O and H_2O, as described by the following equation:

$$2\,NO + 2\,e^- + 2\,H^+ \longrightarrow N_2O + H_2O \qquad \text{(eq. 4.1)}$$

In addition NORs present oxidoreductase activity. The reduction of O_2 seems to follow the same stoichiometry as the HCuOs, without proton translocation, since NORs do not pump protons against the gradient, for energy generation. During O_2 reduction, the protons are up taken from the periplamatic space [2, 10]. The reaction catalysed by *Ps. nautica* NOR involves four electrons for the complete reduction to H_2O (eq. 4.2), as it was demonstrated in the previous chapter (chapter 3, section 3.5.1).

$$O_2 + 4\,e^- + 4\,H^+ \longrightarrow 2\,H_2O \qquad \text{(eq. 4.2)}$$

This chapter of the thesis deals with the kinetic characterization of the enzyme under NO and O_2 catalysis. The main goals of the kinetic experiments are:

i) The kinetic characterization of the NO reduction and oxidoreductase activities of the *Ps. nautica* NOR, using two electron donors: the cyt. *c*$_{552}$ and the direct electrochemical response of the immobilized enzyme in an electrode surface, in which, the electrode can deliver the electrons directly to the protein.

ii) New insights into the structural and functional mechanism of NO and O_2 reduction, based on the pH dependence of the enzymatic activity.

In order to establish a kinetic model for each of the substrates reduction, velocity equations were deduced for several kinetic hypotheses, followed by simulations that could fit the experimental data. For each model it was taken into account the enzyme/substrate stoichiometry, and two assumptions were made:

i) initial rate conditions: when t=0, velocity and product concentration are both equal to zero;

ii) the measurements are made under steady-state kinetic conditions: the catalytic reaction is irreversible and the intermediate species formed between the substrate and the enzyme have constant concentration during the reaction time.

Different models where assumed, such as the Michaelis-Menten, substrate inhibition, the non-productive binding and consecutive substrate binding.

In same cases, the Lineweaver–Burk and Hanes-Woolf linearization were used to estimate the kinetic features, to use as a first approach in the fitting process.

4.2. Physiological Electron Donor

4.2.1. The *Pseudomonas nautica* Cytochrome c_{552}

The cNORs seem to present two physiological electron donors, pseudoazurin or azurin, described in *Pa. denitrificans* and in *Ps. aeruginosa* or *nautica*, a soluble *c*-type cytochrome, such as the cyt. c_{551} or cyt. c_{552}, respectively [4, 11, 12]. Many chemical electron donors are reported in the literature, either used alone or in combination with ascorbate , PMS [1, 11], TMPD [13] or HH cyt. *c* combined with TMPD [2].

The interaction of *Ps. nautica* NOR with the cyt. c_{552} under NO reduction as been described previously [11]. It could be assumed that in the presence of O_2, the enzyme would use the same redox partner. To confirm this assumption, several isolated cytochromes were tested as physiological electron donors. Figure 4.1 shows the re-oxidation of *c*-type cytochromes in the presence of *Ps. nautica* NOR under aerobic conditions. For all the cytochromes tested, only the cyt. c_{552} was able to rapidly transfer electrons to the NOR, because its re-oxidation is observed immediately (red line in figure 4.1).

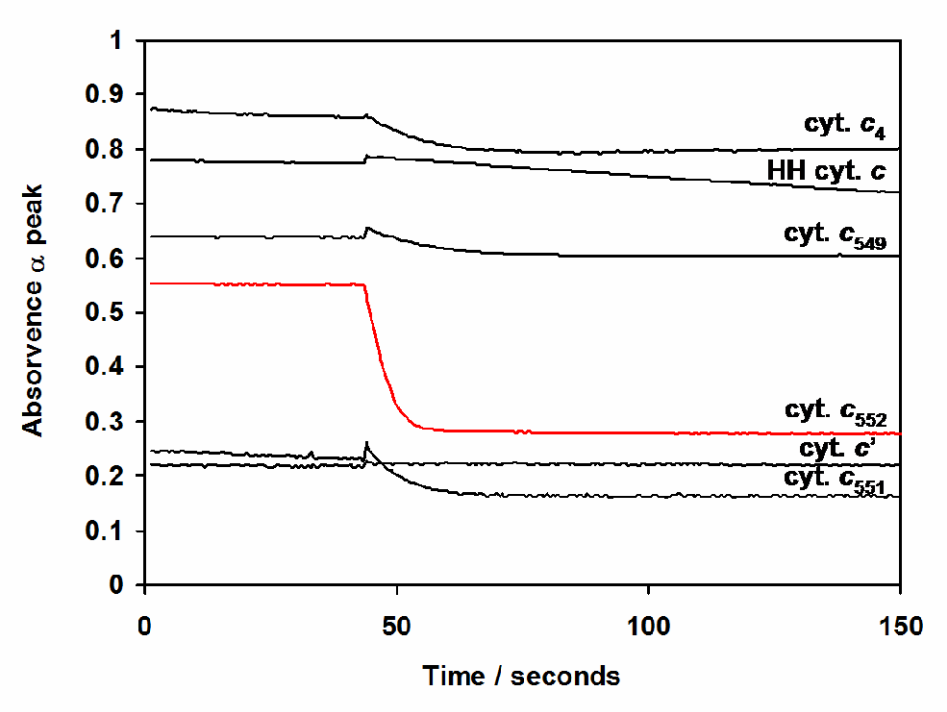

Figure 4.1 – Oxygen reduction by *Pseudomonas nautica* NOR, using different *c*-type cytochromes used as electron donors, isolated from the same microorganism. The representation shows the decay in the α peak of each cytochrome.

In order to conduct steady-state kinetics of the NOR with both substrates, it is imperative to search an optimal protein and electron donor concentration. In NO reduction, previous works point to a NOR concentration of 70 nM and 20 μM for the cyt. c_{552}, creating a ratio of approximately 300 times (supporting information S.6) [14]. The same study was done for the O_2 reduction, pointing a higher enzyme concentration, 0.5 μM and a 600 times larger concentration (300 μM) of electron donor (supporting information S.7).

4.3. Steady-Sate Kinetics Using Cytochrome c_{552}

Nitric oxide reduction

The available literature on steady-sate kinetics for cNORs presents an inhibitory pattern for the NO reduction when the substrate is present at high concentrations (in the low μM range). The substrate inhibition was justified by different interpretations: the first study which came out in 1997 [3] defends that NO binds to the reduced form of the enzyme consecutively, generating the N_2O product. The binding of a substrate molecule to the oxidized form of the enzyme would generate a non-catalytic species. Two years later, a different research group claim that the deduced velocity equation previously deduced was inappropriate for the associated mechanism. A new mechanism was proposed based in the sequential binding of NO molecules, but the inhibitory species being a complex of the enzyme with three NO molecules [15]. Controversy around these mechanisms continued. Recently, in 2010, a different group based on flow-flash experiments in single turnover conditions proposed a new catalytic mechanism and substrate concentration inhibition. Their results showed an obligatory binding of NO to the non-heme Fe_B before ligation to heme b_3, reducing NO trough a *trans*-mechanism and claiming this reaction to be highly inhibited by substrate [16]. In the same year, the first solved crystallographic structure at 2.7 Å, suggests that the catalytic center cavity undergoes structural rearrangements upon NO binding and reduction [4].

Work done in our group in *Ps. nautica*, demonstrated that the fully reduced state is the active form of the enzyme, and that the six-coordinated heme b_3 prompts the possibility of the initial step for NO catalysis to be the binding of the substrate to the Fe_B site. In this case the presence of a six ligand would weaken the affinity of NO binding to heme b_3 and promote the formation of an intermediate species at the Fe_B metal center [14].

Here, to determine the kinetic features under steady-state conditions, NO reduction experiments were conducted using the *Ps. nautica* NOR and the reduced cyt. c_{552} as the electron donor. The experimental data shows an inhibitory pattern (figure 4.2) characteristic of the reported cNORs.

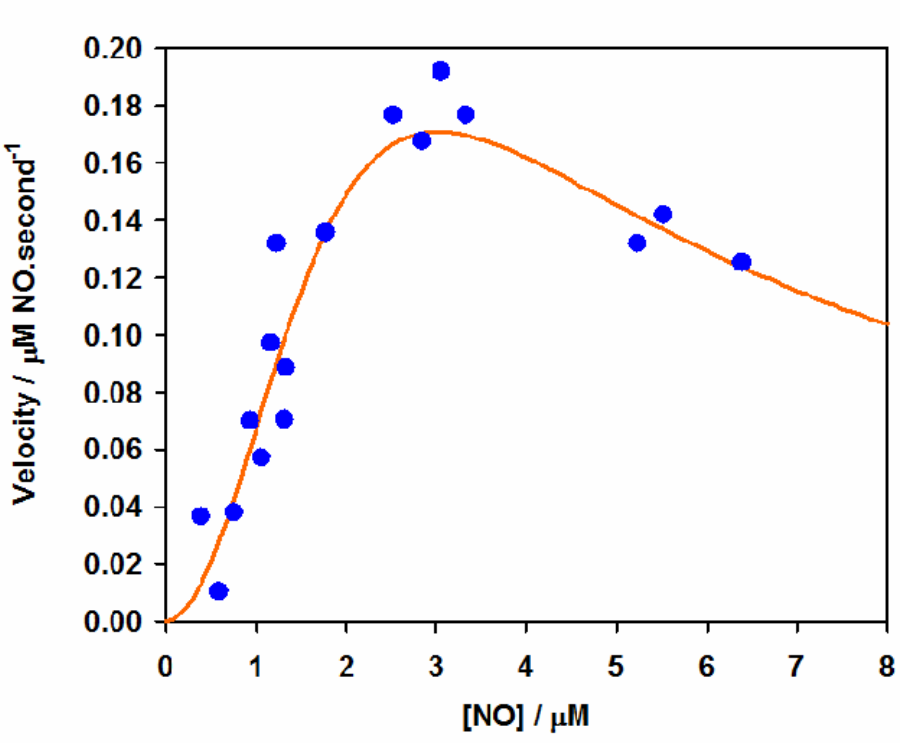

Figure 4.2 – Nitric oxide reduction by *Pseudomonas nautica* NOR, using reduced cyt. c_{552} as the electron donor. The plot exhibits the experimental data (blue dots) and the proposed fit (orange line, equation presented in figure 4.3) with the following kinetic parameters: k_{cat} = 30.4 ± 1.7 s^{-1}, K_1 = 3.6 ± 0.8 μM, K_2 = 6.2 ± 0.7 μM, and K_i = 9.7 ± 0.4 μM

The deduced kinetic model which could better describe the experimental data, is shown in figure 4.3.

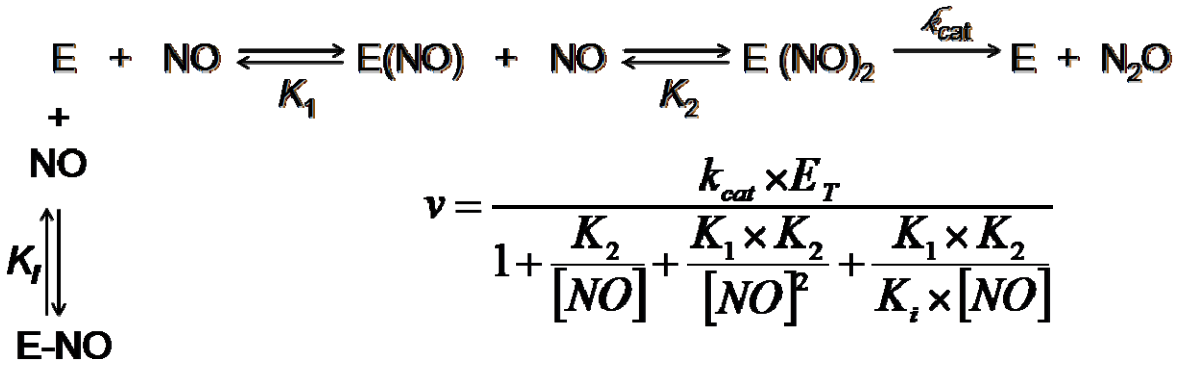

Figure 4.3 – Sequential binding mechanism for NO reduction. The scheme traduces the substrate binding and reaction steps, not showing the electrons and protons involved in the reaction. Rate equation is presented, as a function of substrate concentration and of the rate constants K_1, K_2, K_i and k_{cat}.

The chosen model (figure 4.3) is a sequential NO binding mechanism, where the substrate molecules bind at the catalytic center one at a time. If the first NO molecule binds the catalytic center in a different conformation, or induces an enzyme conformation which does not allow the ligation of the second substrate molecule, and consequent catalysis, then an inhibitory species is formed and leads to a substrate inhibition scenario. This model can be supported by both *cis* and *trans*-mechanisms [17]. The model shown in figure 4.2 fits well the experimental data with the following kinetic parameters k_{cat} = 30.4 ± 1.7 s^{-1} , K_1 = 3.6 ± 0.8 μM, K_2 = 6.2 ± 0.7 μM, and K_i = 9.7 ± 0.4 μM. The kinetic turnover obtained is in agreement with other values mentioned in the literature, from different denitrifying bacteria [2, 4, 5, 16].

During the modulation process other mechanisms were tested. The simultaneous entrance of two NO molecules or the inhibitory effect from the incorrect binding of a second NO molecule, could not fit well the experimental data and were excluded.

The three NO molecule inhibition complex hypothesis proposed by *Koutny et al.* [15] was also tested to fit the experimental data. However, X-ray data reveals not even enough space in the active site pocket to accommodate two NO molecules, explained by the short distance between the two catalytic irons (3.9 Å) and the presence of the Glu residue coordinating the non-heme Fe [4].

An inevitable consequence in enzyme kinetics is the case of product inhibition. There is no reference in the literature for the reversibility in NO reduction. However product inhibition must be expected if the product formed is also bound to the enzyme, even if the reversible reaction is negligible, because it can block the binding of a new substrate molecule to the active site. The modulation of the present kinetic data is not adequate to investigate a product inhibition mechanism. To address this subject, this possible behaviour should be analyzed in steady-state kinetic experiments in the presence of controlled concentrations of the reaction product, with the reaction assays being started by the addition of substrate [18].

Oxygen reduction

To characterize the proton uptake, the O_2 reduction by NORs has been intensively studied by flow-flash experiments in single turnover conditions, using the wild type and single mutant proteins [2, 19]. In C*c*O, studies are predominantly focused in the

characterization of relevant kinetic intermediates and in the proton pathways, since these oxidases are proton pumps [20].

The O_2 reduction by NOR has been reported for several isolated enzymes [2, 5]. However no detailed steady-state kinetic data is reported, with only some kinetic features using chemical electron donors being mentioned. In the oxidoreductase experiments, it is assumed that the active form is the fully reduced form, in analogy to the active form for NO reduction. Many authors assume that this reduced form can be obtained by incubation of the enzyme with ascorbate and mediators, such as HARC [19]. For the enzyme under study, it is reported that the incubation with ascorbate and PMS produces a reduced form equivalent to the reduced with dithionite, as characterized by spectroscopy [14].

In this section the O_2 consumption by *Ps. nautica* NOR using the reduced cyt. c_{552} as the electron donor was investigated. Analogously to the NO reduction studies, the velocity *vs.* substrate dependence in the O_2 reduction profile presents an inhibition pattern (figure 4.4).

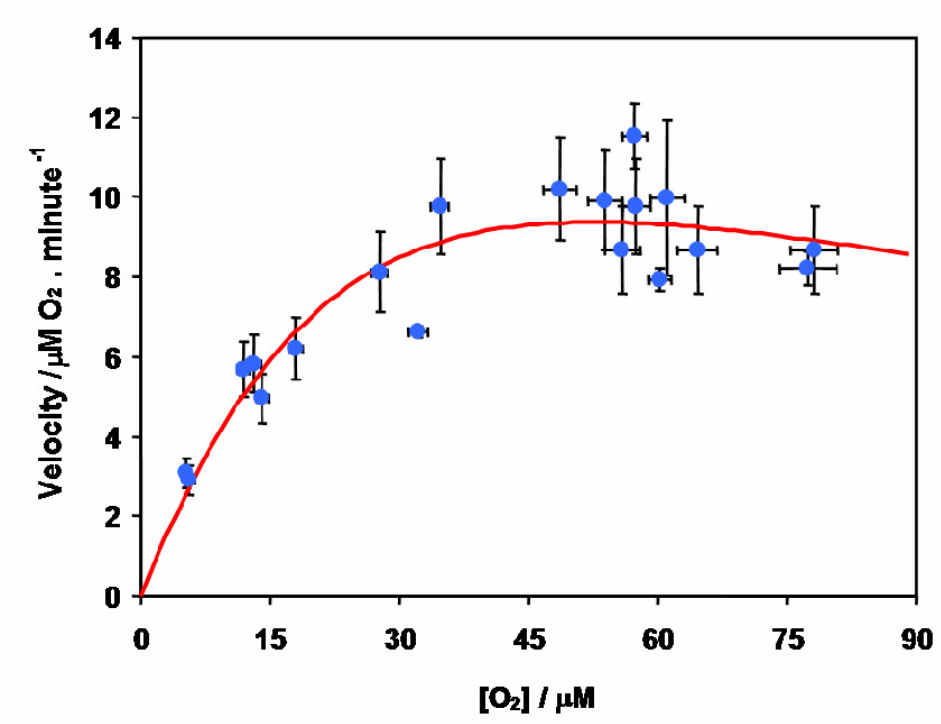

Figure 4.4 – Oxygen reduction by *Pseudomonas nautica* NOR, using reduced cyt. c_{552} as the electron donor. The plot exhibits the experimental data (blue dots) and the proposed fit (red line, equation presented in figure 4.5) with the following kinetic parameters: V'_{max} = 26.9 ± 2.2 μM O_2. minute^{-1}, K'_M= 49.1 ± 3.2 μM, K_i= 56.3 ± 2.8 μM.

For this situation, a simple kinetic mechanism is assumed, since only one substrate molecule binds to the catalytic center (figure 4.5).

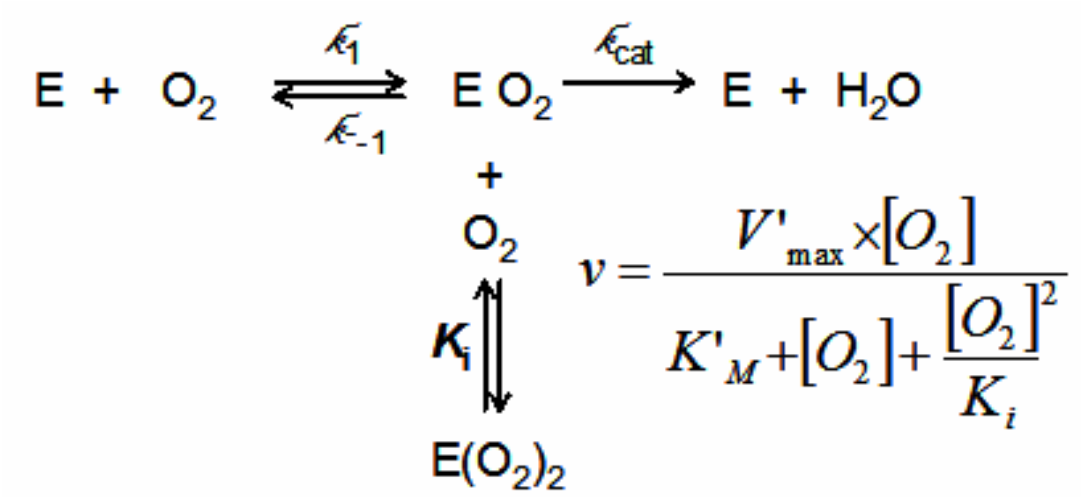

Figure 4.5 – Mechanism for oxygen reduction. The scheme traduces the substrate binding and reaction steps, not showing the electrons and protons involved in the reaction. Rate equation is presented, as a function of substrate concentration and of the kinetic parameters V'_{max}, K'_M, and K_i

The Lineweaver-Burk and Hanes-Woolf linearization of this rate equation are not straight lines, but instead they describe a hyperbola and a parabola respectively. If the K_i is larger than K'_M, it is possible to use the experimental data obtained at low substrate concentration to estimate the kinetic parameters: V'_{max} and K'_M [21]. These parameters were used as a first attempt to fit all the experimental data. The final fit is presented in figure 4.4 (red line) with the following rate constants k_{cat} = 0.89 ± 0.07 s^{-1}; K_M 49.1 ± 3.2 μM; K_i = 56.3 ± 2.8 μM. The determined turnover rate is in agreement with the previously reported for other isolated cNOR [5], but lower when compared with a typical oxidoreductase activity from a C*c*O, as expected [22].

In parallel, during the modulation process a non-productive binding mechanism was tested, but the fit was inadequate to describe the experimental data and was excluded.

Mechanisms for O_2 reduction by members of the HCuO superfamily point to the O_2 molecule binding to the ferrous heme iron, with the formation of a well characterized ferryl compound, which afterwards forms a series of reasonable known intermediates [20]. In NOR, it is assumed that O_2 binds to the catalytic heme iron. However there is no evidence for a catalytic mechanism or the possible catalytic intermediates.

Remarks on NO and O_2 Reduction Using Cyt. c_{552} as Electron Donor

A summary of the information obtained for the steady-state kinetics using the NOR's physiological electron donor, cyt. c_{552} is presented in table 4.1 for an easier comparison of the kinetic parameters.

Table 4.1 – Kinetic parameters obtained for the *Pseudomonas nautica* NOR with NO or O_2 as substrates. *Pseudomonas nautica* cyt.c_{552} was used as the electron donor.

	NO reduction	O_2 reduction
k_{cat} (s-1)	30.4 ± 1.7	0.89 ± 0.07
K_1(μM)	3.6 ± 0.8	-
K_2 (μM)	6.2 ± 0.7	-
K'_M (μM)	-	49.1 ± 3.2
K_i(μM)	9.7 ± 0.4	56.3 ± 2.8

The *Ps. nautica* NOR exhibits a higher affinity for NO than for O_2, since the K'_M value for the oxidoreductase activity is much higher than the kinetic dissociation constants K_1 and K_2 determined for NO reduction. In addition, the high k_{cat} value for NO reduction reveals the high turnover of this enzyme. All the kinetic parameters of the table 4.1 agree with those of others [5], obtained by different methodologies. However, this is the first time that oxidoreductase experiments were done in steady-state conditions and using the enzyme physiological electron donor. The cyt. c_{552} was able to interact with NOR in both substrate reductions. Moreover oxidoreductase conditions required a higher ratio between the reduced cyt. c_{552}/NOR (600×) than when the enzyme was under NO reduction (≅ 300×) demonstrating that oxidoreductase activity demands a higher amount of electron donor. This result is here reported for the first time. This is also in agreement with the electrochemical results (section 3.5.1) showing that O_2 reduction requires four electrons wile NO reduction requires only two electrons.

4.4. Steady-State Kinetics Using Immobilized NOR

Electrochemistry can be used to study enzyme kinetics. Literature has an extensive series of examples for this approach [23-28], whereas electrode interacts directly with the protein giving rise to a catalytic response.

In order to continue the kinetic studies for the *Ps. nautica* NOR, steady-state kinetic assays where performed electrochemically adsorbing the enzyme to a graphite electrode (as described in chapter 3). In this case the electrode will deliver the electrons directly to the enzyme and as shown in section 3.5, the electrons can be transferred immediately to the catalytic binuclear center, enhancing catalysis. The study of a different electron donor system helps to understand the possible mechanism for catalysis and since the enzyme is immobilized at the electrode surface, it is possible to switch the bulk solution and produce variation of different parameters such as the ionic strength or pH.

The protein film preparations made on the electrode surface proved to be physically adsorbed, like the ones previously mentioned in chapter 3. However the produced enzyme films had different stability when they were in the presence of the different substrates. When NO was added, the protein kept immobilized and the preparation lasted for several assays (different scan rates and different pH values). The use of O_2 as substrate, especially at high concentration, seems to enhance the loss of the protein film from the electrode surface.

To conduct the kinetic assays, a RDE with a graphite surface was used. The choice of a rotative over a stationary electrode was done on purpose, because (as explained in section 3.5) in this system a convection flow is generated, that maintains the concentration of all the species in solution uniform and equal to the bulk solution, avowing the diffusion process existent in a stationary system. The use of a dynamic system will maintain the substrate concentration constant (substrate added to the bulk solution).

Cyclic voltammetry at high scan rate (1-5 Vs^{-1}) was used to estimate the electrode surface coverage (Γ), as described in section 3.3 of the previous chapter. To determine this value, it was used the well-define redox process II (section 3.3 and 3.3.3). The current measured in a normal linear sweep voltammetry assay was used to determine the catalytic current difference, at defined substrate concentrations. Figure 4.6 show an example of

two cathodic current increases, using the *Ps.* nautica NOR modified RDE, in the presence of NO and O_2.

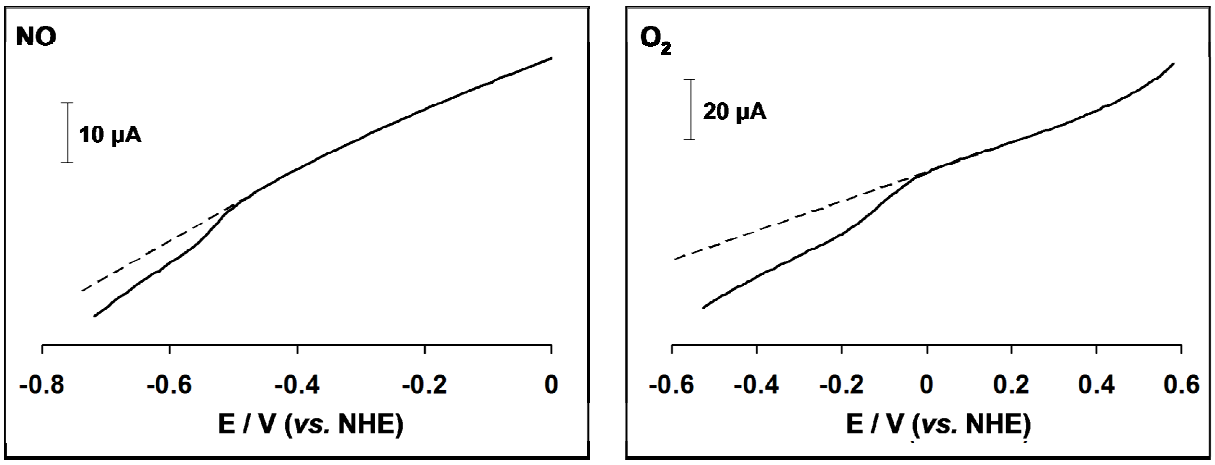

Figure 4.6 – Cathodic current increase in the presence of NO and O_2 obtained with the *Ps.* nautica NOR modified graphite RDE (ν = 50mVs^{-1}, 2000 RPM, [NO] = 50 µM, [O2] = 27.5 µM). The experiments were conducted in 20 mM mixture buffer (experimental details), pH 6.85 and 7.63 for NO and O_2 reduction, respectively.

All the kinetic assays were performed at a scan rate of 50 mVs$^{-1,}$ with an angular speed of 2000 RPM. The increase of the substrate concentration was traduced on an increase on the intensity of the catalytic current. Theses variations were determined taken, as it is exemplified in figure 4.6, and the values were transformed into velocities (µmol substrate.minute^{-1}) using the Faqraday law and according to the following equations:

$$Q = I_{\lim it} \times \Delta t \qquad \text{(eq. 4.1)}$$

$$Q = n_{mol} \times F \times n_{electrons} \qquad \text{(eq. 4.2)}$$

If there is a limit current, the charge at a certain potential value is proportional to the limit current at that same potential for the time that was applied. It is known for a redox process, that the charge is directly proportional to the number of electrons involved in the process and the amount of transformed compound. Therefore, for NO reduction and O_2 reduction there are two and four electrons, respectively, as quantified in the chapter 3.

Combining the two equations (eq. 4.1 and 4.2) and applying correction factors it is possible to transform the limit current measured at a certain potential to a substrate consumption value (eq. 4.3).

$$v \quad (\mu mol.substrate.\min^{-1}) = \frac{i_{\lim} \times 60 \times 10^{-6}}{F \times n_{electrons}} \qquad \text{(eq. 4.3)}$$

The enzyme kinetics study could be performed using the data obtained, without transforming the I_{lim} in a rate of substrate consumption, since I_{lim} is proportional to the number of electrons involved in the reduction process (n) and the electrode surface coverage (Γ) - I_{lim} = n. F A Γ*k*cat. However, this equation has some restrictions when used to study enzyme kinetics in substrate dependence. This equation can be applied when $I_{lim} = I_{max}$ (the maximum catalytic current attained in a substrate concentration) and this is only possible when [S] >> K_M (see following sections). In the rest of the cases, I_{lim} is different from I_{max}, therefore it was imperative the transformation of the kinetic data.

The data were collected for different substrate concentrations at different pH values. The previously kinetic assumptions are equally assumed: the steady-state, the initial rates and the irreversibility of the catalytic reaction.

4.4.1. Experiments Preformed at pH = 7.6

Nitric Oxide Reduction

The *Ps. nautica* NOR was adsorbed to a rotative disk graphite electrode and kinetic features towards NO reduction were evaluated (figure 4.7).

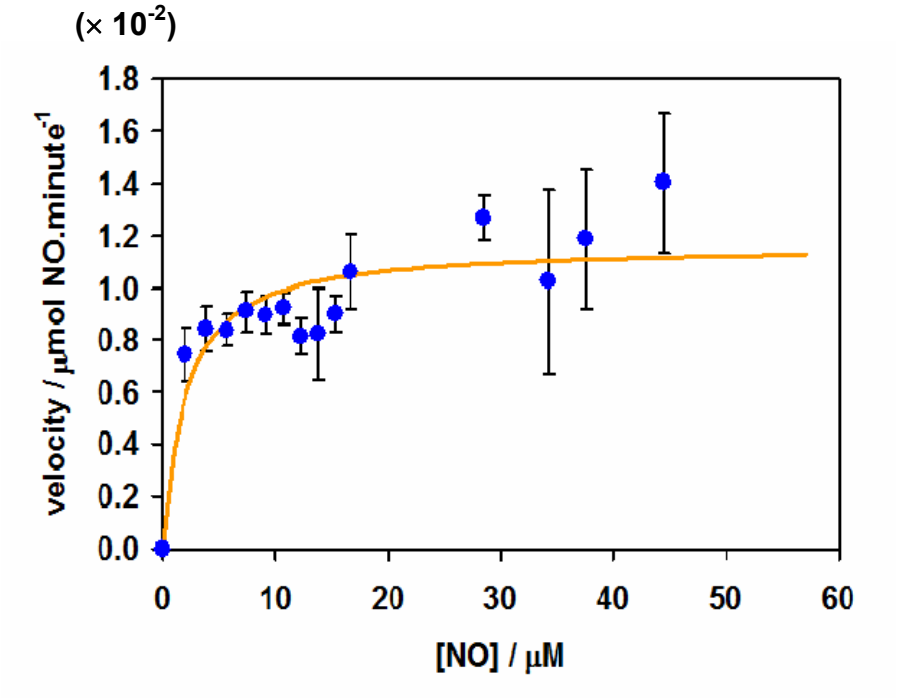

Figure 4.7 – Nitric oxide reduction by *Pseudomonas nautica* NOR using the immobilized enzyme on a graphite RDE (ν= 50 mV.s^{-1}, ω = 2000 RPM). The plot exhibits the experimental data (blue dots) and the proposed fit (orange line) with the following kinetic parameters: V'_{max} = 1.2 ± 0.1 × 10^{-2} µmol NO.minute^{-1}, K_1= 1.0 ± n.d. × 10^{-3} µM and K_2= 2.2 ± 0.2 µM.

The experimental data show (figure 4.7) that is a hyperbolic behaviour with no signs of substrate inhibition. In order to fit the experimental data, different kinetic models were tested in parallel. The two models seem to fit equally well the experimental data: a consecutive substrate binding with the formation of two intermediate species, and a second model with the simultaneous binding of two substrate molecules to the enzyme active site. Figure 4.8 shows the mechanism of consecutive binding. The kinetic

parameters obtained were: V'_{max}= 1.2 ± 0.1 × 10^{-2} μmol NO.$minute^{-1}$, K_1 = 1.0 ± n.d.[1] × 10^{-3} μM. and K_2 =2.2 ± 0.2 μM. The error for the first dissociation constant was not determined, since the smaller this value became, better became the theoretical fit, without considerable changes in K_2 or V'_{max} value. Using the electrode coverage and the electrode area, it is possible to determine the amount of active enzyme adsorved to the electrode ($\Gamma^{**} = \Gamma \times$ Electrode Area → Γ^{**} = 2.71 × 10^{-12} mol NOR), and determine the pseudo-first-order rate constant, since V'max = $k_{cat} \times [E_T]$, and $[E_T] = \Gamma^{**}$, therefore k_{cat} = 71.9 ± 2.88 s^{-1}. Unfortunately the initial part of the fit has a lack of experimental data (figure 4.7), this is due experimental limitations. As seen from the experimental kinetic features, NOR presents a high affinity for NO in its two binding steps, proved by the low values of the dissociation constants (K_1 and K_2). In addition, the high turnover can explain the limitations when working at low substrate concentrations.

$$E + NO \underset{K_1}{\rightleftharpoons} E(NO) + NO \underset{K_2}{\rightleftharpoons} E(NO)_2 \xrightarrow{k_{cat}} E + N_2O$$

$$v = \frac{V'_{max}}{1 + \frac{K_2}{[NO]} + \frac{K_1 \times K_2}{[NO]^2}}$$

Figure 4.8 – Sequential binding mechanism for NO reduction. The scheme traduces the substrate binding and reaction steps, not showing the electrons and protons involved in the reaction. Rate equation is presented, as a function of substrate concentration and of the kinetic parameters V'_{max}, K_1 and K_2 .

Simulations of the simultaneous binding NO molecules rate equation resembled a characteristic Michaelis-Menten model for two substrate molecules binding (data not shown). The rate equation was deduced, fitted and the kinetic parameters achieved were K_M=1.99 μM and V'_{max}= 1.1 ± 0.1 × 10^{-2} μmol NO.$minute^{-1}$. The values are close to the predicted for the first model, but this mechanism would not describe the possible subtract ligation to the binuclear catalytic center of the enzyme, since the active site presents a short Fe-Fe distance and it would be difficult to perform the binding of two NO

[1] n.d.- not determinated

molecules to the same or to different Fe atom(s) (depending on the mechanism, *cis* or *trans*) [4, 17].

Oxygen reduction

Oxidoreductase was measured under similar conditions using the *Ps. nautica* NOR adsorbed to the same graphite RDE. The results show a substrate inhibitory pattern (figure 4.5).

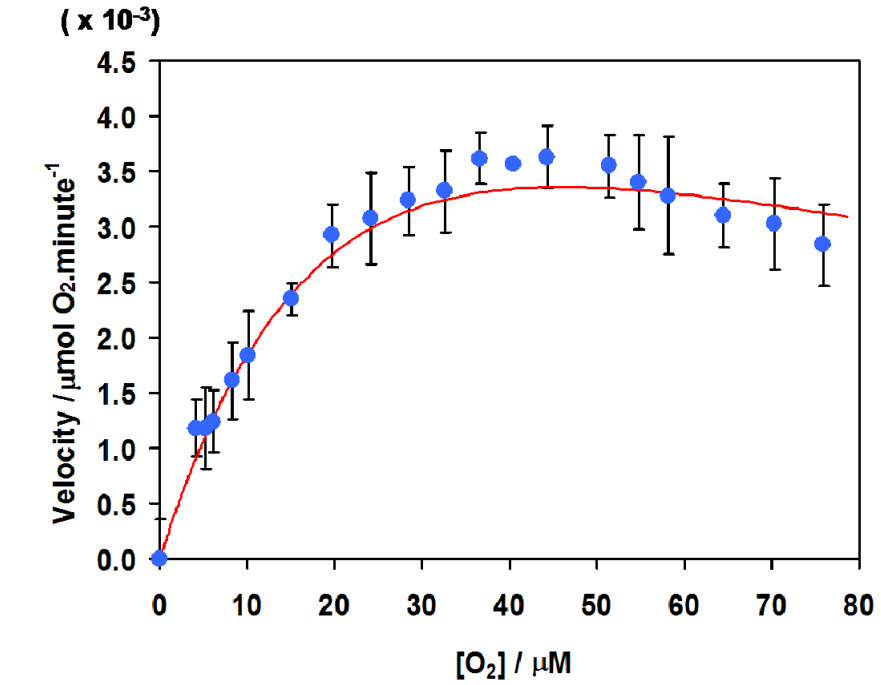

Figure 4.9 – Oxygen reduction by *Pseudomonas nautica* NOR using the enzyme immobilized on a graphite RDE (ν= 50 mV.s^{-1}, ω = 2000 RPM). The plot exhibits the experimental data (blue dots) and the proposed fit (red line) with the following kinetic parameters: V'_{max} = 8.1 ± 0.1 × 10^{-3} µmol O_2.minute^{-1}, K'_M= 32.4 ± 2.64 µM and K_i= 65.0 ± 5.6 µM

The kinetic model chosen to fit the experimental data was the previously described for the assays in the presence of the enzyme physiological electron donor (figure 4.5). The kinetic parameters achieved were: V'_{max} = 8.1 ± 0.5 × 10^{-3} µmol O_2.minute $^{-1}$, K'_M= 32.4 ± 2.6 µM and K_i = 65.2 ± 5.6 µM. Analogous to the previous result analysis, using Γ^{**}= [E_T] = 5.83 × 10^{-13} mol, the kinetic constant k_{cat}= 231.6 ±12.9 s^{-1} was determined, since V'max = k_{cat} × [E_T].

Remarks in NO and O_2 Reduction Using the immobilized Ps. nautica NOR at pH 7.6

Possible diffusion limitations can occur when adsorbed enzymes are used to study enzyme kinetics by electrochemical techniques. To overcome this issue a RDE can be used, in order to insure that the substrate bulk concentration is the same as at the electrode surface.

The results confirm that the *Ps. nautica* NOR has a higher affinity for NO than for O_2. NO reduction seems to occur in a two step mechanism, where the substrate molecules bind consecutively and quickly to the active site. This is suggested by the extremely low dissociation constants (table 4.2). O_2 is also reduced by NOR, but the enzyme presents a lower affinity for this substrate, exhibiting a higher dissociation constant (K_M).

Table 4.2 – Kinetic parameters obtained for the immobilized *Pseudomonas nautica* NOR in the presence of NO and O_2.

	NO reduction	**O_2 reduction**
V'_{max}	$1.2 \pm 0.1 \times 10^{-2}$	$8.1 \pm 0.1 \times 10^{-3}$-
k_{cat} (s^{-1})	71.9 ± 2.9	231.6 ± 12.9
K_1(μM)	$1.0 \pm$ n.d. $\times 10^{-3}$	-
K_2 (μM)	2.2 ± 0.2	-
K'_M (μM)	-	$32.4. \pm 2.6$
K_i(μM)	-	65.0 ± 5.6

It is not possible to compare the pseudo-first order rate constants (in grey) between the two substrate reductions. The comparison of these values would require the study of the kinetics in function of the electrode surface coverage, as it was done for the previous electron donor system; in function of the protein concentration is solution.

The low affinity for O_2 and the presence of a substrate inhibition pattern can justify the instability of the protein film on the electrode surface, when O_2 is present. During the assays, the O_2 concentration was raised to values close to 100 μM. It is predicted that this enzyme has a low turnover for O_2 and it will be possible the entrapment of O_2 in the

protein film, since it has a percentage of detergent in its constitution that could enhance the protein film release.

4.4.2. pH Dependence Experiments

The study of the kinetic activity in a pH scale is not physiologically relevant, but it may give hints in the structural and functional motifs of the protein, and information in its active kinetic form. The main objective in these experiments is to determine the dissociation constant values, in order to index possible protonable residues, crucial to the NO and O_2 reduction. Both substrate reductions were investigated by electrochemical assays with the *Ps. nautica* NOR adsorbed to the graphite RDE.

Nitric oxide reduction

Characterization of the NO reduction at pH 7.6 assumed a consecutive two substrate molecule binding mechanism, with the formation of two intermediate species. The K_1 value found was very small, and therefore, it is possible to assume that in the presence of NO the enzyme is in its form binding two NO molecules. The observed pattern at pH 7.6 was similar for all pH values tested ($2.5 < pH < 9.7$). All literature data is situated between $5 < pH < 9$ [2, 29], this is the first report on a wide range of pH.

To perform the analysis of the data, the first step will be to estimate the number of protons involved in the kinetic mechanism, where a plot of $V"_{max}$ *vs.* pH dependence is required. From now on, the velocity values obtained in the pH dependence are designated as $V"_{max}$ in order to differentiate these values from the $V"_{max}$ obtained at pH 7.6 ($V"_{max}$ = $1.2 \pm 0.1 \times 10^{-2}$ μmol NO. $minute^{-1}$). To determine $V"_{max}$ in all the investigated pH values is possible to assume that at substantially high substrate concentrations, similar to the Michaelis-Menten models, velocity is equal to $V"_{max}$. The results obtained are present in figure 4.10.

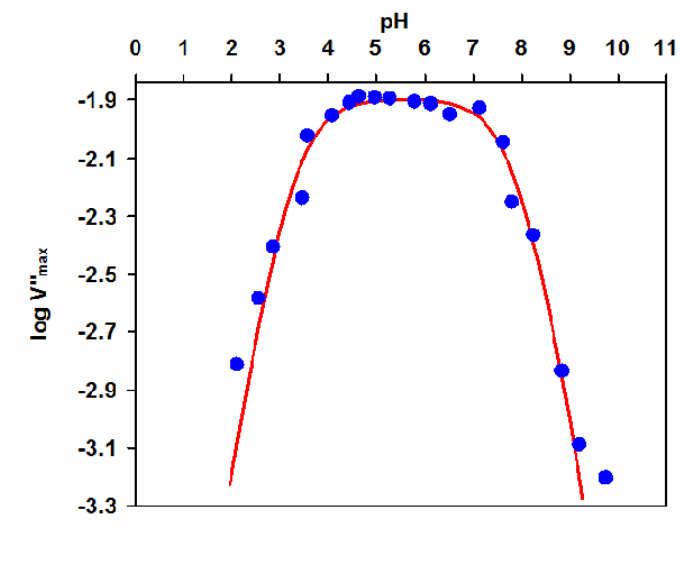

Figure 4.10 – pH dependence of the nitric oxide maximum reduction velocity. The plot exhibits the experimental data (blue dots) and the proposed fit (red line, eq. 4.4) with the following kinetic parameters: V'_{max} = 1.3 ± 0.1 × 10-2 μmol NO.minute^{-1}, pK_{a1} = 3.27 ± 0.03 and pK_{a2} = 7.92 ± 0.06.

The plot of the V'_{max} decimal logarithmic in function of the pH produces a bell shape curve, typical for a pH dependence enzyme kinetics, showing a maximum activity between 4 and 6. This result agrees with those obtained for steady-state NO reduction by NOR, that revealed to be strongly pH dependent between pH 6 and 8 [2, 19, 29].

The results are consistent with a two p*K* process. A complete diagram of the kinetic mechanism, presenting all the possible forms with only two protons, is showed in figure 4.11.

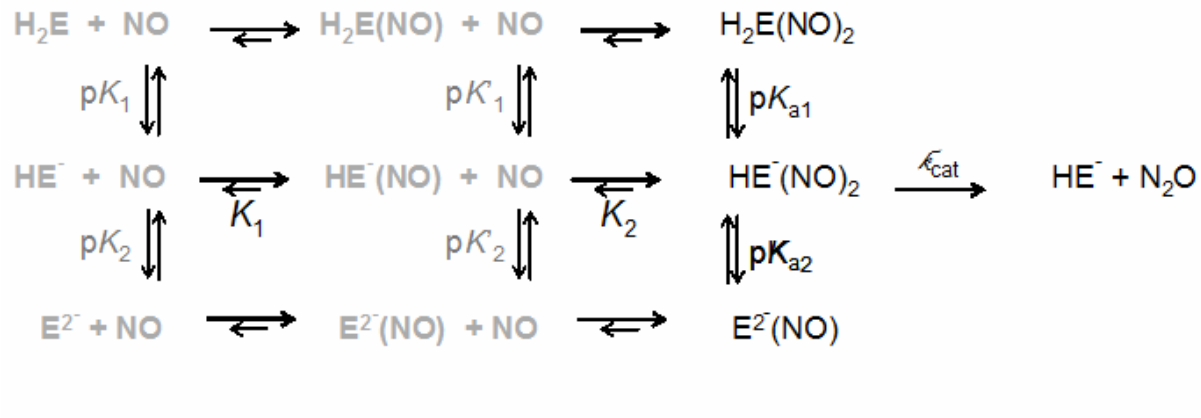

Figure 4.11 – Nitric oxide reduction mechanism assuming two protonable residues in the *Pseudomonas nautica* NOR.

Although it is possible to have a larger number of protonable residues. From the observation of the experimental results, it seems reasonable to assume the existence of only two major inflections in the graphic (two pK_as).

Besides the double protonation, the model assumes another restriction: only the single protonated form of the enzyme is able to catalyse the NO reduction. The assumption is reasonable since the activity approaches zero at high and low pH values.

For the deduction of the velocity rate equation (eq. 4.4), it should be noted that [NO] >>> K_1 and [NO] >> K_2, with this observation, a last assumption must be applied to this model: the free form of the enzyme is inexistent, so the equilibriums will be dislocated towards the protonated forms that are binding two substrate molecules (figure 4.11, written in black), and the remaining species will have a concentration near zero (figure 4.11, written in grey).

A velocity equation can be written for the proposed mechanism, with the above applied constraints:

$$E_T = [H_2E(NO)_2] + [HE^-(NO)_2] + [E^{2-}(NO)_2] +$$

$$+ \underbrace{[H_2E] + [H_2E(NO)] + [HE^-] + [HE^-(NO)] + [E^{2-}(NO)] + [E^{2-}]}_{=0}$$

$$v = k_{cat} \times [HE^-(NO)_2]$$

$$v = V''_{max} = \frac{V'_{max}}{\left(1 + \frac{[H^+]}{K_{a1}} + \frac{K_{a2}}{[H^+]}\right)} \qquad \text{(eq. 4.4)}$$

Therefore, the velocity equation in function of the pH (eq. 4.4) is totally independent from the substrate concentration. Using the equation it is possible to determine pK_{a1} and pK_{a2} by fitting a theoretical line in the V''_{max} *vs.* pH plot (figure 4.10, red line). The values obtained where pK_{a1}= 3.27 ± 0.03, pK_{a2}= 7.92 ± 0.06 and V'_{max} = 1.3 ± 0.1 × 10^{-2} μmol NO.minute^{-1}.

The only value obtained for a pK reported in the literature was 6.6 for the *Pa. denitrificans* NOR. This value was achieved in a pH dependence developed in a smaller pH

range (between 5 < pH < 9) and under O_2 reduction measurements, that were assumed to be similar for the NO reduction. The identity of the residue is unknown, but conserved Glu residues were proposed to be the responsible for this loss of activity [29].

The pK_{a2} = 7.92 determined here may correspond to a conserved Glu residue of the *Ps. nautica* enzyme. The higher value suggests that the aminoacid residue is buried inside the protein hydrophobic core, rising the pK_a (to values close to 8.8) [30].

It is hypothesized here that the pK_{a1} = 3.27 can probably be due to a conserved acidic aminoacid residue, for instance the Glu 125 or 202, (*Pa. denitrificans* numbering), since these residues are conserved among cNORs, and they all belong to the conserved proton pathway [2, 31].

Oxygen reduction

The pH dependence analysis for O_2 reduction proved more complicated. First, in all in the pH scale tested was noted a substrate inhibition effect, as it was described for pH 7.6 (section 4.4.1) additionally, the basic part of the curve is not very well defined and more experiments should be conducted at extremer basic pH values. The reason why these experiments were not done here was the choice to use the same combination of buffers for all the assays, with a maximum useful pH range around 9.75. A different component could be introduced to the mixture to increase the useful pH range, but that would lead to a new characterization of the enzyme kinetics for both substrates.

The assumptions made for the analysis of the NO reduction results can not be applied to O_2 reduction, since it exhibits an inhibitory pattern. For this reason v (velocity) ≠ V'_{max} and $[O_2] \cong K'_M$, making the condition of substrate saturation not valid. From now on, and similarly to the NO reduction pH dependence analysis, the kinetic parameters obtained in this section are named V'_{max}, K'_M and K'_i, in order to differentiate these values from the V'_{max}, K'_M and K_i obtained at pH 7.6.

The unique way to extract information from the experimental data is to fit an inhibitory model, as done for pH=7.6, in all the pH experiments and therefore, plot the kinetic parameters in function of the pH. From the analysis of the shape of the curves, it is, in principle, possible to infer how many protons are involved in the kinetic mechanism. Experimental results are shown in figure 4.12.

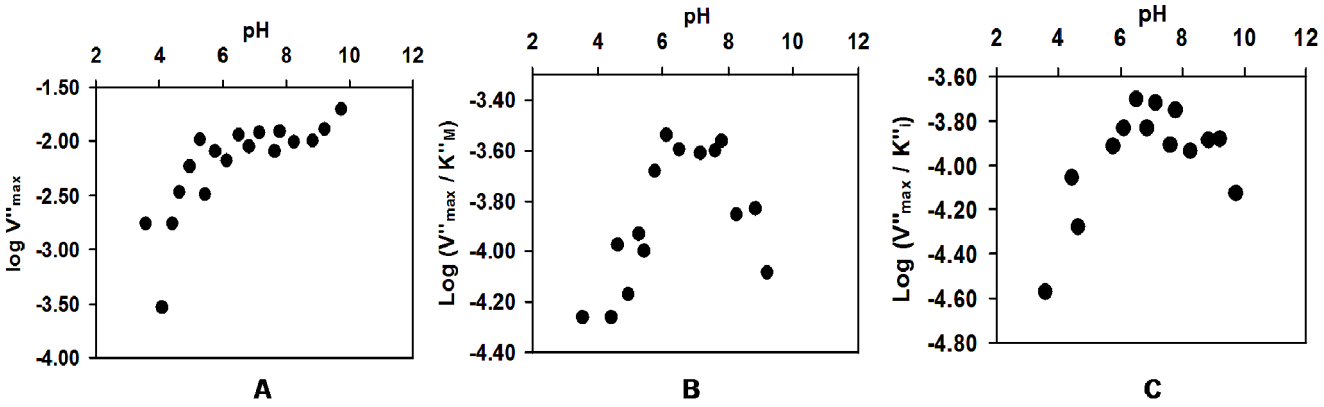

Figure 4.12 – pH dependence of the oxygen maximum reduction velocity. The plots show the decimal logarithmic for: A - $V"_{max}$, B - $V"_{max}/K"_M$ and C – $V"_{max}/K_i$ in function of the pH.

The results obtained have to be considered with reservations since the required higher O_2 concentrations destabilized the protein film. Although the experimental points could not be fitted by any predictable steady-state kinetic model, it is possible to make some qualitative considerations:

i) log $V"_{max}$ *vs.* pH suffered a shift of the optimal pH for higher values (when compared with NO), with an imperfect bell shape curve. This suggests the presence of at least one proton and if there is a second protonable residue, will have a smaller dissociation constant (higher p*K*).

ii) log $V"_{max}/K"_M$ and log $V"_{max}/K"_I$ *vs.* pH present a bell shape trend, suggesting at least the involvement of two protons in the kinetic mechanism.

At this point it is not possible to make any further conclusions. A hypothetical working hypothesis which includes the involvement of two protons is presented in figure 4.13.

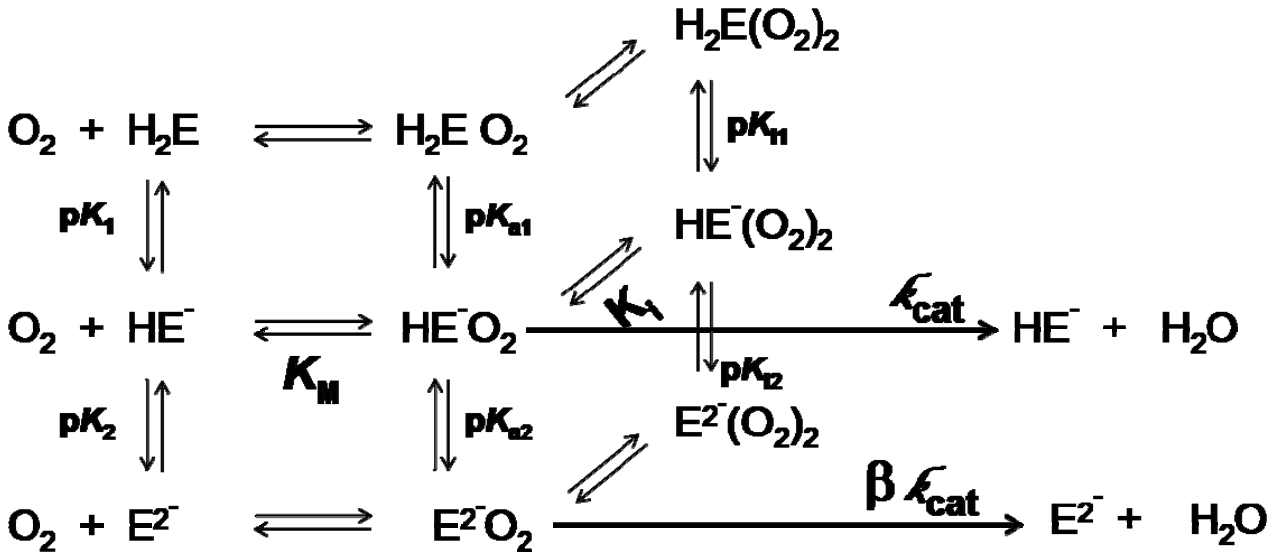

Figure 4.13 – Working hypotheses for an oxygen reduction mechanism assuming two protonable residues in the *Pseudomonas nautica* NOR.

The previous working model was assumed in order to fulfil the following assumptions:

i) The binding of two protons. log V'_{max} *vs.* pH shows that the enzyme is extremely active at pH values higher than 5. Since the data do not present a define trend in the graphic basic region, it is possible to predict the presence of one or two protonable residues. The assumption of two protonable residues is supported by the log V'_{max}/K'_M and log V''_{max}/K'_i vs. pH graphics.

ii) Unprotonated and single-protonated forms of the enzyme may catalyse O_2. The relation log V'_{max} *vs.* pH also suggests the possibility of product formation by the unprotonated and single protonated forms.

iii) The presence of all the putative enzyme species in solution. The $K'_M \cong [O_2]$ for all the analysed pH values, therefore the reaction for all the protonated and deprotonated forms are in equilibrium.

This working hypothesis can be used as a platform for future works.

Remarks on the pH dependence of nitric oxide and oxygen reduction

The main goal of the experiments was to search for enzymatic kinetics modifications that could reflect structural modifications, namely due to protonation/deprotonation of aminoacid residues.

It is the first time that steady state kinetic experiments are described for a NOR using electrochemical techniques. The applied methods revealed to be excellent for studying the pH dependence of the enzyme kinetics. Not only was it possible to achieve reproducible experimental data, as well as the enzyme modified electrode could be immersed in different pH solutions, in order to quickly check the enzyme activity.

Under NO reduction, the enzyme exhibits an optimal pH between 4 and 6, and under oxidoreductase activity this optimal pH is shifted towards higher pH values.

NO reduction presents two pK_as, 3.27 and 7.92, that can rise from different residues in the protein. It is most likely that they belong to the NOR proton pathway, since these residues are important for NO reduction performing the translocation of protons, towards the catalytic center or by coordinating the non-heme Fe_B (Glu residue coordinating the non-heme Fe_B is believed to be the last residue in the proton pathway).

The pK_{a1} = 3.27 was determined here for the first time, predicting a protonable residue with high solvent exposure. The value of 7.92 corresponding to pK_{a2} is probably related to the protonation of a conserved Glu berried in the protein core.

For elucidating the kinetic model and proton uptake that could explain NO and O_2 reduction the experiments must be extended to a broader range of pH with a grater sampling.

4.5. Experimental Details

Protein purification and preparation: NOR was purified from *Ps. nautica* membrane extracts, and it was biochemically characterized as described in chapter 2. Cytochromes c_{552}, c_{549}, c_4, c_{551} and *c'* were purified from *Ps. nautica* extracts as described in the literature and quantified using the correspondent molar extinction coefficients [32-38]. Samples containing each of the purified cytochromes, or the horse heart cytochromes *c* (*Sigma*), were concentrated and reduced with excess of sodium ascorbate, briefly centrifuged and applied into a His-Trap column (*Amersham*), equilibrated in 100 mM KPB pH 7.0 The eluted fraction was immediately collected, closed in an anaerobic flask and the atmosphere was replaced by argon, in order to prevent re-oxidation.

Electron donor assays: were performed in aerobic conditions, at room temperature, in 100 mM KPB pH 7, 0.02 (v/v) % DDM, with a cytochrome/NOR molar ratio of 100. Spectroscopic changes were monitored using the wavelength of each cytochrome α-band.

NO reduction assays: NO consumption was measured by an ISO-NO Mark II electrode, connected to Quad 16/EFA-400 and a computer. Data were collected and treated using DataTrax™ software (World Precision Instruments). The reaction was performed at room temperature, in anaerobic conditions, in 20 mM mixture buffer, (sodium citrate, MES, HEPES, AMPSO) pH 7.6, 0.02 (v/v) % DDM. The reduced cyt. c_{552} was used as the electron donor (20 μM), NO was dissolved in water and added to the solution with a gastight syringe, as described previously (chapter 3, experimental details), NOR was added in order to start the reaction (0.07 μM).

Oxidoreductase assays: O_2 consumption was measured by chronoamperometry, using an adapted Clarck electrode. Platinum was set as the working electrode, silver as the counter electrode and a SCE was introduced as the reference electrode. The potential was set to –0.7 V during the experiments. The three electrodes were connected to a μAUTOLAB type II potentiostat, and data acquired using GPES software. Assays were done in anaerobic environment, at room temperature, in 20 mM mixture buffer, (sodium citrate, MES, HEPES, AMPSO) pH 7.6, 0.02 (v/v) % DDM. Ascorbate reduced cyt. c_{552}

was used as the electron donor, O_2 dissolved in water was added to the anaerobic cell, with a gastight syringe and reaction started with NOR addiction (0.5 μM).

pH dependence assays: protein was immobilized in a graphite RDE, using the solvent casting technique as described in chapter 3 and the support electrolyte solution was a 20 mM mix buffer (sodium citrate, MES, HEPES, AMPSO), at different pH values. Substrate was added to the electrochemical cell, using different volumes of water solutions saturated with NO or O_2 (experimental details, Chapter 3). Surface coverage was determined by CV at high scan rates and kinetic data acquired inputting a linear sweep voltammogram at a scan rate of 50 $mV.s^{-1}$ and an ω of 2000 RPM. Experiments were made at room temperature, in anaerobic conditions.

4.6. References

[1] Dermastia, M., T. Turk and T.C. Hollocher, *Nitric oxide reductase. Purification from Paracoccus denitrificans with use of a single column and some characteristics.* J Biol Chem, 1991. **266**(17): p. 10899-905.

[2] Flock, U., P. Lachmann, J. Reimann, N.J. Watmough and P. Adelroth, *Exploring the terminal region of the proton pathway in the bacterial nitric oxide reductase.* J Inorg Biochem, 2009. **103**(5): p. 845-50.

[3] Girsch, P. and S. de Vries, *Purification and initial kinetic and spectroscopic characterization of NO reductase from Paracoccus denitrificans.* Biochim Biophys Acta, 1997. **1318**(1-2): p. 202-16.

[4] Hino, T., Y. Matsumoto, S. Nagano, H. Sugimoto, Y. Fukumori, T. Murata, S. Iwata and Y. Shiro, *Structural basis of biological N2O generation by bacterial nitric oxide reductase.* Science, 2010. **330**(6011): p. 1666-70.

[5] Sakurai, N. and T. Sakurai, *Isolation and characterization of nitric oxide reductase from Paracoccus halodenitrificans.* Biochemistry, 1997. **36**(45): p. 13809-15.

[6] Fujiwara, T. and Y. Fukumori, *Cytochrome cb-type nitric oxide reductase with cytochrome c oxidase activity from Paracoccus denitrificans ATCC 35512.* J Bacteriol, 1996. **178**(7): p. 1866-71.

[7] Butler, C., E. Forte, F. Maria Scandurra, M. Arese, A. Giuffre, C. Greenwood and P. Sarti, *Cytochrome bo(3) from Escherichia coli: the binding and turnover of nitric oxide.* Biochem Biophys Res Commun, 2002. **296**(5): p. 1272-8.

[8] Forte, E., A. Urbani, M. Saraste, P. Sarti, M. Brunori and A. Giuffre, *The cytochrome cbb3 from Pseudomonas stutzeri displays nitric oxide reductase activity.* Eur J Biochem, 2001. **268**(24): p. 6486-91.

[9] Giuffre, A., G. Stubauer, P. Sarti, M. Brunori, W.G. Zumft, G. Buse and T. Soulimane, *The heme-copper oxidases of Thermus thermophilus catalyze the reduction of nitric oxide: evolutionary implications.* Proc Natl Acad Sci U S A, 1999. **96**(26): p. 14718-23.

[10] Flock, U., J. Reimann and P. Adelroth, *Proton transfer in bacterial nitric oxide reductase.* Biochem Soc Trans, 2006. **34**(Pt 1): p. 188-90.

[11] Conrath, K., A.S. Pereira, C.E. Martins, C.G. Timoteo, P. Tavares, S. Spinelli, J. Kinne, C. Flaudrops, C. Cambillau, S. Muyldermans, I. Moura, J.J. Moura, M. Tegoni and A. Desmyter, *Camelid nanobodies raised against an integral membrane enzyme, nitric oxide reductase.* Protein Sci, 2009. **18**(3): p. 619-28.

[12] Field, S.J., F.H. Thorndycroft, A.D. Matorin, D.J. Richardson and N.J. Watmough, *The respiratory nitric oxide reductase (NorBC) from Paracoccus denitrificans.* Methods Enzymol, 2008. **437**: p. 79-101.

[13] Hendriks, J., A. Warne, U. Gohlke, T. Haltia, C. Ludovici, M. Lubben and M. Saraste, *The active site of the bacterial nitric oxide reductase is a dinuclear iron center.* Biochemistry, 1998. **37**(38): p. 13102-9.

[14] Timoteo, C.G., A.S. Pereira, C.E. Martins, S.G. Naik, A.G. Duarte, J.J. Moura, P. Tavares, B.H. Huynh and I. Moura, *Low-Spin Heme b3 in the Catalytic Center of Nitric Oxide Reductase from Pseudomonas nautica.* Biochemistry, 2011. **50**(20): p. 4251-4262.

[15] Koutny, M. and I. Kucera, *Kinetic analysis of substrate inhibition in nitric oxide reductase of Paracoccus denitrificans.* Biochem Biophys Res Commun, 1999. **262**(2): p. 562-4.

[16] Lachmann, P., Y. Huang, J. Reimann, U. Flock and P. Adelroth, *Substrate control of internal electron transfer in bacterial nitric-oxide reductase.* J Biol Chem, 2010. **285**(33): p. 25531-7.

[17] Watmough, N.J., S.J. Field, R.J. Hughes and D.J. Richardson, *The bacterial respiratory nitric oxide reductase.* Biochem Soc Trans, 2009. **37**(Pt 2): p. 392-9.

[18] Bissawanger, H., *Enzyme Kinetics Principles and Methods* W. -VCH, Editor. 2008.

[19] Reimann, J., U. Flock, H. Lepp, A. Honigmann and P. Adelroth, *A pathway for protons in nitric oxide reductase from Paracoccus denitrificans.* Biochim Biophys Acta, 2007. **1767**(5): p. 362-73.

[20] Brzezinski, P. and R.B. Gennis, *Cytochrome c oxidase: exciting progress and remaining mysteries.* J Bioenerg Biomembr, 2008. **40**(5): p. 521-31.

[21] Cornish-Bowde, A., *Fundamentals of Enzyme Kinetics*. third edition ed. 2004: Portland Press.

[22] Urbani, A., S. Gemeinhardt, A. Warne and M. Saraste, *Properties of the detergent solubilised cytochrome c oxidase (cytochrome cbb(3)) purified from Pseudomonas stutzeri.* FEBS Lett, 2001. **508**(1): p. 29-35.

[23] Cordas, C.M., I. Moura and J.J. Moura, *Direct electrochemical study of the multiple redox centers of hydrogenase from Desulfovibrio gigas.* Bioelectrochemistry, 2008. **74**(1): p. 83-9.

[24] Cordas, C.M., A.S. Pereira, C.E. Martins, C.G. Timoteo, I. Moura, J.J. Moura and P. Tavares, *Nitric oxide reductase: direct electrochemistry and electrocatalytic activity.* Chembiochem, 2006. **7**(12): p. 1878-81.

[25] Leger, C. and P. Bertrand, *Direct electrochemistry of redox enzymes as a tool for mechanistic studies.* Chem Rev, 2008. **108**(7): p. 2379-438.

[26] Paes de Sousa, P.M., S.R. Pauleta, M.L. Simoes Goncalves, G.W. Pettigrew, I. Moura, J.J. Moura and M.M. Correia dos Santos, *Artefacts induced on c-type haem proteins by electrode surfaces.* J Biol Inorg Chem. **16**(2): p. 209-15.

[27] Dell'Acqua, S., S.R. Pauleta, P.M. Paes de Sousa, E. Monzani, L. Casella, J.J. Moura and I. Moura, *A new CuZ active form in the catalytic reduction of N(2)O by nitrous oxide reductase from Pseudomonas nautica.* J Biol Inorg Chem, 2010. **15**(6): p. 967-76.

[28] Correia dos Santos, M.M., P.M. Sousa, M.L. Goncalves, M.J. Romao, I. Moura and J.J. Moura, *Direct electrochemistry of the Desulfovibrio gigas aldehyde oxidoreductase.* Eur J Biochem, 2004. **271**(7): p. 1329-38.

[29] Flock, U., N.J. Watmough and P. Adelroth, *Electron/proton coupling in bacterial nitric oxide reductase during reduction of oxygen.* Biochemistry, 2005. **44**(31): p. 10711-9.

[30] Fitch, C.A., D.A. Karp, K.K. Lee, W.E. Stites, E.E. Lattman and E.B. Garcia-Moreno, *Experimental pK(a) values of buried residues: analysis with continuum methods and role of water penetration.* Biophys J, 2002. **82**(6): p. 3289-304.

[31] Butland, G., S. Spiro, N.J. Watmough and D.J. Richardson, *Two conserved glutamates in the bacterial nitric oxide reductase are essential for activity but not assembly of the enzyme.* J Bacteriol, 2001. **183**(1): p. 189-99.

[32] Fauque, G.M., J. J. G.; Besson , S.; Saraiva, L.; Moura I. , *Caractérisation préliminaire de système cytochromique de la bactérie marine dénitrifiante Pseudomonas nautica 617.* Océans, 1992. **18**(2): p. 211-216.

[33] Gilmour, R., C.F. Goodhew and G.W. Pettigrew, *Cytochrome c′ of Paracoccus denitrificans.* Biochim Biophys Acta, 1991. **1059**(2): p. 233-8.

[34] Giudici-Orticoni, M.T., G. Leroy, W. Nitschke and M. Bruschi, *Characterization of a new dihemic c(4)-type cytochrome isolated from Thiobacillus ferrooxidans.* Biochemistry, 2000. **39**(24): p. 7205-11.

[35] Saraiva, L.M., S. Besson, G. Fauque and I. Moura, *Characterization of the dihemic cytochrome c549 from the marine denitrifying bacterium Pseudomonas nautica 617.* Biochem Biophys Res Commun, 1994. **199**(3): p. 1289-96.

[36] Saraiva, L.M., S. Besson, I. Moura and G. Fauque, *Purification and preliminary characterization of three c-type cytochromes from Pseudomonas nautica strain 617.* Biochem Biophys Res Commun, 1995. **212**(3): p. 1088-97.

[37] Saraiva, L.M., G. Fauque, S. Besson and I. Moura, *Physico-chemical and spectroscopic properties of the monohemic cytochrome C552 from Pseudomonas nautica 617.* Eur J Biochem, 1994. **224**(3): p. 1011-7.

[38] Wilson, M.T., C. Greenwood, M. Brunori and E. Antonini, *Electron transfer between azurin and cytochrone c-551 from Pseudomonas aeruginosa.* Biochem J, 1975. **145**(3): p. 449-57.

CHAPTER 5

MAIN CONCLUSIONS

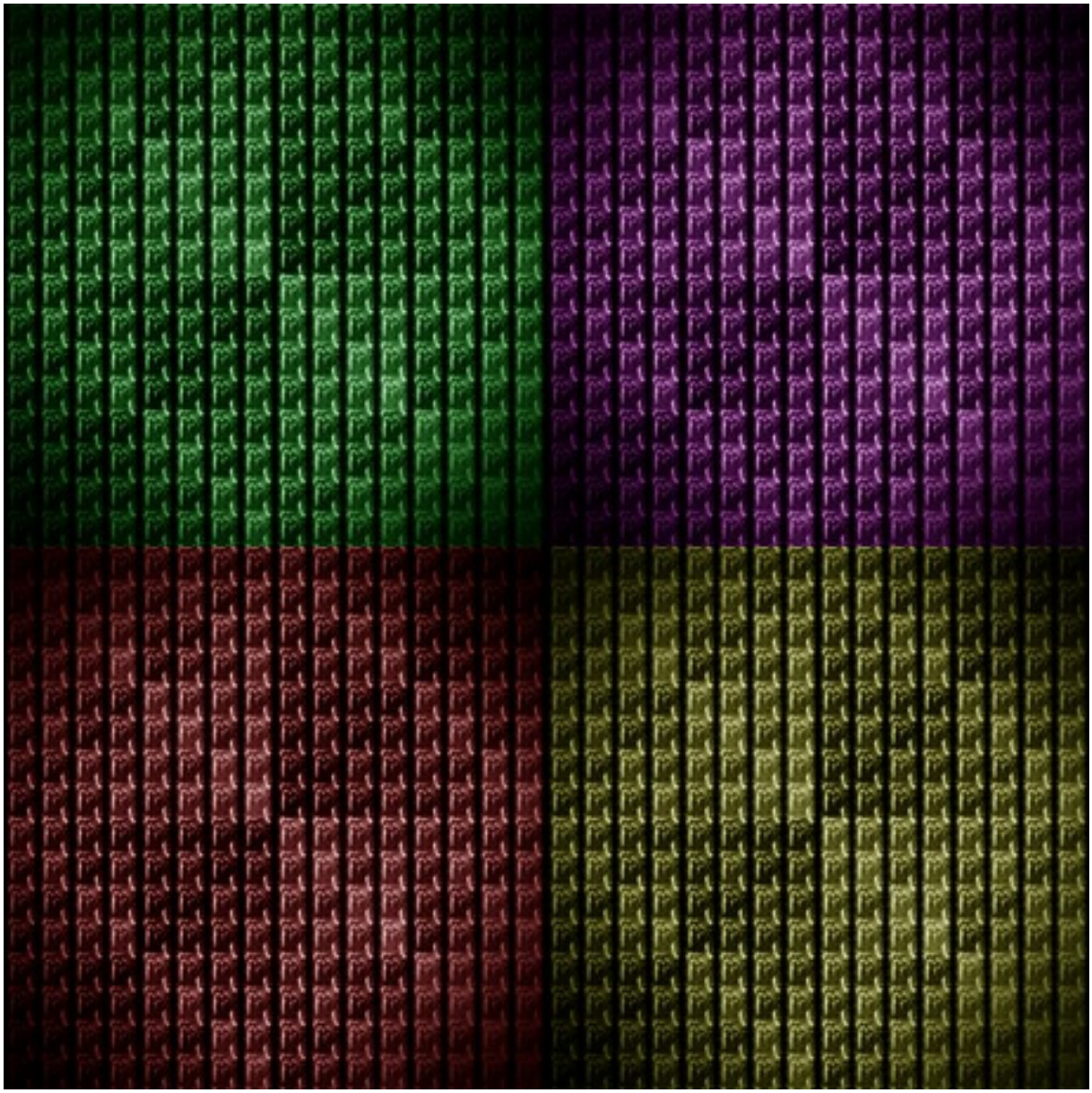

5. Main Conclusions

The *Pseudomonas nautica* NO reductase (NOR) is a metaloenzyme from the denitrification pathway, present in different denitrifying organisms and able to reduce NO to N_2O, and O_2 to H_2O. This class of enzymes carries a unique binuclear Fe center composed by a heme/non-heme Fe cluster where the substrate is reduced. Studies on this particular class of enzymes can bring light to the functional relevance of this single diiron center.

The main objective of this work was to isolate *Ps. nautica* NOR and characterize the enzyme metal co-factors, using different biochemical and spectroscopic techniques.

The optimized protocol for the purification of the native enzyme was developed. This is an integral membrane protein, isolated as a heterodimer formed by the subunits NorC and NorB. This enzyme presents a high homology with other cNORs such as the ones isolated from *Ps. stutzeri* and *aeruginosa*. The achieved enzyme fractions presented high purity, a correct metal stoichiometry, and therefore reproducible results could be obtained.

The NOR presents four iron centers. The low-spin heme *c*, covalently bound to the NorC subunit, a low-spin heme *b* and the catalytic diiron center, composed by a low-spin heme b_3 and a non-heme Fe_B.

The spectroscopic characterization made using different techniques revealed new structural features.

The UV-visible absorption spectroscopy analysis suggests that the heme b_3 is in a low-spin conformation. Previously, this catalytic heme center was thought to be high-spin [1]. The results obtained here are in agreement with a recent report which demonstrated unequivocally that it is in fact a low-spin center, for both ferric and ferrous states [2].

EPR spectroscopy proved the existence of a new integer-spin species rising from the diiron antiferromagnetic coupled center. This is the first time an integer-spin signal is detected in a NOR enzyme. The binuclear Fe center was believed to be EPR silent. However, the EPR results presented here and the Mössbauer data obtained in our research group [2] leads beyond doubt the presence of an integer-spin species, composed by a heme b_3-Fe^{III}-Fe_B^{III}.

The UV-visible absorption spectroscopy showed that the low-spin electron transfer heme *c* and heme *b* present a small reduced fraction in the as-isolated form of the enzyme, which is in agreement with Mössbauer spectroscopy analysis [2]. This was expected since the midpoint redox potential for these centers is believed to be highly positive [2, 3], a fact that was also demonstrated in this thesis.

In order to study the midpoint redox potential of the enzyme iron co-factors, direct electron transference between the immobilized *Ps. nautica* NOR and a pyrolytic graphite electrode was accomplished. This was the first time that the four redox processes were distinguished using this approach (figure 5.1, in bold). Figure 5.1 shows a summary of the midpoint redox potentials reported in the literature, which were obtained by different techniques applied to NORs from different microorganisms.

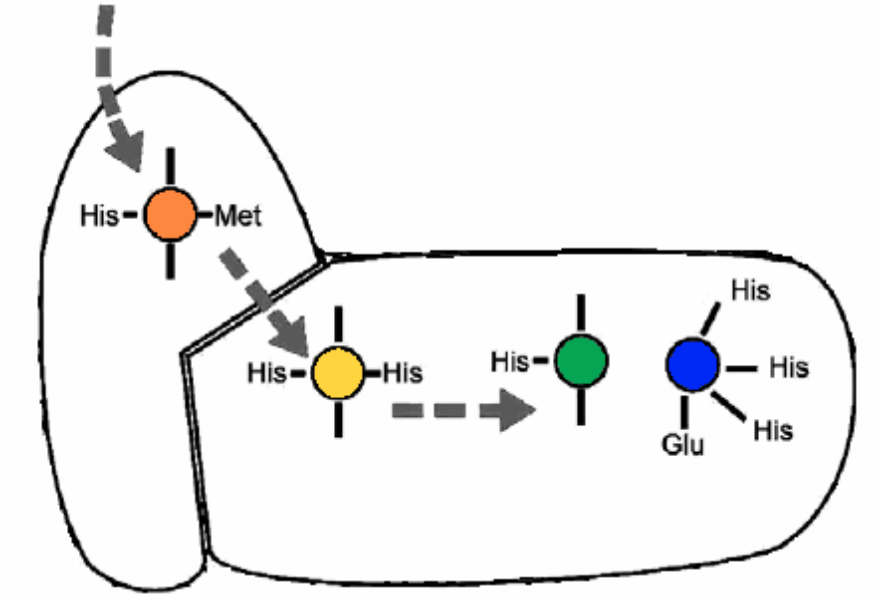

enzyme/organism	Heme *c*	Heme *b*	Heme b_3	Fe_B	method /Ref.
cNOR/*Ps. nautica*	**208**	**43**	**-162**	**- 369**	**DE / this work**
	n.d.	n.d.	-126	n.d.	DE / [4]
	215	n.d.	-38	n.d.	RT / [2]
cNOR/*Pa. denitrificans*	310	345	60	320	RT / [3]
	≅ 300	≅ 300	80	80	RT / [5]
Fe-myoglobin/ recombinant	n.d.	n.d.	-158/-46	n.d.	SE/ [6, 7]

n.d. – not determined

DE – Direct electrochemical measurements

RT – Visible redox titration

SE – Spectroelectrochemical measurements

Figure 5.1 – Midpoint redox potentials for the NOR metal centers. Top, schematic representation of the NOR structure emphasising the four co-factors, with the correspondent ligands. Bottom, summary table of the midpoint redox potentials. The results obtained in this work are in bold.

The results presented in this work show that:

i) The non-heme Fe_B presents a very low midpoint redox potential. Previously it was believed that the catalytic heme b_3 was the Fe center with the lowest redox potential, and therefore, responsible for the thermodynamic barrier between the low-spin heme electron transfer groups and the catalytic center.

ii) The binuclear catalytic cluster presents a low redox potential. It was thought that only the catalytic heme b_3 had a negative midpoint redox potential. The results presented here show that both catalytic iron atoms have low redox potentials. This is supported by the spectroscopic results published by our research group, showing the reduction of the NOR catalytic center only in the presence of strong reducing agents.

iii) The higher midpoint redox potential of the protein is the low-spin heme *c*. This is in agreement with the literature [2, 3] (and rNorC subunit, below in the text), since this is metal center that is predicted to interact with the electron physiological donor, and to be responsible for the electrons entrance in the protein. The high redox potential of this center, when compared with the remaining metal irons, promotes the intramolecular electron transfer.

iv) The results obtained for the midpoint redox potentials in a pH dependence, for all the Fe centers, suggest the presence of a hydrogen bond network surrounding the heme propionate side chains, most likely due to the presence of several conserved aminoacid residues in the NOR subclass. More experiments should be conducted in order to elucidate the relevance of these residues and confirm this hypothesis.

In parallel to the native NOR, the rNorC subunit was used in direct electrochemical experiments. This was is the first time that direct electron transfer was studied with this subunit, separately from the catalytic subunit NorB. The results showed that:

i) the heme *c* is unequivocally the metal center with the highest positive redox potential. The recombinant subunit presents a midpoint redox potential of the same magnitude of the one determined for the heme *c* present in the native protein.

ii) The 100 mV difference between the heme *c* potencial of the rNorC and the determined for the native enzyme can be justified by the subunit separation. This may suggest that the NOR subunits have strong interaction interface (also predicted by the determined x-ray crystal structure [8]. Moreover the separation of the subunits may produces severe structural changes on the heme *c* vicinity.

The enzyme under study is capable of NO reduction in a two proton/two electron reaction, producing N_2O and also presents oxidoreductase activity, reducing O_2 in a four electron/four protons reaction. This result agrees with the literature [9].

In this work are reported direct electrochemical measurements for the immobilized *Ps. nautica* NOR, under catalytic conditions, showing the electrocatalytic response for both substrates. This approach was already described in literature [4]. However, in this work one of the goals was to use it to quantify the number of electrons involved in each substrate reduction. This is the first time that the quantification of electrons involved in these reactions was performed using an electrochemical method. Until now the mentioned electron/protons stoichiometry reported were achieved by the steady-state kinetics [9]. The results here presented, showed beyond doubt that O_2 is reduced to H_2O, without the formation of H_2O_2.

Steady-state kinetic assays were made in order to deduce the kinetic mechanisms and to determine the kinetic parameters for the NO and O_2 reduction. The experiments were done using the reduced *Ps. nautica* cyt.c_{552} or *Ps. nautica* NOR immobilized to a graphite RDE (where the enzyme receives the electrons directly from the electrode). This is the first report on oxidoreductase activity measurements assayed with the enzyme's physiological electron donor.

Both electron donor systems show beyond doubt:

i) A higher affinity for NO than for O_2. This can be concluded by the lower dissociation constant determined for the NO reduction assays.

ii) Two NO molecules bind to the enzyme in a consecutive mechanism. This was expected, since the reaction requires two substrate molecules and the binding of two substrate molecules simultaneously to the catalytic center is not predicted by the proposed catalytic neither by the determined crystal structure [1, 8].

iii) O_2 reduction presents inhibitory pattern for the steady-state assays made with the cyt. c_{552} and the immobilized enzyme. This can be due to the inhibitory effect of the substrate.

The pH dependence experiments of the immobilized *Ps. nautica* NOR show the presence of a protonable residue probably an acidic residue (Glu or Asp), that has never been reported before. This residue is probably a glutamate residues essential for the protons translocation [10, 11].

The information discussed in this thesis can be useful in future works, since it brings new insights to the catalytic binuclear center, in issues such as the heme b_3 coordination and spin state, or the non-heme Fe_B redox potential value. The presented kinetic study on the secondary substrate, O_2, for this enzyme can be seen as a platform for further kinetic experiments. Therefore, these results can be used to claim reconsiderations in the NO reduction mechanism, a subject under discussion during the last 20 years, and bring to light hypothesis on the alternative substrate reduction by this class of proteins. Moreover, applications can be developed in the biosensors area, in order to apply it in the different research fields such as bioremediation.

5.1. References

[1] Watmough, N.J., S.J. Field, R.J. Hughes and D.J. Richardson, *The bacterial respiratory nitric oxide reductase.* Biochem Soc Trans, 2009. **37**(Pt 2): p. 392-9.

[2] Timoteo, C.G., A.S. Pereira, C.E. Martins, S.G. Naik, A.G. Duarte, J.J. Moura, P. Tavares, B.H. Huynh and I. Moura, *Low-Spin Heme b3 in the Catalytic Center of Nitric Oxide Reductase from Pseudomonas nautica.* Biochemistry, 2011. **50**(20): p. 4251-4262.

[3] Gronberg, K.L., M.D. Roldan, L. Prior, G. Butland, M.R. Cheesman, D.J. Richardson, S. Spiro, A.J. Thomson and N.J. Watmough, *A low-redox potential heme in the dinuclear center of bacterial nitric oxide reductase: implications for the evolution of energy-conserving heme-copper oxidases.* Biochemistry, 1999. **38**(42): p. 13780-6.

[4] Cordas, C.M., A.S. Pereira, C.E. Martins, C.G. Timoteo, I. Moura, J.J. Moura and P. Tavares, *Nitric oxide reductase: direct electrochemistry and electrocatalytic activity.* Chembiochem, 2006. **7**(12): p. 1878-81.

[5] Field, S.J., M.D. Roldan, S.J. Marritt, J.N. Butt, D.J. Richardson and N.J. Watmough, *Electron transfer to the active site of the bacterial nitric oxide reductase is controlled by ligand binding to heme b(3).* Biochim Biophys Acta, 2011. **1807**(4): p. 451-7.

[6] Yeung, N., Y.W. Lin, Y.G. Gao, X. Zhao, B.S. Russell, L. Lei, K.D. Miner, H. Robinson and Y. Lu, *Rational design of a structural and functional nitric oxide reductase.* Nature, 2009. **462**(7276): p. 1079-82.

[7] Lin, Y.W., N. Yeung, Y.G. Gao, K.D. Miner, S. Tian, H. Robinson and Y. Lu, *Roles of glutamates and metal ions in a rationally designed nitric oxide reductase based on myoglobin.* Proc Natl Acad Sci U S A, 2010. **107**(19): p. 8581-6.

[8] Hino, T., Y. Matsumoto, S. Nagano, H. Sugimoto, Y. Fukumori, T. Murata, S. Iwata and Y. Shiro, *Structural basis of biological N2O generation by bacterial nitric oxide reductase.* Science, 2010. **330**(6011): p. 1666-70.

[9] Flock, U., N.J. Watmough and P. Adelroth, *Electron/proton coupling in bacterial nitric oxide reductase during reduction of oxygen.* Biochemistry, 2005. **44**(31): p. 10711-9.

[10] Butland, G., S. Spiro, N.J. Watmough and D.J. Richardson, *Two conserved glutamates in the bacterial nitric oxide reductase are essential for activity but not assembly of the enzyme.* J Bacteriol, 2001. **183**(1): p. 189-99.

[11] Flock, U., P. Lachmann, J. Reimann, N.J. Watmough and P. Adelroth, *Exploring the terminal region of the proton pathway in the bacterial nitric oxide reductase*. J Inorg Biochem, 2009. **103**(5): p. 845-50.

SUPPORTING INFORMATION

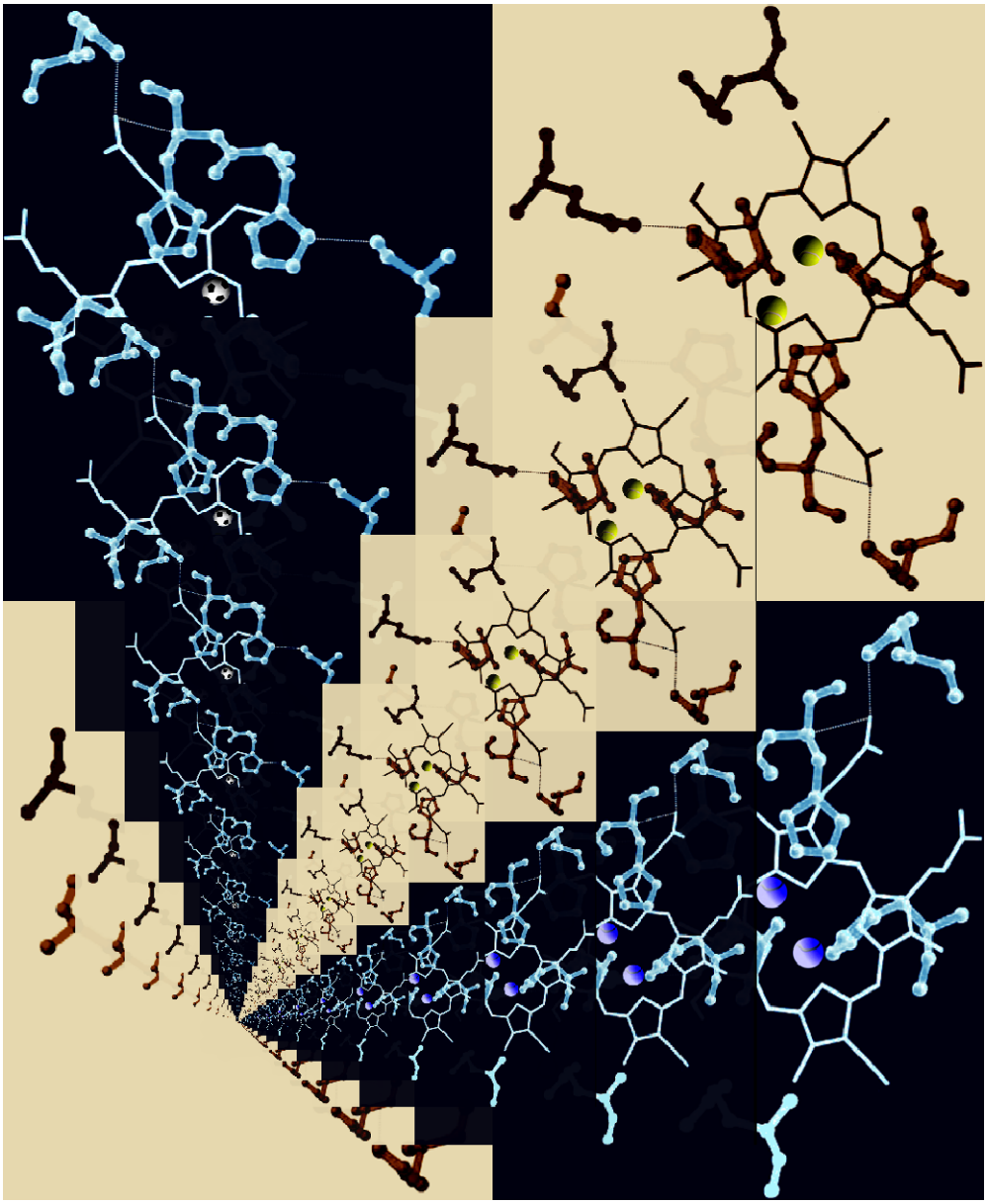

Supporting information

S.1 Primary Sequence Alignment

```
                                        10        20        30        40        50
                                ....|....|....|....|....|....|....|....|....|....|
NOR B Ps. nautica               --------------------------------------------------
NOR B Ps. aeruginosa            --------------------------------------------------
NOR B Ps. stutzeri              --------------------------------------------------
NOR B Pa. denitrificans         --------------------------------------------------
qNOR Ralstonia eutropha H16     MGSYRRLWFLLIAVLAVTFSLLGYYGVEVYRQAPPMPAKVVTTEGRTLFT
qNOR Achromobacter xylosoxidan  MGPYRKLWFTLIAVLAVTFALLGFYGGEVYRQAPPIPGQVVTADGKPLFG
qNOR Neisseria gonorrhoeae      MGQYKKLWYLLFAVLAVCFTILGYMGSEVYKKAPPYPEQVVSASGKVLMT
qNOR Haemophilus parainfluenza  MGQYKKFWYLLVAVLIGAFSILGYYGFEVYREAPPIPQQYVSESGEKVIT
qNOR Pyrobaculum aerophilum     --MKNGWTYFVLAATVLVYVVYIAMAVWTFYNLPPIPERVVTKSGELLFT

                                        60        70        80        90       100
                                ....|....|....|....|....|....|....|....|....|....|
NOR B Ps. nautica               --------------------------------------------------
NOR B Ps. aeruginosa            --------------------------------------------------
NOR B Ps. stutzeri              --------------------------------------------------
NOR B Pa. denitrificans         --------------------------------------------------
qNOR Ralstonia eutropha H16     GEEILDGQTAWQSVGGMQLGSIWGHGAYQAPDWTADWLHRELSAWLELAA
qNOR Achromobacter xylosoxidan  RDDILDGQTAWQSVGGMQLGSVWGHGAYQAPDWTADWLHRELTAWLDLAA
qNOR Neisseria gonorrhoeae      KDDILAGQSAWQSTGGMEVGSILGHGAYQAPDWTADWLHRELSAWLDLTA
qNOR Haemophilus parainfluenza  HDDILHGQTAWQTTGGMQVGSVWGHGAYQAPDWTADWLHRELTNWLDITA
qNOR Pyrobaculum aerophilum     AQDIIEGKTLAQKYGLLDYGSFLGFGGYFGIDYTAYTMKFFVDKIGQLKG

                                       110       120       130       140       150
                                ....|....|....|....|....|....|....|....|....|....|
NOR B Ps. nautica               --------------------------------------------------
NOR B Ps. aeruginosa            --------------------------------------------------
NOR B Ps. stutzeri              --------------------------------------------------
NOR B Pa. denitrificans         --------------------------------------------------
qNOR Ralstonia eutropha H16     QDANGRPYAQLDAPAQAALREHVRTEYRGNATDPATNVLTVSKRRAQAIA
qNOR Achromobacter xylosoxidan  REQHGQDYAQLDARAQAALRADLKAEYRANRSDAATDTLTVSPRRARAMA
qNOR Neisseria gonorrhoeae      QQAYGKKFDEVSPEEQAVLKTRLADEYRNQSRIKEDGSVVISDTRVKAIE
qNOR Haemophilus parainfluenza  NQEFGKNFADLNDEQQTLLKARLTKEYRGSK--VENGTVVLSNTRLAAME
qNOR Pyrobaculum aerophilum     ---------TALASEIKHLMTPQFSAKTSSLFAPAAGVAVVSDEFGAAYK

                                       160       170       180       190       200
                                ....|....|....|....|....|....|....|....|....|....|
NOR B Ps. nautica               --------------------------------------------------
NOR B Ps. aeruginosa            --------------------------------------------------
NOR B Ps. stutzeri              --------------------------------------------------
NOR B Pa. denitrificans         --------------------------------------------------
qNOR Ralstonia eutropha H16     DTAAYYDQLFSDAPALHTTREHYAMKENTLPSAERREQLTHFFFWTAWAA
qNOR Achromobacter xylosoxidan  QTAAYYGQLFSDAPALHRSRENFAMKENTLPDAARRTQLTHFFFWTAWAA
qNOR Neisseria gonorrhoeae      SILPYYHGVYGDDPKLQTTREHFAMKNNTLPSQEAREKLFDFFFWTSWSA
qNOR Haemophilus parainfluenza  KTAQYYISLYGDDPATKVTREHFAMKDNTLPDLQARKDLAKFFFWTAWTA
qNOR Pyrobaculum aerophilum     QAVDFYKQLFG------PKAEEIGLKPNLITDPEHVRKIVSFFTWGVMIA

                                       210       220       230       240       250
                                ....|....|....|....|....|....|....|....|....|....|
NOR B Ps. nautica               --------------------------------------------------
NOR B Ps. aeruginosa            --------------------------------------------------
NOR B Ps. stutzeri              --------------------------------------------------
NOR B Pa. denitrificans         --------------------------------------------------
qNOR Ralstonia eutropha H16     STARPGHEATYTNNWPHEPLIGNQPTSENVVWSVISVVVLLAGVGFLVWA
qNOR Achromobacter xylosoxidan  ATEREGKNVTYTNNWPHEPLIDNVPSAENVMWSIISVVVLLAGIGFLVWA
qNOR Neisseria gonorrhoeae      STNRPGEVFTYTNNWPHEPLINNVPTTENYMWSFTSVVLLLMGIGLLMWG
qNOR Haemophilus parainfluenza  SAERPNTHASYTNNWPHEPLINNVPTPENVVWSIASVVFLIAGIGFVVWI
qNOR Pyrobaculum aerophilum     MAN-------YTNGFPYMPGILTPNIHVTVATWVTFFILLLVIMPLAGWI
```

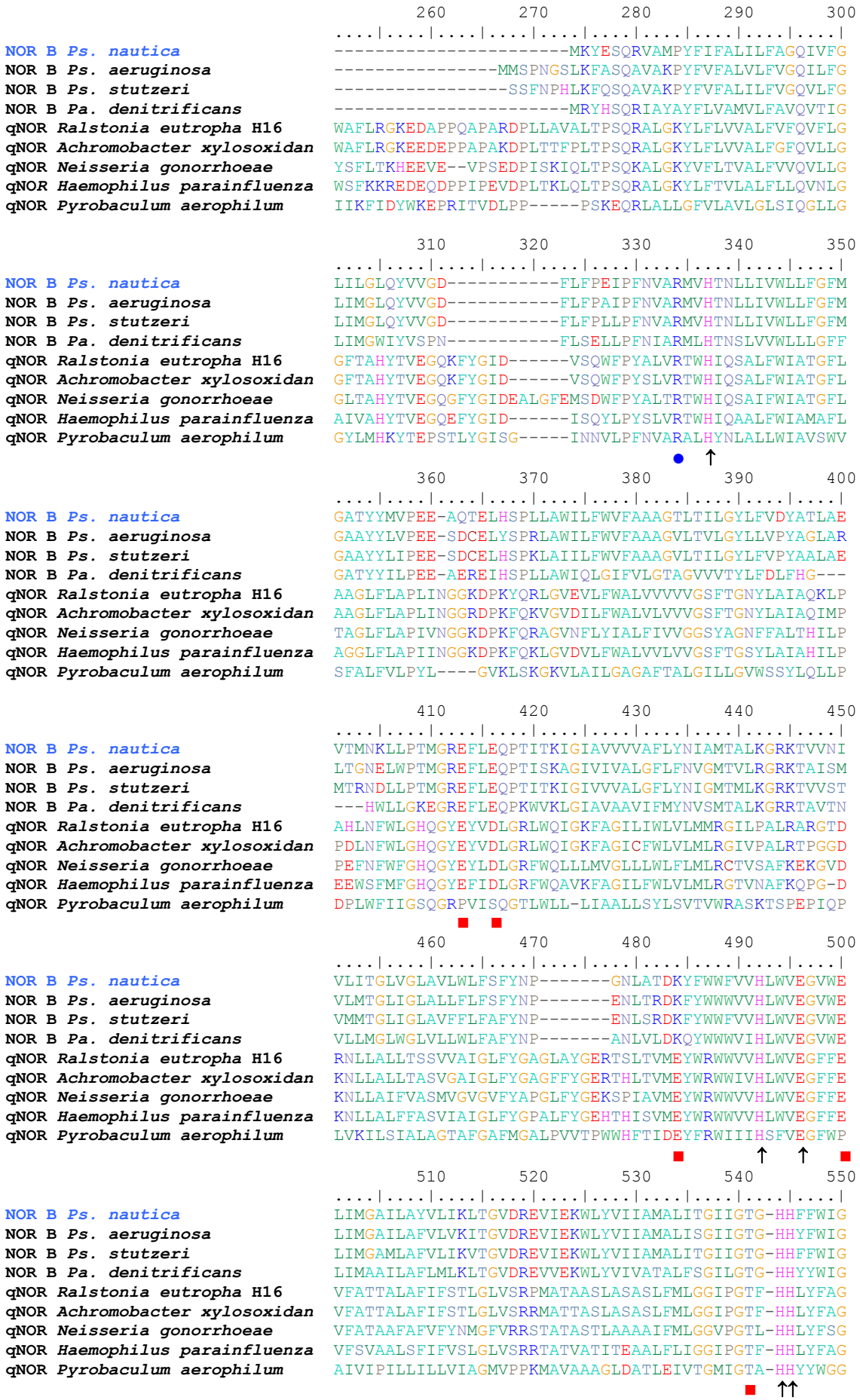
260 270 280 290 300
NOR B Ps. nautica ----------MKYESQRVAMPYFIFALILFAGQIVFG
NOR B Ps. aeruginosa ----------MMSPNGSLKFASQAVAKPYFVFALVLFVGQILFG
NOR B Ps. stutzeri ----------SSFNPHLKFQSQAVAKPYFVFALILFVGQVLFG
NOR B Pa. denitrificans ----------MRYHSQRIAYAYFLVAMVLFAVQVTIG
qNOR Ralstonia eutropha H16 WAFLRGKEDAPPQAPARDPLLAVALTPSQRALGKYLFLVVALFVFQVFLG
qNOR Achromobacter xylosoxidan WAFLRGKEEDEPPAPAKDPLTTFPLTPSQRALGKYLFLVVALFGFQVLLG
qNOR Neisseria gonorrhoeae YSFLTKHEEVE--VPSEDPISKIQLTPSQKALGKYVFLTVALFVVQVLLG
qNOR Haemophilus parainfluenza WSFKKREDEQDPPIPEVDPLTKLQLTPSQRALGKYLFTVLALFLLQVNLG
qNOR Pyrobaculum aerophilum IIKFIDYWKEPRITVDLPP-----PSKEQRLALLGFVLAVLGLSIQGLLG
310 320 330 340 350
NOR B Ps. nautica LILGLQYVVGD----------FLFPEIPFNVARMVHTNLLIVWLLFGFM
NOR B Ps. aeruginosa LIMGLQYVVGD----------FLFPAIPFNVARMVHTNLLIVWLLFGFM
NOR B Ps. stutzeri LIMGLQYVVGD----------FLFPLLPFNVARMVHTNLLIVWLLFGFM
NOR B Pa. denitrificans LIMGWIYVSPN----------FLSELLPFNIARMLHTNSLVVWLLLGFF
qNOR Ralstonia eutropha H16 GFTAHYTVEGQKFYGID------VSQWFPYALVRTWHIQSALFWIATGFL
qNOR Achromobacter xylosoxidan GFTAHYTVEGQKFYGID------VSQWFPYSLVRTWHIQSALFWIATGFL
qNOR Neisseria gonorrhoeae GLTAHYTVEGQGFYGIDEALGFEMSDWFPYALTRTWHIQSAIFWIATGFL
qNOR Haemophilus parainfluenza AIVAHYTVEGQEFYGID------ISQYLPYSLVRTWHIQAALFWIAMAFL
qNOR Pyrobaculum aerophilum GYLMHKYTEPSTLYGISG-----INNVLPFNVARALHYNLALLWIAVSWV
360 370 380 390 400
NOR B Ps. nautica GATYYMVPEE-AQTELHSPLLAWILFWVFAAAGTLTILGYLFVDYATLAE
NOR B Ps. aeruginosa GAAYYLVPEE-SDCELYSPRLAWILFWVFAAAGVLTVLGYLLVPYAGLAR
NOR B Ps. stutzeri GAAYYLIPEE-SDCELHSPKLAIILFWVFAAAGVLTILGYLFVPYAALAE
NOR B Pa. denitrificans GATYYILPEE-AEREIHSPLLAWIQLGIFVLGTAGVVVTYLFDLFHG---
qNOR Ralstonia eutropha H16 AAGLFLAPLINGGKDPKYQRLGVEVLFWALVVVVVGSFTGNYLAIAQKLP
qNOR Achromobacter xylosoxidan AAGLFLAPLINGGRDPKFQKVGVDILFWALVLVVVGSFTGNYLAIAQIMP
qNOR Neisseria gonorrhoeae TAGLFLAPIVNGGKDPKFQRAGVNFLYIALFIVVGGSYAGNFFALTHILP
qNOR Haemophilus parainfluenza AGGLFLAPIINGGKDPKFQKLGVDVLFWALVVLVVGSFTGSYLAIAHILP
qNOR Pyrobaculum aerophilum SFALFVLPYL----GVKLSKGKVLAILGAGAFTALGILLGVWSSYLQLLP
410 420 430 440 450
NOR B Ps. nautica VTMNKLLPTMGREFLEQPTITKIGIAVVVVAFLYNIAMTALKGRKTVVNI
NOR B Ps. aeruginosa LTGNELWPTMGREFLEQPTISKAGIVIVALGFLFNVGMTVLRGRKTAISM
NOR B Ps. stutzeri MTRNDLLPTMGREFLEQPTITKIGIVVVALGFLYNIGMTMLKGRKTVVST
NOR B Pa. denitrificans ---HWLLGKEGREFLEQPKWVKLGIAVAAVIFMYNVSMTALKGRRTAVTN
qNOR Ralstonia eutropha H16 AHLNFWLGHQGYEYVDLGRLWQIGKFAGILIWLVLMMRGILPALRARGTD
qNOR Achromobacter xylosoxidan PDLNFWLGHQGYEYVDLGRLWQIGKFAGICFWLVLMLRGIVPALRTPGGD
qNOR Neisseria gonorrhoeae PEFNFWFGHQGYEYLDLGRFWQLLLMVGLLLWLFLMLRCTVSAFKEKGVD
qNOR Haemophilus parainfluenza EEWSFMFGHQGYEFIDLGRFWQAVKFAGILFWLVLMLRGTVNAFKQPG-D
qNOR Pyrobaculum aerophilum DPLWFIIGSQGRPVISQGTLWLL-LIAALLSYLSVTVWRASKTSPEPIQP
460 470 480 490 500
NOR B Ps. nautica VLITGLVGLAVLWLFSFYNP-------GNLATDKYFWWFVVHLWVEGVWE
NOR B Ps. aeruginosa VLMTGLIGLALLFLFSFYNP-------ENLTRDKFYWWWVVHLWVEGVWE
NOR B Ps. stutzeri VMMTGLIGLAVFFLFAFYNP-------ENLSRDKFYWWFVVHLWVEGVWE
NOR B Pa. denitrificans VLLMGLWGLVLLWLFAFYNP-------ANLVLDKQYWWWVIHLWVEGVWE
qNOR Ralstonia eutropha H16 RNLLALLTSSVVAIGLFYGAGLAYGERTSLTVMEYWRWWVVHLWVEGFFE
qNOR Achromobacter xylosoxidan KNLLALLTASVGAIGLFYGAGFFYGERTHLTVMEYWRWWIVHLWVEGFFE
qNOR Neisseria gonorrhoeae KNLLAIFVASMVGVGVFYAPGLFYGEKSPIAVMEYWRWWVVHLWVEGFFE
qNOR Haemophilus parainfluenza KNLLALFFASVIAIGLFYGPALFYGEHTHISVMEYWRWWVVHLWVEGFFE
qNOR Pyrobaculum aerophilum LVKILSIALAGTAFGAFMGALPVVTPWWHFTIDEYFRWIIIHSFVEGFWP
510 520 530 540 550
NOR B Ps. nautica LIMGAILAYVLIKLTGVDREVIEKWLYVIIAMALITGIIGTG-HHFFWIG
NOR B Ps. aeruginosa LIMGAILAFVLVKITGVDREVIEKWLYVIIAMALISGIIGTG-HHYFWIG
NOR B Ps. stutzeri LIMGAMLAFVLIKVTGVDREVIEKWLYVIIAMALITGIIGTG-HHFFWIG
NOR B Pa. denitrificans LIMAAILAFLMLKLTGVDREVVEKWLYVIVATALFSGILGTG-HHYYWIG
qNOR Ralstonia eutropha H16 VFATTALAFIFSTLGLVSRPMATAASLASASLFMLGGIPGTF-HHLYFAG
qNOR Achromobacter xylosoxidan VFATTALAFIFSTLGLVSRRMATTASLASASLFMLGGIPGTF-HHLYFAG
qNOR Neisseria gonorrhoeae VFATAAFAFVFYNMGFVRRSTATASTLAAAAIFMLGGVPGTL-HHLYFSG
qNOR Haemophilus parainfluenza VFSVAALSFIFVSLGLVSRRTATVATITEAALFLIGGIPGTF-HHLYFAG
qNOR Pyrobaculum aerophilum AIVIPILLILLVIAGMVPPKMAVAAAGLDATLEIVTGMIGTA-HHYYWGG

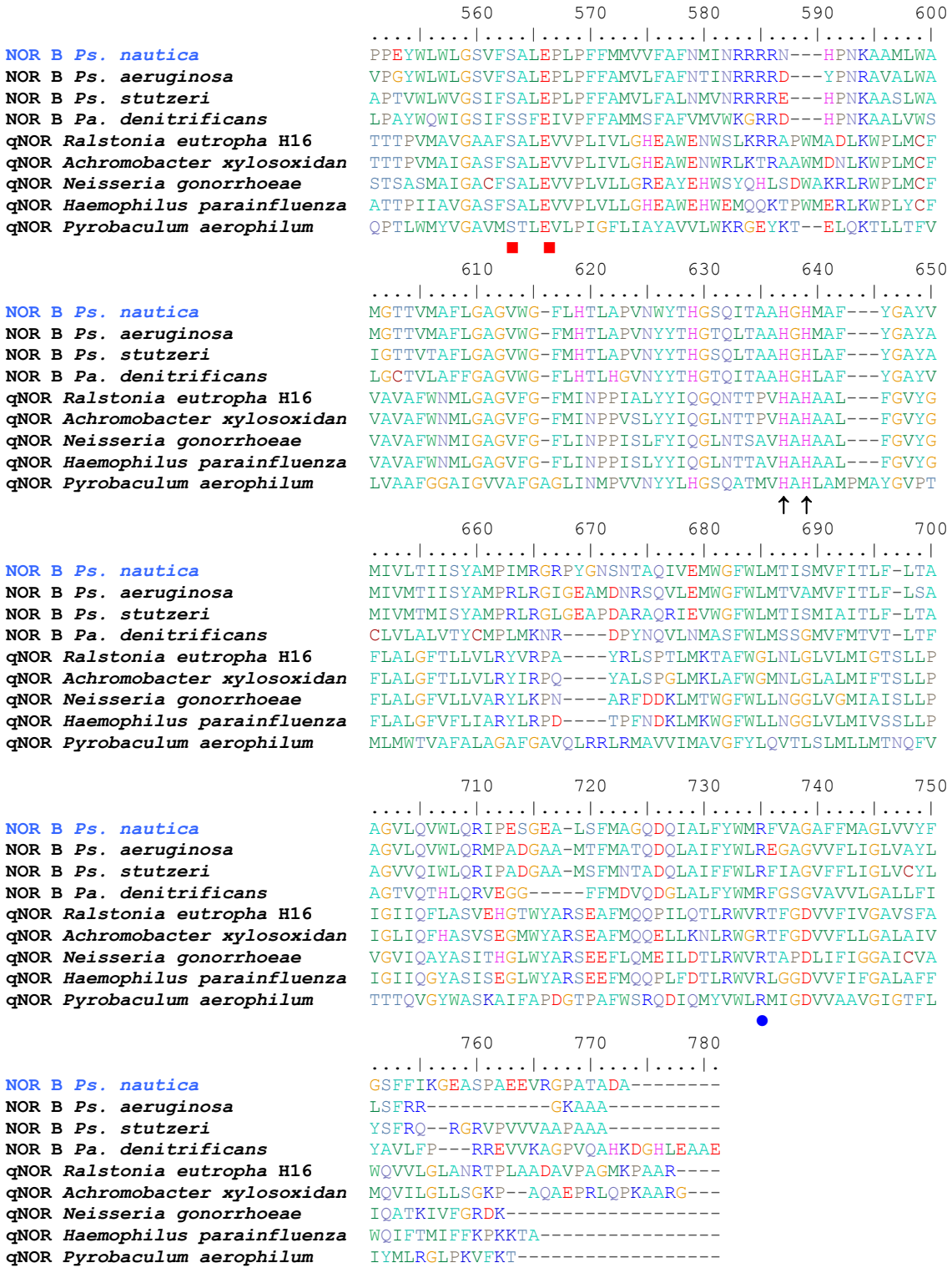

Figure S.1 – Primary sequence alignment from different NOR catalytic subunits. The sequences presented are from *Pseudomonas nautica*, *aeruginosa*, *stutzeri* and *Paracoccus denitrificans*. qNOR from R*alstonia eutropha H16, Achromobacter xylosoxidan*, *Neisseria gonorrhoeae* and *Pyrobaculum aerophilum*. Black arrows point the iron co-factors ligands, ● show the conserved Arg residues and ■ indicate the conserved protonable residues proposed for proton translocation towards the active site.

S.2 Spin Quantitation

The *Pseudomonas nautica* NOR heterodimeric complex, presents a low-spin heme *c*, two low-spin, the heme *b* and heme b_3, and one non-heme Fe_B [1]. The highly anisotropic heme *c* signal is very complicated to simulate. However, the low spin heme *b* is bis-His coordinated and presents the g signals well defined, and therefore using specific software (WINEPR and SimFonia) it is possible to simulate the low-spin heme *b* signal present in the *Ps. nautica* NOR sample (figure S.2).

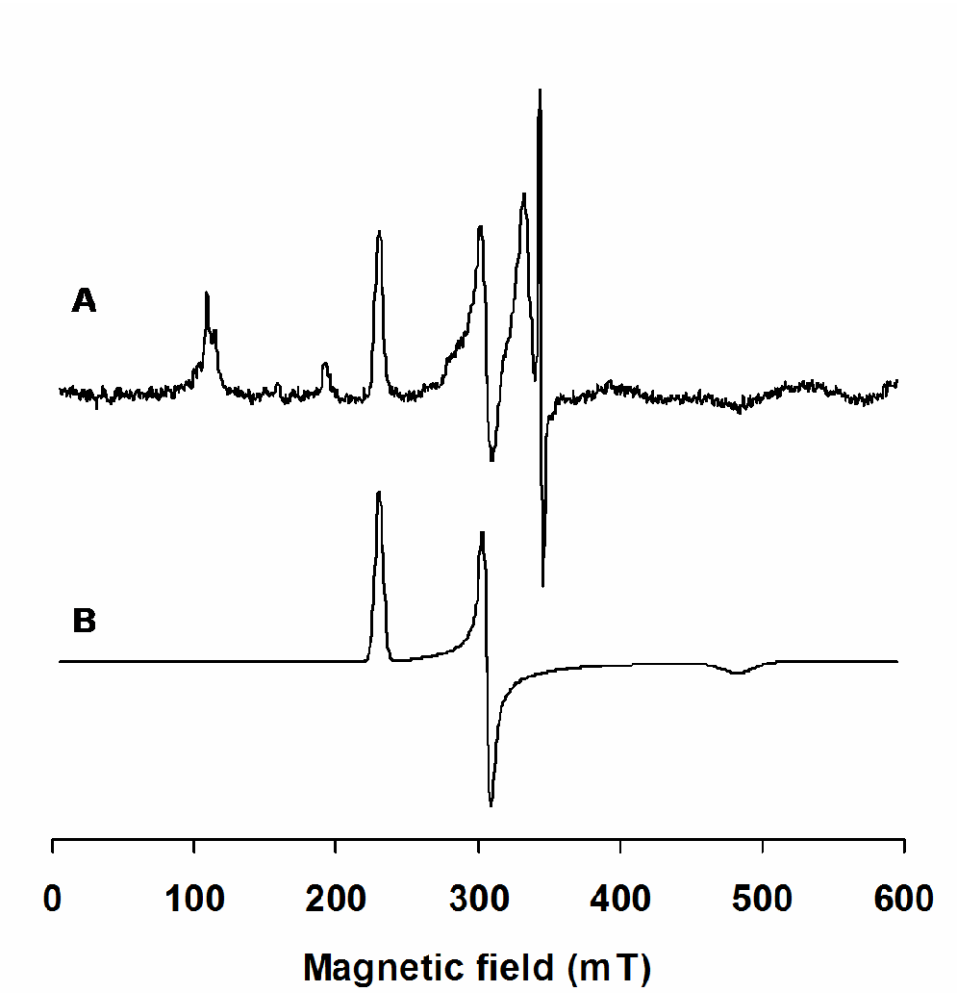

Figure S.2 – Low-spin heme *b* simulation spectrum. A - Shows the EPR spectrum at 9.653 GHz of the as-isolated, *Pseudomonas nautica* NOR (265 µM in 100 mM KPB, pH 7, 0.02 % (w/v) DDM, 0.01 % (v/v) PE). B - is the low-spin heme *b* theoretical simulation using a g_x = 2.9971, g_y=2.2535 and g_z = 1.4276. Experimental conditions of the acquired spectrum (spectrum A): temperature = 12 K, microwave power = 0.2 mW, modulation frequency = 100 kHz, modulation amplitude = 0.5 mT, receiver gain = 1×10^5.

Combining the simulated spectrum with other spectrum in which is known the spin amount (CuEDTA, figure S.3), the spin quantitation for the low-spin hemes *b* and *c* signals can be determined, using the method described by De Vries and Albracht [2]. This method is used to estimate the spin concentration of highly anisotropic low-spin heme EPR signals and is based on the mathematical expressions that account the proportionality factor reported by Aasa and Väänngård [3].

Table S.1 – Spin quantitation for the low-spin heme *b* and heme *c*.

	Spin
heme *b*	0.9 ± 0.18
heme *c*	0.7 ± 0.14

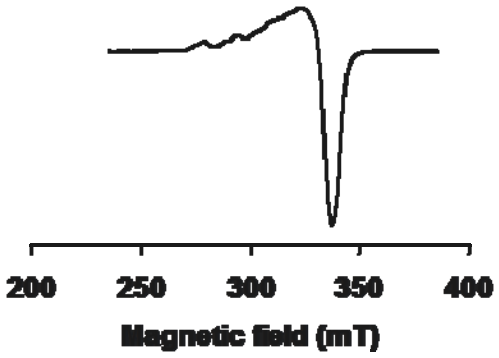

Figure S.3 – CuEDTA (3.076 mM) EPR spectrum at 9.653 GHz. Experimental conditions of the acquired spectrum: temperature = 12 K, microwave power = 0.02\ mW, modulation frequency = 100 kHz, modulation amplitude = 0.5 mT, receiver gain = 2×10^5.

S.3 Cloning the *Pseudomonas nautica* NorC subunit

The NorC subunit coding sequence was amplified, by PCR. Using the *Pseudomonas nautica* 617, partially purified genomic DNA and the flowing forward and reverse primers: NORC_primer1 $^{5'}$ATTGGATCCCATATGGCCGAGCGCTTTACC$^{3'}$ and NORC_primer2 ^{5}TATAAGCTTCTCGAGTTACCCCTCGATGTTGGGTGGC$^{3'}$, the 450 bp fragment containing the protein sequence was amplified. The fragment was inserted into the pCRII-TOPO vector (*Invitrogen)*, according the manufactures specifications [4]. The resultant plasmid was transformed in *Escherichia coli* competent cells as mention in the protocol [4] (alternative protocol for transformation of competent cells is described in the supporting information S.8.5). The transformation reaction was platted in solid LB/ampicillin/x-gal medium and incubated overnight at 37 ºC. This commercial cloning system permits the white/blue screening (positive/negative). Different white colonies were isolated through a plasmidic DNA purification kit (midiprep, *Genomed*) and further sequenced. One of the positive clones was used to double hydrolysis, using previously chosen restriction enzymes (*Nde*I and *Xho*I). The vector, pET-21-c was equally treated with the same restriction enzymes. The hydrolysis products were separated in an agarose gel 1.0 % (w/v) migrated by electrophoresis. The desired fragments were sliced from the agarose gel and purified with a DNA gel extraction kit (*Genomed*). The double-hydrolysed vector and fragment containing the coding sequence of the NorC subunit, were quantified and ligated in a reaction mixture, using the T4 DNA ligase (*Invitrogen*), in order to achieve the pAD11 vector (figure S.4). The reaction product was transformed in *E. coli* competent cells (protocol described in supporting information S.8). Figure S.4 show a schematic resume of the process done for cloning the NorC subunit coding sequence into the pET-21-c. For a detailed description of this cloning strategy, and proceedings check the reference [5].

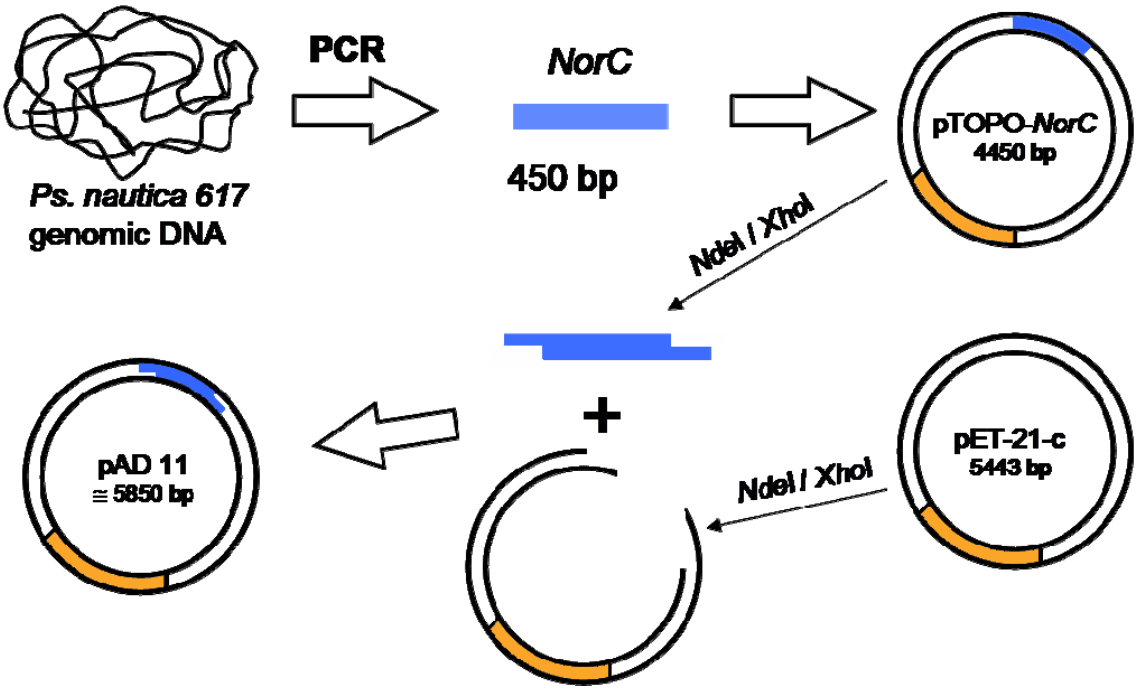

Figure S.4 – Cloning the *Pseudomonas nautica* NorC subunit. The scheme represents the steps for cloning NorC subunit into pCRII-TOPO, subsequent hydrolysis with restriction enzymes and insertion into the pET-21-c vector, in order to achieve the pAD11 vector.

Positive clones were isolated as described earlier in the text and sequenced. The results shown the correct ORF of the NorC subunit in the pAD11 vector, as it can be seen in the alignment present in figure S.5 [1, 6]. The overexpression optimization, the biochemical and spectroscopic characterization of the recombinant NorC subunit (rNorC) is described by Mesquita work [7].

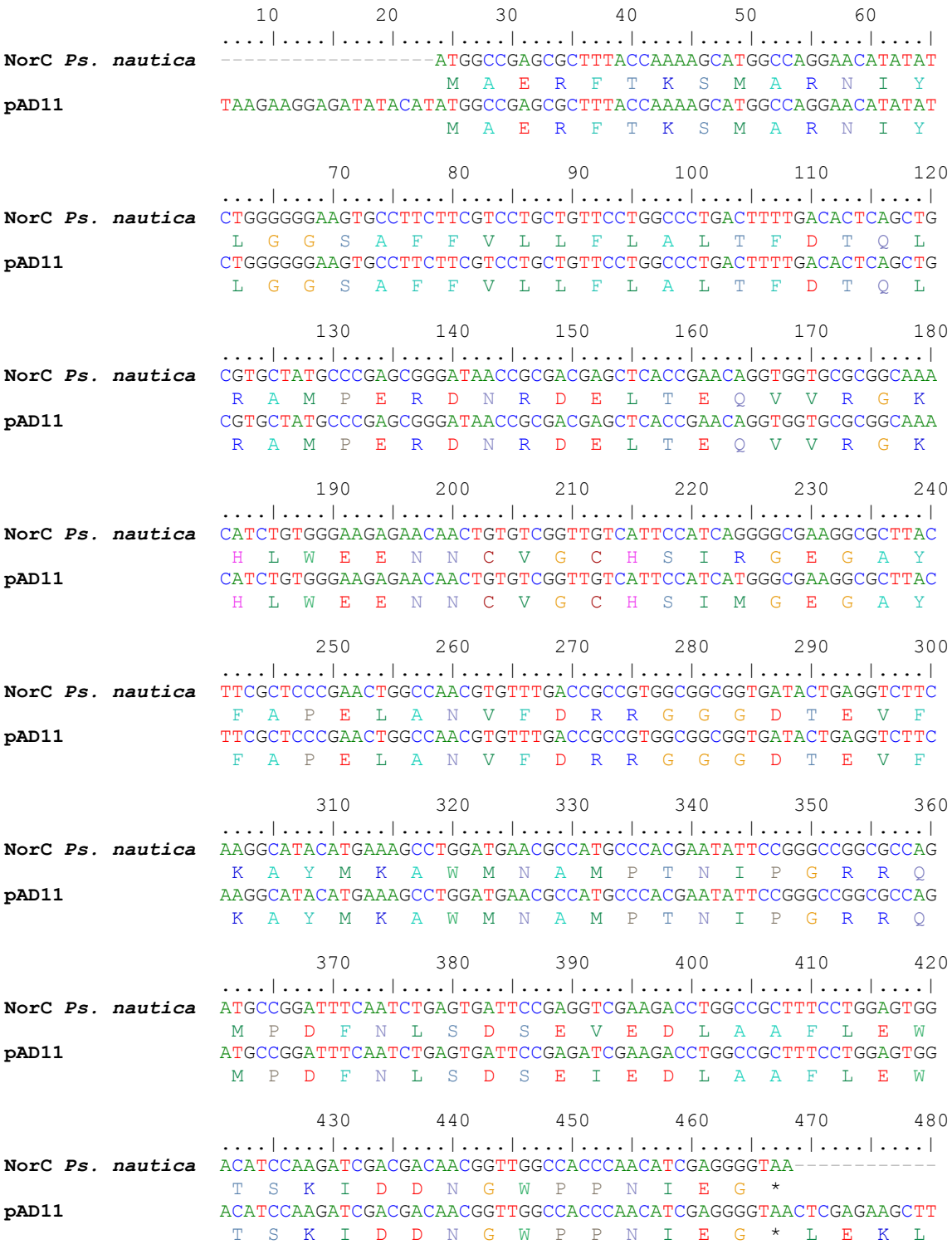

Figure S.5 – Nucleotide sequence alignment of the pAD11 vector with the *Pseudomonas nautica* NorC coding sequence. Under the nucleotide sequences it is shown the correspondent primary sequence [6].

S.4 Laviron's Mathematical Approach

The use of a layer diffusionless regime, allows the application of Laviron's mathematical formulation, to determine kinetic parameters. In this section is presented a brief description of the mathematical approach to determine the heterogeneous rate constant k_s.

When the reduced and oxidised species are strongly adsorbed to the electrode surface, the electrochemical reaction concerns exclusively the adsorbed molecules, thus:

$$i = nFAk_s\{\Gamma_O \exp\left[\frac{-\alpha nF(E-E'^{o})}{RT}\right] - \Gamma_R \exp\left[\frac{(1-\alpha)nF(E-E'^{o})}{RT}\right] \quad \text{(eq. S.1)}$$

$$\Gamma_O + \Gamma_R = \Gamma_T \quad \text{(eq. S.2)}$$

$$i = -nFAd\Gamma_O / dt \quad \text{(eq. S.3)}$$

Where, Γ_O and Γ_R are the surface concentration of the oxidised and reduced species (mol.cm^{-2}) respectively, Γ_R the constant sum of the latest two, and A the electrode area (cm^2). N, F, α, R, and T have the usual significance and the current is expressed in amperes (A).

The current can be defined by the dimensionless function (eq. S.4):

$$\Psi = \frac{i}{(F^2/RT)n^2\nu A\Gamma_T} = m\left[(\Gamma_O/\Gamma_T)\eta^{-\alpha} - (\Gamma_R/\Gamma_T)\eta^{1-\alpha}\right] \quad \text{(eq. S.4)}$$

$$m = \frac{RTk_s}{Fn\nu} \quad \text{(eq. S.5)}$$

When m $\rightarrow\infty$ ($\nu\rightarrow 0$) the system tends to the reversibility and the peak width at mid height tends to 90.6 /n (mV). For m $\rightarrow 0$ (high scan rates), the system tends to irreversibility and in this total irreversible case, the width of the cathodic and anodic peaks are equal to $62.5/\alpha n$ and $62.5/(1-\alpha)n$ (mV) respectively.

From the experimental difference between the anodic and cathodic peaks (ΔEp), and for a known α value, the K_s can be calculated. However, two cases can be considered

$\Delta Ep > 200/n$ mV and $\Delta Ep < 200/n$ mV. The obtained results were all in the second case ($\Delta Ep < 200/n$ mV), so the determination of α can not be precise. For α values close to 0.5 (between 0.3 and 0.7), the k_s can still be determined with a negligible error. Using a theoretical curve of $n\Delta Ep$ as a function of 1/m, and from direct interpolation of the experimental ΔEp values, the k_s can be estimated, according to equation S.5 [8].

S.5 Oxidoreductase Activity Assays Using a Coupled Enzyme System

In order to investigate the formation of H_2O_2 in the O_2 reduction process developed by the *Ps. nautica* NOR, oxidoreductase activity assays were conducted in the presence of peroxidase (*Sigma*).

Experiments were accomplished in 100 mM KPB buffer pH 6, 0.02 % (w/v) DDM, at room temperature, in an aerobic environment. TMPD (1mM) was used as the electron donor for both enzymes (NOR-0.5 μM and peroxidase-0.5 μM). The reaction was monitorized spectophotometrically, following the TMPD oxidation, recording the absorbance changes at 520 nm ($\varepsilon_{520\ nm} = 6.1\ mM^{-1}\ cm^{-1}$) [9]. The assays were performed in a quartz cuvette, and the reaction was started by the addiction of the *Ps. nautica* NOR. Control experiments were assayed in parallel to test TMPD self oxidation and peroxidase activity with this chemical electron donor, in the presence and absence of H_2O_2.

S.6 The *Pseudomonas nautica* NOR Activity

Kinetic experiments using a NO sensor (ISO NO, World Precision Instruments) were accomplished in our research group for the *Ps. nautica* NOR. The detailed experimental procedures for these assays are described in the supporting information S.8.4.

The following unpublished data (figure S.6 and S.7) were kindly given by Carlos E. Martins, member of our research group. The results show the *Ps. nautica* NOR activity in the presence of NO, with different protein concentrations, using two electron donors: the sodium ascorbate/PMS (ASC/PMS) and the reduced *Ps. nautica* cyt.c_{552} (the enzyme's physiological electron donor).

Chemical Electron Donors (ASC/PMS)

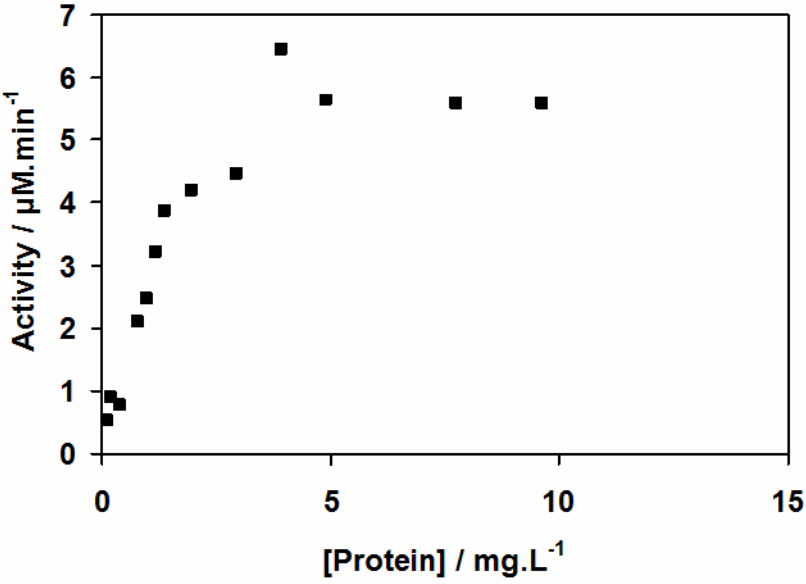

Figure S.6 – The *Pseudomonas nautica* NOR activity (µM NO reduced.minite^{-1}) using ASC (10 mM) /PMS (100 µM) as electron donor. The experimental details are described in the supporting information S.8.4.

Physiologic Electron Donor (*Ps. nautica* cyt.c_{552})

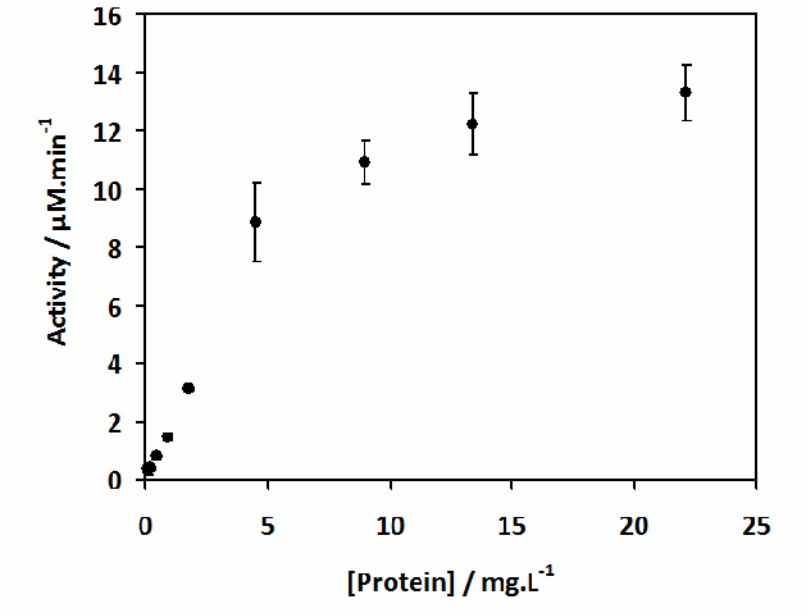

Figure S.7 – The *Pseudomonas nautica* NOR activity (µM NO reduced.minite^{-1}) using reduced *Pseudomonas nautica* cyt.c_{552} (20 µM). The experimental details are described in the supporting information S.8.4.

S.7. The *Pseudomonas nautica* NOR Oxidoreductase Activity

Chemical Electron Donor (TMPD)

The NOR oxidoreductase activity was investigated using TMPD (1 mM) as the chemical electron donor. The assays were monitored by absorbance changes at 520 nm ($\varepsilon_{520\ nm}$= 6.1 mM^{-1} cm^{-1}) [9]. The experiments were made in a quartz cuvette, in 100 mM KPB buffer pH 7, 0.02 % (w/v) DDM, at room temperature, in an anaerobic environment. O_2 was inserted into the system by additions of different volumes of O_2 saturated water, maintained in a sealed flask and using a gastight syringe. Control experiments were assayed in parallel to test the TMPD self oxidation in the presence of O_2. The reactions were initiated by the substrate addiction, in different enzyme concentrations. The results are shown in figure S.8.

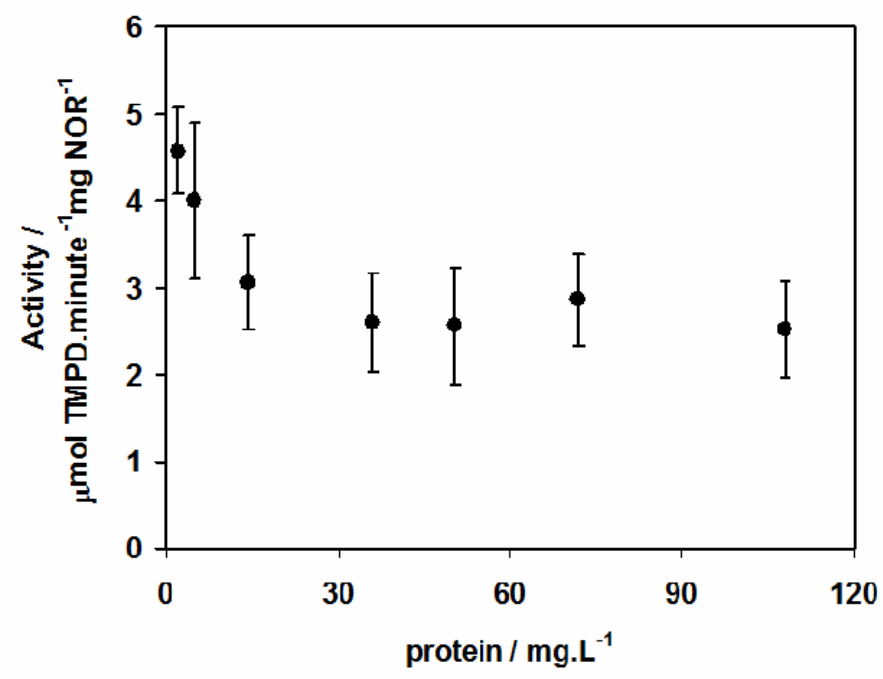

Figure S.8 – The *Pseudomonas nautica* NOR oxidoreductase specific activity (µmol TMPD.minite^{-1}. mg NOR^{-1}) using TMPD (1 mM) as the electron donor.

Concentration Dependence of the Physiological Electron Donor

The NOR oxidoreductase activity was investigated, using a modified Clarck type electrode. Platinum and silver were set as the working and counter electrodes respectively.

A SCE was inserted as the reference electrode, and the three electrodes were connected to a μAUTOLAB type II potentiostat with the potential set to – 0.7 V during the experiments. The data were acquired using the GPES software. Assays were done in an anaerobic environment, at room temperature, in 20 mM mixture buffer, (sodium citrate, MES, HEPES, AMPSO) pH 7.6, 0.02 % (v/v) DDM. The reduced *Ps. nautica* cyt. c_{552} was used as the electron donor. The substrate was dissolved in water and introduced in the reaction from a sealed flask using a gastight syringe.

In order to determine the optimal concentration for the physiological electron donor, oxidoreductase was assayed in different concentrations of cyt. c_{552}, maintaining the substrate and enzyme concentration constant. The achieved results are presented in figure S.9.

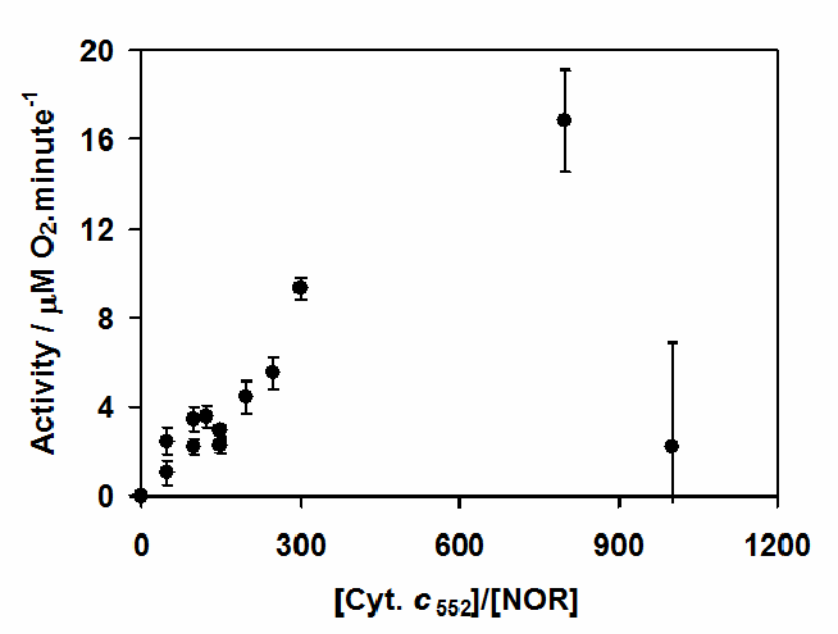

Figure S.9 – The *Pseudomonas nautica* NOR oxidoreductase activity (μM O_2 reduced.minite^{-1}) using different concentration of reduced *Pseudomonas nautica* cyt. c_{552}.

S.8 Methodologies and solutions

S.8.1 Tricine Sodium Dodecyl Sulfate Electrophoresis

Table S.2 – Solutions for tricine sodium dodecyl sufate gel electrophoresis [10].

Solution	Reagents	Amount	Notes
I Acrylamide/bisacrylamide (49.5% T, 3 % C)[1]	Acrylamide Bisacrylamide H_2O	48 g 1.5 g up to 100 ml	
II Gel buffer	Tris SDS H_2O	36.34 g 0.3 g up to 100 ml	Adjust the pH to 8.45
III Ammonium persulfate	Ammonium persulfate H_2O	0.1 g up to 100 ml	
IV Cathodic buffer	Tris Tricine SDS H_2O	121,2 g 179.2 g 10 g up to 1000 ml	Should be at pH 8.45 (without adjustment)
V Anodic buffer	Tris H_2O	121,2 g up to 1000 ml	Adjust the pH to 8.9
VI Sample buffer	SDS β-Mercaptoethanol Glycerol Coomassie blue Tris –HCl pH 7 (1 M)	1.2 g 600 µl 2.44 ml (3 g) 5 mg up to 1.5 ml	When using for heme staining, change β-Mercaptoethanol for H_2O.

[1] % T stands for the total percentage of acrylamide and bis- acrylamide, determined by the following equation: %T=a + b/V. %C stands for the bisacrylamide percentage, compared with the total amount, it is estimated by the equation: %C = a × 100/ (a + b). a, b and V stand for amount of acrylamide, bisacrylamide and the volume, respectively

Table S.3 – Volumes required for tricine sodium dodecyl sulfate gel preparation.

Stock solution	Running gel		Stacking gel
	10 % T, 3 % C[1]	16 % T, 3 % C[1]	4 %
I	1 ml	1.67 ml	166 µl
II	1.67 ml	1.67 ml	500 µl
Glycerol	400 µl	400 µl	-
H_2O	1930 ml	1260 ml	1334 ml
III	25 µl	25 µl	15 µl
TEMED	2.5 µl	2.5 µl	1.5 µl

The tricine SDS-PAGE gels were done by mixing the solutions I, II and III with glycerol, TEMED (table S.3) and water in the proportions described in table S.3. After the running gel polymerization, the stacking gel was prepared as indicated in the previous table (table S.3) and polymerization was attended. Protein samples were prepared and diluted with sample buffer (table S.2) in a ratio 1:4. (v/v), and heated at 40 ºC during 30 minutes. After applying the samples in the gel, these were submitted to a constant current (35 or 70 mA, if one or two gels) using a 1:10 dilution of the cathode and anode buffers (table S.2). After sample migration in the gel, these were stained properly.

Coomassie staining: total protein was detected by immersion of the tricine SDS-PAGE gels in a 0.05 % (p/v) brilliant blue R250, 7.5 % (v/v) glacial acetic acid, 45 % (v/v) methanol solution during 30 minutes. Distaining was accomplished by switching the previous solution to a 7.5 % (v/v) glacial acetic acid, 45 % (v/v) methanol solution.

Heme staining: peroxidatic heme detection was achieved by immersion of the tricine SDS-PAGE gels in a 30 % (p/v) TMBZ, 0.3 % (v/v) methanol, 1.75 mM sodium acetate, 0.7 mM acetic acid solution (freshly prepared) during 30 minutes in the dark. Peroxidatic activity was initiated by addiction of 400 to 800 µl of a commercial 30 % H_2O_2 solution. Reaction was maintained in the dark until developing the blue bands, indicating the peroxidatic hemes presence. To inactivate the reaction, the gels were immersed in a 0.3 % (v/v) isopropanol, 1.75 mM sodium acetate, 0.7 mM acetic acid solution.

S.8.2 Protein Quantification

Protein quantification was assayed using a commercial BCA kit (*Sigma*). The calibration curve was accomplished using bovine serum albumin (BSA) as a standard. After rigorous biochemical characterization, protein (*Ps. nautica* NOR) concentration was estimated through its molar extinction coefficient at 411 nm (295 $mM^{-1}cm^{-1}$) for the as-isolated sample [1].

S.8.3 Simultaneous Detection of Heme *b* and Heme *c*

Protein samples can harbour different heme types. Berry and Trumpower [11] developed a method to quantify independently different type hemes, when they are present in the same biological sample. The principle of the method consists in the complexation of the heme co-factor with pyridine in an alkaline medium. The addiction of sodium dithionite will enhance the heme-pryridine complex reduction, that can be distinguished by slightly changes in their molar extinction coefficients [11]. Gathering the difference spectrum of the complex pyridine-porphyrin (reduced menus oxidised) and the reported molar extinction coefficients at different wavelengths, it is possible to determine the total concentration of the different hemes present in the same sample.

From freshly prepared stock solutions, a 40% (v/v) pyridine, 200 mM NaOH, 0.6 mM $K_3[Fe(CN)_6]$ solution was prepared. This solution was diluted 1:2 with a known amount of the biological sample to analyse. After obtaining the oxidised spectrum, the mixture is reduced by the addition of sodium dithionate. The mixture must be homogenized quickly and the spectra recorded for several minutes, until the soret band stops increasing. Calculations must be done using the spectrum with the maximum absorbance at the soret peak [11].

S.8.4 NO Activity Assays

Kinetic assays for NO reduction were performed using a ISO NO sensor (World Precision Instruments). Electrode calibration was performed using an acidic KI solution

(10 mM, 4.15 g KI, 1.4 ml H_2SO_4, H_2O up 250 ml) and a standard NO_2^- standard solution. According with the chemical reaction:

$$2\,KNO_2 + 2\,KI + H_2SO_4 \longrightarrow 2\,NO + I_2 + 2\,H_2O + 2\,K_2SO_4$$

NO is formed and detected in the sensor. The addition of different NO_2^- amounts can be made, in order to achieve a calibration curve.

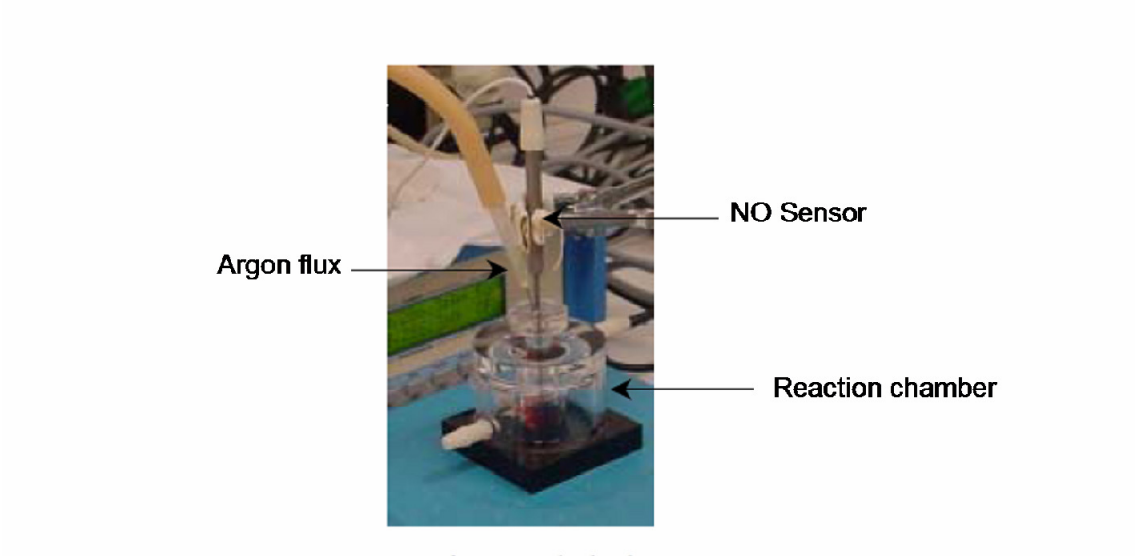

Figure S.10 – ISO NO (World Precision Instruments) sensor setup. The figure shows the specific chamber to install the NO sensor, the introduction of an argon flux in order to maintain the anaerobic environment for reaction.

Reactions where made in a specific chamber (figure S.10) where the electrode is inserted vertically. Oxygen was removed by a constant positive argon flux. Anaerobic solutions were added to the reaction chamber with the use of gastight syringes and the reaction was started with the addiction of the enzyme (*Ps. nautica* NOR) or the crude protein extract in study. Assays were done using combined chemical electron donors Asc/PMS (10 mM and 100 μM, respectively) or reduced *Ps. nautica* cyt. c_{552}. Pure protein samples or crude extracts were quantified as mentioned and used in a concentration of 6 mg/l concentration. ISO-NO Mark II electrode was connected to a Quad 16/EFA-400 and computer. Data were collected and treated using DataTrax™ software (World Precision Instruments).

S.8.5 Molecular biology

Table S.4 – Reagents and correspondent amounts for Luria broth and S.O.C. solutions

	Concentration (g/l)	
Reagent	**LB**	**S.O.C.**
Bactotryptone	10	20
Yeast extract	5	5
NaCl	10	10
KCl	-	0.19
MgCl2	-	2.0
Glucose	-	3.6
agar	20 only to use in solid LB	-
Adjust the pH to 7.2-7.6		

Culture mediums were prepared by dissolving all the reagents in water and adjusting the pH according table S.4. Sterilization was done by heat, at 130 ºC during 30 minutes (autoclave). The desired antibiotics as ampicillin or any other chemical such as x-gal was incorporated in the medium by the addition of the correspondent volume taken from a sterile stock solution. Manipulations were taken in aseptic conditions.

Transformation protocol

1. Thaw competent cells gently on ice (if needed, aliquot the cells to pre-chilled tubes).
2. Add to each tube the DNA for transformation, swirl gently and keep on ice 30 minutes. The volumes used can go from 1-2 μl for a constructed plasmid 4-6 μl if is for transformation of a ligation product.
3. Heat-shock the transformation reactions at 42 ºC for 45-90 seconds.
4. Incubate the reaction on ice 2 minutes.
5. Add 900 μl pre-heated S.O.C solution (37ºC).
6. Incubate the mixture on an orbital shaker, 250 RPM, 37 ºC for 60 minutes.
7. Plate different volumes of the incubated mixture in LB plates, containing the antibiotics for selection, or any other desired chemical.
8. Incubate overnight at 37 ºC.

S.9 Voltammograms and Experimental Parameters

S.9.1 The *Ps. nautica* NOR Redox Potentials

Several voltamograms will be presented in order to elucidate the presence of the four redox processes explained in chapter 3. It will be shown in the following figures the voltammograms obtained with and without a protein film adsorbed to the electrode, as well as the correspondent voltammogram subtraction.

The electron transfer heme *b* and heme *c*

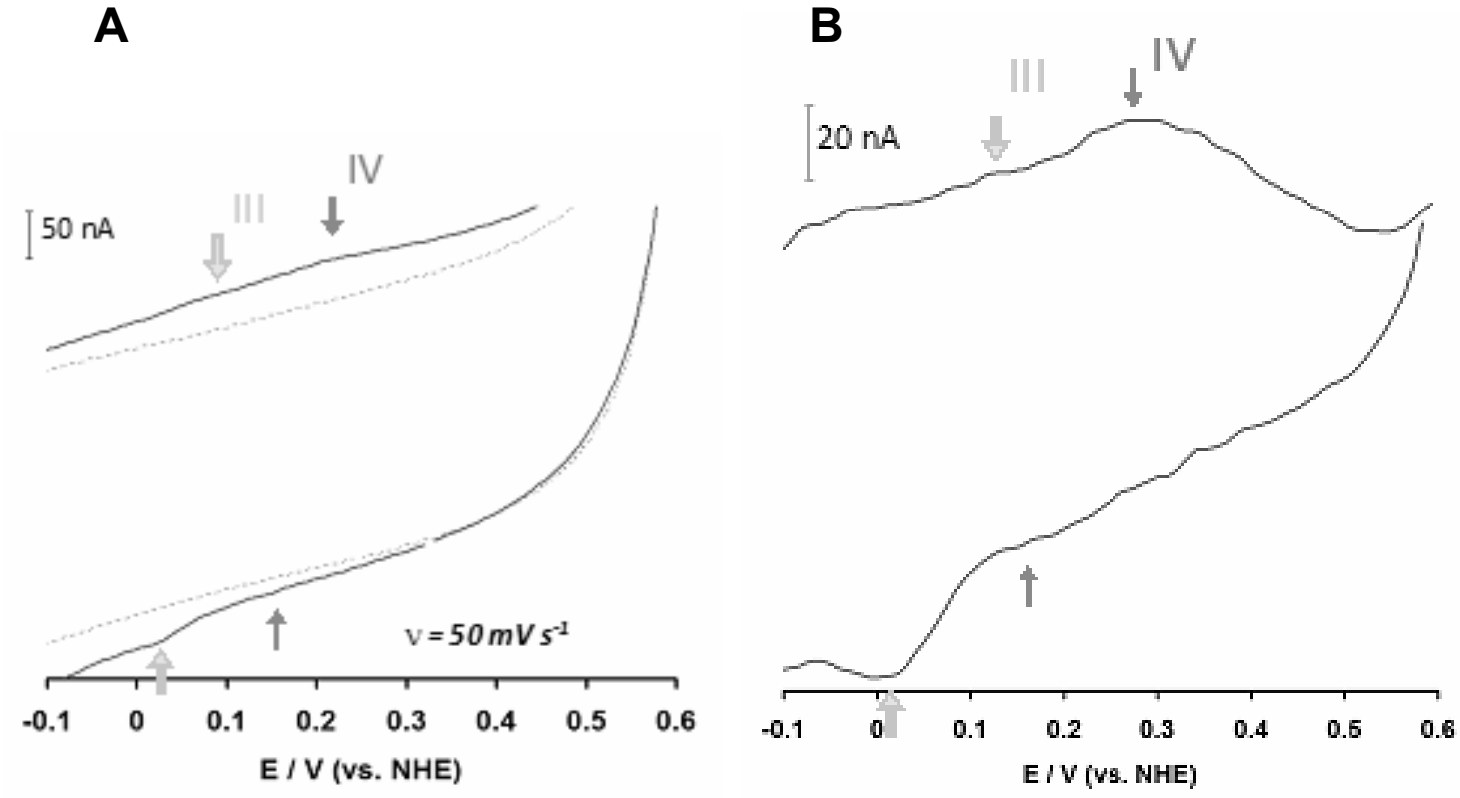

Figure S.11 – Cyclic voltammogram of the immobilized *Pseudomonas nautica* NOR. Panel A shows a detail from the cyclic voltammogram performed at 50 $mV.s^{-1}$ (black line) and the correspondent control experiment (without protein, dashed line). Panel B shows the previous voltammograms subtraction (black line minus dashed line). The arrows point towards the anodic and cathodic peaks for the identified redox processes. Experiments were conducted in 20 mM mixture buffer (experimental details) pH 6.85

The diiron catalytic center

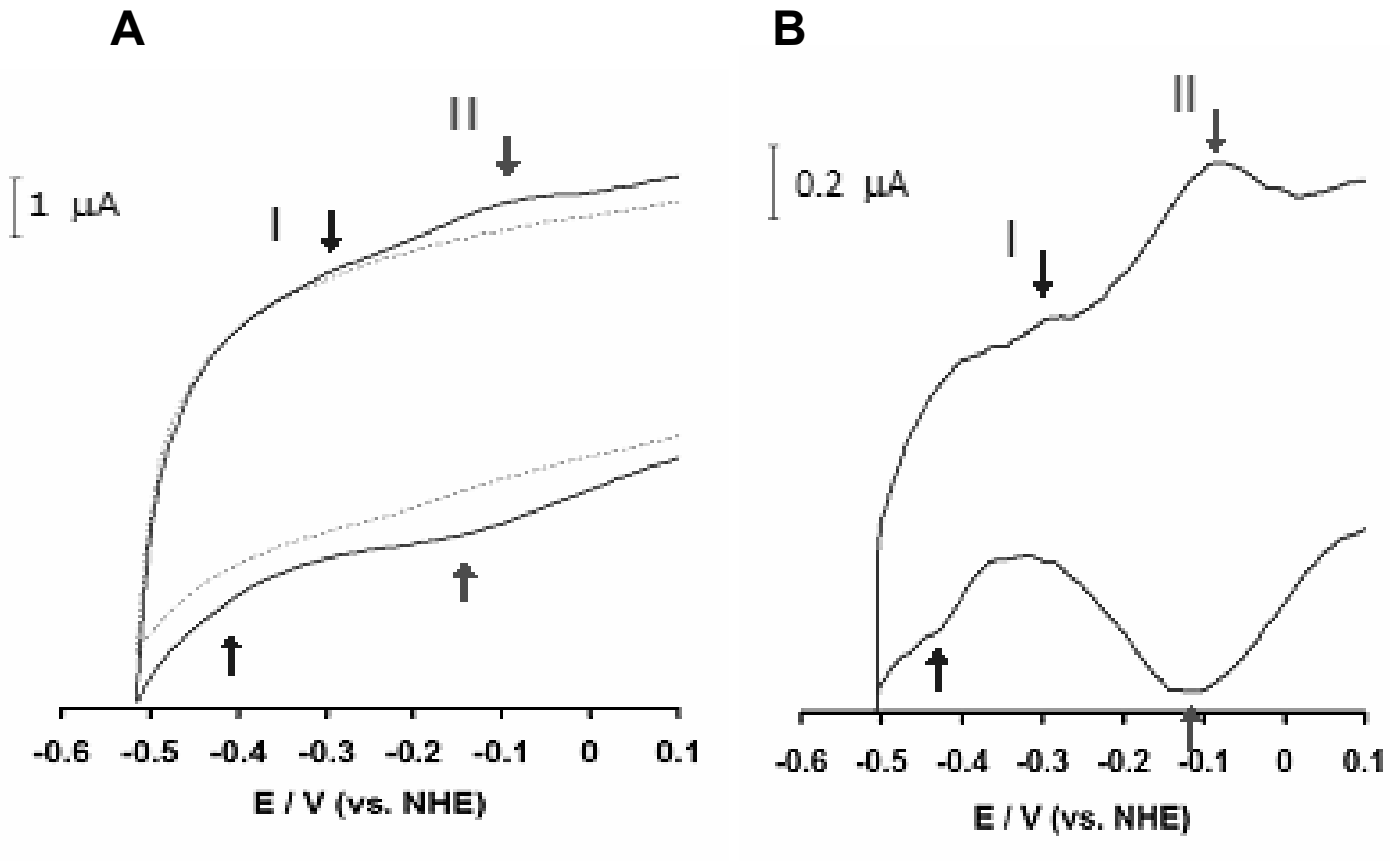

Figure S.12 – Cyclic voltammogram of the immobilized *Pseudomonas nautica* NOR. Panel A shows a detail from the cyclic voltammogram performed at 500 $mV.s^{-1}$ (black line) and the correspondent control experiment (without protein, dashed line). Panel B shows the previous voltammograms subtraction (black line minus dashed line). The arrows point towards the anodic and cathodic peaks for the identified redox processes. Experiments were conducted in 20 mM mixture buffer (experimental details) pH 6.85

S.9.2 ΔEp and $Ep_{w\,½}$

Table S.5 – Values determined for the ΔEp and $Ep_{w,1/2}$ from the anodic and cathodic peak, achieved from the analysis of several voltammograms. It is also the presented the number of electrons (n) estimated for the each redox processe.

pH		I Fe_B	II Heme b_3	III Heme *b*	IV Heme *c*
9.75	ΔEp	58 ± 28	40 ± 20	75 ± 20	41 ± 20
	$Ep_{w,1/2\,a}$	55 ± 6	201 ± 15	70 ± 30	88 ± 30
	$Ep_{w,1/2\,c}$	42 ± 20	150 ± 80	80 ± 40	76 ± 20
	n	1.8 ± 0.6	0.5 ± 0.1	1.2 ± 0.1	1.1 ± 0.1
7.63	ΔEp	57 ± 21	57 ± 27	76 ± 26	60 ± 30
	$Ep_{w,1/2\,a}$	57 ± 22	202 ± 35	69 ± 41	85 ± 40
	$Ep_{w,1/2\,c}$	33 ± 16	122 ± 56	61 ± 32	68 ± 20
	n	2.1 ± 0.8	0.6 ± 0.2	1.4 ± 0.2	1.2 ± 0.2
6.52	ΔEp	83 ± 52	50 ± 18	89 ± 27	80 ± 10
	$Ep_{w,1/2\,a}$	73 ± 30	214 ± 13	60 ± 12	74 ± 19
	$Ep_{w,1/2\,c}$	35 ± 6	153 ± 60	67 ± 21	55 ± 13
	n	1.9 ± 0.9	0.5 ± 0.1	1.4 ± 0.1	1.4 ± 0.3
5.44	ΔEp	58 ± 27	69 ± 10	88 ± 15	46 ± 13
	$Ep_{w,1/2\,a}$	58 ± 37	204 ± 13	60 ± 14	73 ± 10
	$Ep_{w,1/2\,c}$	41 ± 21	169 ± 45	71 ± 27	53 ± 10
	n	1.8 ± 0.5	0.5 ± 0.1	1.4 ± 0.2	1.5 ± 0.3
4.09	ΔEp	17 ± 6	80 ± 14	78 ± 48	23 ± 6
	$Ep_{w,1/2\,a}$	59 ± 10	171 ± 47	35 ± 13	33 ± 15
	$Ep_{w,1/2\,c}$	45 ± 6	166 ± 24	55 ± 18	63 ± 38
	n	1.7 ± 0.3	0.5 ± 0.1	2.0 ± 0.7	2.0 ± 0.9
2.54	ΔEp	84 ± 50	65 ± 27	84 ± 20	67 ± 6
	$Ep_{w,1/2\,a}$	47 ± 11	191 ± 25	76 ± 33	40 ± 19
	$Ep_{w,1/2\,c}$	45 ± 7	106 ± 69	64 ± 26	81 ± 36
	n	1.9 ± 0.4	0.7 ± 0.3	1.3 ± 0.2	1.6 ± 0.8

n (number of electrons involved in each redox process) was estimated using the $Ep_{w,1/2}$ from the anodic and cathodic peak ΔEp, . $Ep_{w,1/2\,a,}$ and $Ep_{w,1/2\,c}$ values are presented in mV

S.9.3 Recombinant NorC Voltammograms

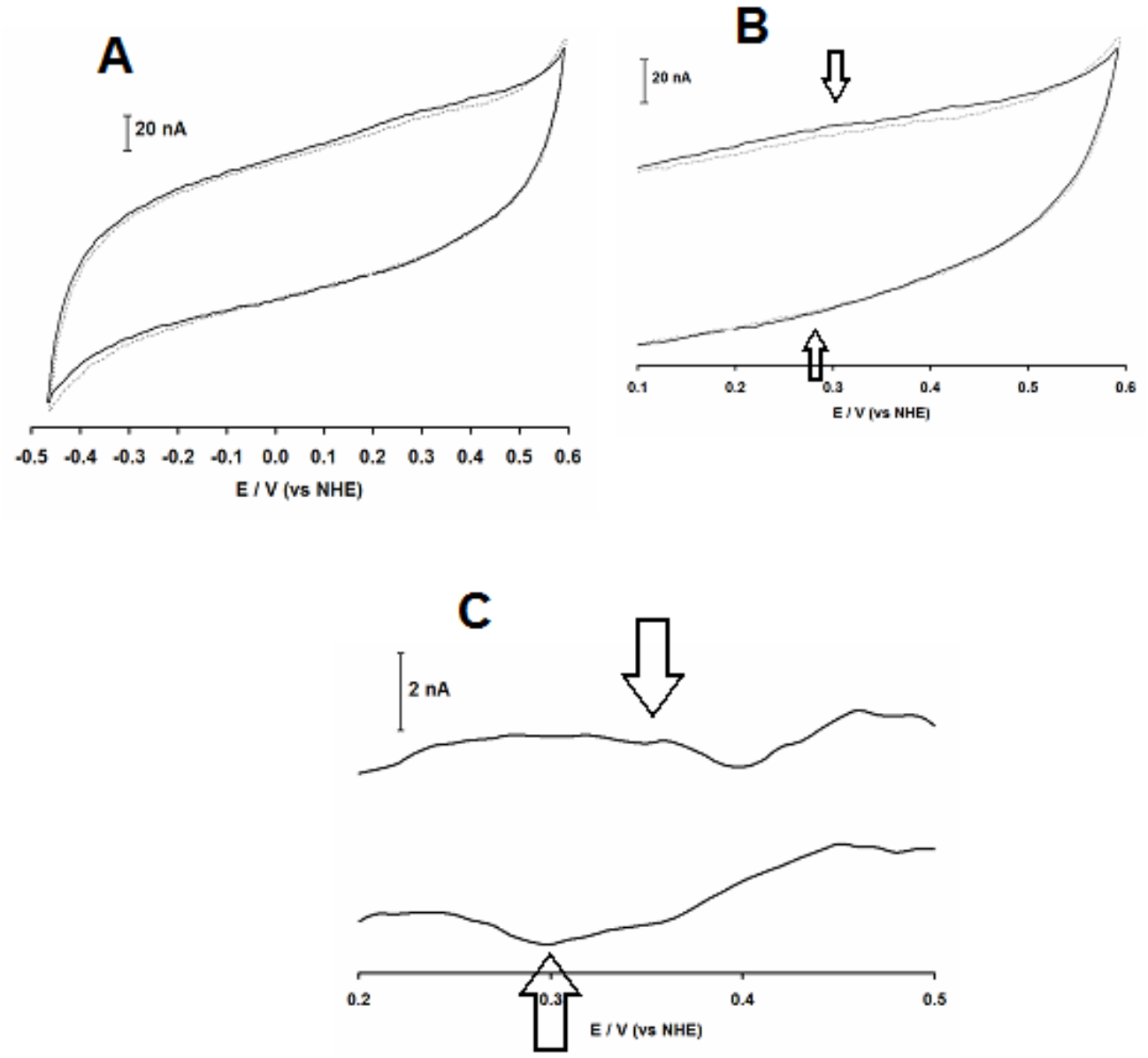

Figure S.13 – Cyclic voltammogram of the immobilized recombinant NorC subuinit . Panel A show a cyclic voltammogram performed at 2.5 $mV.s^{-1}$ (black line) and the correspondent control experiment (without protein, dashed line). Panel B presents a detail from the previous group of voltammograms. Panel C show the previous voltammograms subtraction (black line minus dashed line). The arrows point towards the anodic and cathodic peaks for the identified redox proces. Experiments were conducted in 20 mM mixture buffer (experimental details) pH 7.63

S.9.4 Behaviour with pH Dependence

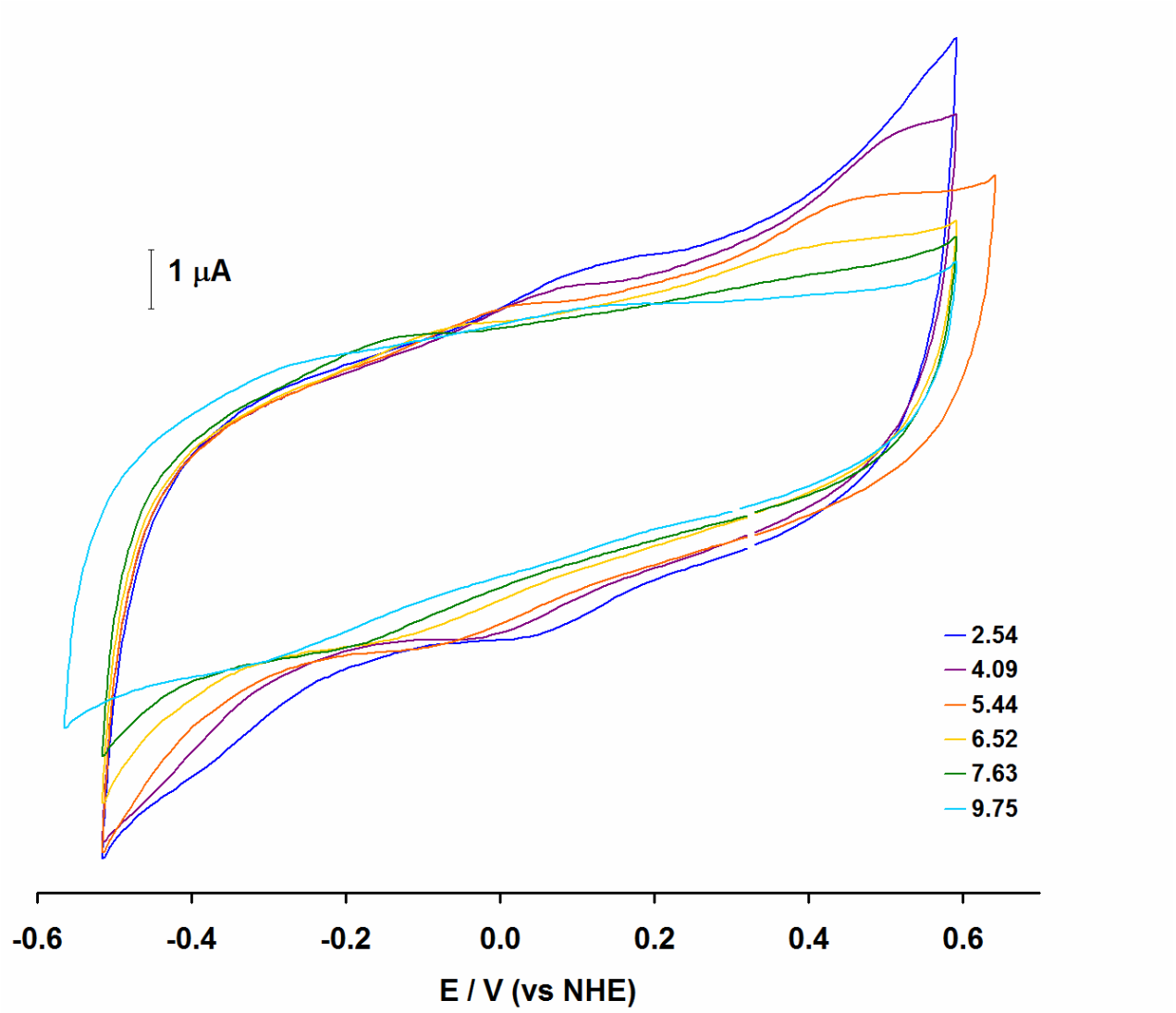

Figure S.14 – Plot of the *Pseudomonas nautica* NOR cyclic voltammograms performed at different pH values. The voltamogramms were obtained with a modified pyrolytic graphite electrode (with the *Ps. nautica* NOR adsorbed to the electrode surface) using a scan rate of 500 mVs^{-1}.

S.9.5 Electrochemical Response in the Presence of Substrate

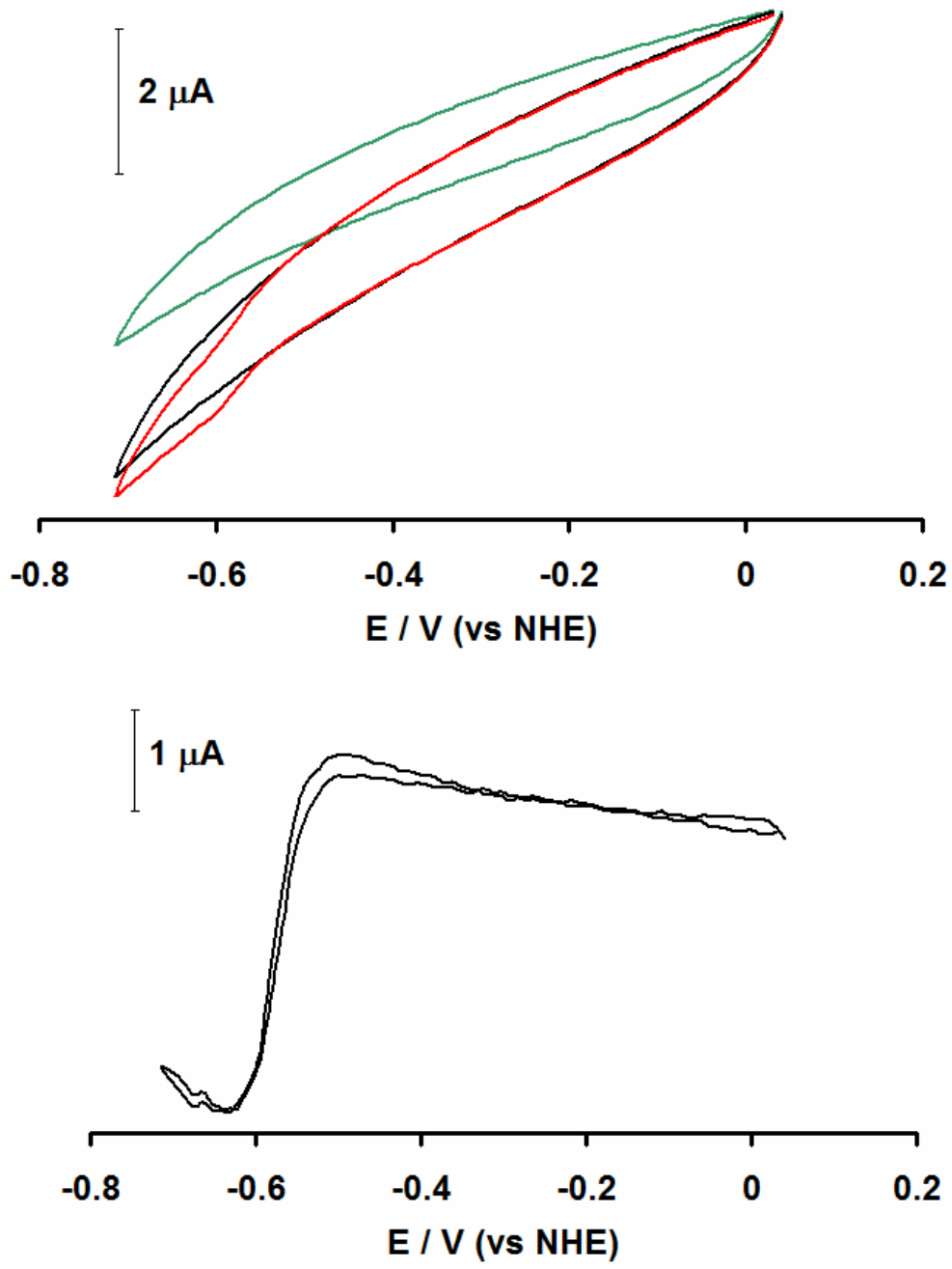

Figure S.15 –Nitric oxide reduction using the *Pseudomonas nautica* NOR modified graphite RDE. Panel A show the results obtained: black and red lines describe the electrochemical response of the NOR modified graphite electrode, in the absence and presence of NO, respectively. The green line describes the control experiment (without protein) in the presence of NO. Panel B is the subtraction of voltammograms performed with the modified electrode, in the presence or not of NO (red menus black), showing beyond dough the presence of a catalytic current. Electrolyte solution was a 20 mM mixture buffer (experimental details, section 3.7) pH 7.6, ν = 50 mV.s^{-1}, (ω = 5000 RPM, RDE), [NO] = 20 μM.

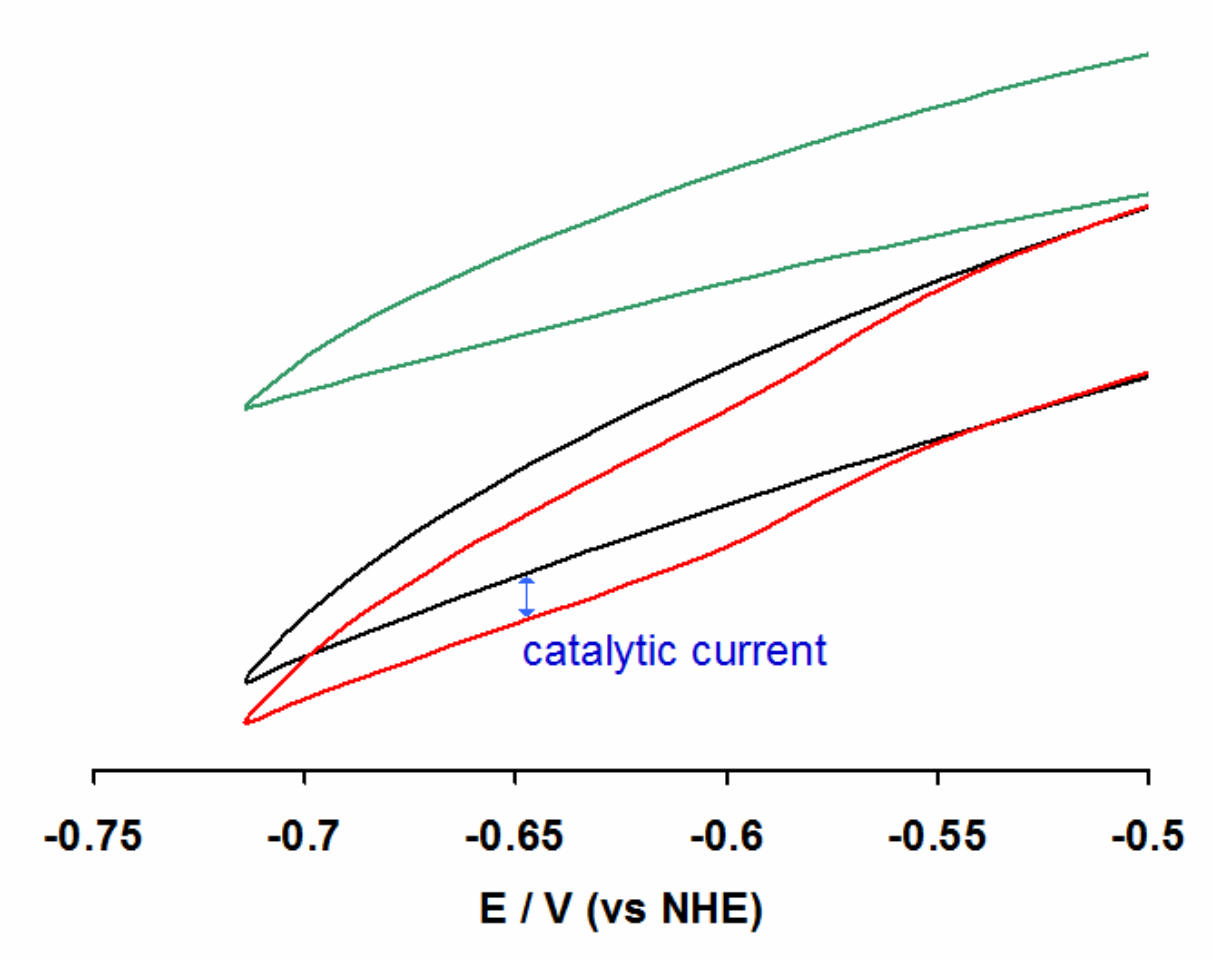

Figure S.16 –Nitric oxide reduction using the *Pseudomonas nautica* NOR modified graphite RDE. The figure shows a detail from the previous figure S.15. Black and red lines describe the electrochemical response of the NOR modified graphite electrode, in the absence and presence of NO, respectively. The green line describes the control experiment (without protein), in the presence of NO. Electrolyte solution was a 20 mM mixture buffer (experimental details, section 3.7) pH 7.6, ν = 50 mV.s^{-1}, (ω = 5000 RPM, RDE), [NO] = 20 μM.

References

[1] Timoteo, C.G., A.S. Pereira, C.E. Martins, S.G. Naik, A.G. Duarte, J.J. Moura, P. Tavares, B.H. Huynh and I. Moura, *Low-Spin Heme b3 in the Catalytic Center of Nitric Oxide Reductase from Pseudomonas nautica.* Biochemistry, 2011. **50**(20): p. 4251-4262.

[2] De Vries, S. and S.P.J. Albracht, *Intensity of Highly Anisotropic Low-Spin Heme Epr Signals.* Biochim Biophys Acta, 1979. **546**(2): p. 334-340.

[3] Aasa, R. and T. Vanngard, *Epr Signal Intensity and Powder Shapes - Re-Examination.* Journal of Magnetic Resonance, 1975. **19**(3): p. 308-315.

[4] Technologies, I.L., *TOPO TA Cloning*, ed. Invitrogen. 2004.

[5] Duarte, A.G., *Biomineralização em bactérias anaerobias. Caracterização de intermediários catalíticos*. 2007, Universidade Nova de Lisboa: Lisboa.

[6] Timoteo, C.G., *Estudos Estruturais e Mecanisticos em enzimas Multihémicas Isoladas de Bactérias Desnitrificantes*. 2004, pHD Thesis Universidade Nova de Lisboa: Lisboa.

[7] Mesquita, K.A., *Produção e caracterização da subunidade c recombinante da redutase do óxido nítrico*, in *Chemistry Department* 2008, Universidade Nova de Lisboa: Lisbon p. 44.

[8] Laviron, E., *General expression of the linear potential sweep voltammogram in the case of diffusionless electochemical system* Journal Electroanal. Chem., 1979. **101**: p. 19-28.

[9] Matsushita, K., E. Shinagawa, O. Adachi and M. Ameyama, *o-Type cytochrome oxidase in the membrane of aerobically grown Pseudomonas aeruginosa.* FEBS Lett, 1982. **139**(2): p. 255-8.

[10] Schagger, H. and G. Vonjagow, *Tricine Sodium Dodecyl-Sulfate Polyacrylamide-Gel Electrophoresis for the Separation of Proteins in the Range from 1-Kda to 100-Kda.* Analytical Biochemistry, 1987. **166**(2): p. 368-379.

[11] Berry, E.A. and B.L. Trumpower, *Simultaneous Determination of Hemes-a, Hemes-B, and Hemes-C from Pyridine Hemochrome Spectra.* Analytical Biochemistry, 1987. **161**(1): p. 1-15.